

Synthesis and characterization  
of bifunctional materials for electro-optical  
applications

Dissertation

for the award of the academic degree of  
Doctor of Natural Science (Dr. rer. nat.)  
from the Faculty of Biology, Chemistry and Geosciences  
University of Bayreuth

submitted by  
Katja Peter  
born in Kronach

Bayreuth, 2005



Synthese und Charakterisierung von  
bifunktionellen Materialien  
für elektro-optische Anwendungen

Dissertation

zur Erlangung des akademischen Grades  
Doktor der Naturwissenschaften  
der Fakultät für Biologie, Chemie und Geowissenschaften  
Der Universität Bayreuth

vorgelegt von  
Katja Peter  
geboren in Kronach

Bayreuth, 2005

Die vorliegende Arbeit wurde vom Juni 2001 bis Dezember 2004 am Lehrstuhl für Makromolekulare Chemie I der Universität Bayreuth angefertigt.

Vollständiger Abdruck der von der Fakultät Biologie, Chemie, Geowissenschaften der Universität Bayreuth genehmigten Dissertation zur Erlangung des akademischen Grades Doktor der Naturwissenschaften (Dr. rer. nat.).

Datum der Einreichung der Arbeit: 12.01.2005

Datum des wissenschaftlichen Kolloquiums: 29.04.2005

Prüfungsausschuß:

<i>Vorsitzender:</i>	<i>Prof. Dr. Georg Krausch</i>
<i>Erstgutachter:</i>	<i>Privatdozent Dr. Mukundan Thelakkat</i>
<i>Zweitgutachter:</i>	<i>Prof. Dr. Helmut Alt</i>
<i>Prüfer:</i>	<i>Prof. Dr. Rainer Schobert</i>

*Diese Arbeit wurde finanziell unterstützt durch die „Deutsche Forschungsgemeinschaft, Sonderforschungsbereich 481“.*

Es gibt eine Reihe von Menschen, denen ich danken möchte, da ohne sie die Anfertigung dieser Arbeit nicht möglich gewesen wäre:

Herrn *Prof. Dr. Hans-Werner Schmidt* danke ich für die Möglichkeit, an seinem Lehrstuhl diese Doktorarbeit verfassen zu können und für das Bereitstellen eines hervorragend ausgestatteten Arbeitsplatzes.

Besonders danken möchte ich Herrn Privatdozenten *Dr. Mukundan Thelakkat*. Seine Fähigkeit, einen auch in Momenten größter Frustration zu motivieren, sowie stete Diskussionsbereitschaft und ein offenes Ohr für alle großen und kleinen Probleme, sind einzigartig und verdienen große Anerkennung.

Den Mitgliedern der Gruppe von *James Durrant* vom Imperial College, London (UK), danke ich sehr für die Durchführung der transienten Absorptionsspektroskopie und *Dr. Bin Peng* gebührt ein großes Dankeschön für die Präparation und Charakterisierung der Solarzellen.

*Helga Wietasch* danke ich für ihre Unterstützung bei der Synthesearbeit, sowie für die zahlreichen netten Unterhaltungen über alle Dinge, die das Leben für einen bereit hält. Danke auch an *Julian Rauh* für seine Unterstützung bei der Synthesearbeit als HIWI.

Den Netzwerk-Administratoren *Martin Sonntag* und *Dr. Christian Neuber* gebührt besonderer Dank für ihre Hilfsbereitschaft und Ausdauer bei allen Computer-Problemen. Außerdem danke ich *Stefan Lindner* und *Daniela Kropp* für ihre Unterstützung bei der Durchführung von SEC-Messungen, bzw. für einen Einblick in die anionische Polymerisation.

Ich danke den *Mitgliedern des Herrenstammtisches* und *Heiko Thiem* dafür, daß sie während meiner Zeit in der MC I zu guten Freunden geworden sind, die immer für einen Scherz zur Aufmunterung zu haben sind.

Meinem ehemaligen Laborkollegen *Dr. Roman Kisselev* möchte ich für seine gute Laune im Labor danken. Auf seine besondere Art hat er es fast immer geschafft, mich zum Lachen zu bringen.

Mein Dank gilt auch *Annette Krökel* und *Frauke Pfeiffer*, die mir die Betreuung des NMR-Gerätes erleichtert, bzw. abgenommen haben, für die netten Gespräche fachlicher und privater Natur.

Mein größter Dank gilt *meiner ganzen Familie*, sowie meinem Freund *Peter*, für ihre stete Unterstützung – besonders in schwierigen Phasen, während der Anfertigung dieser Arbeit.



*...in Dankbarkeit  
für meine Eltern...*



## List of abbreviations

AM 1.5	air mass 1.5 solar spectrum
ATRP	atom transfer radical polymerization
a. u.	arbitrary unit
bpy	2,2'-bipyridine
bl-TiO <sub>2</sub>	TiO <sub>2</sub> blocking layer
C <sub>60</sub>	fullerene
<sup>13</sup> C-NMR	carbon nuclear magnetic resonance
CRP	controlled radical polymerization
d	doublet
DMF	N,N-dimethylformamide
DMSO	dimethylsulfoxide
DNPP	2,5-dimethyl-4-(4-nitrophenylazo)phenol
DSC	differential scanning calorimetry
FTO	fluorinated tin oxide
GC	gas chromatography
h	hour
HC	hole conductor
HEMA	hydroxyethylmethacrylate
<sup>1</sup> H-NMR	proton nuclear magnetic resonance spectroscopy
HOMO	highest occupied molecular orbital
HTL	hole transport layer
IPCE	incident photon to current conversion efficiency
ITO	indium tin oxide
LUMO	lowest unoccupied molecular orbital
m	multiplet
MCP	α-chloromethylpropionate
MEK	ethyl methyl ketone
MLCT	metal-to-ligand charge transfer

MPP	maximum power point
MS	mass spectrometry
nc	nanocrystalline
NLO	non-linear optical
Pc	phthalocyanine
PDI	polydispersity [ $M_w/M_n$ ]
PMDETA	1,1,4,7,7-pentamethyldiethylene triamine
ppm	parts per million
PPV	poly(p-phenylene vinylene)
s	singlet
SEC	size exclusion chromatography
spiro-OMeTAD	2,2',7,7'-tetrakis(N,N-di-p-methoxy-phenylamine)-9,9'-spirobifluorene
TBAB	<i>tert</i> -butylammoniumbromide
t	triplet
TBDMS	<i>tert</i> -butyldimethyldimethylsilyl protective group
TD-DFT	time-dependent density functional theory
TGA	thermo gravimetric analysis
THF	tetrahydrofurane
TLC	thin layer chromatography
TPA	triphenylamine
TPD	N,N,N',N'-tetraphenyl-1,1'-biphenyl-4,4'-diamine derivative
vTPA	4-vinyltriphenylamine

## List of symbols and physical terms

$c$	concentration [ $\text{mol l}^{-1}$ ]
$\delta$	chemical shift [ppm]
$\epsilon$	extinction coefficient [ $\text{l mol}^{-1} \text{cm}^{-1}$ ]
FF	fill factor [%]
$\eta$	power conversion efficiency [%]
$I_{\text{SC}}$	short circuit current density [ $\text{mA cm}^{-2}$ ]
$l$	thickness of sample for UV-Vis spectroscopy [cm]
$\lambda$	wavelength [nm]
$\lambda_{\text{max}}$	wavelength of maximum absorption [nm]
$M$	molecular weight [ $\text{g mol}^{-1}$ ]
$M_n$	number average molecular weight [ $\text{g mol}^{-1}$ ]
$M_p$	peak molecular weight [ $\text{g mol}^{-1}$ ]
$M_w$	weight average molecular weight [ $\text{g mol}^{-1}$ ]
OD	optical density
$T_g$	glass transition temperature [ $^{\circ}\text{C}$ ]
$T_{\text{onset}}$	onset temperature for weight loss in TGA [ $^{\circ}\text{C}$ ]
$U_{\text{OC}}$	open circuit voltage [V]
wt %	weight percentage

# Table of contents

<b>1</b>	<b>Introduction.....</b>	<b>1</b>
1.1	<b>Organic materials in electro-optical applications.....</b>	<b>2</b>
1.2	<b>Organic solar cells.....</b>	<b>3</b>
1.2.1	P/n-heterojunction thin-layer photovoltaic devices .....	4
1.2.2	Dye-sensitized nc-TiO <sub>2</sub> solar cells .....	9
1.2.3	Ru(II) dyes in dye-sensitized TiO <sub>2</sub> solar cells .....	16
1.2.4	Solar cell characterization.....	20
1.3	<b>Organic photorefractive systems .....</b>	<b>22</b>
1.4	<b>Atom transfer radical polymerization (ATRP).....</b>	<b>27</b>
<b>2</b>	<b>Motivation and aim .....</b>	<b>33</b>
<b>3</b>	<b>Low molecular weight Ru(II) dyes carrying TPA units.....</b>	<b>41</b>
3.1	<b>Synthetic strategy .....</b>	<b>42</b>
3.2	<b>Synthesis of bis(triarylamino)bipyridine ligands .....</b>	<b>43</b>
3.2.1	Synthesis of 4,4'-bis(chloromethyl)-2,2'-bipyridine ( <b>3</b> ) .....	43
3.2.2	Synthesis of 4,4'-bis[4-(diphenylamino)styryl]-2,2'-bipyridine (bpy-TPA ligand, <b>6</b> ).....	46
3.2.3	Synthesis of 4,4'-bis[N-(phenyl)-N'-(styryl)-N,N'-bis(3-methyl phenyl)-1,1'- biphenyl-4,4'-diamino]2,2'-bipyridine ( <b>11</b> ) .....	47
3.2.4	NMR-spectroscopy of <b>6</b> and <b>11</b> .....	50
3.2.5	UV-Vis spectroscopy of <b>6</b> and <b>11</b> .....	52
3.3	<b>Synthesis of Ru(bpy<sub>COOH</sub>)<sub>2</sub>Cl<sub>2</sub> · 2 H<sub>2</sub>O (<b>13</b>).....</b>	<b>54</b>
3.3.1	Synthesis of 4,4'-dicarboxy-2,2'-bipyridine ( <b>12</b> ) .....	54

3.3.2	Metallation of 4,4'-dicarboxy-2,2'-bipyridine (12) .....	55
3.3.3	Characterization of Ru(bpy <sub>COOH</sub> ) <sub>2</sub> Cl <sub>2</sub> · 2 H <sub>2</sub> O (13) .....	56
<b>3.4</b>	<b>Synthesis of Ru(II) dyes carrying hole conductor units (14, 15) ....</b>	<b>57</b>
3.4.1	Synthesis of Ru(II) dye carrying TPA-units (14) .....	57
3.4.2	Synthesis of Ru(II) dye carrying TPD-units (15) .....	59
<b>3.5</b>	<b>Characterization of bifunctional dyes 14 and 15.....</b>	<b>61</b>
3.5.1	UV-Vis spectroscopy .....	61
3.5.2	Application of bifunctional dye in dye-sensitized nc-TiO <sub>2</sub> solar cells.....	64
3.5.3	Transient absorption spectroscopy .....	70

## **4 Bifunctional polymers carrying Ruthenium (II) core and poly(vTPA) chains.....76**

<b>4.1</b>	<b>Synthesis and characterization of 4,4'-bis[poly(4-bromostyryl)methyl]-2,2'-bipyridine (16 a – f) .....</b>	<b>81</b>
4.1.1	GC analysis of ATRP of 4-bromostyrene .....	83
4.1.2	Size exclusion chromatography (SEC) .....	86
4.1.3	NMR-spectroscopy .....	88
4.1.4	Thermal properties: DSC and TGA .....	90
<b>4.2</b>	<b>Synthesis and characterization of 4,4'-bis[poly(4-vinyltriphenylamino) methyl]-2,2'-bipyridine (17 c – f).....</b>	<b>91</b>
4.2.1	NMR-spectroscopy .....	93
4.2.2	Elemental analysis.....	95
4.2.3	Molecular weight determination .....	97
4.2.4	Thermal analysis.....	98
4.2.5	UV-Vis spectroscopy .....	99
<b>4.3</b>	<b>Synthesis and characterization of bis[bipyridyl]-[4,4'-bis[poly(4-vinyltri-phenylamino)methyl]-2,2'-bipyridyl]-Ru(II) trifluoro-sulfonate (18).....</b>	<b>100</b>

4.3.1	Thermal analysis of polymers <b>18</b> .....	101
4.3.2	Molecular weight determination .....	103
4.3.3	UV-Vis spectroscopy .....	105
4.3.4	Transient absorption spectroscopy of <b>18</b> .....	106

## **5 Fully functionalized AB-diblock copolymers carrying hole transport and NLO-dye blocks ..... 109**

<b>5.1</b>	<b>Synthesis and characterization of poly(4-bromo-styrene) macroinitiators (19).....</b>	<b>111</b>
5.1.1	GC analysis of ATRP of 4-bromostyrene with standard initiator MCP .....	113
5.1.2	Size exclusion chromatography (SEC) .....	114
5.1.3	Thermal analysis.....	115
5.1.4	NMR-spectroscopy.....	116
<b>5.2</b>	<b>Synthesis and characterization of poly(4-bromo-styrene)-block-poly(HEMA-TBDMS) (21) .....</b>	<b>117</b>
5.2.1	Synthesis and characterization of <i>t</i> -butyldimethylsiloxyethyl methacrylate (HEMA-TBDMS) ( <b>20</b> ) .....	117
5.2.2	Synthesis of poly(4-bromostyrene)- <i>block</i> -poly(HEMA-TBDMS) ( <b>21</b> ) .....	119
5.2.3	Size exclusion chromatography (SEC) .....	121
5.2.4	NMR-spectroscopy.....	123
5.2.5	Calculation of composition.....	124
5.2.6	Thermal analysis.....	126
<b>5.3</b>	<b>Synthesis and characterization of poly(4-vinyl-triphenylamine)-block-poly(HEMA-TBDMS) (22b, 22c).....</b>	<b>127</b>
5.3.1	Size exclusion chromatography (SEC) .....	128
5.3.2	NMR-spectroscopy.....	129
5.3.3	Thermal analysis.....	131
<b>5.4</b>	<b>Synthesis and characterization of poly(4-vinyl-triphenylamine)-block-poly (HEMA-DNPP) (28) .....</b>	<b>132</b>

5.4.1	Synthesis of poly(4-vinyltriphenylamine)- <i>block</i> -poly(HEMA) ( <b>23</b> ).....	132
5.4.2	Size exclusion chromatography (SEC) .....	133
5.4.3	NMR-spectroscopy .....	133
5.4.4	Thermal analysis.....	134
5.4.5	Synthesis and characterization of 1-[(2,5-dimethyl-4-(4-nitrophenylazo) phenoxy] butyric acid chloride ( <b>27</b> ).....	135
5.4.6	Synthesis and characterization of poly(4-vinyltriphenyl-amine)- <i>block</i> -poly(HEMA-DNPP) .....	139
5.4.7	Size exclusion chromatography (SEC) .....	140
5.4.8	NMR-spectroscopy .....	141
5.4.9	Thermal analysis.....	142
5.4.10	UV-Vis Spectroscopy .....	143
<b>6</b>	<b>Summary .....</b>	<b>146</b>
<b>7</b>	<b>Zusammenfassung.....</b>	<b>159</b>
<b>8</b>	<b>Experimental .....</b>	<b>173</b>
<b>8.1</b>	<b>Methods and devices for characterization .....</b>	<b>174</b>
8.1.1	Differential scanning calorimetry (DSC) .....	174
8.1.2	Elemental analysis.....	174
8.1.3	Fluorescence spectroscopy .....	174
8.1.4	Fourier transformed infrared spectroscopy (FT-IR) .....	174
8.1.5	MALDI-TOF spectrometry .....	175
8.1.6	Mass spectrometry.....	175
8.1.7	Nuclear magnetic resonance spectroscopy (NMR) .....	175
8.1.8	Size exclusion chromatography (SEC) .....	175
8.1.9	Thermo gravimetric analysis (TGA) .....	176
8.1.10	Thin layer chromatography (TLC) .....	176
8.1.11	UV-Vis spectroscopy.....	177
8.1.12	Preparation and characterization of solar cells .....	177

<b>8.2</b>	<b>Solvents, chemicals and inert gas</b> .....	<b>179</b>
<b>8.3</b>	<b>Synthesis and characterization</b> .....	<b>182</b>
8.3.1	4,4'-bis(trimethylsilylmethyl)-2,2'-bipyridine ( <b>2</b> ) .....	182
8.3.2	4,4'-bis(chloromethyl)-2,2'-bipyridine ( <b>3</b> ).....	183
8.3.3	4,4'-bis(triphenylphosphonium-methyl)-2,2'-bipyridyl chloride ( <b>4</b> ) .....	184
8.3.4	4,4'-bis[4-(diphenylamino)styryl]-2,2'-bipyridine ( <b>6</b> ) .....	184
8.3.5	Synthesis of 4,4'-bis[N-(phenyl)-N'-(styryl)-N,N'-bis(3-methyl phenyl)-1,1'- biphenyl-4,4'-diamino]-2,2'-bipyridine ( <b>11</b> ).....	186
8.3.6	4,4'-dicarboxy-2,2'-bipyridine ( <b>12</b> ).....	189
8.3.7	Bis(4,4'-dicarboxy-2,2'-bipyridyl) Ru(II)dichloride ( <b>13</b> ).....	190
8.3.8	Synthesis of bifunctional dyes <b>14</b> and <b>15</b> .....	191
8.3.9	4,4'-bis[poly(4-bromostyryl)methyl]-2,2'-bipyridine ( <b>16</b> ) .....	193
8.3.10	4,4'-bis[poly(4-vinyltriphenylamino)methyl]-2,2'-bipyridine ( <b>17</b> ) .....	194
8.3.11	Bis[bipyridyl]-[4,4'-bis[poly(4-vinyltriphenylamino)methyl]-2,2'-bipyridyl]-Ru(II) trifluorosulfonate ( <b>18</b> ).....	196
8.3.12	Synthesis of poly(4-bromostyrene) macroinitiator ( <b>19</b> ) .....	198
8.3.13	<i>Tert.</i> -butyldimethylsiloxyethylmethacrylate ( <b>20</b> ).....	199
8.3.14	Poly(4-bromostyrene)-b-poly(HEMA-TBDMS) ( <b>21</b> ) .....	200
8.3.15	Poly(4-vinyltriphenylamine)-b-polyHEMA-TBDMS ( <b>22</b> ) .....	202
8.3.16	Poly(4-vinyltriphenylamine)-b-polyHEMA ( <b>23</b> ) .....	203
8.3.17	2,5-dimethyl-4-(4-nitrophenylazo)phenol ( <b>24</b> ) .....	204
8.3.18	1-[(2,5-dimethyl-4-(4-nitrophenylazo) phenoxy] ethyl-butyrate ( <b>25</b> ) .....	205
8.3.19	1-[(2,5-dimethyl-4-(4-nitrophenylazo) phenoxy]butyric acid ( <b>26</b> ).....	207
8.3.20	1-[(2,5-dimethyl-4-(4-nitrophenylazo) phenoxy] butyric acid chloride ( <b>27</b> ).....	208
8.3.21	Poly(4-vinyltriphenylamine)-b-poly-(HEMA-DNPP) ( <b>28</b> ) .....	208

# 1 Introduction

*In this chapter an overview of developments and breakthroughs in the field of semiconducting materials and their application in electro-optics are given. Different concepts of photovoltaic devices will be introduced with particular focus on dye-sensitized nanocrystalline(nc) TiO<sub>2</sub> hybrid solar cells and the materials employed in these cells. Challenges and problems in optimization of dye-sensitized nc-TiO<sub>2</sub> solar cells concerning the interface of Ru(II) dyes and the organic semiconductor are reported emphasizing the need of design and development of novel materials. Thus, a new synthetic strategy for the preparation of bifunctional materials suitable for interface modification in dye-sensitized nc-TiO<sub>2</sub> solar cells is presented. As modern methods of polymer synthesis atom transfer radical polymerization (ATRP) will be introduced giving the chance to realize the first fully functionalized AB-diblock copolymer suitable for photorefractive holography. A short outline of this application will also be given here.*

## 1.1 Organic materials in electro-optical applications

In the past organic materials and polymers had been regarded as insulators in electronic industry. The breakthrough for organic semiconductors began with the discovery of doping of poly(acetylene) in 1977 which led to an increase in conductivity of poly(acetylene) by eleven orders of magnitude (Nobel prize in chemistry, 2000)<sup>1, 2</sup>. Since then design and synthesis of new semiconducting materials were pushed forward emphasizing on their conductivity and electro-optical properties. The fast progress in material science was leading to the development of different types of functional materials for the application in a variety of electro-optical devices: In 1987 a novel electroluminescent device was constructed in Kodak laboratories using organic materials as emitting elements which was the breakthrough for the era of high-performance organic-light emitting diodes (OLEDs)<sup>3, 4, 5</sup> which still has not reached its climax. Another approach in the field of electro-optics was the development of semiconducting organic materials, e. g. based on thiophene derivatives, with high-field effect charge mobilities in thin films for the application in organic field-effect transistors (OFETs)<sup>6, 7, 8</sup>.

---

<sup>1</sup> C. K. Chiang, C. R. Fischer, Y. W. Park, A. J. Heeger, H. Shirakawa, E. J. Louis, S. C. Gau, A. G. McDiarmid *Phys. Rev. Lett.* **1977**, 39, 1098.

<sup>2</sup> H. Shirakawa, E. J. Louis, A. G. McDiarmid, C. K. Chiang, A. J. Heeger *J. Chem. Soc. Chem. Commun.* **1977**, 578.

<sup>3</sup> C. W. Tang, S. A. VanSlyke *Appl. Phys. Lett.* **1987**, 51, 913.

<sup>4</sup> J. H. Burroughes, D. D. C. Bradley, A. R. Brown, R. N. Marks, K. Mackay, R. H. Friend, P. L. Burns, A. B. Holmes *Nature* **1990**, 347.

<sup>5</sup> N. C. Greenham, S. C. Moratti, D. D. C. Bradley, R. H. Friend, A. B. Holmes *Nature* **1993**, 365, 628.

<sup>6</sup> C. J. Drury, C.M. J. Mutsaers, C. M. Hart, M. Matters, D. M. de Leeuw *Appl. Phys. Lett.* **1998**, 73, 108.

<sup>7</sup> (a) F. Garnier, G. Horowitz, X. Peng, D. Fichou *Solid State Comm.* **1989**, 72, 4; (b) F. Garnier, R. Hajlaoui, M. El Kassmi *Appl. Phys. Lett.* **1998**, 73, 1721.

<sup>8</sup> (a) H. Sirringhaus, N. Tessler, R. H. Friend *Science* **1998**, 280, 1741; (b) X. C. Li, H. Sirringhaus, F. Garnier, A. B. Homes, S. C. Moratti, N. Feeder, W. Clagg, S. J. Teat, R. H. Friend *J. Am. Chem. Soc.* **1998**, 120, 2206.

<sup>9</sup>. Research is also proceeding with the ambition to replace magnetic data storage with alternative optical processes. This resulted in the synthesis of materials for photorefractive holography<sup>10, 11</sup> – a technique, which might satisfy the urgent need of high data density and high data transfer rates. Another concept in the field of electro-optical devices involves organic and inorganic/organic hybrid solar cells providing a low-cost alternative to the well established Silicon solar cells.

This thesis is based on the synthesis of tailor-made bifunctional materials for application in dye-sensitized *nc*-TiO<sub>2</sub> solar cells as well as on the development of a new type of fully functionalized block copolymers suitable for photorefractive applications. The novel bifunctional materials should combine hole-transport and dye function within one molecule and therefore special synthetic approaches had to be found for their preparation. Although the present work does not focus on device technologies, a brief introduction into different types of materials and devices is given in the following sections underlining the complexity involved in the design and development of organic materials for electro-optical applications.

## 1.2 Organic solar cells

There is a variety of models for the realization of organic solar cells based on different concepts which can be divided into a) organic solar cells and b) inorganic/organic hybrid solar cells. The materials for the application in these photovoltaic devices generally require high photo-chemical stability and excellent absorption in the visible spectrum.

For this reason, strongly absorbing materials belonging to the classes of phthalocyanines and perylenes are investigated.

---

<sup>9</sup> (a) Z. Bao, A. J. Lovinger, J. Brown *J. Am. Chem. Soc.* **1998**, 120, 207; (b) Z. Bao, A. Dodabalapur, A. J. Lovinger *Appl. Phys. Lett.* **1996**, 69, 4108; (c) Z. Bao, A. J. Lovinger *Chem. Mater.* **1999**, 11, 2607.

<sup>10</sup> U. Hofmann; S. Schlöter, A. Schreiber, K. Hochtetter, G. Bauml, S. J. Zilker, D. Haarer, M. Thelakkat, H.-W. Schmidt, K. Ewert, C.-D. Eisenbach *Proc. SPIE-Int. Soc. Opt. Eng.* **1998**, 3417, 124.

<sup>11</sup> S. J. Zilker *ChemPhysChem* **2000**, 1, 72.

But great interest exists also for research and development of conjugated polymers for the application in photovoltaics<sup>12</sup>. Moreover, within the setup of an organic solar cell an internal field must be created enabling the release of electrons and holes from electronic levels to diffuse to the electrodes with the recombination rate being as low as possible. The internal field can be generated either by constructing an interface between organic semiconductor and metal electrode (Schottky-type cell)<sup>13</sup> or building up a p/n heterojunction (p/n type cell). A p/n heterojunction is defined as the interface between an electron donor (p-type material, hole conductor) and an electron acceptor (n-type material, electron conductor) and can be generated by different ways (see next section). The different types of organic solar cells are generally classified as p/n heterojunction thin layer solar cells and systems applying a dye-sensitized semiconducting metal oxide, e. g. TiO<sub>2</sub>, SnO<sub>2</sub>. In the next sections the different concepts and materials used for building up organic photovoltaic devices and solar cells will be described in detail.

### 1.2.1 P/n-heterojunction thin-layer photovoltaic devices

#### *Multi-layer vapour deposited solar cells*

In 1986 the breakthrough in the field of p/n type organic solar cells occurred with the preparation of a two-layer solar cell based on phthalocyanine and perylenebisimide by Tang and co-workers (*Tang cell*)<sup>14</sup>. A glass plate coated with indium-tin oxide (ITO) served as transparent substrate on which subsequently thin films of hole transporting and electron transporting material were applied in high vacuum vapour deposition processes. A 30 nm layer of Cu-phthalocyanine (CuPc) served as p-type material and hence as hole conductor whereas a perylene bisimidazole derivative (50 nm) acted as electron transporting component. Ag-electrodes were vapour deposited on top completing the device.

---

<sup>12</sup> G. Horowitz *Adv. Mater.* **1990**, 2, 287.

<sup>13</sup> D. Wöhrle, D. Meissner *Adv. Mater.* **1991**, 3, 129.

<sup>14</sup> C. W. Tang *Appl. Phys. Lett.* **1986**, 48, 183.

On illumination both photo-active layers exhibit excitation of electrons and thus the generation of electron-hole pairs (excitons) which can diffuse within the bulk of the films. But only at the interface between CuPc and perylene the charge separation takes place. Holes are preferentially transported in the CuPc layer whereas electrons diffuse into the perylene bisimidazole phase. The efficiency of this exciton dissociation process can be attributed to the internal field and is dependent on the field strength. The Tang cell is characterized by power conversion efficiency of 0.95 %. Improvement of the original *Tang cell* with CuPc as hole transport material was achieved by doping phthalocyanine with fullerene C<sub>60</sub>. This was realized via depositing a mixture of ZnPc and C<sub>60</sub> between the actual layers of ZnPc and perylene bisimide. All layers had been prepared by vapour deposition processes controlling the desired geometry by using appropriate masks. With the described setup it was possible to increase power conversion efficiency of this type of solar cell to 1.05 %<sup>15</sup>.

#### *Polymer / fullerene solar cells*

Another approach of thin-layer photovoltaic devices was applying C<sub>60</sub> in combination with hole transport polymers and this was investigated intensively using a sandwich structure with a blend of p-type and n-type materials embedded between electrodes consisting of ITO and aluminium. Successful realization of this concept was carried out using a layer structure with the poly(p-phenylenevinylene) derivative poly[2-methoxy-5-(2'-ethylhexoxy)-p-phenylene]vinylene (MEH-PPV) as electron donor and C<sub>60</sub> as electron acceptor – materials which provide satisfying results in solar cells due to compatible HOMO (highest occupied molecular orbital) and LUMO (lowest unoccupied molecular orbital) levels:

Holes can be transferred easily from HOMO of MEH-PPV to the ITO electrode and electrons from LUMO of C<sub>60</sub> to the aluminium electrode<sup>16</sup>.

---

<sup>15</sup> J. Rostalski, D. Meissner *Sol. En. Mat. & Solar Cells* **2000**, 61, 87.

<sup>16</sup> C. J. Brabec, N. S. Sariciftci, J. C. Hummelen *Adv. Funct. Mat.* **2001**, 1, 15

The interface for the generation and separation of charges is limited to the surface area of the layers offering the possibility of device improvement via increasing the internal interface. This was achieved by applying a phase separated blend-system as photo-active unit consisting of substituted PPV and the soluble C<sub>60</sub> derivative [6,6]-phenyl-C<sub>61</sub>-butyric acid methyl ester (PCBM)<sup>17</sup>. With this concept in the whole volume of the photoactive material charge separation is possible and recently power conversion efficiencies of 2.5 – 3 % were reported for mixtures of substituted PPVs and PCBM solution-processed from chlorobenzene<sup>18, 19</sup>. A further improvement upto 4 % was achieved using better light absorbing hole conductors such as poly(3-hexylthiophene) instead of PPVs<sup>20</sup>.

#### *Polymer / polymer heterojunction solar cells*

Another strategy for converting sun light into electricity is the use of phase separated polymer blends of hole transporting (donor) and electron transporting (acceptor) polymers. A large internal interface can be generated by controlling the morphology of the phase separation with the structure of the polymers. Moreover the light sensitivity of the system can be regulated by choosing polymers with adequate  $\pi \rightarrow \pi^*$  energy gaps which also enables the application for broad illumination wavelengths. First results in efficient charge generation and transfer were obtained using a phase separated blend system of MEH-PPV (p-type, donor) and a dimethoxy-cyano PPV-derivative poly[dimethoxy-cyano(phenylene)vinylene] (CN-PPV, n-type, acceptor)<sup>21</sup>. The structures of the two compounds are shown in Figure 1-1.

---

<sup>17</sup> G. Yu, A. J. Heeger *J. Appl. Phys.* **1995**, 78, 4510.

<sup>18</sup> S. E. Shasheen, C. J. Brabec, N. S. Sariciftci, F. Padinger, T. Fromherz, J. C. Hummelen *Appl. Phys. Lett.* **2001**, 78, 841.

<sup>19</sup> C. J. Brabec, N. S. Sariciftci, J. C. Hummelen *Adv. Funct. Mat.* **2001**, 11, 15.

<sup>20</sup> C. J. Brabec *Sol. En. Mat. & Solar Cells* **2004**, 83, 273.

<sup>21</sup> J. J. M. Halls, C. A. Walsh, N. C. Greenham, E. A. Marseglia, R. H. Friend, S. C. Moratti, A. B. Homes *Nature* **1995**, 376, 498.

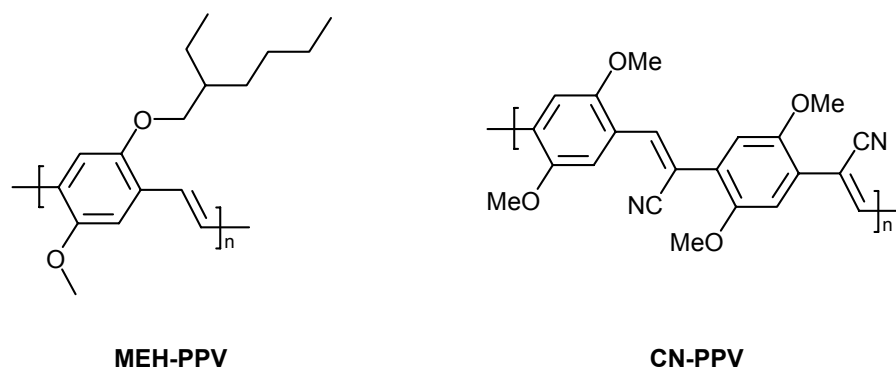


**Figure 1-1:** Chemical structures of poly[2-methoxy-5-(2'-ethyl)-hexyloxy-p-phenylene vinylene] (MEH-PPV) and poly[dimethoxy-cyano(p-phenylene)vinylene] (CN-PPV).

The solar cells were prepared via solution-casting of polymer thin films (150 nm – 200 nm) from xylene onto a glass substrate partly covered with ITO. Calcium or aluminium was vapour deposited as counter electrode. An increase in overall efficiency seemed to be possible by better control of the morphology and thus suppressing recombination processes.

In the group of Friend, a two-layer concept was developed consisting of conjugated, polymeric hole and electron conductors which were coated by a special lamination technique<sup>22</sup>. As photo-active materials a CN-PPV derivative (electron conductor) and poly[3-(4-octylphenyl)thiophene] (POPT, see Figure 1-2) were spin-coated onto two ITO covered glass substrates from different solution compositions. One substrate was coated with a solution consisting of CN-PPV and 5 wt% POPT, the second substrate with a solution of POPT and 5 wt% CN-PPV. The two substrates were arranged one on top of the other and set under pressure which resulted in a p/n heterojunction device. Aluminium or calcium served as electrode materials which were deposited onto the substrates before coating the photo-active layers.

<sup>22</sup> R. H. Friend, M. Granstroem, K. Petrisch, A. C. Arias, A. Lux, M. R. Andersson *Nature* **1998**, 395, 257.

With this setup power conversion efficiency of 1.9 % was achieved at irradiation with solar spectrum A.M. 1.5 (see chapter 1.2.4)<sup>22</sup>.

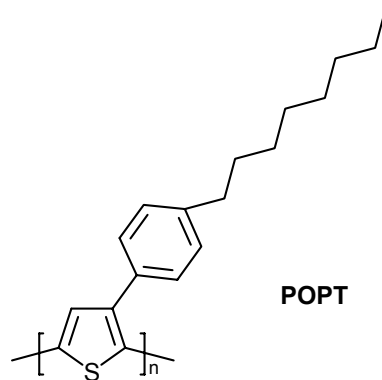


**Figure 1-2:** Chemical structure of poly[3-(4-octylphenyl)thiophene] (POPT).

The main problems in this concept still are charge separation and charge transport to the electrodes. The light has to be absorbed directly at the donor-acceptor interface and at the same time the contact of the materials with the matching electrodes has to be guaranteed which turned out to be the limiting factor of this device structure. The reproducibility of the lamination technique also was not guaranteed for large area devices.

#### *Polymer / semiconductor solar cells*

Another concept in the development of solar cells are hybrid systems involving both conjugated polymers and inorganic semiconductor nanoparticles.

The first system of this kind was reported by Alivisatos et al. and employed MEH-PPV as conjugated polymer and CdSe and CdS as inorganic nanoparticles<sup>23</sup>. With this approach it is possible to combine the easy processability of polymeric materials with the favourable absorption profile of inorganic materials and the charge transport properties of the inorganic particles can be optimized by tuning their size.

---

<sup>23</sup> N. C. Greenham, X. Peng, A. P. Alivisatos *Phys. Rev. B* **1996**, 54, 17628.

For optimized hybrid devices applying poly(3-hexylthiophene) as conjugated low band gap polymer and CdSe nanoparticles a power conversion efficiency of 1.7 % could be obtained<sup>24</sup>.

### 1.2.2 Dye-sensitized *nc*-TiO<sub>2</sub> solar cells

A totally different strategy for conversion of sun light are solar cells applying a mesoporous nanocrystalline(*nc*) TiO<sub>2</sub> layer sensitized with a dye. In this concept the light absorption takes place in dye molecules chemisorbed onto the TiO<sub>2</sub> surface. Under irradiation, exciton generation occurs in the dye transferring an electron to an excited state and leaving a positive counter-charge (hole) in the ground state level. The electron is transferred to the conduction band of the electron transport material which is *nc*-TiO<sub>2</sub> and finally to the ITO electrode. The hole left behind in the HOMO of the dye has to be filled by contact with an electron donating species, a hole transport material respectively. Suitable hole conductors in dye-sensitized *nc*-TiO<sub>2</sub> solar cells are either liquid electrolyte systems using I<sub>2</sub>/I<sub>3</sub><sup>-</sup> or solid state organic materials like triphenylamine derivatives, resulting in either electrolyte or solid-state solar cells respectively.

#### *Dye-sensitized nc-TiO<sub>2</sub> solar cells with electrolyte*

In the dye-sensitized *nc*-TiO<sub>2</sub> cell introduced by Graetzel in the 80s the hole transport and dye regeneration was guaranteed using an I<sub>2</sub>/I<sub>3</sub><sup>-</sup> redox-electrolyte which was reproduced by several other research groups<sup>25, 26, 27, 28</sup>. The *Graetzel cell* prepared as follows:

On top of an ITO electrode the electron transport material (*nc*-TiO<sub>2</sub>) is coated from a colloidal solution followed by sintering at 500 °C.

---

<sup>24</sup> W. U. Huynh, J. J. Dittmer, A. P. Alivisatos *Science* **2002**, 295, 2425.

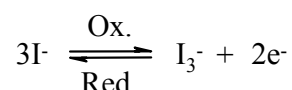
<sup>25</sup> B. O'Reagan, M. Graetzel *Nature*, **1991**, 353, 737.

<sup>26</sup> R. Knödler, J. Sopka, F. Harbach, H. W. Gruenling *Sol. En. Mat. & Solar Cells* **1993**, 30, 277.

<sup>27</sup> A. Hagfeldt, B. Didriksson, T. Plamqvist, H. Lindstroem, S.-E. Lindquist, *Sol. En. Mat. & Solar Cells* **1994**, 31, 481.

<sup>28</sup> H. Lindstroem, H. Rensmo, S. Soedergren, A. Solbrand, S.-E. Lindquist *J. Phys. Chem.* **1996**, 100, 3084.

It is possible to control and optimize the surface of the TiO<sub>2</sub> by the particle size and the thickness of this layer (5 – 20 μm). The pore size in the nanocrystalline layer had to be sufficient for the diffusion of the liquid redox-electrolyte. The tri-nuclear complex<sup>29</sup> [Ru(bipyridyl)<sub>2</sub>(cyano)<sub>2</sub>]-Ru[bpy(COO)<sub>2</sub>]<sub>2</sub><sup>2-</sup> was chemisorbed onto the TiO<sub>2</sub> surface producing a monomolecular dye layer. The dye coated layer was embedded into the electrolyte solution containing the I<sub>2</sub>/I<sub>3</sub><sup>-</sup> redox-couple and the cell is completed by another ITO glass substrate placed on top coated with platinum. Under irradiation the following processes are taking place: Light is absorbed by the dye molecules resulting in the generation of an electron – hole pair (exciton). Within the life time of the excited state, the electron can be injected into the conduction band of the TiO<sub>2</sub> which is an instantaneous process. However, the electron injection is competing with recombination processes limiting the performance of the device. For satisfying power conversion efficiency the rate of electron injection has to be 100-fold higher than the recombination rate. The oxidized dye molecule has to accept an electron and be reduced to its initial state to be again available for absorption. For regeneration of the dye molecules the redox-electrolyte is taking care via oxidizing the I<sup>-</sup> species in an electrochemical process to I<sub>3</sub><sup>-</sup> and thus providing electrons for dye regeneration:



Then electrons have to diffuse through TiO<sub>2</sub> to the ITO electrode. The consumption of iodide I<sup>-</sup> at dye / electrolyte interface has to be compensated by continuous reduction of tri-iodide happening at the platinized counter-electrode. For this purpose a facile diffusion of respective ions to the corresponding interfaces has to take place which depends on the viscosity of the medium as diffusion constant of these ions in the medium.

In this way the solar cell is regenerating itself which is the basic requirement for permanent conversion of sun light.

---

<sup>29</sup> R. Amadelli, R. Argazzi, C. A. Bigozzi, F. Scandola *J. Am. Chem. Soc.* **1990**, 112, 7099.

At irradiation the maximum voltage of the cell is limited by the difference of potential between Fermi-level of  $\text{TiO}_2$  and the electrochemical potential of the  $\text{I}^-/\text{I}_3^-$  redox-couple of the electrolyte.

The greatest benefit of the *Graetzel cell* are the low production costs and minor requirements in purity of the materials. A power conversion efficiency of 10 % which is already achieved appears to be very promising for the commercialization of these devices. At present dye-sensitized  $\text{TiO}_2$  solar cells employing liquid electrolyte for charge transport as developed by Graetzel and co-workers still are one of the most efficient organic solar cells<sup>25, 30, 31, 32</sup>. However, the liquid electrolyte applied in such cells creates both short-term and long-term sealing problems. This has activated the search for alternative hole transporting systems like gelled, molten salt electrolytes, polymer electrolytes etc., but still using the inorganic  $\text{I}_3^-/\text{I}^-$  as hole transport medium<sup>33, 34, 35, 36</sup>.

In the next chapter the replacement of the electrolyte by solid-state hole transport materials will be introduced and all solar cells prepared in this research work are based on this strategy.

---

<sup>30</sup> K. Tennakone, G. R. R. A. Kumara, I. R. M. Kottegoda, V. P. S. Perera *Chem. Commun.* **1999**, 16, 15.

<sup>31</sup> A. Hinsch, J. M. Kroon, R. Kern, I. Uhlendorf, J. Holzbock, A. Meyer, J. Ferber *Prog. Photovoltaics: Research and Applications* **2001**, 9, 425.

<sup>32</sup> Z. S. Wang, C. H. Huang, Y. Y. Huang, Y. J. Hou, P. H. Xie, B. W. Zhang, H. M. Cheng *Chem. Mater.* **2001**, 13, 678.

<sup>33</sup> F. Cao, G. Oskam, P. C. Searson *J. Phys. Chem.* **1995**, 99, 17071.

<sup>34</sup> H. Matsumoto, T. Matsuda, T. Tsuda, R. Hagiwara, Y. Ito, Y. Miyazaki *Chem. Lett.* **2001**, 1, 26.

<sup>35</sup> N. Papageorgiou, Y. Athanassov, M. Armand, P. Bonhôte, H. Pettersson, A. Azam, M. Graetzel *J. Electrochem. Soc.* **1996**, 143, 3099.

<sup>36</sup> W. Kubo, K. Murakoshi, T. Kitamura, Y. Wada, K. Hanabusa, H. Shirai, S. Yanagida *Chem. Lett.* **1998**, 1241.

*Solid-state dye-sensitized nc-TiO<sub>2</sub> solar cells*

In the past decade the use of low molecular weight organic hole transport materials in dye-sensitized TiO<sub>2</sub> solar cells and conjugated p-type polymers instead of liquid electrolyte as charge transport medium was reported<sup>37, 38, 39</sup>. It has been shown that an efficient class of hole transport compounds with triarylamine units which are well-known for high hole transport mobility could be used instead of the liquid electrolyte to obtain a solid-state dye-sensitized solar cell<sup>37</sup>. This type of solid-state cell was further optimized in the group of Graetzel by using a low molecular weight spiro-compound as hole conductor and additional additives like lithium salt and dopants to increase the conductivity of such a cell to obtain higher power conversion efficiencies<sup>40, 41</sup>. One of the major differences between the electrolyte and p-type semiconductor solar cell lies in the nature of charge transport: ionic transport controlled by diffusion prevails in the former, whereas electronic transport influenced by conductivity and charge transport mobility plays the deciding role in the latter. The basic physical processes like light absorption in the chemisorbed dye layer followed by electron transfer to the TiO<sub>2</sub> layer remains the same in both types of cells. Figure 1-3 shows schematically the different layers in a solid-state dye-sensitized nc-TiO<sub>2</sub> solar cell with organic hole conductor.

In this cell, a layer of fluorinated tin-oxide (FTO) serves as conducting electrode which is transparent to let light through to reach dye-TiO<sub>2</sub> junctions. The next layer, a compact TiO<sub>2</sub> film acts as a blocking layer to prevent holes formed in the dye or hole-transport layer (HTL) from contacting the lower FTO layer, which would otherwise short-circuit the cell.

---

<sup>37</sup> J. Hagen, W. Schaffrath, P. Otschik, R. Fink, A. Bacher, H.-W. Schmidt, D. Haarer *Synth. Met.* **1997**, 89, 215.

<sup>38</sup> C. Jaeger, R. Bilke, M. Heim, D. Haarer, H. Karickal, M. Thelakkat *Synth. Met.* **2001**, 121, 1543.

<sup>39</sup> M. Thelakkat, J. Hagen, D. Haarer, H.-W. Schmidt *Synth. Met.* **1999**, 102, 1125.

<sup>40</sup> U. Bach, D. Lupo, P. Compte, J. E. Moser, F. Weissoertel, J. Salbeck, H. Spreiter, M. Graetzel *Nature* **1998**, 395, 583.

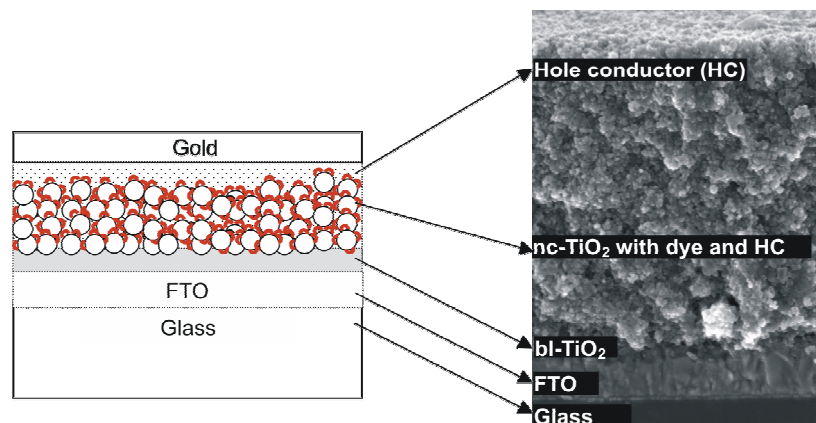


**Figure 1-3:** Device structure and SEM picture of a complete solid-state dye-sensitized  $\text{TiO}_2$  solar cell showing the different layers and interfaces.

The porous structure of nanocrystalline ( $nc$ -)  $\text{TiO}_2$  enormously enlarges the surface area up to a factor of about 1000 as compared to a flat surface, which enables most of the light to be absorbed, or reflected and then absorbed, resulting in maximum light harvesting. The  $nc$ - $\text{TiO}_2$  itself is a network, making it possible for the transferred electrons to reach the anode through this perforated network. A molecular layer of Ru-dye is self-assembled on the  $nc$ - $\text{TiO}_2$  surface by chemisorption, forming a hetero-junction which functions as an interface for the separation of charges from excitons formed. Typically for this device dye N 719 is applied as sensitizing agent; its structure is shown in Figure 1-4.

The charge separation occurs at the interface, the electron is transferred to  $\text{TiO}_2$  and the hole in the dye is compensated by electron transfer from the hole transport layer (HTL)<sup>37, 41</sup>. The HTL is prepared from a mixture of *spiro*-OMeTAD (Figure 1-5), radical cation salt of *spiro*-OMeTAD (ox-*spiro*), and a Li-salt (N-lithiotrifluoromethanesulfonimide,  $(\text{CF}_3\text{SO}_2)_2\text{NLi}$ ). The ox-*spiro* acts as a dopant to enrich charge concentration and the Li-salt is added to increase the conductivity as well as to manipulate the surface potential of  $\text{TiO}_2$  to enhance electron injection.

<sup>41</sup> J. Krüger, R. Plass, L. Cevey, M. Piccirelli, M. Grätzel *Appl. Phys. Lett.* **2001**, 79, 2085.

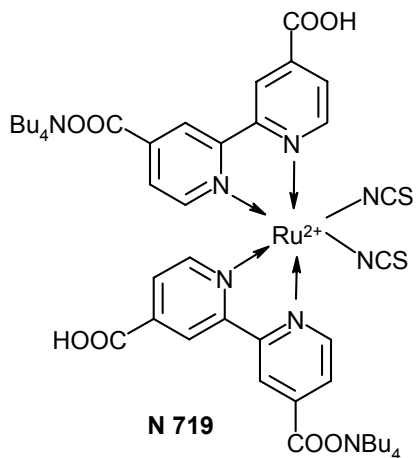


**Figure 1-4:** Chemical structure of dye N 719, *cis-bis(isothiocyanato)-bis-(2,2'-bipyridyl-4,4'-dicarboxylato)-ruthenium(II)-bis(tetrabutylammonium)*.

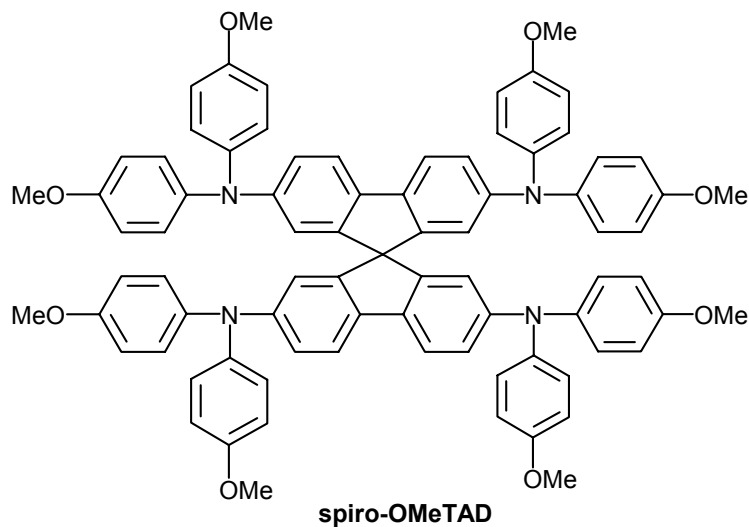


**Figure 1-5:** Chemical structure of 2,2',7,7'-tetrakis(*N,N*-di-*p*-methoxy-phenylamine)-9,9'-spirobifluorene (*spiro-OMeTAD*).

In this work typically four cells on one substrate were prepared to check the reproducibility. The effective area of each cell is 8 mm x 2 mm (0.16 mm<sup>2</sup>). Solar cell samples were prepared by successive deposition of the component layers.

First a compact layer of blocking  $\text{TiO}_2$  was deposited via spray-pyrolysis from 0.2 M solution of Titan(IV)-bis(acetylacetonato)-diisopropylate in ethanol followed by preparation of the *nc*- $\text{TiO}_2$  film by screen-printing of colloidal  $\text{TiO}_2$ -paste. After sintering the *nc*- $\text{TiO}_2$ , the substrate was first treated with  $\text{TiCl}_4$  solution and sintered again to guarantee better interconnection between the particles. Subsequently the substrates were immersed into the Ru-dye solution for dye-coating. Physisorbed dye molecules were then washed away and a HTL layer was spin-coated as a next step. Finally, with a mask, a thin Au-film was vapour-deposited. The details of cell preparation are given in literature<sup>42</sup>. A picture of a dye-sensitized *nc*- $\text{TiO}_2$  solid-state solar cell is shown in Figure 1-6.

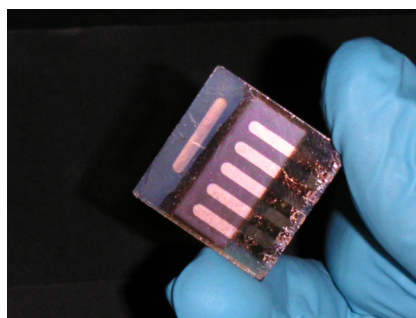


**Figure 1-6:** Dye-sensitized solid-state *nc*- $\text{TiO}_2$  solar cell as prepared in this work.

Both in electrolyte and solid-state dye-sensitized  $\text{TiO}_2$  solar cells, bulk properties of the charge transport materials have been intensively studied and reported<sup>43, 44</sup>. But little work, in contrast, has been done on surface and interface properties in such cells. A hole, moving from the dye to the gold cathode, crosses at least two interfaces, the dye-HTL and the HTL-Au interface. Taking into consideration that the HTL has a thickness of several hundred nanometers, these two interfaces must play very important roles in the whole charge transport process.

---

<sup>42</sup> B. Peng, G. Jungmann, C. Jaeger, D. Haarer, H.-W. Schmidt, M. Thelakkat *Coord. Chem. Rev.* **2004**, 248, 1479.

<sup>43</sup> H. Baessler, *Phys. Status Solidi B* **1993**, 175, 15.

<sup>44</sup> J. Salbeck, N. Yu, J. Bauer, F. Weissoertel, H. Bestgen *Synth. Met.* **1997**, 91, 209.

Moreover, in a photovoltaic cell of the dye-sensitized nano-crystalline TiO<sub>2</sub> type, the charge separation step takes place in a very fast way<sup>45, 46</sup>: Upon absorbing a photon by the ruthenium dye molecule, an electron in the ruthenium d-orbital is excited to the ligand's (bipyridine)  $\pi^*$ -orbital, via metal-to-ligand charge transfer (MLCT) process, in which ruthenium is oxidized from +2 to +3. Owing to an energetically favourable situation, the electron in the  $\pi^*$ -orbital is subsequently injected into the conduction band of TiO<sub>2</sub>. The charge separation step is in this way completed, the electron being in the TiO<sub>2</sub> conduction band and the hole in the dye. The electron injection from dye to TiO<sub>2</sub> takes place within a time scale of femto-second, actually one of the fastest chemical processes ever investigated<sup>47</sup>. The backward electron transfer, i.e., from TiO<sub>2</sub> to dye, happens at least three orders of magnitude slower than the forward injection.

### 1.2.3 Ru(II) dyes in dye-sensitized TiO<sub>2</sub> solar cells

Much work has to be done in improving light absorption and charge transport. In the first report of a dye-sensitized TiO<sub>2</sub> solar cell Graetzel described the application of a trinuclear Ru(II) complex as sensitizing dye (Figure 1-7). Then the new high performance dyes N 3<sup>48, 49</sup> and its bis(tetrabutylammonium) salt N 719 (Figure 1-8) had been investigated and are still considered as standard dyes for future developments in this regard. However the main drawback of this sensitizers is the lack of absorption in the red region of the visible spectrum and thus panchromatic dyes mainly based on terpyridyl or poly(pyridyl) Ru(II) complexes have been designed and synthesized.

---

<sup>45</sup> A. Hagfeldt, M. Graetzel *Chem. Rev.* **1995**, 95, 49.

<sup>46</sup> D. Cahen, G. Hodes, M. Graetzel, J. F. Guillemoles, H. Riess *J. Phys. Chem. B* **2000**, 104, 2053.

<sup>47</sup> A. Hagfeldt, M. Graetzel *Acc. Chem. Res.* **2000**, 33, 269.

<sup>48</sup> P. Liska, N. Vlachopoulos, M. K. Nazeeruddin, P. Comte, M. Graetzel *J. Am. Chem. Soc.* **1988**, 110, 3686.

<sup>49</sup> M. K. Nazeeruddin, A. Kay, I. Rodicio, R. Humphrey-Baker, E. Mueller, P. Liska, N. Vlachopoulos, M. Graetzel *J. Am. Chem. Soc.* **1993**, 115, 6382.

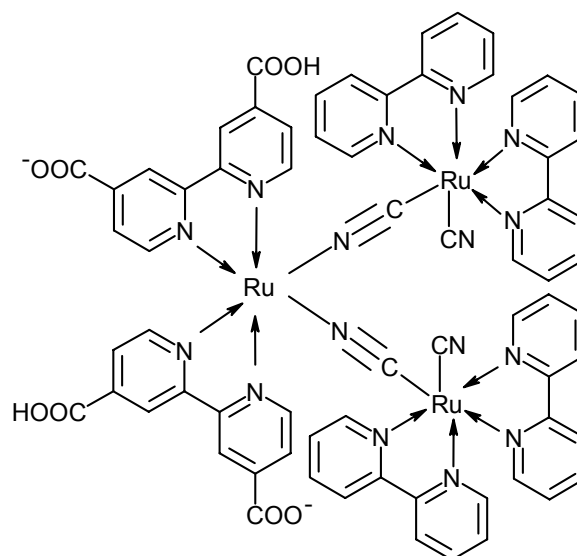


**Figure 1-7:** Chemical structure of the trinuclear Ru(II) complex  $[Ru(bpy)_2(CN)_2]_2Ru(bpy(COO^-))(COOH))_2$  used in the group of Graetzel for the first dye-sensitized *nc*-TiO<sub>2</sub> solar cell with electrolyte (bpy = bipyridine).

They show satisfactory absorption into the red and infrared regions (“black dye”, wavelength > 700 nm)<sup>50, 51</sup> (Figure 1-8). Although an impressive 10 % solar-to-electricity conversion efficiency could be obtained using a panchromatic dye, the achievement of long-term stability at operating temperatures has remained a major challenge for a long time. Recently a new class of sensitizers for light absorption in TiO<sub>2</sub> solar cells was introduced in which Ru(II) complexes carry amphiphilic ligands<sup>52, 53, 54</sup> (see Figure 1-8).

<sup>50</sup> M. K. Nazeeruddin, P. Péchy, T. Renouard, S. M. Zakeeruddin, R. Humphry-Baker, P. Comte, P. Liska, L. Cevey, E. Costa, V. Shklover, L. Spiccia, G. B. Deacon, C. A. Bignozzi, M. Graetzel *J. Am. Chem. Soc.* **2001**, 123, 1613.

<sup>51</sup> A. Islam, H. Sugihara, H. Arakawa *J. Photochem. Photobio. A: Chemistry* **2003**, 158, 131.

<sup>52</sup> J. J. Lagref, M. K. Nazeeruddin, M. Graetzel *Synth. Met.* **2003**, 138, 333.

<sup>53</sup> P. Wang, S. M. Zakeeruddin, R. Humphry-Baker, J. E. Moser, M. Graetzel *Adv. Mater.* **2003**, 15, 2101.

<sup>54</sup> M. K. Nazeeruddin, S. M. Zakeeruddin, J. J. Lagref, P. Liska, P. Comte, C. Barolo, G. Viscardi, K. Schenk, M. Graetzel *Coord. Chem. Rev.* **2004**, 248, 1317.

These amphiphilic complexes exhibiting alkyl chains attached to the bipyridine ligand have already been tested in electrolyte cells resulting in IPCE (incident photon to current efficiencies) values up to 80 %<sup>52</sup> and an overall power conversion efficiency of 7.3 % (on irradiation with 1 sun, AM 1.5) for optimized devices using a Ru(II) dye with nonyl-substituents on one of the bipyridine ligands (dye Z 907, see Figure 1-8)<sup>53</sup>.

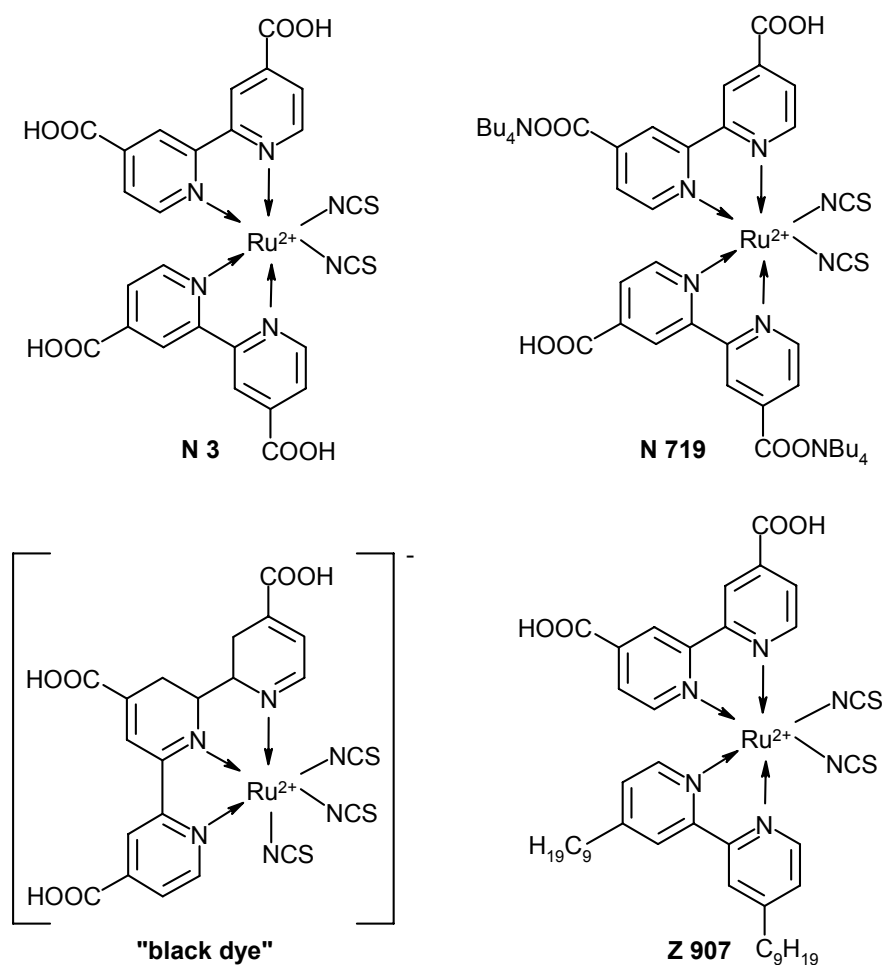


**Figure 1-8:** Chemical structures of different sensitizers for light absorption in dye-sensitized *nc*-TiO<sub>2</sub> solar cells: N 3, N 719, (tricarboxyterpyridine)-Ru(II)(NCS)<sub>3</sub> "black dye" and Z 907.

This work focusses on the interface between the dye monolayer and the solid-state hole transport layer (HTL). At this interface, a hole is transferred from the dye to the HTL, offering an electron to the ruthenium d-orbital and reducing the dye molecule to its former +2 state. The idea is to separate the two processes of absorption and charge separation locally as observed in nature in the process of photosynthesis to increase the efficiency of the system by preventing recombination. Simultaneously the wetting problem of a relatively non-polar hole conductor on to the polar surface of dye-coated TiO<sub>2</sub> should be addressed. First approaches towards this concept had been very recently investigated by Durrant, Graetzel and co-workers using a heteroleptic Ru(II) dye N 845 provided with a electron-donor group on one of the ligands<sup>55</sup>. The structure of this new dye N 845 is presented in Figure 1-9.

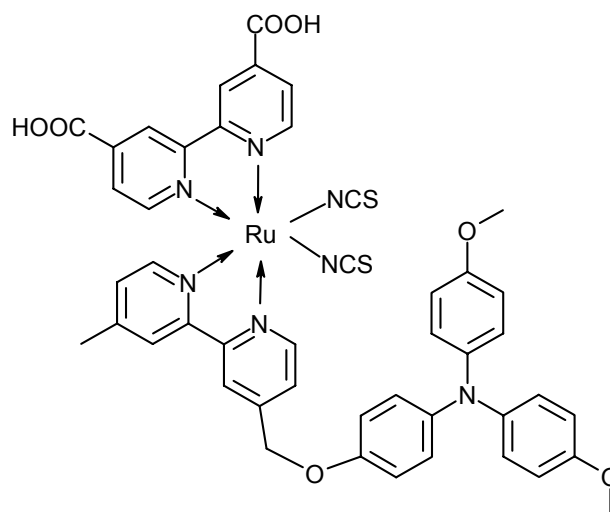


**Figure 1-9:** Chemical structure of heteroleptic Ru(II) dye N 845<sup>55</sup>.

The novel bifunctional dye exhibit a remarkably long-lived charge separated state ascertained by monitoring the charge-recombination dynamics using transient absorption spectroscopy.

<sup>55</sup> N. Hirata, J.-J. Lagref, E. J. Palomares, J. R. Durrant, M. K. Nazeeruddin, M. Graetzel, D. Di Censo *Chem. Eur. J.* **2004**, 10, 595.

The retardation of recombination dynamics presumably is a consequence of an increase in physical separation of the dye cation centre from the  $\text{TiO}_2$  surface which was confirmed by semiempirical calculations locating the HOMO of the modified dye-molecule on the electron-donor group. Thus it could be shown that by appropriate design of the sensitizing dye it is possible to achieve molecular control and hindrance of the back transfer of electrons from  $\text{TiO}_2$  to the positive dye centre which otherwise would result in recombination of charges.

### 1.2.4 Solar cell characterization

Most important for solar cell characterization and comparison are standard conditions especially concerning the irradiation of the solar cells. For this reason, the power of incident light of 1 sun ( $100 \text{ mWcm}^{-2}$ ) was set as standard. To determine characteristic photovoltaic parameters of a solar cell the device is irradiated with a lamp providing AM(air mass) 1.5 solar spectral conditions (see Figure 1-10).

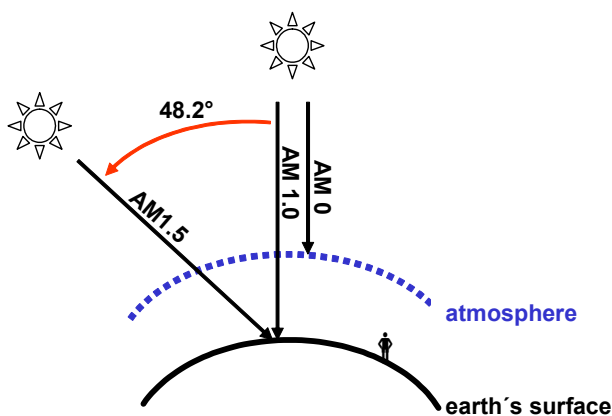


**Figure 1-10:** Schematic definition of the solar spectrum standards AM(air mass) 0, AM 1 and AM 1.5. Irradiation under zenith angle zero down to the atmosphere or the earth's surface is defined as AM(air mass) 0 and AM 1, respectively. Irradiation under zenith angle of  $48.2^\circ$  is specified as AM 1.5 solar spectral conditions.

AM 1.5 is defined as sun light irradiation under a zenith angle of  $48.2^\circ$  as it is schematically outlined in Figure 1-10 together with the corresponding parameters AM 0 and AM 1. The specification of a solar spectrum standard is important for the reasonable comparison of photovoltaic parameters of different solar cells prepared in various research groups.

For characterization of a solar cell a countervoltage is applied to the device and the dependence of current on voltage is measured. The measurements are subsequently carried out with and without irradiation yielding photo current and dark current, respectively. From the resulting current-voltage characteristic curve the following photovoltaic parameters can be determined: Open circuit voltage ( $U_{OC}$ , voltage at zero current), short circuit current ( $I_{SC}$ , current at zero voltage), fill factor (FF) and power conversion efficiency ( $\eta$ ) as depicted in Figure 1-11.

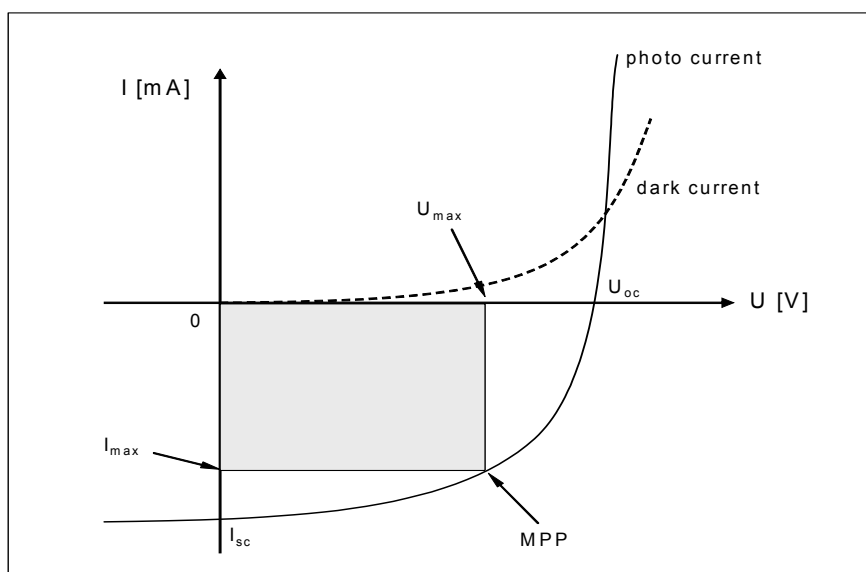


**Figure 1-11:** Current-voltage characteristic of a solar cell with photovoltaic parameters.

The maximum power point (MPP) is defined as the coordinate where the product of current and voltage in the curve is maximum:

$$MPP = U_{\max} \cdot I_{\max} \quad (\text{Equation 1})$$

Using this information the fill factor (FF) of the solar cell can be calculated as follows:

$$FF = \frac{U_{\max} \cdot I_{\max}}{U_{OC} \cdot I_{SC}} = \frac{MPP}{U_{OC} \cdot I_{SC}} \quad (\text{Equation 2})$$

The fill factor (FF) is a measure of quality of the current-voltage characteristic of a solar cell. Graphically it corresponds to the ratio of the rectangular area limited by  $U_{\max}$  and  $I_{\max}$  as plotted in Figure 1-11 and the rectangular area limited by  $U_{OC}$  and  $I_{SC}$ . In order to determine power conversion efficiency ( $\eta$ ) which is the most important parameter of a solar cell MPP has to be divided with the power of light  $P_{\text{light}}$  delivered by the lamp or solar simulator used in the experiment setup (Equation 3):

$$\eta = \frac{MPP}{P_{\text{light}}} = \frac{U_{\max} \cdot I_{\max}}{P_{\text{light}}} = \frac{FF \cdot U_{OC} \cdot I_{SC}}{P_{\text{light}}} \quad (\text{Equation 3})$$

All solar cells described in this work haven been characterized under AM 1.5 solar spectral conditions at a power of light of  $77 \text{ mWcm}^{-2}$ . Details of the experimental setup are given in the experimental part.

### 1.3 Organic photorefractive systems

Photorefractivity is an intriguing phenomenon which was initially perceived as a disturbance in measurement: Laser illumination generates large internal electric fields which, in turn, modify the optical properties of the material.

It was first discovered in 1966 by researchers at Bell Laboratories in inorganic crystals<sup>56</sup>. Potential applications such as digital holographic data storage, image processing, medical imaging etc. led to intensive research effort. However, nearly 25 years after the discovery of inorganic photorefractive crystals photorefractivity was observed for the first time in 1990 in organic materials. Shortly after that in 1991 polymeric materials have been reported exhibiting photorefractive properties.

Photorefractive polymers feature high optical quality, are relatively cheap and enable the introduction of dopants. Consequently charge generation and transport properties as well as the optical characteristics can be tuned individually by incorporating the required functionalities for photorefractivity<sup>57</sup>. In general polymeric photorefractive materials need to have photoconducting properties for charge transport. Moreover photosensitizers are necessary in order to obtain light absorption and charge generation. The NLO-chromophores, which are one of the main components in a photorefractive composite, react to the internal space-charge field to generate a refractive index modulation. The principle of the photorefractive effect is presented in Figure 1-12:

- a) A spatial light intensity modulation is created by the interference of two laser beams resulting in the bright and dark regions in the sample.
- b) In the bright areas electron-hole pairs are generated by photoexcitation of the sensitizer / photoconductor charge transfer state. Since most of the organic photoconductors exhibit hole conducting properties, the electrons are immobile. For this reason the holes are able to drift in the external electric field until they are trapped.
- c) Due to the drift of the holes a space-charge distribution  $\rho_{SC}$  is caused, in which the holes are located predominantly in the dark areas, the maxima of  $\rho_{SC}(x)$  respectively. The electrons remain immobile in the bright areas.

---

<sup>56</sup> A. Ashkin, G. D. Boyd, J. M. Dziedzic, R. G. Smith, A. A. Ballman, J. J. Levinstein, K. Nassau *Appl. Phys. Lett.* **1966**, 9, 72.

<sup>57</sup> S. J. Zilker *ChemPhysChem* **2000**, 1, 72.

- d) The space-charge field  $E_{SC}(x)$  leads to orientation of NLO dye-molecule which lead to a local modulation of the refractive index  $\Delta n$ . There is a phase shift  $\phi$  between the light intensity grating and the resulting refractive index modulation  $\Delta n$ .

The nature of the index grating is a unique feature of the photorefractive effect and distinguishes it from other grating mechanisms such as photochromism or thermochromism<sup>58</sup>.

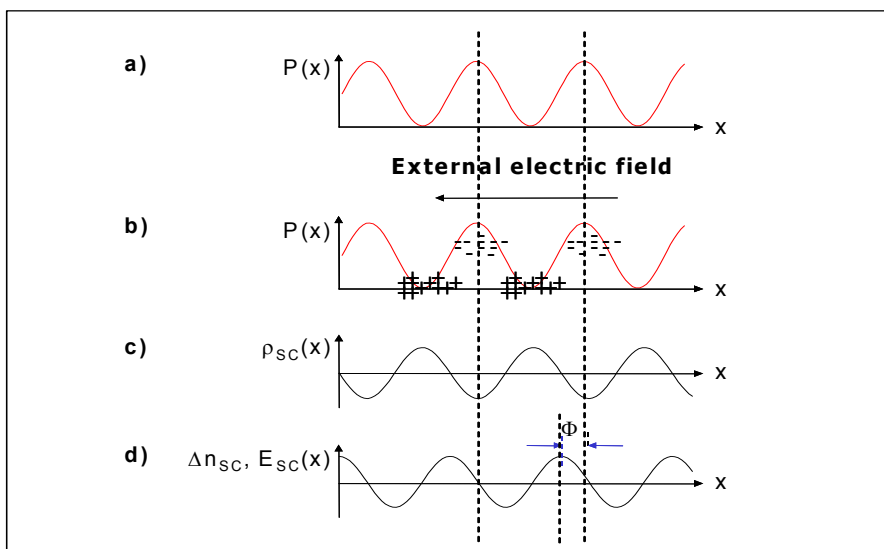


**Figure 1-12:** Principle of the photorefractive effect. A) Spatial light intensity modulation  $P(x)$  of two laser beams. B) Generation and drift of the charge carriers in the external electric field. C) Resulting space-charge distribution  $\rho_{SC}(x)$ . D) Space-charge field  $E_{SC}(x)$ , refractive index modulation  $\Delta n$  and phase shift of photorefractive hologram with respect to incident light ( $\phi$ ).

<sup>58</sup> M. Levitus, P. F. Aramendía *J. Phys. Chem. B* **1999**, 103, 1864.

Starting from inorganic crystals, a variety of different material concepts have been developed:

Low-molecular weight glasses, host-guest polymers, fully-functionalized polymers or liquid crystals – preferably materials exhibiting low glass transition temperatures ( $T_g$ ).

Low molecular weight glasses have been developed which form stable amorphous phases and generally exhibit appreciably high compositional stability combined with low viscosity for chromophore reorientation. The glass forming components mostly are bifunctional materials with both photoconductive and nonlinear optical properties<sup>59,60</sup>. The major drawbacks of this system however are immense amounts of plasticizers required for tuning glass transition towards room temperature so that the orientation of the chromophores is enhanced.

In the first studies of host-guest polymers a polymer was doped with a charge transport agent, a sensitizer and a NLO-chromophore to provide the necessary functionalities for photorefractivity<sup>61</sup>. Most recent systems use photoconducting polymers as hosts which are readily available. The problem is that most of the well known photoconducting polymers exhibit  $T_g$  above room temperature making the application of a plasticizing agent essential. Moreover host-guest polymer systems incline to a lack of compositional stability as the polar chromophores tend to crystallize in the apolar host material. What is needed are alternative concepts to improve material compatibility and overcome the use of additional compounds for lowering  $T_g$ . A synthetic approach to reach this goal is monolithic materials like fully functionalized polymers with photoconducting moieties and chromophores covalently attached to a polymer backbone; typical examples for this class of materials are shown in Figure 1-13. It has to be considered that so far with most systems consisting of fully functionalized polymers only poor refractive index modulations,  $\Delta n$  have been obtained.

---

<sup>59</sup> C. Hohle, U. Hofmann, S. Schlöter, M. Thelakkat, P. Strohriegel, D. Haarer, S. J. Zilker *J. Mater. Chem.* **1999**, 9, 2205.

<sup>60</sup> S. Schlöter, A. Schreiber, M. Grasruck, A. Leopold, M. Kol'chenko, J. Pan, C. Hohle, P. Strohriegel, S. J. Zilker, D. Haarer *Appl. Phys. B* **1999**, 68, 899.

<sup>61</sup> S. Ducharme, J. C. Scott, R. J. Twieg, W. E. Moerner *Phys. Rev. Lett.* **1991**, 66, 1846.

These polymers do not satisfy the need for high hole conductivity and thus have not yet fulfilled the high expectations connected with their development. Most recently the idea arose to prepare AB-diblock copolymers consisting of hole conductor and NLO-dye block<sup>62</sup>.

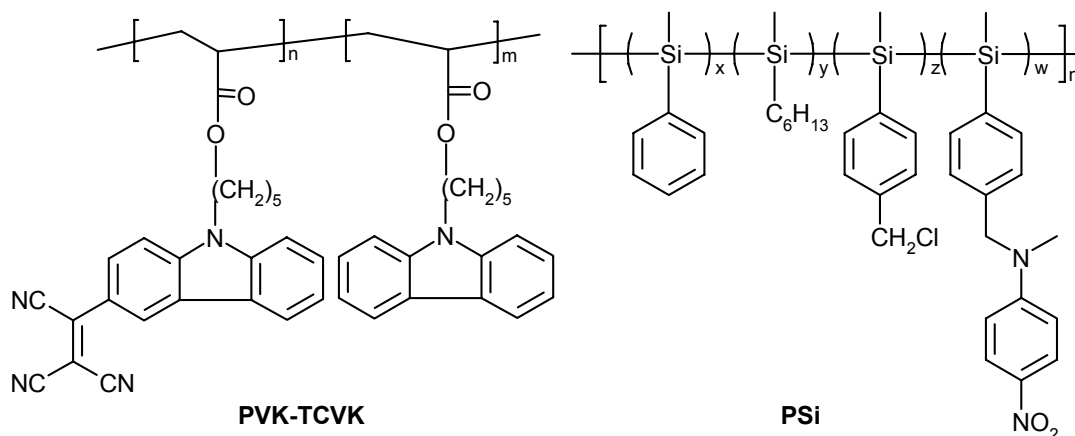


**Figure 1-13:** Fully functionalized photorefractive materials: Carbazole-tricyanovinyl-carbazole (PVK-TCVK)<sup>63</sup> with photoconducting and electro-optic side groups; polysilane PSi with photoconducting main chain and NLO-dye as side chains<sup>64</sup>.

This approach has the advantage of a fully functionalized system with nanometer phase separation which is thermodynamically stable. Here nano-domains of NLO-chromophores embedded in a hole transport matrix can be prepared. With this concept an increase in hole mobility was expected in combination with the possibility to tune  $T_g$  by variation of comonomers making plasticizing additives unnecessary. Among other things this work deals with the development of a modern synthetic strategy for the preparation of such block copolymers which exhibit the desired properties.

<sup>62</sup> M. Behl, R. Zentel *Macromol. Chem. Phys.* **2004**, 205, 1633.

<sup>63</sup> B. Kippelen, K. Tamura, N. Peyghambarian *Phys. Rev. B* **1993**, 48, 10710.

<sup>64</sup> E. Hendrickx, D. Van Steenwinckel, A. Persoons *Macromolecules* **1999**, 32, 2232.

The method of ATRP was chosen for the challenge of synthesizing a new class of bifunctional AB-diblock copolymers suitable for photorefractive applications.

Since ATRP turned out to be a very promising method for the synthesis of functional polymers a short introduction into this method will be given in the next sub-section.

## 1.4 Atom transfer radical polymerization (ATRP)

One of the main objectives in modern synthetic polymer chemistry is to prepare polymers with controlled molecular weight and well-defined architecture. Living polymerizations developed in the past forty years including cationic and anionic polymerization provide the opportunity to reach that goal<sup>65</sup>. In living polymerization neither chain transfer nor termination processes occur. One of the major drawbacks of these living polymerizations that prevents them from wider industrial application is the stringent conditions required for the polymerization reactions. In contrast, free radical polymerizations are still the most important processes in industry for preparation of high molecular weight polymers. But they lack control due to termination and chain transfer processes. Thus gaining control over radical polymerization has become one of the important topics in polymer chemistry. Free radical polymerization has been shown to be controlled under conditions in which a fast, dynamic equilibrium between an active and dormant species exist and only low concentration of the active species is present. This is the basis of controlled / living radical polymerization (CRP) which is quite similar to conventional free radical polymerization; however, the radical formation is reversible. Similar values for the equilibrium constants during initiation and propagation in CRP ensure that the initiator is consumed at the early stages of the polymerization, generating chains which slowly and continuously grow. The most important difference between conventional and controlled / living radical polymerization is the life-time of the average chain. In conventional systems the chain is born, grows and dies within a time scale of approximately 1s.

---

<sup>65</sup> O. Webster *Science* **1991**, 251, 887.

During this time it is not possible to perform any synthetic manipulation such as chain extension, end functionalization, variation of monomer feed, etc.. But in controlled / living polymerizations the principle of equilibrium between growing free radicals (active species) and various types of dormant species makes a control in molecular weights together with low polydispersities and active end groups feasible.

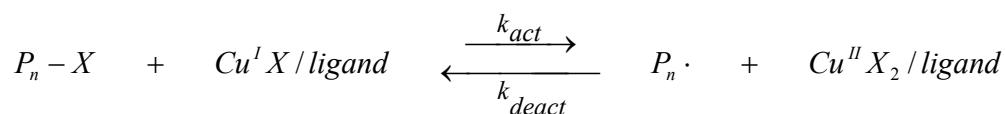
The different approaches towards control in radical polymerization can be classified depending on mechanism and chemistry of the equilibrium processes as well as on the structure of the dormant species. Currently three methods appear to be most efficient and can be successfully applied to a large number of monomers: Nitroxide-mediated polymerization (NMP), reversible addition-fragmentation chain transfer (RAFT) and atom transfer radical polymerization (ATRP).

Each technique has its special advantages from which particularly ATRP enables the synthesis of special block copolymers by utilizing a halogen exchange process.<sup>66</sup> The general mechanism of ATRP involves (Scheme 1-1) the abstraction of a halogen  $X$  from a dormant species  $P_n - X$  by a transition metal centre, mostly complexes of Cu(I) coordinated by various amine ligands, in a redox process. Upon halogen abstraction a radical  $P_n \cdot$  is formed which can undergo chain propagation by reacting with olefinic monomers as in conventional free radical polymerization. The halogen is accepted by the Cu(I) complex which is consequently oxidized to Cu(II). However, the radical  $P_n \cdot$  is also able to abstract the halogen back from the metal reproducing the dormant species and reducing Cu(II) to its initial state. These very fast processes with the rate constants for activation and deactivation  $k_{\text{act}}$  and  $k_{\text{deact}}$  establish an equilibrium favouring the dormant species  $P_n - X$  (see Scheme 1-1)<sup>67</sup>.

---

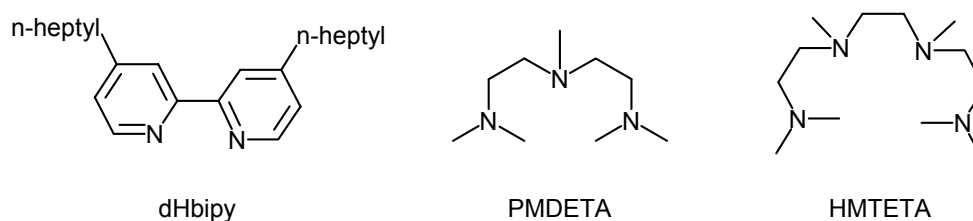
<sup>66</sup> K. Matyjaszewski *Macromol. Symp.* **2003**, 195, 25.

<sup>67</sup> J.-L. Wang, T. Grimaud, K. Matyjaszewski *Macromolecules* **1997**, 30, 6507.



**Scheme 1-1:** General principle of atom transfer radical polymerization (ATRP): Equilibrium between active ( $P_n \cdot$ ) and dormant ( $P_n - X$ ) species controlled by reversible abstraction of halogen  $X$  via a  $Cu$ /ligand complex.

Typical for ATRP is the application of  $Cu(I)$ -halides like  $CuBr$  and  $CuCl$  in combination with ligands like 4,4'-di(*n*-heptyl)-2,2'-bipyridine (dHbipy),  $N,N,N',N'',N'''$ -penta-methyldiethylenetriamine (PMDETA) or 1,1,4,7,10,10-hexamethyltriethylenetetramine (HMTETA) the structures of which are shown in Scheme 1-2. These catalytic systems are intensively studied as reported in literature<sup>68</sup>.



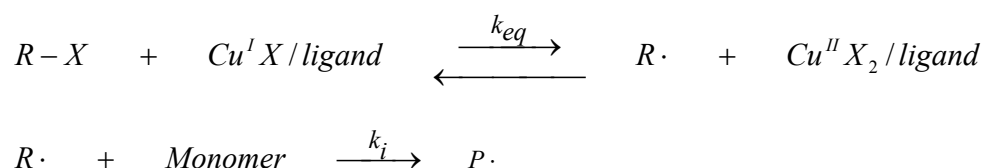
**Scheme 1-2:** Chemical structures of multidentate amine ligands commonly used for atom transfer radical polymerization (ATRP).

The ligands not only improve solubility of the  $Cu$ -halides in organic solvents and monomers but also influence the redox behaviour of the  $Cu(I) / Cu(II)$  systems. By choosing appropriate ligands homolytic cleavage of the carbon-halide bond of the dormant species is facilitated resulting in the formation of an active radical species for attaching monomer and propagation of the polymer chain. As initiators organic halides with active carbon-halide bonds are employed which may easily generate a radical species:

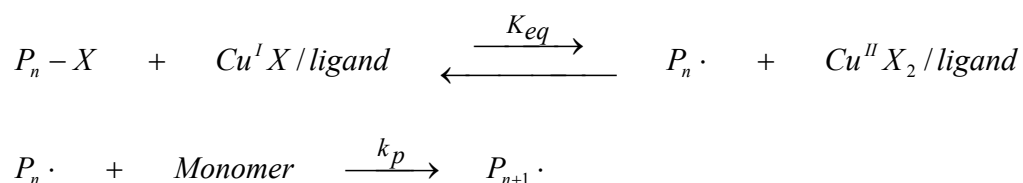
<sup>68</sup> J. Xia, K. Matyjaszewski *Macromolecules* **1997**, 30, 7697.

Compounds like carbon tetrachloride, 1-phenylethyl halide, p-toluenesulfonyl chloride or  $\alpha$ -halo esters (methyl- $\alpha$ -chloropropionate, MCP; ethyl- $\alpha$ -bromoisobutyrate, EBIB) meet these requirements as initiators<sup>69</sup>. The reaction mechanism of ATRP, which consists of the initial atom transfer equilibrium followed by addition of olefinic monomers during initiation, propagation as well as termination steps is shown in Scheme 1-3<sup>67</sup>.

*Initiation:*



*Propagation:*



*Termination:*



**Scheme 1-3:** Mechanism of ATRP including the three major reaction steps: Initiation by abstraction of a halogen from the initiator, propagation by reaction of the radical of the active species with a monomer and termination via recombination of radicals.

Assuming insignificant termination reactions, fast initiation and steady concentration of propagating radicals the following rate laws were derived: The constant of the

---

<sup>69</sup> M. Kamigaito, T. Ando, M. Sawamoto *Chem. Rev.* **2001**, 101, 3689.

equilibrium of the propagation step ( $K_{eq}$ ) is given by the ratio of the constants for the activation and deactivation process,  $k_{act}$  and  $k_{deact}$ , respectively (Equation 4). The square brackets symbolize the molar concentrations for the respective species.

$$K_{eq} = \frac{k_{act}}{k_{deact}} = \frac{[P_n \cdot][Cu^{II}X]}{[P-X][Cu^I]} \quad (\text{Equation 4})$$

Using this equation the rate of polymerization  $R_p$  can be determined by taking into account the rate constant for radical propagation  $k_p$  which results in the following equation. Equation 5 predicts the direct proportionality of rate of polymerization to initiator concentration:

$$R_p = k_p [P_n \cdot][M] = k_p K_{eq} [I]_0 \frac{[Cu^I]}{[Cu^{II}X]} [M] \quad (\text{Equation 5})$$

As is the case in all CRP processes, in ATRP also all chains begin to grow at essentially the same time and the concentration of free radicals (active species) is low resulting in markedly reduced termination by recombination of radicals. For this reason, the degree of polymerization (DP) can be predetermined (Equation 6) and the polydispersities may be quite low.

$$DP = \frac{[M]_0 - [M]_t}{[I]_0} \quad (\text{Equation 6})$$

$DP$  = degree of polymerization

$[M]_0$  = initial monomer concentration

$[M]_t$  = monomer concentration after reaction time  $t$

$[I]_0$  = concentration of initiator

In conclusion, the advantages of ATRP is control in molecular weight in combination with low polydispersities. The reactions via ATRP exhibit relatively low sensitivity to water, oxygen and the purity of the reactands is not as significant as for example in anionic polymerization. For ATRP there are no stringent conditions necessary and the method is applicable to a broad variety of monomers. Another outstanding feature of ATRP is that virtually all polymer chains contain an active halogen end group when the polymerization reaction is finished.

These polymers can then be extended by utilizing them as macroinitiators, i. e. initiating the polymerization of a second monomer and thus enabling the synthesis of block copolymers<sup>70, 71</sup>. With the method of ATRP it is possible to obtain copolymers with various architectures like graft copolymers<sup>72</sup> and rod-coil block copolymers<sup>73</sup>. This opens a field of great opportunities for polymer synthesis which still has not been fully investigated. In this work especially the capability of ATRP to produce diblock copolymers which carry an non-linear optic (NLO)-dye functionality in one block and hole transport functionality in the other will be investigated. Polymers exhibiting this bifunctionality can be applied in photorefractive systems to study the photorefractive properties in such a diblock copolymers system.

---

<sup>70</sup> C. Burguière, S. Pascual, C. Bui, J.-P. Vairon, B. Charleux, K. A. Davis, K. Matyjaszewski *Macromolecules* **2001**, 34, 4439.

<sup>71</sup> N. V. Tsarevsky, T. Sarbu, B. Göbel, K. Matyjaszewski *Macromolecules* **2002**, 35, 6142.

<sup>72</sup> H. Shinoda, P. J. Miller, K. Matyjaszewski *Macromolecules* **2001**, 34, 3186.

<sup>73</sup> P. K. Tzolakis, J. K. Kallitsis, A. Godt *Macromolecules* **2002**, 35, 5758.

## 2 Motivation and aim

### *Interface modification in solid-state dye-sensitized nc-TiO<sub>2</sub> solar cells*

In the state-of-the-art solid-state dye-sensitized nc-TiO<sub>2</sub> solar cell, charge recombination is still one of the most limiting factors for device performance. The question arises, if there is a possibility to overcome this problem by developing new material concepts using modern synthetic methods. Therefore, the challenges, questions and possible synthetic approaches to interfacial problems related with charge recombination in solid-state dye-sensitized TiO<sub>2</sub> solar cells will be discussed in this chapter. Despite active research in this field one of the crucial issues in solid-state dye-sensitized TiO<sub>2</sub> solar cells still is the undefined interface between dye and hole conductor (spiro-MeO-TAD) prepared via spin-coating. The differences in polarity between the ionic Ru(II) dye and the non-polar hole transporting spiro-compound leads to difficulties in wetting and in filling the mesoporous dye-coated TiO<sub>2</sub> layer with hole conductor. This leads to accumulation of holes in the dye and electrons in TiO<sub>2</sub> without much spatial separation. Moreover, the time scale of charge transfer for regeneration of the dye by donation of electrons from the hole conductor to the dye is much slower compared to the analogous process at the dye / TiO<sub>2</sub> interface. Consequently this leads to recombination of the electron in TiO<sub>2</sub> with the hole in the excited dye molecule which reduces device performance drastically as schematically presented in Figure 2-1.

Recently it has been observed that one of the key factors controlling the charge recombination dynamics in dye-sensitized nc-TiO<sub>2</sub> solar cells is the spatial separation of the dye cation HOMO from the TiO<sub>2</sub> surface<sup>74</sup>.

---

<sup>74</sup> J. N. Clifford, E. Palomares, M. K. Nazeerudin, M. Graetzel, J. Nelson, X. Li, N. Long, J. R. Durrant *J. Am. Chem. Soc.* **2004**, 126, 5225.

By increasing the distance between the positive centre of the dye radical cation (HOMO) and the  $\text{TiO}_2$  surface, recombination can be suppressed drastically. This was studied using Ru(II) dyes having different anions which influence the HOMO distribution<sup>74</sup>.

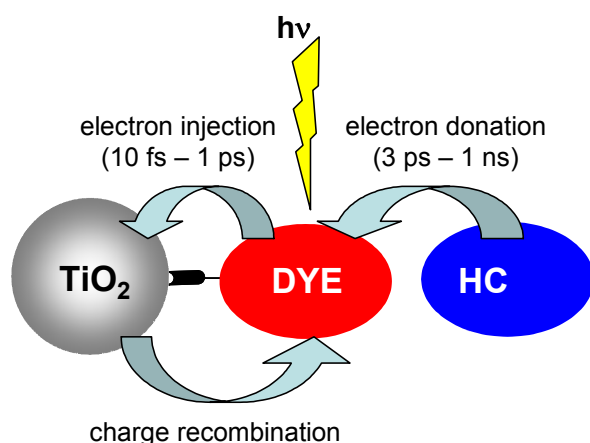


**Figure 2-1:** Schematic representation and time scales of charge transfer and recombination processes occurring at the  $\text{TiO}_2$  / dye and dye / hole conductor (HC) interfaces in a standard solid-state  $nc\text{-TiO}_2$  solar cell<sup>55</sup>.

Graetzel and co-workers also developed amphiphilic Ru(II) dyes which improved the polarity issue in electrolyte cells<sup>52</sup>. Therefore, the question arises how to exploit this fact for developing novel sensitizers for solid-state  $nc\text{-TiO}_2$  solar cells. Is it possible to increase this spatial separation by synthetic approaches? What would happen when hole conducting (donor) antenna groups would be covalently attached to a light absorbing Ru(II) complex? A possible effect might be the delocalization of the HOMO orbitals of the dye radical cation over the hole conducting antenna group and consequently an increased spatial separation of the HOMO of the dye cation to the  $\text{TiO}_2$  surface. In this way, the desired retardation of recombination processes can be realized as suggested in Figure 2-2. Furthermore, the donor antenna groups can help the wetting of the dye-coated  $\text{TiO}_2$  surface by the spiro hole conductor.

A right choice of donor groups can also allow the energy cascading from donor to dye, thus improving the light harvesting as well. Any delocalization of HOMO in the ligand also can lead to higher extinction coefficients for the dye. Structures which are thought to be suitable as bifunctional dyes and a synthetic strategy are presented in Figure 2-3.

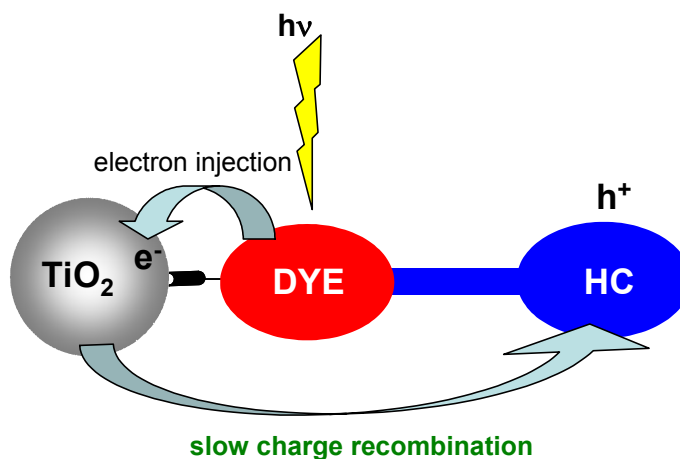


**Figure 2-2:** Schematic representation of electron injection into  $\text{TiO}_2$  and delocalization of the dye radical cation ( $h^+$ ) over a hole transport unit covalently attached to the Ru(II) dye resulting in retarded recombination processes.

The aim of this work is to develop an appropriate synthetic strategy with which the suggested bifunctional materials could be prepared. Then the charge recombination dynamics can be investigated by transient absorption spectroscopy and concretely the effect in a solar cell device could be tested.

The next question is, if it is possible to extend the concept of low molecular weight bifunctional dyes to polymers with a Ru(II) dye unit carrying polymeric donor chains, thus extending the donor groups extensively. This may help to move the HOMO in Ru(II) dye further away from the  $\text{TiO}_2$  surface resulting in much improved spatial separation.

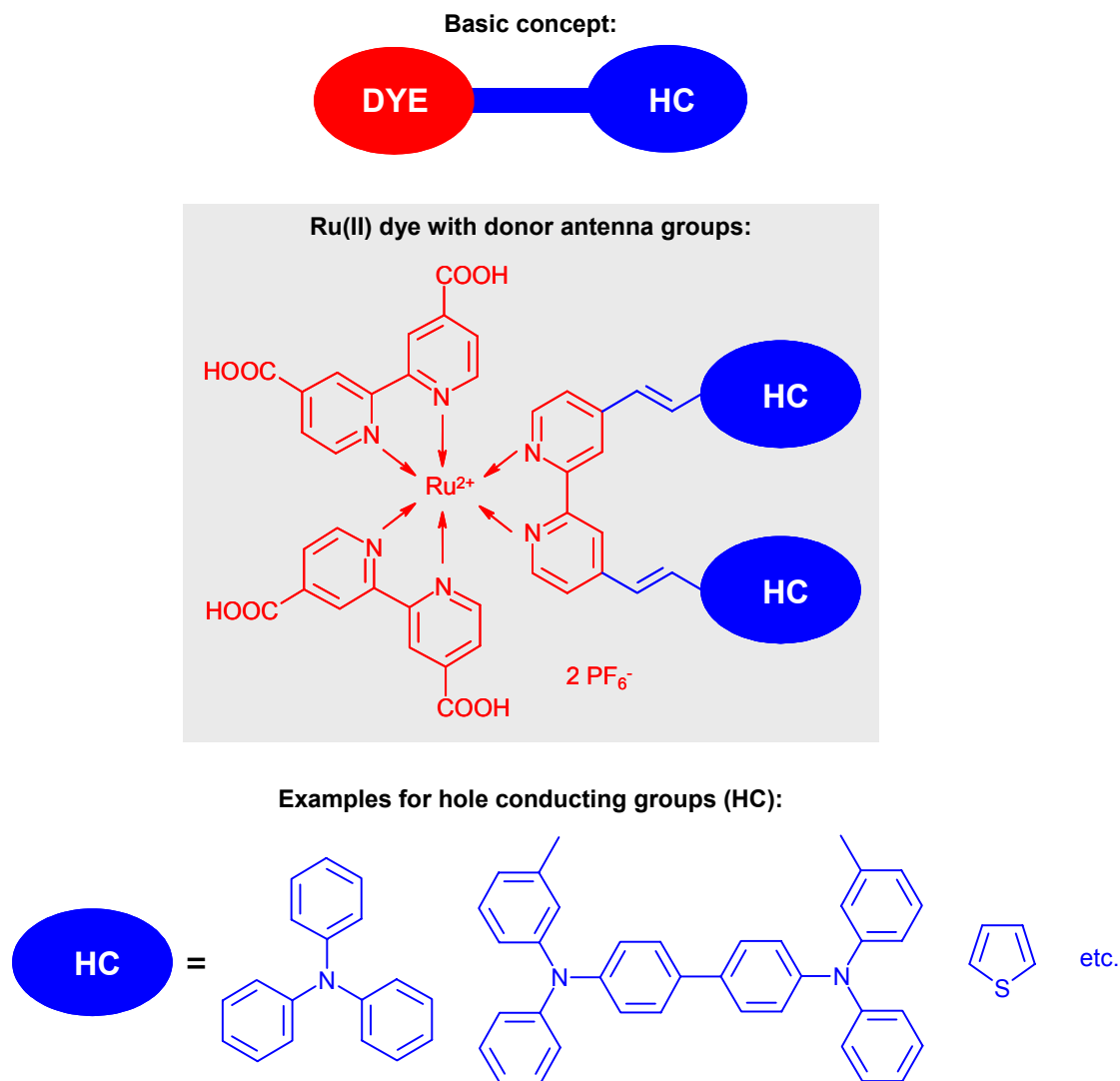


**Figure 2-3:** Suggested chemical structures of new bifunctional materials with delocalization of HOMO resulting in spatial separation of HOMO away from  $TiO_2$ /dye interface.

The question is then: What effect will such a hole transport polymer chain consisting of several repeating units have on the recombination dynamics? A conceivable chemical structure for this approach is given in Figure 2-4.

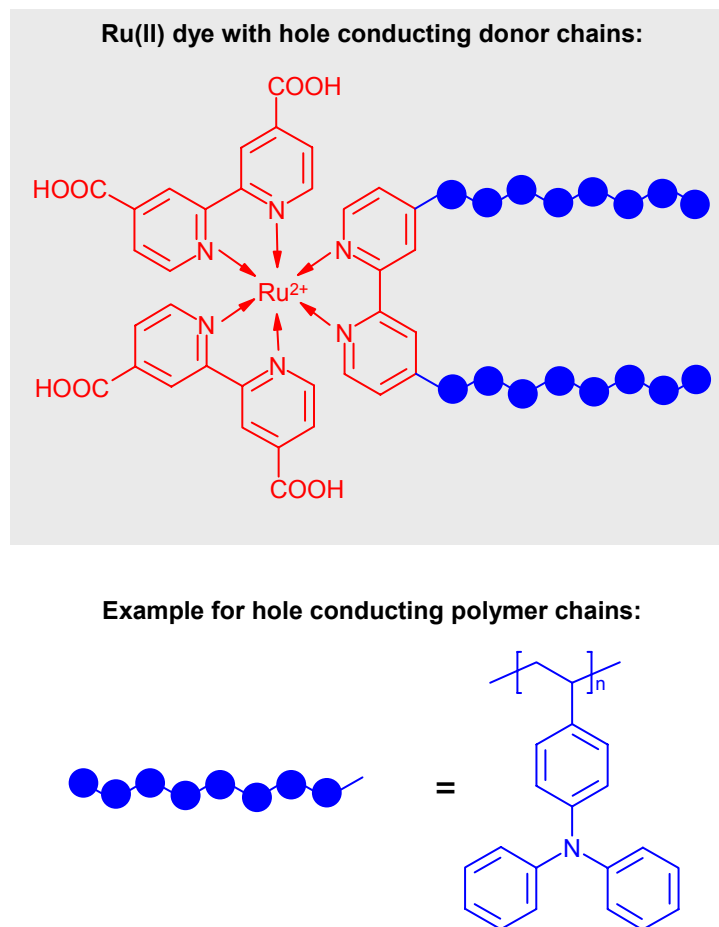


**Figure 2-4:** Chemical structure of a bifunctional polymer with hole transport chains covalently attached to a Ru(II) dye core.

For the synthesis of the planned polymers a controlled polymerization method has to be found in order to define molecular weight as well as chain length of the hole conductor and thus to enable the control of dye content within the macromolecules. Due to its low sensitivity against water, oxygen and impurities, atom transfer radical polymerization (ATRP) would be very promising for this purpose and therefore this technique will be applied for the synthesis of the suggested bifunctional polymers. After successful synthesis of polymers with different dye contents, the influence of these novel polymeric structures on recombination might be studied with transient absorption spectroscopy.

A comparison with the low-molecular weight dyes may give further insight into the issue of spatial separation and recombination. The motivation thus is to use ATRP, starting from a bipyridine initiator to build up polymeric hole conductor and then to complex the macroligand with Ru(II) bis(bipyridyl) precursors to get the desired dye.

### *Fully functionalized AB-diblock copolymers for photorefractive applications*

A variety of different approaches have been developed to obtain a well operating photorefractive system, but most of them have some drawbacks: Molecular glasses require huge amounts of additives to tune the glass transition temperature ( $T_g$ ), guest-host polymers systems suffer from poor material compatibility and high  $T_g$  and the fully functionalized random copolymers exhibit only low refractive index modulations<sup>57</sup>. There is still no system existing which might satisfy all criteria required for efficient photorefractive application such as light sensitization and charge separation followed by a fast reorientation of the NLO-dye in the space charge field to induce the refractive index modulation. Thus the aim of this work is to prepare fully functionalized AB-diblock copolymers with charge transport blocks as well as NLO-dye blocks. Such materials may form stable phase separated systems in nanometer range with NLO-dye domains embedded in a hole transport matrix (see Figure 2-5). With this concept the hole mobility can be improved which may increase the response time of the system and the possibility to tune  $T_g$  by variation of the comonomers is feasible.

In order to reach the goal of fully functionalized AB-diblock copolymers, an appropriate polymerization method has to be found. The knowledge gained in the method of ATRP in the first part of this work should be utilized here for the preparation of block copolymers via a controlled polymerization technique.

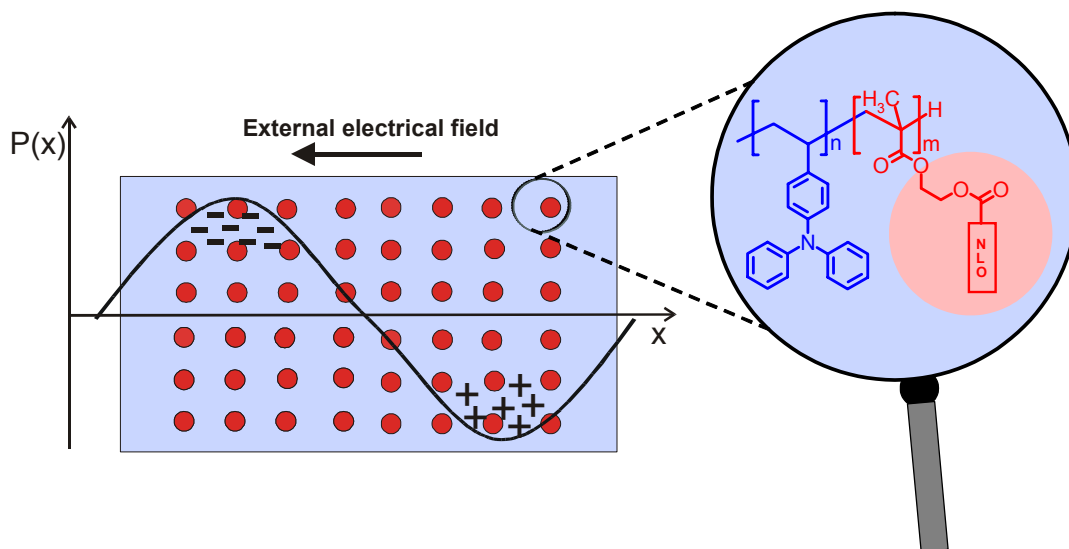


**Figure 2-5:** Schematical representation of nanoscale NLO-dye domains embedded in a hole transport matrix: The red spheres represent the dye moieties and the blue area displays the hole transport matrix. A photorefractive experiment is indicated as described in chapter 1.3 and in the magnifier a possible chemical structure of the desired material is suggested.

ATRP should be optimized for the preparation of an AB-diblock copolymer with functional pendant groups on the monomer units. Then the desired functionalities can be attached in polymeranalogous reactions. The advantage of this method clearly lies in the fact that various photoconductor units and different NLO-dyes can be introduced on the same AB-diblock precursor polymer. The challenges and limitations of the concept should be tested while going for a final AB-diblock copolymer structure as proposed in Figure 2-6.

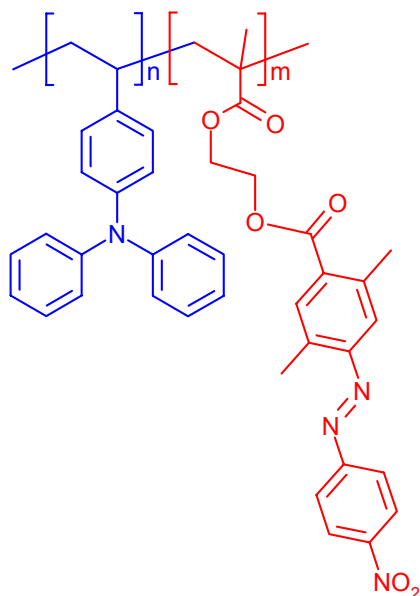


**Figure 2-6:** Chemical structure of fully functionalized AB-diblock copolymer carrying hole transport block and NLO-dye block.

Successful realization of this synthetic strategy would clear the way towards a totally new class of bifunctional materials which should be investigated in photorefractive measurements.

### 3 Low molecular weight Ru(II) dyes carrying TPA units

*In this chapter the synthesis and characterization of low molecular weight bifunctional molecules for interface modification in solid-state dye-sensitized TiO<sub>2</sub> solar cells are described. The intention of the synthesis was to obtain materials which carry hole transport moieties as antenna groups attached to a Ru(II) dye centre so that a facile transfer of holes away from the Ru(II) core to the hole transport unit takes place. These materials should be thermally stable in an appropriate range for the application in dye-sensitized solar cells and should be able to chemisorb onto a TiO<sub>2</sub> surface. Different triarylamine units chosen as hole transport moieties were connected to a 2,2'-bipyridine ligand with a conjugated vinylene spacer. A bis(bipyridine)Ru(II) precursor carrying carboxylic acid anchor groups was synthesized and subsequently tris(bipyridyl)-Ruthenium(II) complexes were prepared from this by reacting with the bipyridine hole transport ligand. The anchor groups serve for chemisorption on the TiO<sub>2</sub> surface in solar cells and the hole transport units should lead to spatial separation of the holes away from the TiO<sub>2</sub> surface. Transient photoinduced absorption (PIA) studies were carried out to determine the efficiency of the dyes in retarding back transfer of electrons from TiO<sub>2</sub>. As an example one of these new materials was tested in solar cells and the results are presented in this chapter.*

### 3.1 Synthetic strategy

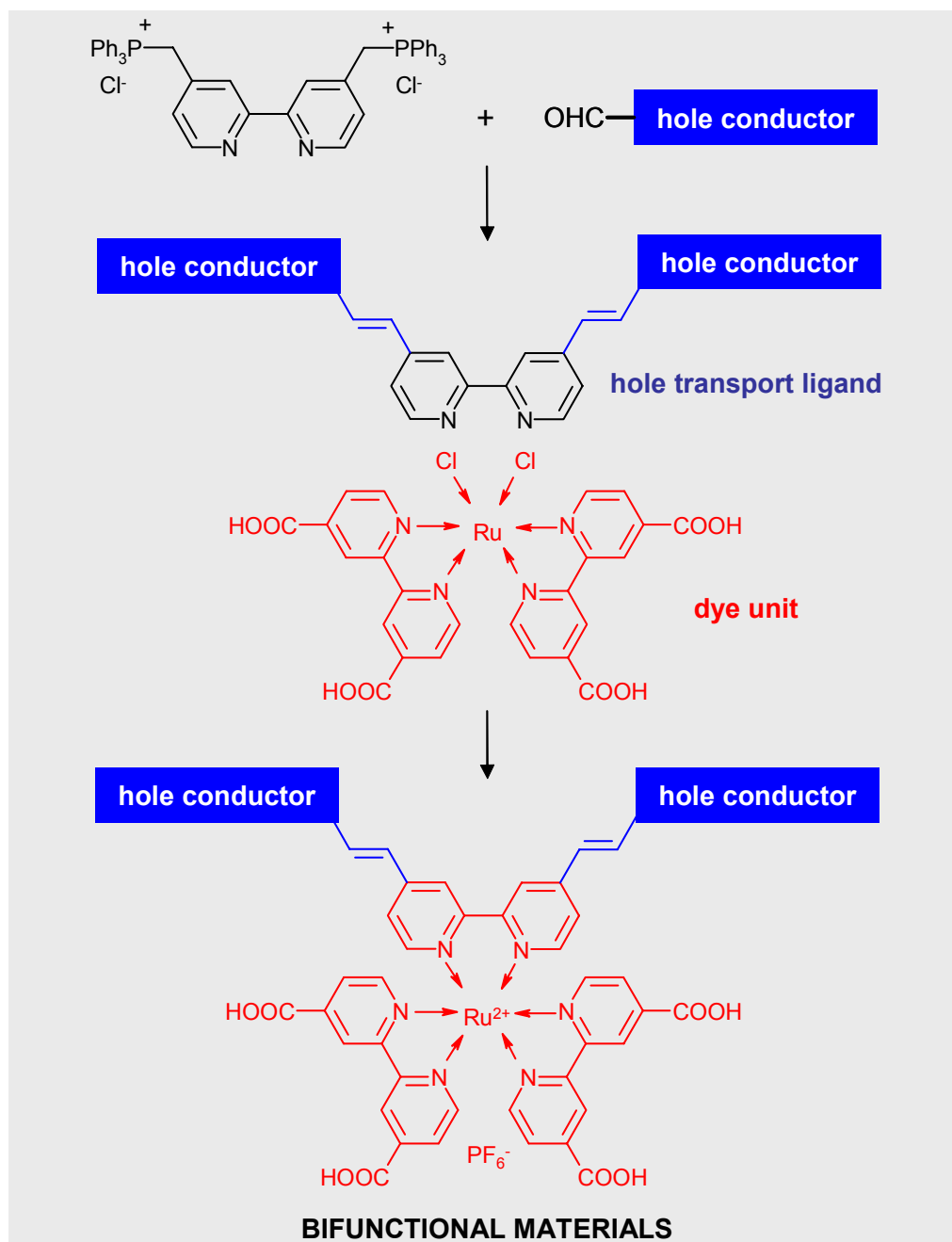


**Figure 3-1:** Schematic presentation of the synthetic strategy for preparation of new bifunctional materials carrying hole conductor (e. g. triphenylamine TPA) as well as light absorbing dye unit (Ru(II) core).

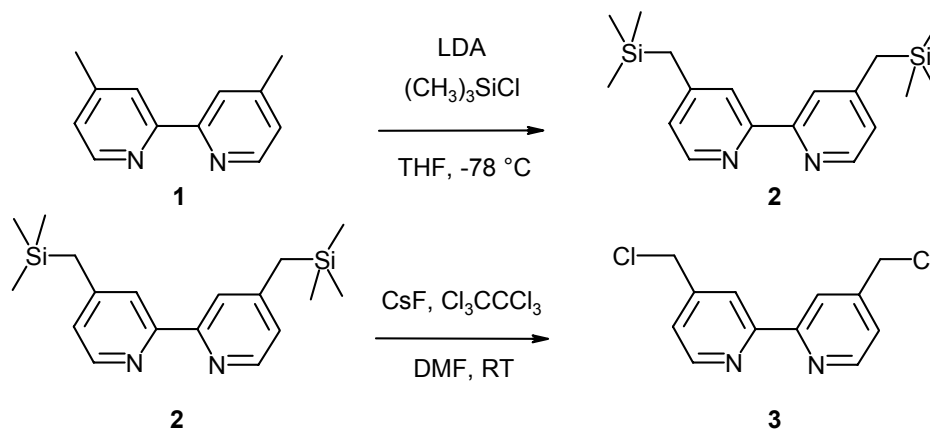
Low molecular weight Ru(II) dyes carrying triarylamine units were prepared by complexing bis[(4,4'-dicarboxy)-2,2'-bipyridyl]dichloro-Ru(II)hydrate with newly synthesized ligands (bpy-TPA) carrying different hole conductor units. The bpy-hole conductor ligands were obtained as follows: In three reaction steps the educt 4,4'-dimethyl-2,2'-bipyridine was converted to a phosphonium salt which made a coupling with an aldehyde via Wittig reaction feasible. By application of a triarylamine aldehyde a bpy-hole transport functionality was attached to the bipyridine via vinylene units resulting in a hole transport ligand for complex formation. In a metallation reaction with bis[(4,4'-dicarboxy)-2,2'-bipyridyl]dichloro-Ru(II)hydrate a light absorbing complex was obtained with the hole transport functionality covalently attached to one of the bipyridyl ligands. The basic idea of this concept and the general strategy of synthesis is schematically outlined in Figure 3-1. The precise synthetic pathway for the different new low molecular weight bifunctional materials carrying triarylamine units and light absorbing Ru(II) dye centre will be described in detail in the following sub-sections.

## 3.2 Synthesis of bis(triarylamino)bipyridine ligands

### 3.2.1 Synthesis of 4,4'-bis(chloromethyl)-2,2'-bipyridine (**3**)

First 4,4'-bis(trimethylsilylmethyl)-2,2'-bipyridine was synthesized by a modified procedure of Fraser et al.<sup>75</sup> starting with the deprotonation of the methyl substituents of 4,4'-dimethyl-2,2'-bipyridine with Lithium-diisopropylamide (LDA) followed by trapping the resulting dianion with trimethylsilylchloride (Scheme 3-1). To prevent oversilylation it is important that the reaction is quenched immediately after silylation is complete. This occurs a few minutes after addition of the TMSCl and is indicated by a colour change from maroon to bluish green. The resulting product was fully characterized as reported in the experimental section and served as starting material for the synthesis of 4,4'-bis(chloromethyl)-2,2'-bipyridine (**3**).

<sup>75</sup> C. L. Fraser, N. R. Anastasi, J. S. Lamba *J. Org. Chem.* **1997**, 62, 9314-9317.

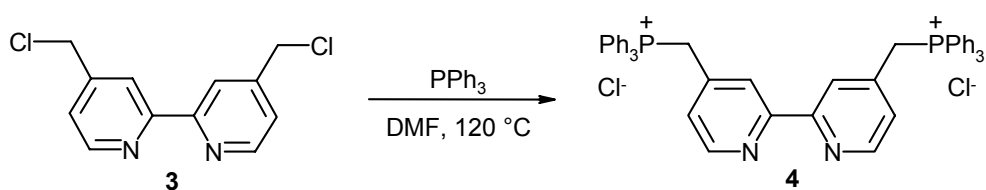


**Scheme 3-1:** Schematic representation of the synthesis of 4,4'-bis(trimethylsilylmethyl)-2,2'-bipyridine (**2**) and 4,4'-bis(chloromethyl)-2,2'-bipyridine (**3**).

For the preparation of **3** anhydrous CsF was used as fluoride source to abstract the TMS substituents. Together with Cl<sub>3</sub>CCl<sub>3</sub> in dry DMF 4,4'-bis(chloromethyl)-2,2'-bipyridine (**3**) could be produced at room temperature in appreciably good yields. In this reaction one equivalent of the Cl<sup>+</sup> source and one equivalent of CsF were used per TMS group. The reaction was controlled via TLC and quenched when compound **2** was fully consumed. The raw product consisted of a mixture of the desired molecule together with traces of the mono-substituted product. The mono-substituted derivative could be removed by washing the raw product several times with cold toluene (cooled with liquid N<sub>2</sub>) resulting in pure 4,4'-bis(chloromethyl)-2,2'-bipyridine (**3**). The purification can also be performed via column chromatography with alox N as stationary phase and diethylether as eluent. But this method resulted in less yield and is time consuming. NMR-spectroscopy, FT-IR as well as mass spectrometry confirm the chemical structure of the product **3** and all the data are agreeable to those published in literature<sup>76</sup>. For example in <sup>1</sup>H-NMR spectroscopy the singlet appearing at 2.18 ppm in compound **2** and representing the methylene groups is clearly shifted to lower field (4.58 ppm) when the

<sup>76</sup> K. Peter, M. Thelakkat *Macromolecules* **2003**, 36, 1779.

chlorine substituents are attached in **3**. According to Fraser et al. yield could be improved by using double excess of  $\text{Cl}_3\text{CCl}_3$  per TMS-group. This could not be reproduced but resulted in a mixture of all possible substitution variations of the methyl group of the bipyridine educt verified by NMR-spectroscopy and mass spectrometry. In the next reaction step triphenylphosphonium salts (**4**) were prepared by the reaction of 4,4'-bis(chloromethyl)-2,2'-bipyridine with  $\text{PPh}_3$  in DMF at 120 °C as shown in Scheme 3-2.

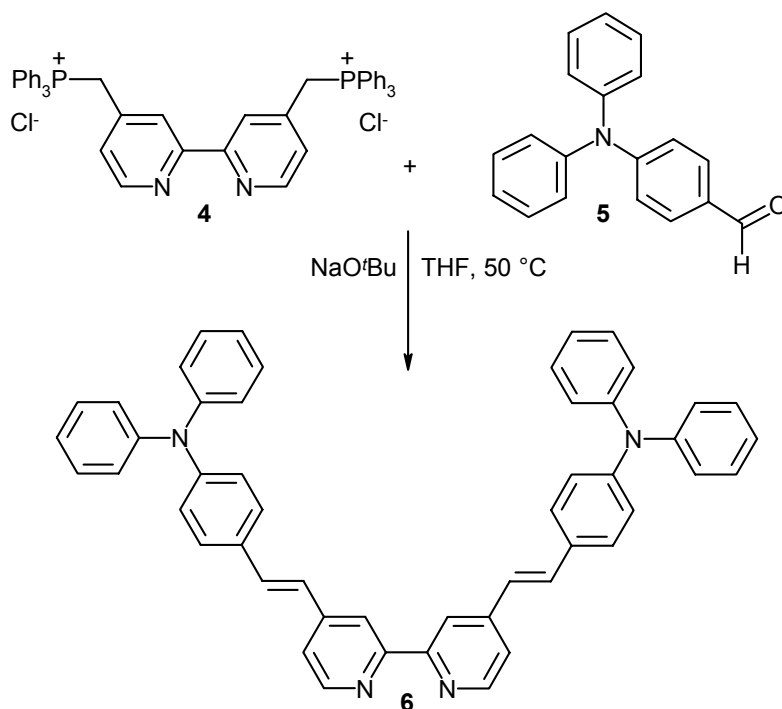


**Scheme 3-2:** Schematic representation of the synthesis of 4,4'-bis(triphenylphosphonium methyl)-2,2'-bipyridyl chloride (**4**) via quaternization of **3** with  $\text{PPh}_3$ .

The characterization was carried out via  $^1\text{H}$ -NMR-spectrometry exhibiting a doublet at 4.84 ppm corresponding to the protons of the methyl group adjacent to the phosphor atom. In the aromatic region (7.70 ppm – 8.38 ppm) the signals of the bipyridine unit are visible partly superposed by the signal of the three phenyl rings. In mass spectrometry the signal of  $\text{M}^+$  is not present but the fragment corresponding to the triphenylphosphine group at  $m/z = 262$  as well as a fragment at  $m/z = 183$  which can be assigned to the bipyridine moiety. All the characterizations are outlined in detail in the experimental section.

### 3.2.2 Synthesis of 4,4'-bis[4-(diphenylamino)styryl]-2,2'-bipyridine (bpy-TPA ligand, **6**)

The hole transporting ligand 4,4'-bis[4-(diphenylamino)styryl]-2,2'-bipyridine (bpy-TPA ligand, **6**) was prepared via coupling of the phosphonium salt **4** with 4-diphenylaminobenzaldehyde. The reaction was carried out in THF and is outlined in Scheme 3-3.



**Scheme 3-3:** Schematic representation of the synthesis of 4,4'-bis[4-(diphenylamino)styryl]-2,2'-bipyridine (bpy-TPA ligand, **6**).

With the application of NaO<sup>t</sup>Bu as strong base it is possible to abstract acidic protons adjacent to the phosphonium group in **4** to convert it into the phosphonium ylides. The phosphonium ylide can react with equimolar amount of aldehyde per phosphonium group in a Wittig reaction resulting in the desired product (**6**) in which a bipyridine unit is connected to two triphenylamine moieties with conjugated vinylene spacers.

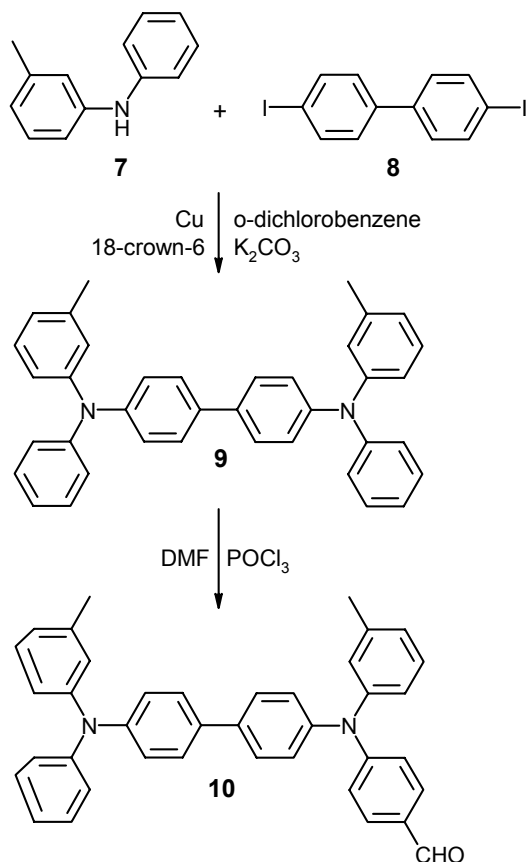
### 3.2.3 Synthesis of 4,4'-bis[N-(phenyl)-N'-(styryl)-N,N'-bis(3-methylphenyl)-1,1'-biphenyl-4,4'-diamino]2,2'-bipyridine (**11**)

The new concept was extended for preparing additional hole transport ligand carrying N,N'-bis(phenyl)-N,N'-bis(3-methylphenyl)-1,1'-biphenyl-4,4'-diamine (TPD) units covalently attached to a bipyridine center via conjugated vinylene spacer. The idea here is to transfer the dye cation more efficiently away from the Ru(II) core to the bulk of the hole transport layer. The TPD unit is more delocalized than TPA and the HOMO value of TPD (5.2 eV) lies still higher than that of TPA (5.4 eV). The synthesis of bpy-TPD ligand **11** was carried out in three reaction steps: First a biphenyl derivative was coupled with a diphenylamine derivative to get the TPD molecule which was followed by mono-formylation resulting in the introduction of the desired aldehyde function. In the final step the aldehyde was coupled with the phosphonium salt (**4**) reported above to yield the target molecule, bpy-TPD ligand (**11**).

#### *Synthesis and characterization of N-phenyl-N'-(4-formylphenyl)-N,N'-bis(3-methylphenyl)-1,1'-biphenyl-4,4'-diamine (**10**)*

The synthesis of the mono-aldehyde (**10**) was carried out in two steps as shown in Scheme 3-4: First 3-methyldiphenylamine (**7**) and 4,4'-diiodobiphenyl (**8**) were coupled via Ullmann reaction using Cu-powder, 18-crown-6 as phase transfer catalyst and K<sub>2</sub>CO<sub>3</sub> as base resulting in N,N'-diphenyl-N,N'-bis(3-methylphenyl)-1,1'-biphenyl-4,4'-diamine (**9**)<sup>77</sup>. The reaction was performed under reflux in o-dichlorobenzene for 24 h. The raw product was purified via extraction with hot methanol to remove the biphenyl educt. Residual Cu and other impurities were removed by column chromatography using cyclohexane and ethylacetate (9 : 1) as eluent. The structure was verified via NMR-spectroscopy and mass spectrometry.

<sup>77</sup> M. Thelakkat, J. Hagen, D. Haarer, H.-W. Schmidt *Synth. Met.* **1999**, 102, 1125.



**Scheme 3-4:** Schematic representation of the synthesis of mono-aldehyde *N*-phenyl-*N'*-(4-formylphenyl)-*N,N'*-bis(3-methylphenyl)-1,1'-biphenyl-4,4'-diamine (**10**).

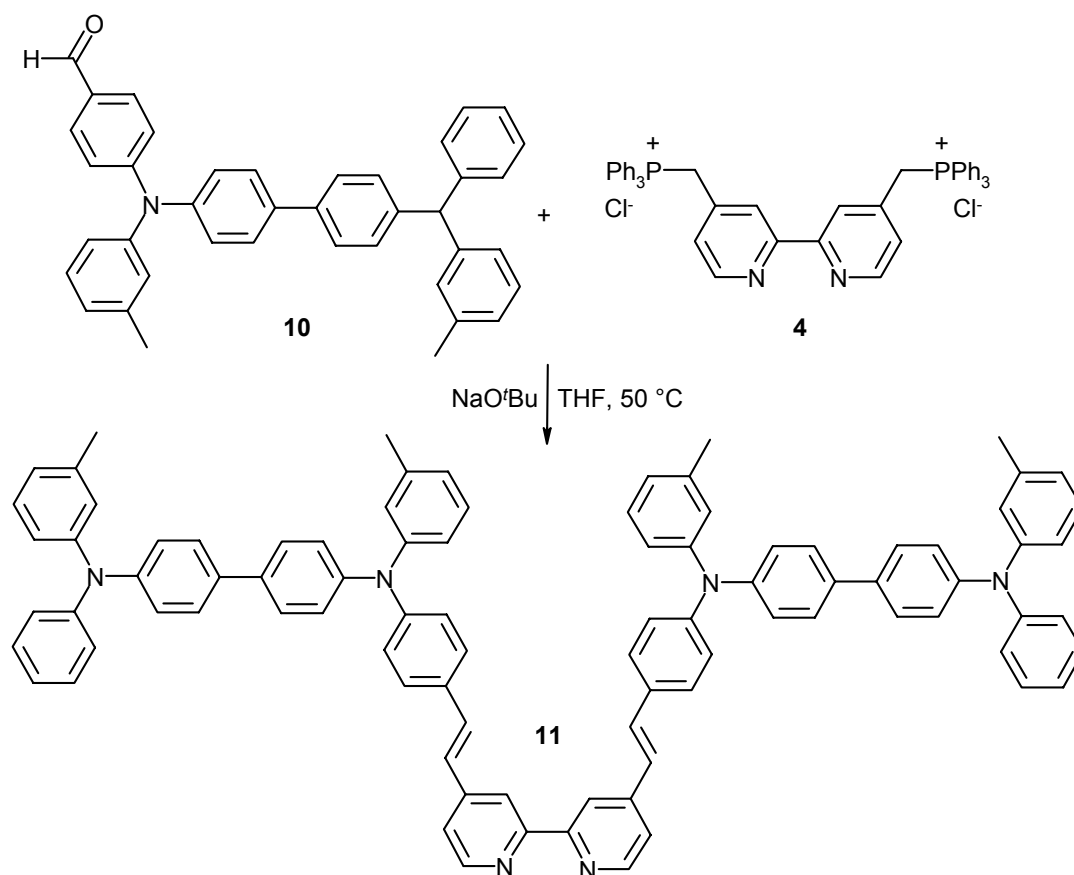
In a second step the aldehyde group was introduced via mono-formylation of **9** with a slight excess of freshly distilled POCl<sub>3</sub> in dry DMF. The aldehyde *N*-phenyl-*N'*-(4-formylphenyl)-*N,N'*-bis(3-methylphenyl)-1,1'-biphenyl-4,4'-diamine (**10**) was precipitated by pouring the reaction mixture into ice-water followed by neutralization with CH<sub>3</sub>COONa. Di-substituted by-product and unreacted educt were removed by column chromatography using cyclohexane and ethylacetate (9 : 1) as eluent yielding the target molecule. As it is reported in the experimental part the characterization of **10** was carried out via NMR-spectroscopy. Singlets at 2.26 and 2.52 ppm with the integral value of 3 protons each are corresponding to the methyl substituents on the unsymmetric substituted aromatic rings. A bulk of resonance signals which will not be analyzed in

detail exhibiting an integral value of 32 protons from 6.79 ppm – 7.65 ppm can be assigned to the aromatic protons of compound **10**. At 10.04 ppm the singlet resonance signal referring to the aldehyde proton is present proving the successful monoformylation of **9**. The structure was also verified via mass spectrometry exhibiting  $M^+$  at  $m/z = 544$ .

*Synthesis of 4,4'-bis[N-(phenyl)-N'-(styryl)-N,N'-bis(3-methylphenyl)-1,1'-biphenyl-4,4'-diamino]2,2'-bipyridine (bpy-TPD ligand, **11**)*

The preparation of hole transport bpy-TPD ligand **11** was carried out in a very similar procedure as reported above for compound **6**. In a Wittig reaction the phosphonium salt **3** and aldehyde **10** are coupled in THF with NaO<sup>t</sup>Bu as base yielding a bipyridine derivative with TPD substituents covalently attached in 4,4'-positions via conjugated vinylene spacer as shown in Scheme 3-5. For isolation of **11** the reaction mixture was cooled to room temperature, neutralized with diluted acetic acid and extracted with CH<sub>2</sub>Cl<sub>2</sub>. After removal of the solvent the raw product was obtained which was further purified by precipitation from CH<sub>2</sub>Cl<sub>2</sub> into petrolether (low boiling fraction, 40 – 60 °C).

The characterization of hole transport ligands **6** and **11** was carried out via <sup>1</sup>H-NMR spectroscopy as well as UV-spectroscopy. The data obtained by these methods will be discussed in the following section and details are given in the experimental part.



**Scheme 3-5:** Schematic representation of the synthesis of bipy-TPD ligand 4,4'-bis[N-(phenyl)-N'-(styryl)-N,N'-bis(3-methylphenyl)-1,1'-biphenyl-4,4'-diamino]-2,2'-bipyridine **11**.

### 3.2.4 NMR-spectroscopy of **6** and **11**

In the <sup>1</sup>H-NMR spectrum of bipy-TPA ligand **6** (Figure 3-2) the resonance signals of two protons of the bipyridine core are visible at 8.49 ppm and 8.62 ppm and the integral value of each was defined as 1. The residual 17 protons are present in a bulk of signals from 6.95 ppm to 7.44 ppm (integral value 17).

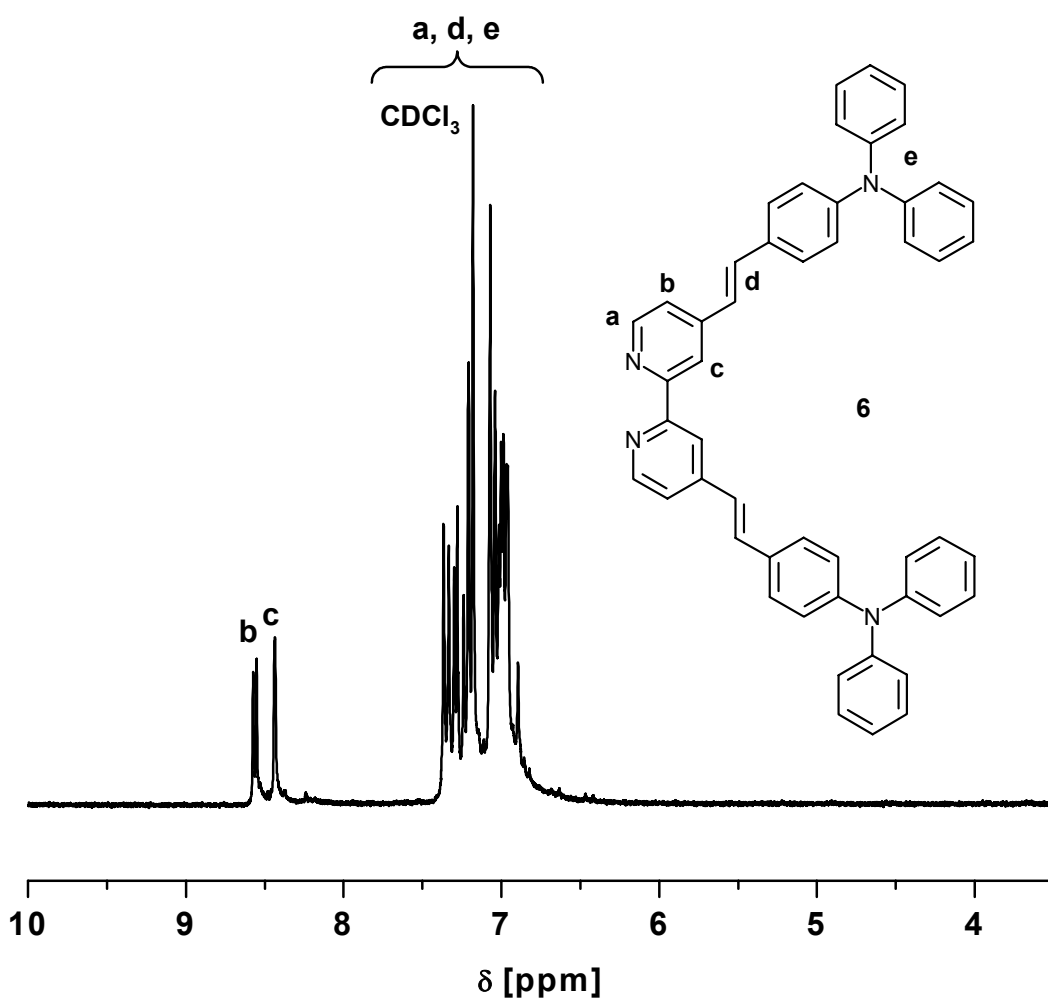


**Figure 3-2:**  $^1\text{H-NMR}$  spectrum of bpy-TPA ligand (6) (in  $\text{CDCl}_3$ , 250 MHz, 298 K).

The proton NMR-spectrum of the TPD-ligand **11** shown in Figure 3-3 exhibits a singlet at 2.25 ppm representing the methyl substituents of the TPD units. Two protons of the bipyridine centre are visible at 8.48 ppm and 8.63 ppm respectively whereas the residual aromatic proton of the bipyridine moiety and the TPD antenna groups are situated in a broad multiplet without resolution from 6.83 ppm to 7.65 ppm.

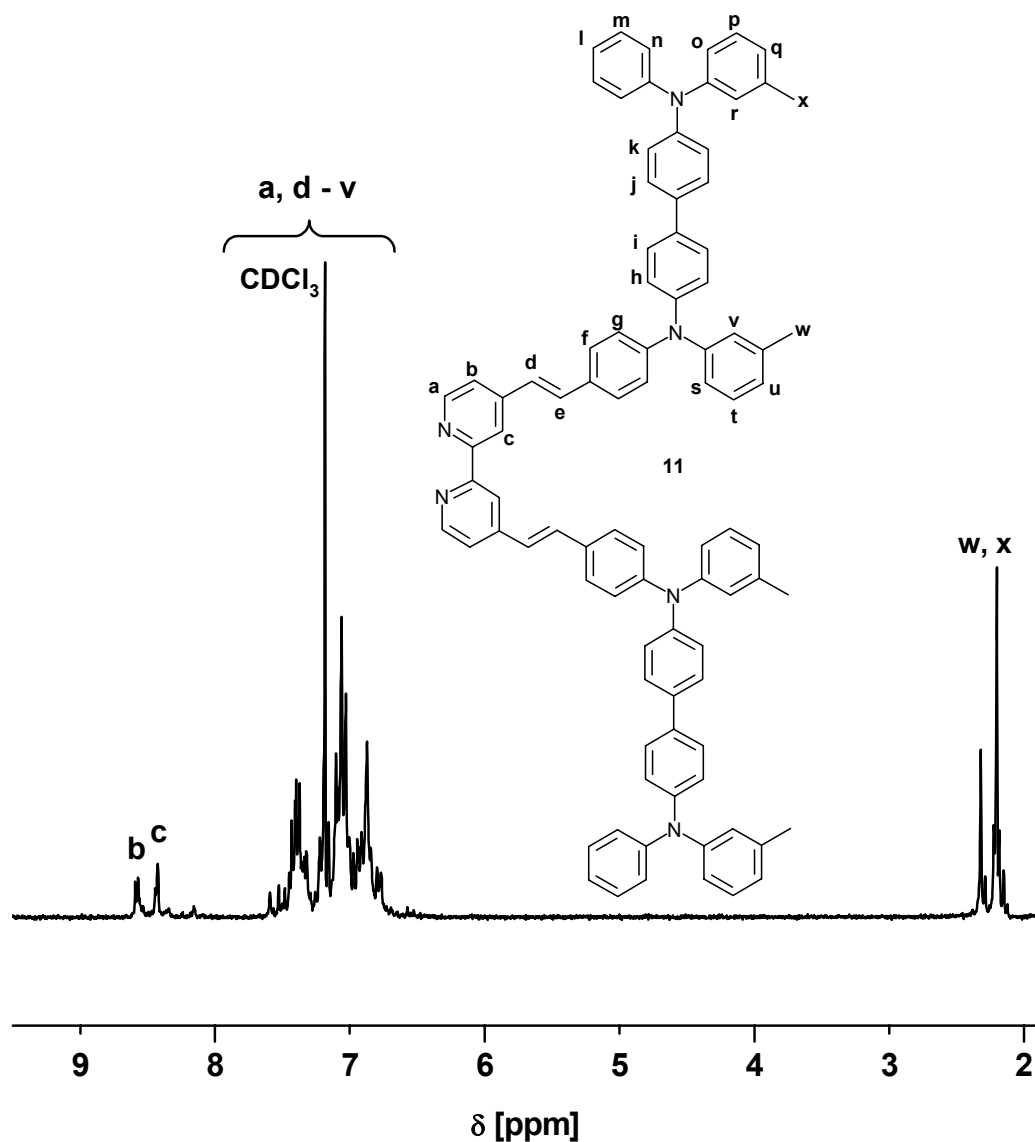


**Figure 3-3:**  $^1\text{H-NMR}$  spectrum of *bpy-TPD* ligand (**11**) (in  $\text{CDCl}_3$ , 250 MHz, 298 K).

### 3.2.5 UV-Vis spectroscopy of **6** and **11**

The normalized UV-Vis spectra of both novel ligands *bpy-TPA* (**6**) and *bpy-TPD* (**11**) are shown in Figure 3-4.

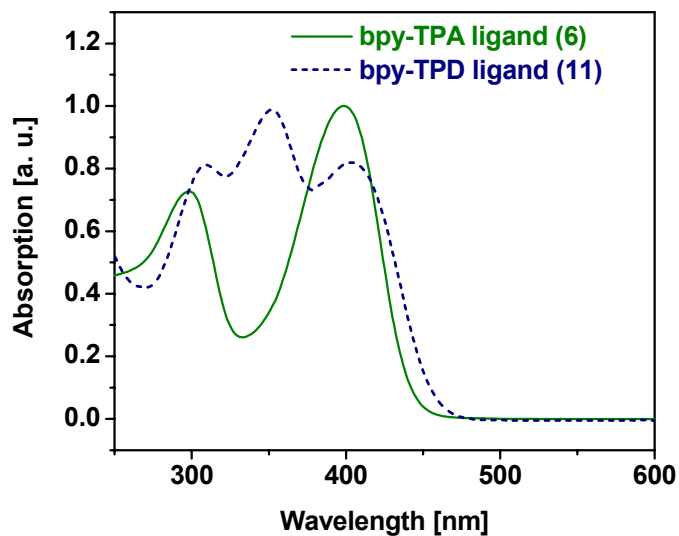


**Figure 3-4:** Normalized UV-Vis spectra of bpy-TPA ligand (**6**, solid line) and bpy-TPD ligand (**11**, dashed line) recorded in  $\text{CHCl}_3$ .

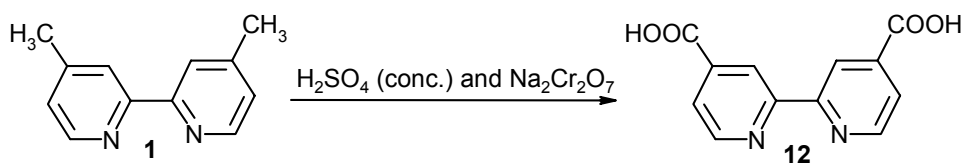
For bpy-TPA ligand **6** two absorption maxima could be detected: The maxima at 298 nm ( $\lambda_{\text{max}1}$ ) and at 398 nm ( $\lambda_{\text{max}2}$ ) correspond to the  $\pi$ - $\pi^*$  transition of the fully conjugated system consisting of triphenylamine units and bipyridine unit connected with vinylene spacers. The spectrum of bpy-TPD ligand **11** exhibits maxima at 309 nm, 352 nm and 403 nm having a much broader absorption range than TPA-ligand **6** which can be attributed to the extended conjugation in structure **11**. Due to the full conjugation in TPA-ligand **6** and TPD-ligand **11** it is not possible to correlate the absorption maxima to different units present in the molecule. Mass spectrometry supported the structures of **6** and **11** exhibiting  $\text{M}^+$  which is detailed in the experimental part. The novel ligands were complexed with a Ru(II) precursor to obtain bifunctional dyes.

### 3.3 Synthesis of Ru(bpy<sub>COOH</sub>)<sub>2</sub>Cl<sub>2</sub> · 2 H<sub>2</sub>O (**13**)

For the application in TiO<sub>2</sub> solar cells it is necessary to have Ru(II)-complexes with carboxylic acid anchor groups for chemisorption on the TiO<sub>2</sub> surface. Therefore bis[(4,4'-dicarboxy)-2,2'-bipyridyl]dichloro-Ru(II)hydrate (**13**) was used as metallation precursor for the new ligands **6** and **11** to produce the bifunctional materials with Ru(II) dye centre. The synthesis of the ligand with the carboxylic acid groups as well as the synthesis of the precursor complex are given in the next section.

#### 3.3.1 Synthesis of 4,4'-dicarboxy-2,2'-bipyridine (**12**)

The ligand 4,4'-dicarboxy-2,2'-bipyridine (**12**) was prepared by oxidation of the methyl groups of 4,4'-dimethyl-2,2'-bipyridine as shown in Scheme 3-6. There are several methods reported in literature to produce this dicarboxylic acid using different oxidizing agents like KMnO<sub>4</sub><sup>78</sup> or concentrated H<sub>2</sub>SO<sub>4</sub><sup>79</sup> but most of them with unsatisfying yields. In this work an excess of Na<sub>2</sub>Cr<sub>2</sub>O<sub>7</sub> in concentrated sulfuric acid was adopted<sup>80</sup>. For purification the raw product was dissolved in 6 M NaOH. After filtration the solution was acidified with HCl (conc.) to precipitate pure 4,4'-dicarboxy-2,2'-bipyridine (**12**) which is almost completely insoluble in most of the organic solvents, alcohols and water.



**Scheme 3-6:** Reaction scheme for the oxidation of 4,4'-dimethyl-2,2'-bipyridine (**1**) to 4,4'-dicarboxy-2,2'-bipyridine (**12**).

<sup>78</sup> G. Sprintschnik, H.W. Sprintschnik, P. P. Kirsch, David G. Witten *J. Am. Chem. Soc.* **1977**, 99, 4974.

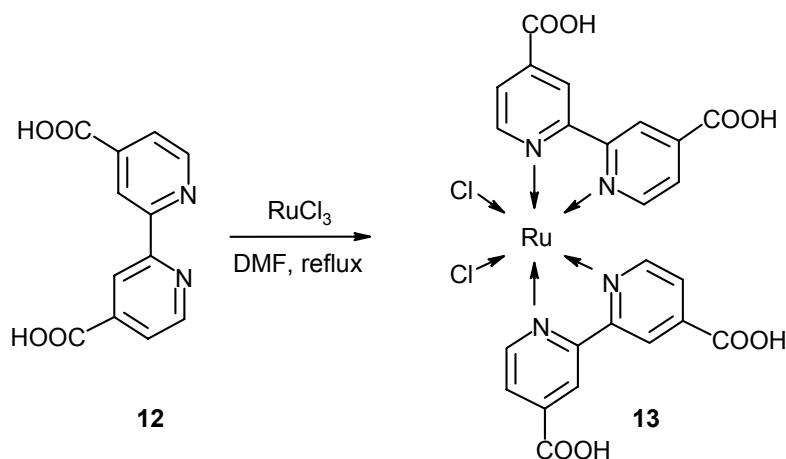
<sup>79</sup> C. Kaes, M. W. Hosseini, A. De Cian, J. Fischer *Tetrahedron Lett.* **1997**, 25, 38, 4389.

<sup>80</sup> A. R. Oki, R. J. Morgan *Synth. Comm.* **1995**, 25, 4093.

The product was characterized via  $^1\text{H-NMR}$  in  $\text{DMSO-d}_6$  and  $^{13}\text{C-NMR}$ -spectroscopy in  $\text{CF}_3\text{COOD}$ . The resonance signals of the bipyridine unit of **12** are present in the  $^1\text{H-NMR}$  spectrum in a singlet (8.84 ppm) and two doublets (7.90 ppm and 8.90 ppm) in the low field aromatic region of the spectrum. The methyl protons (2.45 ppm) of **1** in  $^1\text{H-NMR}$  have disappeared as well as the carbons of the methyl-groups (14.3 ppm) in  $^{13}\text{C-NMR}$  followed by appearance of the resonance signal of the carboxylic acid proton in  $^1\text{H-NMR}$  (13.81 ppm) and the carboxy carbon signal at 167 ppm in the  $^{13}\text{C-NMR}$  spectrum. Mass spectrometry also supports the structure of **12** indicating  $\text{M}^+$  at  $m/z = 244$ .

### 3.3.2 Metallation of 4,4'-dicarboxy-2,2'-bipyridine (**12**)

The preparation of the precursor complex **13** was carried out as presented in Scheme 3-7:



**Scheme 3-7:** Schematic representation of the synthesis of the Ru(II) precursor bis[(4,4'-dicarboxy)-2,2'-bipyridyl]dichloro-Ru(II)hydrate (**13**).

One equivalent of  $\text{RuCl}_3 \cdot 3\text{H}_2\text{O}$  and a slight excess of the ligand **12** were refluxed in dry DMF to develop a black solution consisting of **13** and traces of tris[(4,4'-dicarboxy)-2,2'-

bipyridyl]dichloro-Ru(II)<sup>81</sup>. The insoluble side product could be removed by filtration of the reaction mixture leaving the raw product which could be purified by recrystallization from acetone.

### 3.3.3 Characterization of Ru(bpy<sub>COOH</sub>)<sub>2</sub>Cl<sub>2</sub> · 2 H<sub>2</sub>O (**13**)

The characterization of **13** was carried out via UV-Vis spectroscopy. In comparison to the educt RuCl<sub>3</sub> ( $\lambda_{\text{max}} = 420 \text{ nm}$ ) the UV-Vis spectrum of **13** exhibits two absorption maxima at 391 nm and 536 nm which represent metal-to-ligand charge transfer (MLCT) bands and confirm the Ru(II) core coordinated by two bipyridyl ligands (see Figure 3-5).

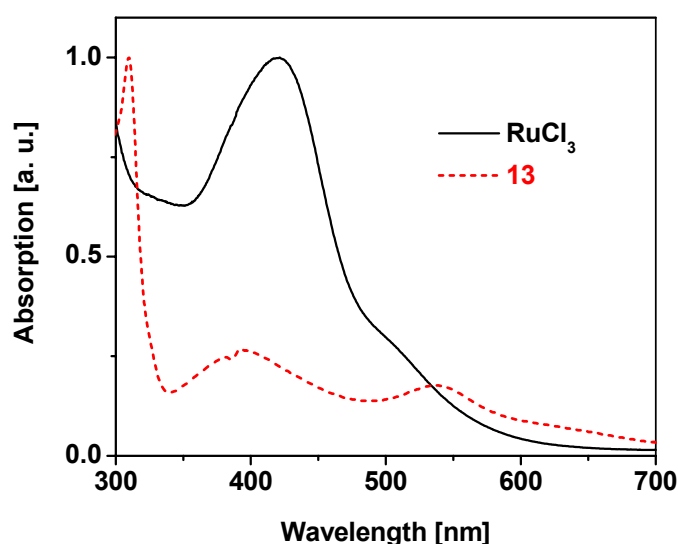


**Figure 3-5:** Normalized UV-Vis spectra of RuCl<sub>3</sub> (solid) and **13** (dashed) recorded in MeOH + 1 wt% KOH.

<sup>81</sup> P. Liska, N. Vlachopoulos, M. K. Nazeeruddin, P. Comte, M. Graetzel *J. Am. Chem. Soc.* **1988**, 110, 3686.

A third maximum at 310 nm can be attributed to the ligand centered (LC) excited state of the bipyridine ligand **12**. The values found for the absorption maxima are in good agreement with analytic data given in literature for Ru(II)(bpy)<sub>2</sub><sup>2+</sup> dyes with different anions<sup>82,83</sup>. According to the poor solubility of **13** in organic solvents and water the characterization via NMR-spectroscopy did not provide further data to confirm the structure of the product.

### 3.4 Synthesis of Ru(II) dyes carrying hole conductor units (**14**, **15**)

The metallation of both ligands **6** and **11** will be discussed here. The Ru(II) precursor (**13**) was used to form the hexa-coordinated Ru(II) dyes **14** and **15** carrying hole transport units as antenna groups. The characterization of the bifunctional target materials will also be detailed.

#### 3.4.1 Synthesis of Ru(II) dye carrying TPA-units (**14**)

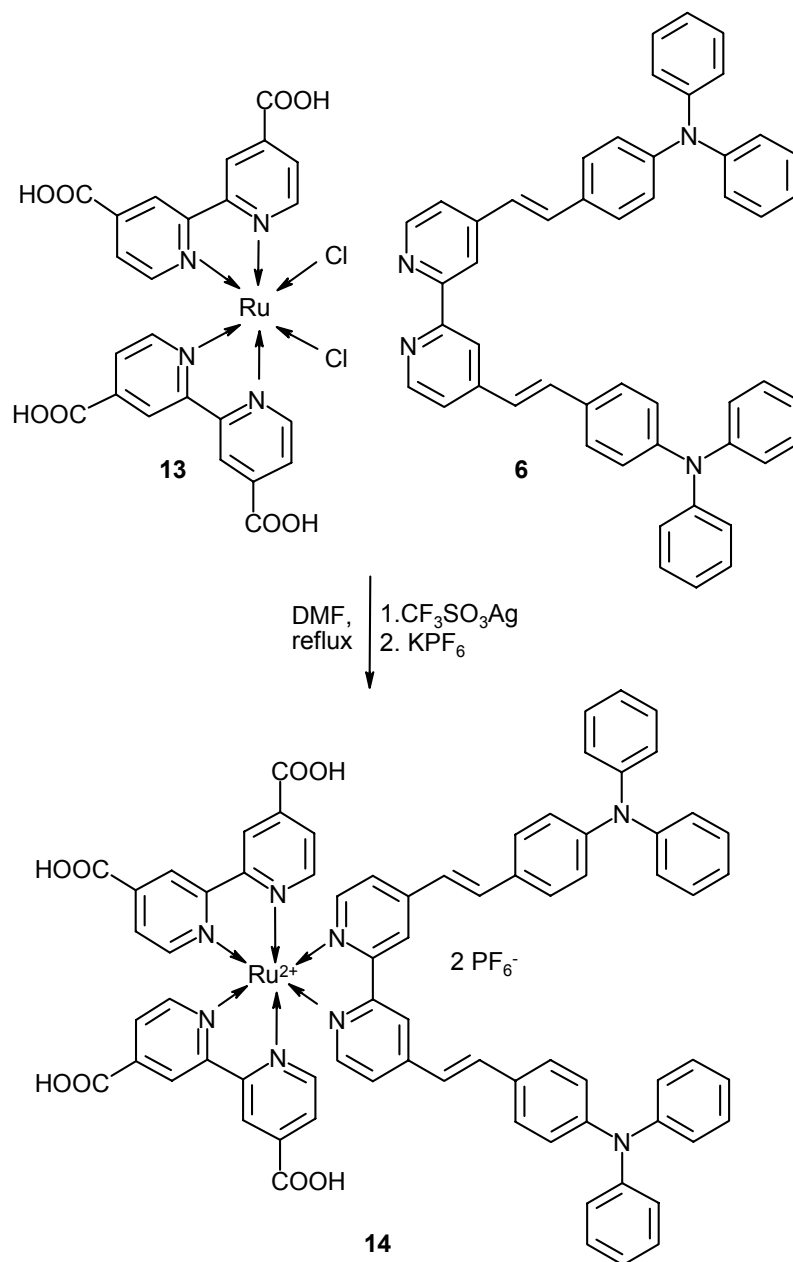
Bis[(4,4'-dicarboxy)-2,2'-bipyridyl]dichloro-Ru(II)hydrate (**13**) was converted to the desired bifunctional Ru(II) dye **14** carrying TPA units by metallation of TPA-ligand **6** as shown in Scheme 3-8. This was carried out by refluxing **6** with the Ru(II) precursor **13** in DMF<sup>84</sup>. To increase the reactivity it was necessary to exchange the chloride anion of the **13** with CF<sub>3</sub>SO<sub>3</sub><sup>-</sup> anion by adding CF<sub>3</sub>SO<sub>3</sub>Ag. The progress of the reaction was controlled via TLC. The metallation was quenched after **6** was fully consumed.

---

<sup>82</sup> M. K. Nazeeruddin, A. Kay, I. Rodicio, R. Humphrey-Baker, E. Mueller, P. Liska, N. Vlachopoulos, M. Graetzel *J. Am. Chem. Soc.* **1993**, 115, 6382.

<sup>83</sup> A. Juris, V. Balzani, F. Barigelletti, S. Campagna, P. Belser, A. Von Zelewsky *Coord. Chem. Rev.* **1988**, 84, 85.

<sup>84</sup> J. E. Collins, J. J. S. Lamba, J. C. Love, J. E. McAlvin, C. Ng, B. P. Peters, X. Wu, C. L. Fraser *Inorg. Chem.* **1999**, 38, 2020.



**Scheme 3-8:** Metallation of the triphenylamine ligand (**6**) with  $\text{Ru}(\text{bpy}_{\text{COOH}})_2\text{Cl}_2 \cdot 2\text{H}_2\text{O}$  (**13**) yielding the bifunctional hole transport dye **14**.

Before isolating the product by crystallization from cooled DMF a saturated aqueous solution of  $\text{KPF}_6$  was added to exchange the  $\text{CF}_3\text{SO}_3^-$  anion with  $\text{PF}_6^-$ .

With the incorporation of  $\text{PF}_6^-$  the photosensitivity of the complex decreases and the tendency to re-chelation or ligand substitution is reduced<sup>85</sup>. Moreover the solubility of the target molecule **14** was increased by exchanging the  $\text{CF}_3\text{SO}_3^-$  anion with  $\text{PF}_6^-$ .

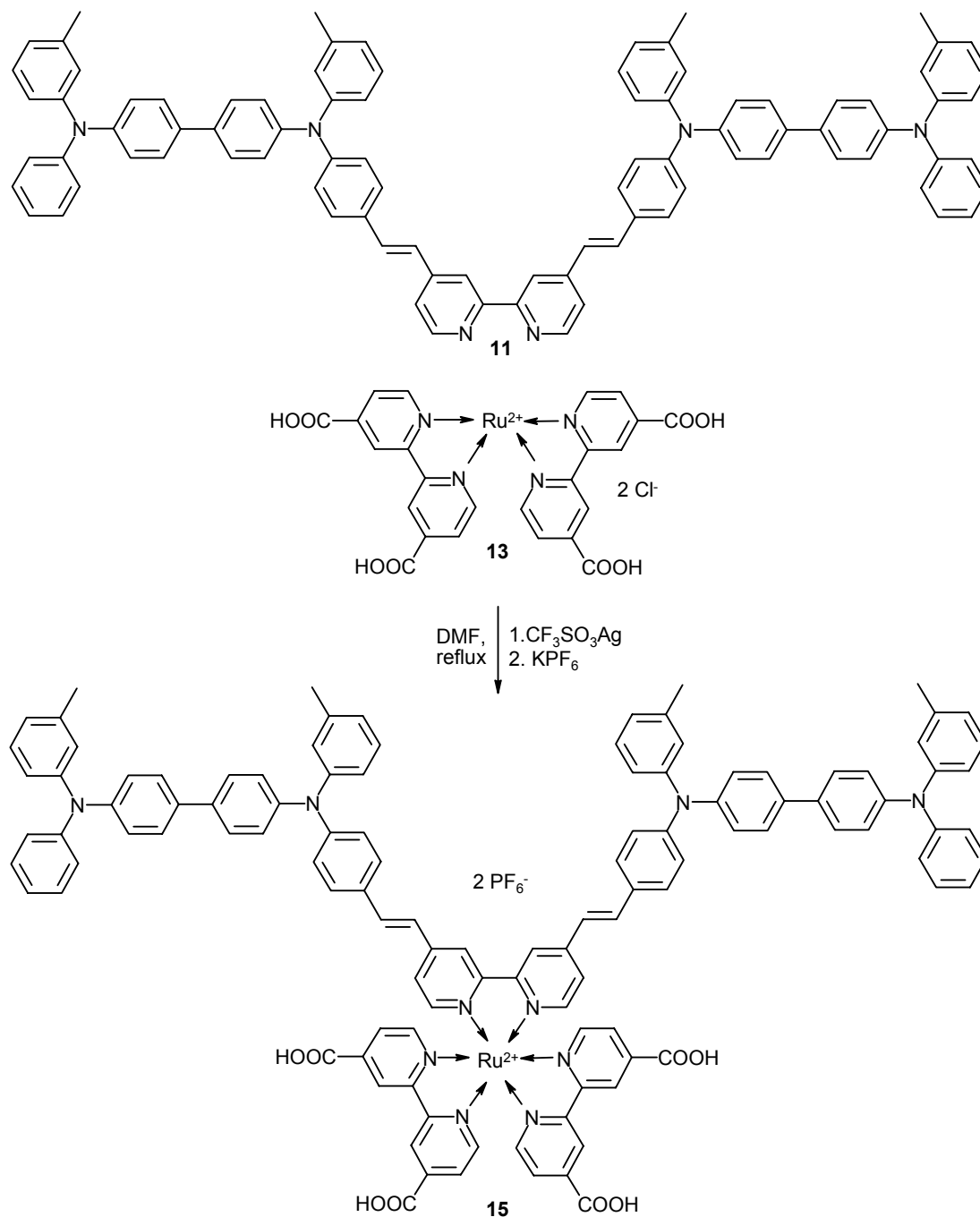
### 3.4.2 Synthesis of Ru(II) dye carrying TPD-units (**15**)

The preparation of the bifunctional Ru(II) complex **15** carrying TPD units as hole transport functionality was carried out according to the procedure reported for the synthesis of the bifunctional dye **14**. The synthesis was carried out in DMF under reflux and the product was precipitated from the reaction mixture. For purification, the raw product was reprecipitated from THF into methanol yielding the reddish-brown target compound. The pathway of synthesis and the structure of the product are presented in Scheme 3-9.

As it is described in the following sections the new bifunctional dyes **14** and **15** were analyzed via UV-Vis spectroscopy. Transient absorption spectroscopy studies were performed by James Durrant and co-workers at Imperial College, London, UK.

---

<sup>85</sup> K. Kalyanasundaram *Coord. Chem. Rev.* **1982**, 46, 159.



**Scheme 3-9:** Metallation of TPD-ligand (11) with  $Ru(bpy_{COOH})_2Cl_2 \cdot 2H_2O$  (13) yielding the bifunctional hole transport dye 15.

## 3.5 Characterization of bifunctional dyes **14** and **15**

The newly synthesized bifunctional dyes **14** and **15** have been characterized via UV-Vis spectroscopy and transient absorption spectroscopy. Moreover a series of solar cells was prepared applying **14** as dye and interface compatibilizer. The results will be discussed in the following sections.

### 3.5.1 UV-Vis spectroscopy

In Figure 3-6 the UV-Vis spectra of the bifunctional dyes **14** and **15** as well as that of the reference dye **N 719** (cis-bis(isothiocyanato)-bis-(2,2'-bipyridyl-4,4'-dicarboxylato)-Ruthenium(II)-bis(tetrabutylammonium)) recorded in methanol containing 1 wt% KOH, concentrations  $\sim 10^{-5} \text{ mol l}^{-1}$ , are plotted. It can be clearly seen that both the new dyes **14** and **15** exhibit stronger absorption than the reference dye **N 719** for the entire range. Especially the bifunctional dye **14** shows almost four times higher absorption intensity than **N 719** at a wavelength of 400 nm. The UV-Vis spectrum of **14** shows maximum absorption wavelength at 301 nm which can be attributed to the  $\pi$ - $\pi^*$  transition of the triphenylamine system and the ligand centered transition due to the 2,2'-bipyridine units at 298 nm. The second maximum at 405 nm represents the MLCT band of the hexacoordinated Ru(II) core<sup>86</sup> and a shoulder at 470 nm corresponds to MLCT transition as well. In the UV-Vis spectrum of **15** absorption maxima are present at a wavelength of 303 nm and 346 nm respectively. These bands can be attributed to the  $\pi$ - $\pi^*$  transition of the TPD substituent. The absorption maximum at 472 nm is corresponding to the MLCT band of the hexacoordinated Ru(II) core proving that the metallation reaction has proceeded as expected.

To compare the intensity of light absorption of the dyes especially concerning their application in dye-sensitized solar cells the extinction coefficients ( $\epsilon$ ) were determined.

---

<sup>86</sup> M. Rehahn, *Habilitation*, Karlsruhe, 1996.

Solutions with defined concentrations ( $c$ ) of about  $10^{-5} \text{ mol l}^{-1}$  were prepared and the optical density (OD) was measured via UV-Vis spectroscopy. The extinction coefficients could be calculated using the Lambert-Beer equation (The parameter  $l$  represents the thickness of the sample and is 1 cm):

$$OD = \log \frac{I}{I_0} = \varepsilon \cdot c \cdot l \quad (\text{Equation 7})$$

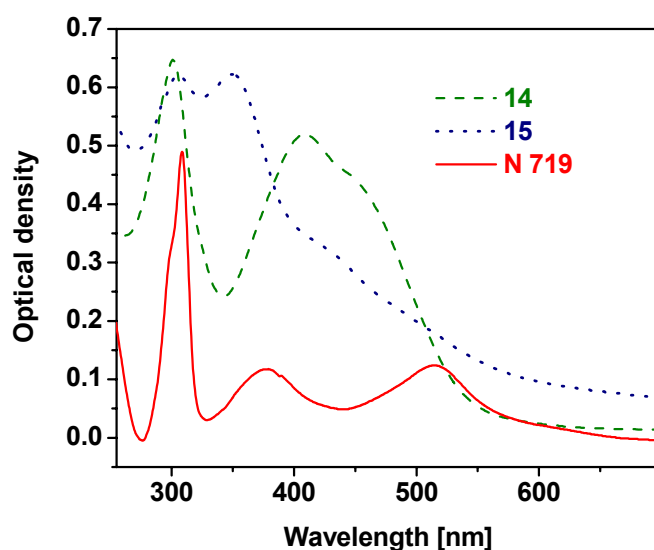


**Figure 3-6:** UV-Vis spectra of **14** (green, dashed line), **15** (blue, dotted line) and **N 719** (red solid line). The spectra have been recorded in MeOH + 1wt % KOH with the concentrations  $c_{14} = 1 \cdot 10^{-5} \text{ mol l}^{-1}$ ,  $c_{15} = 1 \cdot 10^{-5} \text{ mol l}^{-1}$  and  $c_{719} = 9.6340 \cdot 10^{-6} \text{ mol l}^{-1}$  (red, solid line).

The extinction coefficients ( $\varepsilon$ ) were calculated for each absorption maximum detected in UV-Vis spectroscopy and are reported in the following table. Also for the standard Ru-dye for dye-sensitized solar cells (**N 719**) the extinction coefficients are given.

**Table 3-1:** Extinction coefficients of **14**, **15** and **N 719** calculated for each absorption maximum for the concentration  $c_{14} = 1 \cdot 10^{-5} \text{ mol l}^{-1}$ ,  $c_{15} = 1 \cdot 10^{-5} \text{ mol l}^{-1}$  and  $c_{719} = 9.6340 \cdot 10^{-6} \text{ mol l}^{-1}$  recorded in MeOH + 1wt% KOH.

	$\lambda_{\text{max}}$ [nm]	optical density [a. u.]	$\epsilon$ [l cm <sup>-1</sup> mol <sup>-1</sup> ]
<b>14</b>	301	0.646	64 600
	408	0.519	51 900
<b>15</b>	305	0.623	62 300
	349	0.645	64 500
<b>N 719</b>	308	0.490	50 861
	379	0.118	12 248
	514	0.124	12 871

The extinction coefficients and the absorption spectra clearly show that the chemical structures of **14** and **15** result in significantly higher light absorption than **N 719**. Taking this facts into account the application of **14** or **15** in dye-sensitized solar cells should bring about a considerable improvement of the photovoltaic parameters of dye-sensitized TiO<sub>2</sub> solar cells. The employment of the new bifunctional dye **14** in solar cells has already been carried out and their optical and photovoltaic properties were investigated as described in the following sub-section.

In comparison with reference dye **N 719** the increase in extinction values for compounds **14** and **15** is extraordinarily high. This can be explained as follows: Any extension of conjugation and delocalization of the bipyridine ligands lead to higher  $\epsilon$  values. In bifunctional dyes **14** and **15** the TPA and TPD units connected to the bipyridine moiety via vinylene spacers extend the delocalization efficiently, thus leading to the excellent UV-Vis absorption properties of the new materials.

Moreover, the antenna groups in **14** and **15** should support the facile transfer of holes away from the Ru(II) centre. In the following sections the application of bifunctional dye **14** in dye-sensitized solar cells and the transient absorption spectroscopy data of both novel materials **14** and **15** will be given.

### 3.5.2 Application of bifunctional dye in dye-sensitized nc-TiO<sub>2</sub> solar cells

As an example the effect of the new bifunctional dye **14** in dye-sensitized TiO<sub>2</sub> solar cells will be discussed in details here. It must be pointed out that the solar cells were prepared and characterized by Dr. Bin Peng who has been working as post-doc in our group.

A series of dye-sensitized solar cells were prepared with TiO<sub>2</sub> layers coated with different combinations of dyes (see experimental section). A series of mixtures of N 719 and **14** with wt/wt% 3 : 1, 1 : 1 and 1 : 3 at concentrations of 10<sup>-5</sup> mol l<sup>-1</sup> were prepared and tested in solar cells along with pure N 719 and pure **14** as dyes. All the dye compositions were prepared in a mixture of acetonitrile / *tert*.butanol (1 : 1 v/v) and the substrates were coated by immersing in the dye solutions for 18 hours under controlled atmosphere in a flow box and carefully washing away the non-chemisorbed dye with absolute ethanol.

The UV-Vis spectra of all dye compositions in solution with concentrations of about 10<sup>-5</sup> mol l<sup>-1</sup> and as chemisorbed on the TiO<sub>2</sub> surface were measured. Both in solution and chemisorbed on TiO<sub>2</sub>, the new dye **14** shows significantly higher (three to four times) optical density (OD) than that of the reference dye N 719 which can be explained with the high extinction coefficient of the new bifunctional dye (see above). But the absorption range of N 719 with an absorption edge of 650 nm is much broader than that of dye **14**. In solution as well as in the chemisorbed state, the absorption spectra of the dye mixtures are roughly linear combinations of the individual components, the measured values being actually a little higher than the theoretical linear combinations which are not shown here. Thus a good compromise between the higher OD of **14** over N 719 and a better absorption range of N 719 over **14** was achieved in the 1:1 mixture co-modification case. The UV-Vis absorption spectra in solution and the OD of samples as chemisorbed on

TiO<sub>2</sub> are given in Figure 3-7 and Figure 3-8 for the cases pure **14**, 3 : 1 (**14** : N 719), 1 : 1 (**14** : N 719), 1 : 3 (**14** : N 719) and pure N 719. The dye-coated TiO<sub>2</sub> substrates were then coated with hole conductor (spiro-OMeTAD) and gold electrodes were deposited on top via vapour deposition.

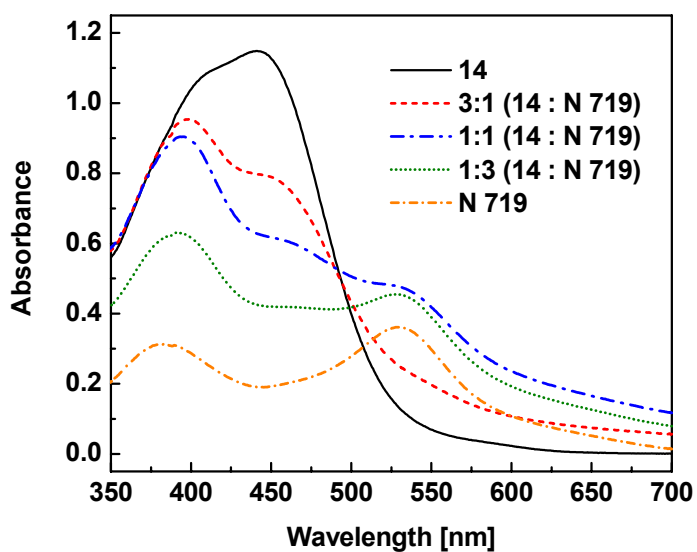


**Figure 3-7:** Absorption spectra of pure standard dye N 719, the co-modifications 3 : 1 (**14** : N 719), 1 : 1 (**14** : N 719), 1 : 3 (**14** : N 719) and pure **14** recorded in solution.

The solar cells were characterized by current (I) - voltage (U) measurements using a white light source with intensity of 77 mW/cm<sup>2</sup> under AM 1.5 solar spectral conditions. The current-voltage characteristics are given in Figure 3-9 and Figure 3-10 and the comparative photovoltaic parameters like short-circuit current ( $I_{SC}$ ), open-circuit voltage ( $U_{OC}$ ), fill factor (FF) and power conversion efficiency ( $\eta$ ) are tabulated in Table 3-2.

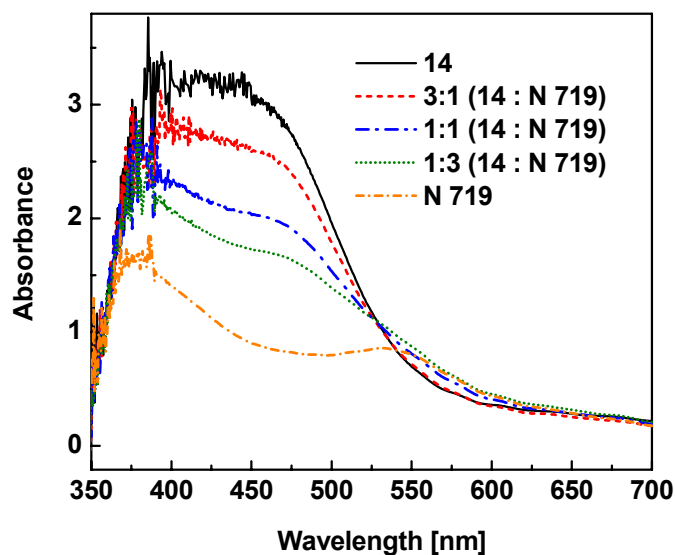


**Figure 3-8:** Absorption spectra of TiO<sub>2</sub> layers coated with monomolecular layers of dye chemisorbed from 10<sup>-5</sup> M solutions of pure standard dye N 719 and the co-modifications 3 : 1 (**14** : N 719), 1 : 1 (**14** : N 719), 1 : 3 (**14** : N 719) and pure **14** (thickness of the TiO<sub>2</sub> layers: 3 μm).

As it is evident from Figure 3-9 the short circuit current I<sub>SC</sub> of a standard dye-sensitized solar cell having N 719 dye is improved dramatically by using the 1 : 1 co-modification of the dyes **14** and N 719.

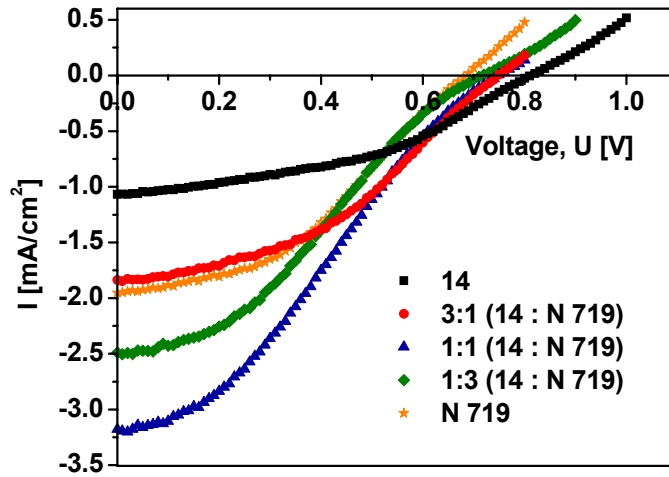


**Figure 3-9:** Current-voltage characteristics for standard solar cell with pure N 719 and solar cells modified with different amounts of 14.

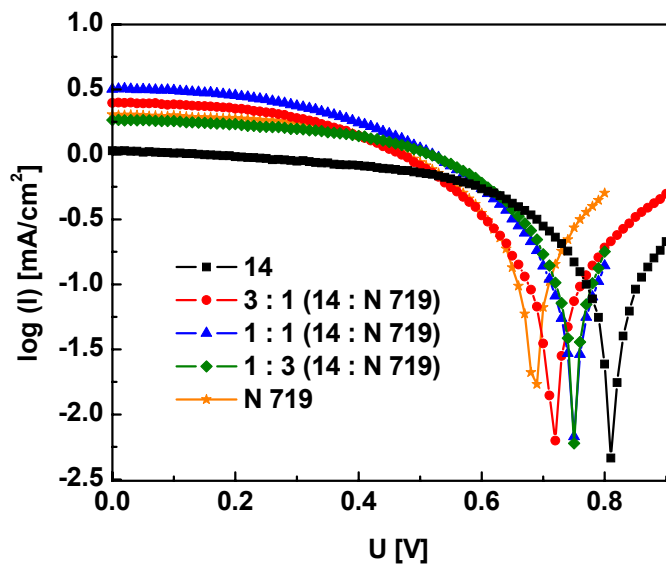


**Figure 3-10:** Semi-logarithmic plots for standard solar cell with pure N 719 and solar cells modified with different amounts of 14.

An increase in  $I_{SC}$  of about 60 % from 1.95 mA/cm<sup>2</sup> to 3.2 mA/cm<sup>2</sup> with 1 : 1 co-modification was achieved. A further increase in concentration of **14** replacing N 719 in dye-sensitized TiO<sub>2</sub> solar cells seems to have adverse effect for the current due to decrease in the absorption range as can be seen by the lowering of  $I_{sc}$  values for modification-case 1 : 3 and finally using pure dye **14** only.

Taking into consideration the high reproducibility of these results the improvement could be attributed to one or more of the following reasons: a) The enhanced hole transfer between the dye and the hole transport layer at the dye/HTL interface, b) improvement in retardation of back transfer of electrons from TiO<sub>2</sub> to dye due to spatial separation of the hole cation centre away from the TiO<sub>2</sub> interface and c) improved adhesion and wetting of hole conductor, spiro-OMeTAD, onto the dye-coated TiO<sub>2</sub> due to the presence of TPA antenna groups in **14**.

**Table 3-2:** Photovoltaic parameters of solar cells prepared using different dye compositions (white light source, AM 1.5, 77 mWcm<sup>-2</sup>).

dye composition N 719 : 14	$I_{sc}$ [mA]	$U_{oc}$ [V]	FF [%]	$\eta$ [%]
N 719	1.95	645	40	0.70
3 : 1	2.49	720	33	0.76
1 : 1	3.18	755	51	1.63
1 : 3	1.84	750	41	0.73
14	1.07	810	42	0.48

In the case of open-circuit voltage  $U_{OC}$ , there should be a linear increase on replacing more and more of N 719 with **14** if there is really a decrease in recombination at the interface due to a fast transfer of the hole from dye to the hole transport layer. Also the increase in HOMO value of the hole conductor triphenylamine (5.4eV) compared to the

spiro-MeOTAD (4.91eV) may cause an increase in  $U_{OC}$ , if TPA attached to the Ru(II) dye acts as the first instance of hole transfer. This is because the maximum value of  $U_{OC}$  is defined as the difference between the HOMO level of the hole conductor and LUMO level of the electron transport layer. This is fully supported by the results shown in Figure 3-10 where a continuous, almost linear increase of  $U_{OC}$  values with increasing amounts of **14** can be observed. Since  $I_{SC}$  of a solar cell is the consequence of its corresponding absorbance and incidental photon-to-current conversion efficiency (IPCE or external quantum efficiency), we also measured the IPCE values for cells with all five dye compositions for a better understanding of the fundamental process of photoinduced charge separation. A selected number of curves are plotted in Figure 3-11. It is obvious that two positive factors such as broad absorption in N 719 and high optical density in **14** results in dramatic improvement in IPCE as well for the 1:1 co-modification.

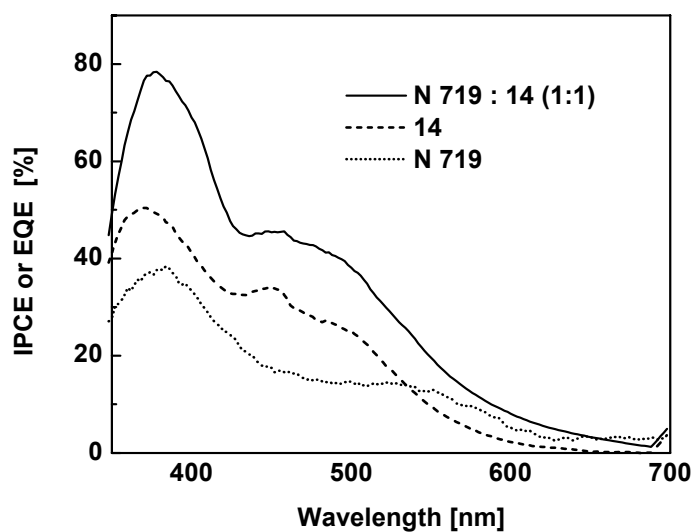


*Figure 3-11: IPCE or external quantum efficiency (EQE) for cells with and without interface modification with bifunctional compound **14**.*

In absolute values, the external quantum efficiency is almost doubled for the whole absorption range from 360 to 500 nm and reaches a remarkable value of about 80 % at the highest absorption peak of 380 nm and more than 40 % at around 500 nm. As pointed out above, the cell with 1:1 co-modified dye interface shows the best results for IPCE and absorbance and exhibit a power conversion efficiency of 1.63 % with corresponding  $I_{SC}$  of  $3.2 \text{ mA/cm}^2$ ,  $U_{OC}$  of 755 mV and a fill factor of 51 % as measured under AM 1.5 solar spectral conditions using a white light intensity of  $77 \text{ mW/cm}^2$ . The high degree of reproducibility observed in Figure 3-12 is an evidence for the control in preparation of each layers of such a complex multi-layer solar cell.

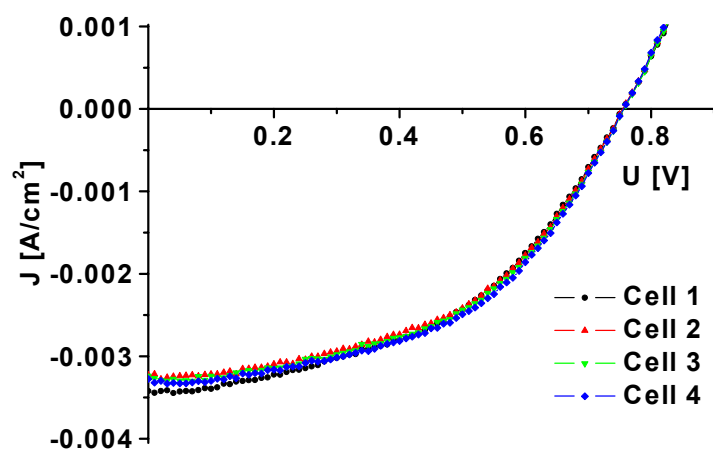


**Figure 3-12:** Current ( $I$ )-voltage ( $U$ ) characteristics for four cells prepared on a single substrate with 1:1-co-modification of the dye layer.

### 3.5.3 Transient absorption spectroscopy

One of the limiting processes in dye-sensitized  $\text{TiO}_2$  solar cells is the recombination of photoinduced electrons injected into  $\text{TiO}_2$  with holes in the dye centre or hole conductor.

In order to improve device function of a solar cell and thus power conversion efficiency it is of great importance to prevent recombination mechanisms. A strategy to reach this goal is the appropriate design of new sensitizing dyes in a way that recombination processes are retarded enabling charge separation of electrons and holes into TiO<sub>2</sub> and spiro-OMeTAD respectively<sup>87</sup>. In the previous section the application of the novel dye **14** in dye-sensitized TiO<sub>2</sub> solar cells is described and a remarkable improvement of all photovoltaic parameters was observed. This fact suggested that the concept of the design of bifunctional dye **14** may lead to a retardation of the back transfer of electrons from TiO<sub>2</sub> to the positive dye centre by spatial separation of the dye cation centre away from TiO<sub>2</sub> and avoiding recombination. For this reason the charge recombination dynamics of both novel dyes **14** and **15** were investigated by photoinduced transient absorption spectroscopy. This method provides the possibility of measuring the time resolved change of absorbance of the dye cation ( $\Delta mOD$ ) generated by laser excitation. The charge recombination dynamics of **14** and **15** were obtained from transient absorption spectroscopy carried out by James Durrant and co-workers (Imperial College, London, UK). The new bifunctional dyes **14** and **15** were chemisorbed onto TiO<sub>2</sub> surface before measurements were performed under pulsed laser excitation at a wavelength of 450 nm at ambient conditions. Figure 3-13 shows the transient absorption spectra observed for the new bifunctional dye **14** chemisorbed on TiO<sub>2</sub> with and without the hole conductor spiro-OMeTAD spincoated on top. For the bifunctional dye **14** coated on TiO<sub>2</sub> without spiro-OMeTAD two broad absorption bands can be detected at 560 nm and 877 nm. These spectral features can be assigned to the formation of the Ru-dye cation (877 nm) and the cation of the TPA-ligand (560 nm) of the complex **14** respectively<sup>88</sup>.

---

<sup>87</sup> J. N. Clifford, G. Yahioglu, L. R. Milgrom, J. R. Durrant *Chem. Commun.* **2002**, 1260.

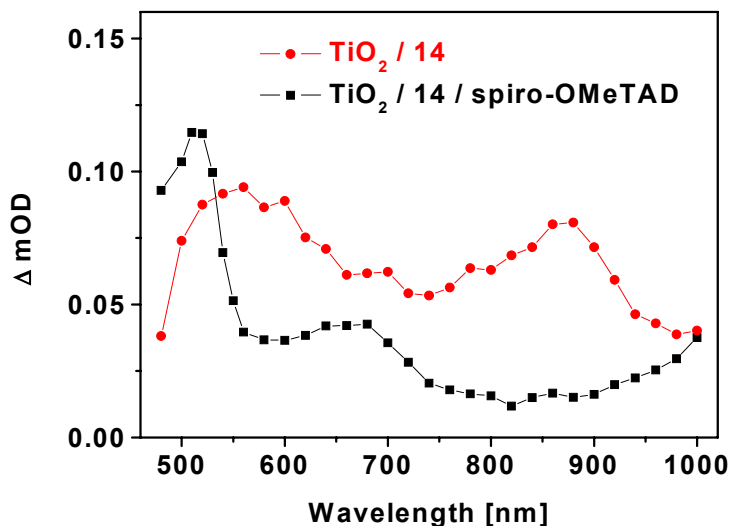


**Figure 3-13:** Transient absorption spectra of **14** adsorbed on TiO<sub>2</sub> (●) and **14** with spiro-OMeTAD spin-coated (■) all measured at a laser excitation wavelength of 450 nm at ambient conditions.

In contrast to this the spectrum of **14** coated on TiO<sub>2</sub> with the spiro-OMeTAD spin-coated on top exhibits a rather sharp absorption band at 520 nm referring to the spiro-cation. The signal of the Ru-cation is lost indicating a fast dye regeneration of approximately 84 % (estimated from transient absorption spectra using ratio of the peaks at 877 nm). In Figure 3-14 the recombination dynamics i. e. the decay curves of the cation at 900 nm of the new bifunctional dyes **14** and **15** are presented. From this graph it is possible to determine the decay half time  $t_{50\%}$  which is defined as time at which the decrease in optical density  $\Delta mOD$  has reached half of its initial value. According to the data obtained from Figure 3-14 the dye radical cations of **14** and **15** are exhibiting decay half times  $t_{50\%}$  of 0.35 ms and 5 ms respectively. In comparison to that N 719 and similar dyes adsorbed onto TiO<sub>2</sub> exhibit  $t_{50\%}$  of 0.06 – 0.8 ms depending on the nature of the ligands<sup>88</sup>.

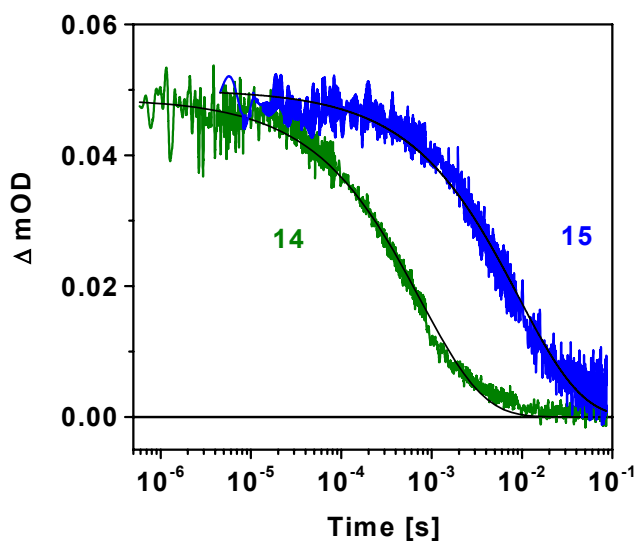


**Figure 3-14:** Charge recombination dynamics: Decay of the cations of **14** and **15** monitored at 900 nm following pulsed laser excitation sensitized  $\text{TiO}_2$  films sensitized with **14** and **15** at 450 nm; experimental data (green, blue) and exponential fits (black solid line).

A strong correlation between recombination dynamics and spatial separation of charges was observed by Durrant et al., suggesting a 10-fold increase in decay half-time  $t_{50\%}$  by increasing the distance of the positive centre in dye cation away from  $\text{TiO}_2$  by 3 Å<sup>88</sup>. Therefore the considerably long decay half times of both **14** and **15** and the enormous retardation of the recombination of the dye cation of **15** in comparison to **14** can be attributed to an increased distance of the positive centre of the dye cation away from the  $\text{TiO}_2$  electrode. In order to support this theory and to visualize the delocalization of the dye cation time dependent density functional theory (TD-DFT) ab-initio calculations have been performed in the group of Durrant. These measurements made clear that the HOMO orbitals of bifunctional dye **14** are delocalized over the bipyridine group and the TPA units with a distance of  $\sim 10.8$  Å from the  $\text{TiO}_2$  surface (Figure 3-15).

<sup>88</sup> J. N. Clifford, E. Palomares, M. K. Nazeerudin, M. Graetzel, J. Nelson, X. Li, N. J. Long, J. R. Durrant *J. Am. Chem. Soc.* **2004**, 126, 5225.

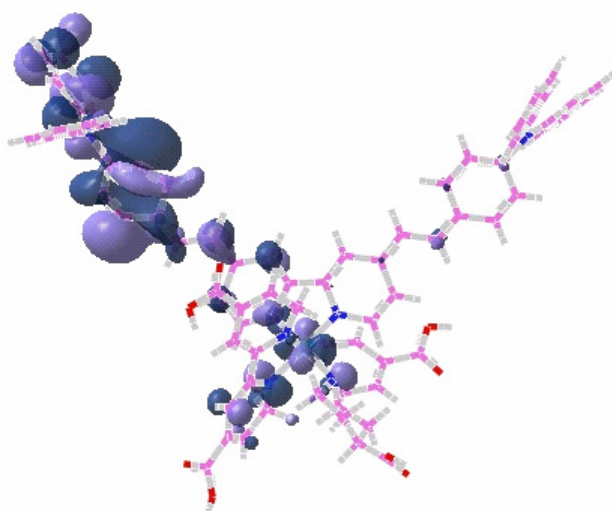


**Figure 3-15:** Graphical representation of the HOMO orbital of Ru-centred bifunctional dye **14** as determined from the TD-DFT *ab-initio* calculations.

An even higher value for this distance was determined for dye **15** with the delocalization of the dye cation HOMO orbitals over the the TPA moieties with a distance of  $\sim 15.6$  Å (Figure 3-16). The distances of the dye radical cation of N 719 (10.2 Å) and similar dyes are much shorter<sup>88</sup> which is suggesting that the goal to prepare new bifunctional dyes for spatial separation of charges reported in this work has been reached.

Taking all these results into account the improvement of photovoltaic parameters in dye-sensitized *nc*-TiO<sub>2</sub> solar cells applying **14** as interface modification agent can be explained not only with to the high extinction coefficient reported before but also with the increased spatial separation of the dye radical cation and consequently the suppression of charge recombination in this device. The application of bifunctional dye **15** in solar cells seems to be very promising and might be tested in the future.

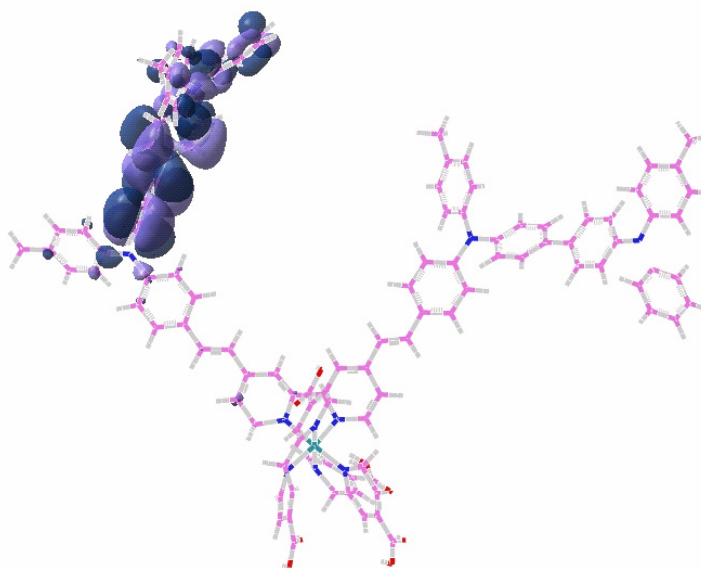


**Figure 3-16:** Graphical representation of the HOMO orbital of Ru-centred bifunctional dye **15** as determined from the TD-DFT ab-initio calculations.

As described in the sections above two new bifunctional materials **14** and **15** were synthesized carrying triarylamine units as hole transport functionality as well as Ru(II) centre for light absorption. Both these dyes exhibit higher  $\epsilon$  values compared to standard dyes used in solar cells. The compound **14** was successfully tested in dye-sensitized TiO<sub>2</sub> solar cells resulting in an increase of efficiency by 100 %. Transient absorption spectroscopy of **14** results in a decay half-time  $t_{50\%}$  of 0.35 ms. The decay half-time  $t_{50\%}$  of compound **15** was 5 ms – which is more than a 10-fold increase in comparison to the value obtained for bifunctional dye **14**. TD-DFT ab-initio calculations proved the spatial separation of the dye radical cation of **14** and **15** away from the TiO<sub>2</sub> surface with distances being  $\sim 10.8$  Å and  $\sim 15.6$  Å.

## 4 Bifunctional polymers carrying Ruthenium (II) core and poly(vTPA) chains

*In this chapter the synthesis of bifunctional polymers carrying Ru(II)-tris(bipyridine) dye core in poly(4-vinyltriphenylamine) chains is reported. The synthetic strategy involves the technique of atom transfer radical polymerization (ATRP) starting from 4,4'-bis(chloromethyl)-2,2'-bipyridine (3) as initiator. With this method 4-bromostyrene could be polymerized in a controlled way followed by polymeranalogous amination reaction to obtain bipyridine-centered poly(4-vinyltriphenylamine) (17). With bis(bipyridine)Ru(II) precursors reported in chapter 3 it is possible to perform a metallation reaction on the new polymers resulting in a tris(bipyridine)Ru(II)-centered hole-transport polymer (18). The application of these new materials in solar cells could help to achieve a spatial separation of hole and electron at the dye-HTL interface. Charge recombination can thus be retarded and the performance of dye-sensitized TiO<sub>2</sub>-solar cells can be improved. To verify this theory time resolved absorption spectra were measured and the results are given in this chapter.*

It has been shown that the concept of copolymerization of different functional monomers is a simple way of incorporating two different material functions into a polymer chain<sup>89,90,91,92</sup>. But in random copolymerization there is no control of polymer architecture and molecular weight. Also a well defined interface between the two functional domains is not present in the bulk due to lack of phase separation of the functional domains. On the other hand living polymerizations and controlled radical polymerizations deliver homopolymers and block copolymers with a low polydispersity which favour nanoscale phase separation between two functional domains. Thus it is possible to define the interface between the two functionalities exactly by attaching the two different functional moieties by a covalent bond. Moreover there may be the chance to manipulate the interface formation between these two moieties using intrinsic polymeric properties like phase separation and aggregation in block copolymers<sup>93,94</sup>.

Some attempts in this regard have been successfully tried out by Hadziioannou et al. by developing bifunctional diblock copolymers carrying para(phenylenevinylene) and fullerene units<sup>95</sup>. For successful exploitation of the nanoscale morphology which creates the desired large internal interface and in turn guarantees charge separation at these internal interfaces, as for example in a solar cell, a good control of the building up of phase domains of the block copolymer is required. In the specific case of a dye sensitized TiO<sub>2</sub>-solar cell in which Ruthenium(II) dye is chemisorbed onto TiO<sub>2</sub>-surface and a triphenylamine derivative functions as the hole conductor, the interface between the chemisorbed monomolecular dye-layer and hole conductor is very crucial for the charge

---

<sup>89</sup> a) W. Y. Ng, W. K. Chan *Adv. Mater.* **1997**, 9, 716; b) P. K. Ng, X. Gong, W. T. Wong, W. K. Chan *Macromol. Rapid. Commun.* **1997**, 18, 1009-1016.

<sup>90</sup> M. Suzuki, S. Kobayashi, S. Uchida, M. Kimura, K. Hanabusa, H. Shirai *Macromol. Chem. Phys.* **1998**, 199, 937-943.

<sup>91</sup> L. Trouillet, A. De Nicola, S. Guillerez *Chem. Mater.* **2000**, 12, 1611-1621.

<sup>92</sup> M. Thelakkat, P. Pösch, H.-W. Schmidt *Macromolecules* **2001**, 34, 7441.

<sup>93</sup> S. A. Jenekhe, X. L. Chen *Science* **1999**, 283, 372.

<sup>94</sup> G. N. Tew, M. U. Pralle, S. I. Stupp *Angew. Chem.* **2000**, 112, 527.

<sup>95</sup> U. Stalmach, B. de Boer, C. Videlot, P.F. van Hutten, G. Hadziioannou *J. Am. Chem. Soc.* **2000**, 122, 5464.

separation and transport<sup>96</sup>. The state of the art preparation of this interface is just by spin coating of a solution of the hole conductor onto the dye surface. This causes insufficient contact between dye and hole conductor which leads to low performance of the cell. One way to overcome this problem is to use additional bifunctional / bipolar compatibilizers which bridge the interface between dye and hole conductor. A chemical approach to solve this problem is to bind the dye with hole transport polymers and use such bifunctional systems in combination with the conventional dyes and hole conductors.

The aim was to realize bifunctional polymers carrying a strongly absorbing polar dye unit attached to well defined polymer chains carrying charge transport moieties based on triaryl amines. The controlled polymerization of the monomer, vinyltriphenylamine (vTPA) using anionic polymerization<sup>97,98</sup> as well as by TEMPO (2,2,6,6-tetramethylpiperidinoxide)-mediated radical polymerization<sup>99</sup> is reported in literature. In order to obtain poly(vTPA) carrying a bipyridine unit in the middle, the synthetic strategy was designed that controlled polymerization starting from a bipyridine derivative was attempted. Fraser et al. has reported the atom transfer radical polymerization (ATRP) of styrene starting from bis(chloromethyl)bipyridine or from the corresponding ruthenium-complex as initiator to obtain poly(styrene) attached to a ruthenium core<sup>100</sup>. It is also possible to carry out ATRP of other substituted styrenes like 4-bromostyrene using conventional initiators like 1-phenylethylbromide as reported in literature by Matyjaszewski et al.<sup>68, 101</sup>.

---

<sup>96</sup> J. Krüger, R. Plass, L. Cevey, M. Piccirelli, M. Grätzel *Appl. Phys. Lett.* **2001**, 79, 2085.

<sup>97</sup> W. J. Feast, R. J. Peace, L. A. Sage, E. L. Wood *Polym. Bull.* **1999**, 42, 167.

<sup>98</sup> E. Bellmann, S. E. Shaheen, R. H. Grubbs, S. R. Marder, B. Kippelen, N. Peyghambarian *Chem. Mater.* **1999**, 11, 399.

<sup>99</sup> M. Behl, E. Hattemer, M. Brehmer, R. Zentel *Macromol. Chem. Phys.* **2002**, 203, 503.

<sup>100</sup> X. Wu, J. E. Collins, J. E. McAlvin, R. W. Cutts, C. L. Fraser *Macromolecules* **2001**, 34, 2812. X. Wu, C. L. Fraser *Macromolecules* **2000**, 33, 4053.

<sup>101</sup> J. Qiu, K. Matyjaszewski *Macromolecules* **1997**, 30, 5643.

In this work a combination of the above two concepts to polymerize 4-bromostyrene in bulk using bis(chloromethyl)bipyridine (**3**) as initiator in order to obtain two poly(4-bromostyrene) chains with well-defined molecular weights and low polydispersity attached to a bipyridyl unit was used. Then a Pd-catalyzed polymer analogous amination reaction was adopted on this macroligand (**16**) carrying two poly(4-bromostyrene) chains to convert the bromophenyl group into triphenylamine moiety resulting in 4,4'-bis[poly(4-vinyltriphenylamino)methyl]-2,2'-bipyridine (**17**). In a final step, the bipyridine moiety in **17** was complexed with bis(bipyridyl) Ru(II) precursors to obtain a highly polar dye functionality covalently bound to two hole transport polymer chains of vinyltriphenylamine (**18**). The synthetic strategy is schematically outlined in Figure 4-1. Although the direct polymerization of the 4-vinyltriphenylamine monomer using **3** as initiator was feasible, this route was not favoured due to lack of reproducibility in the control of polymerization under the conditions that we used.

The following chapter describes the details of synthetic strategy, characterization and different physical properties of a series of metal-free macroligands and its Ru(II) polymer complexes having variable chain length of either poly(4-bromostyrene)s or poly(vinyltriphenylamine)s.

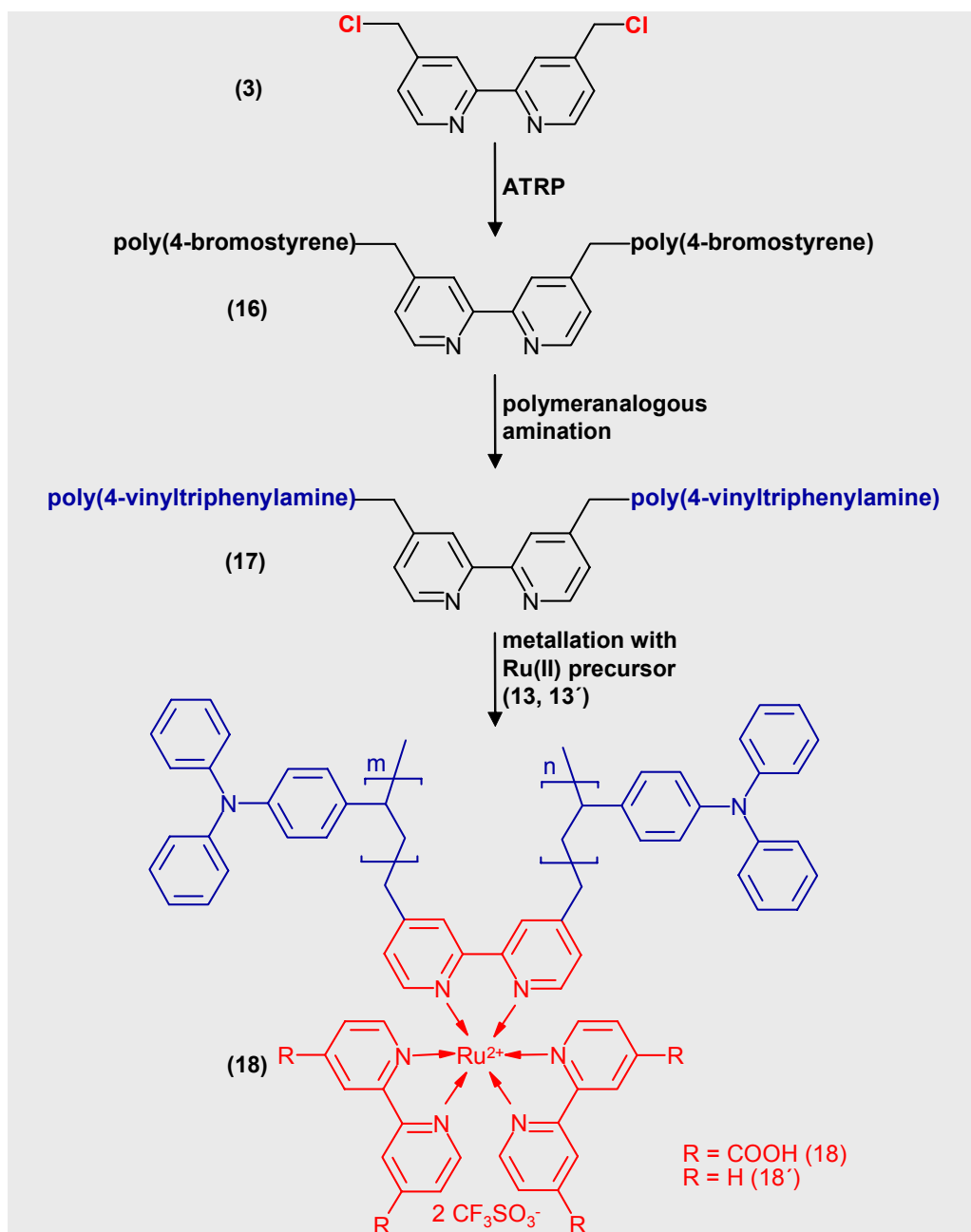


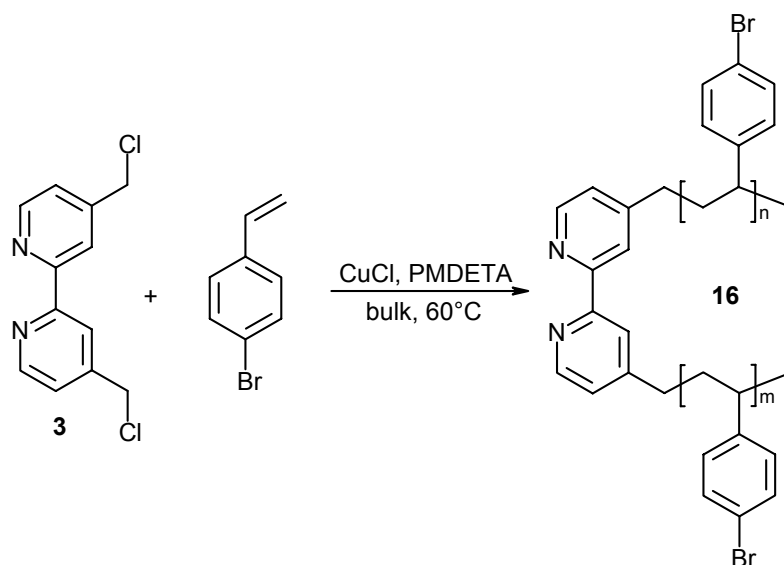
**Figure 4-1:** Schematic representation of the synthetic strategy for the preparation of bifunctional polymers carrying poly(vTPA) chains and Ru(II) dye centre (**18**).

## 4.1 Synthesis and characterization of 4,4'-bis[poly(4-bromostyryl)methyl]-2,2'-bipyridine (**16 a – f**)

At the very beginning of this work the concept of ATRP in bulk using the bipyridine derivative **3** as initiator was tested with styrene in bulk at 110 °C. In ATRP usually bipyridine derivatives are used as ligands and phenyl ethylbromide or esters substituted with an halide in  $\alpha$ -position as initiators<sup>101</sup>. Fraser et al. have also used **3** as initiator for ATRP. In the first experiments it was found, that using 4,4'-nonyl-2,2'-bipyridine ligands as reported in literature did not lead to well defined polymers and control in polymerization of styrene. But it could be confirmed that, as Fraser and co-workers have shown, 4,4'-bis(chloromethyl)-2,2'-bipyridine **3** in combination with a catalytic system very similar to CuCl / PMDETA (1,1,4,7,7-pentamethyldiethylene triamine) can be used to polymerize styrene in a controlled way<sup>102</sup>. The reported catalytic system was tested for styrene as monomer and the combination CuCl / PMDETA was found to result in controlled proceeding of the polymerization of styrene yielding polymers with defined molecular weights and appreciably low polydispersities. Similarly 4-vinyltriphenylamine was tested as monomer in combination with **3** as initiator in order to get a hole transport polymer in a one step reaction. The reaction also applying **3** as initiator either did not proceed at all or resulted in non-reproducible results as presumably thermally initiated uncontrolled radical polymerization of the monomer has taken place. Therefore the idea to apply a monomer having a functional group which could be further converted to the desired functionality in a polymeranalogous reaction was tested. This approach also allows to convert the functional group with different hole transport moieties as well. The concept was successfully carried out using 4-bromostyrene as monomer, **3** as initiator and CuCl / PMDETA as catalytic system at 60 °C. The first step of the reaction as it is shown in Scheme 4-1 involves the controlled radical polymerization of 4-bromostyrene in bulk using CuCl / PMDETA as catalytic system.

---

<sup>102</sup> A. P. Smith, C. L. Fraser *Macromolecules* **2002**, 35, 594.



**Scheme 4-1:** Schematic representation of the polymerization of 4-bromostyrene via ATRP in bulk at 60 °C with **3** as initiator and CuCl / PMDETA as catalytic system. Molar ratio of the reagents [monomer] : [initiator] : [CuCl] : [PMDETA] = 150 : 1 : 1 : 2.

PMDETA acts as ligand for the  $\text{CuCl} \rightleftharpoons \text{CuCl}_2$  system thus making it soluble in the organic medium. The  $\text{Cu(I)} \rightleftharpoons \text{Cu(II)}$  system controls the equilibrium between active radical and dormant bromide species in the reaction mixture as discussed in the introduction part. The initiator **3** was synthesized from the corresponding 4,4'-(trimethylsilylmethyl) derivative **2** by a modified procedure of the CsF-method which is already described in section 3.2.1 and in detail in the experimental part.

The synthesis of a series of 4,4'-bis[poly(4-bromostyryl)methyl]-2,2'-bipyridines (**16**) was carried out in bulk in a sealed flask immersed into an oil bath maintained at 60 °C with the molar ratio of the reagents [monomer] : [initiator] : [CuCl] : [PMDETA] = 150 : 1 : 1 : 2. Monomer, copper salt and the ligand PMDETA were placed in an argon flushed three-neck flask and stirred for an hour to form the copper complex. Then the initiator was added and the mixture was degassed three times by the freeze-pump-thaw method described by Matyjaszewski et al.<sup>101</sup>.

To obtain polymers with defined molecular weights reaching from 2000  $\text{gmol}^{-1}$  up to  $\sim 30\,000\ \text{gmol}^{-1}$  a series of polymerization reactions were performed and each reaction was quenched after a definite reaction time by rapid cooling with liquid  $\text{N}_2$  and exposing the reaction mixture to air and the polymers **16** were precipitated in methanol or n-hexane. The aim was to obtain polymers with rather low molecular weight of about 2000  $\text{gmol}^{-1}$ . Only with low molecular weight polymers it is possible to obtain high dye contents within the polymer chain. But if the polymerization was terminated at low degrees of conversion there is a lot of monomer left which makes the precipitation of the product in methanol or n-hexane difficult. In this case it is important to remove the remaining monomer via high vacuum distillation to achieve a proper precipitation of the polymer. The resulting products had a light blue colour pointing out to the presence of copper salts left from the catalytic system. Residual copper salts can be removed by washing the bluish product successively with methanolic and aqueous  $\text{NH}_4\text{Cl}$ -solution<sup>103</sup> until the blue colour disappears. With this method the rest copper content could be reduced to 0.048 wt%, determined by elemental analysis of such a polymer after purification with  $\text{NH}_4\text{Cl}$ -solution. A series of polymerization of 4-bromostyrene was carried out for the different analysis, characterization and synthetic purposes and each batch of these polymers is named as **16 a – f**.

#### 4.1.1 GC analysis of ATRP of 4-bromostyrene

The method of ATRP belongs to the species of controlled polymerization reactions because it is satisfying the following criterium: Termination and transfer reactions can be neglected because the rate of the polymerization reaction is exceeding the rate of termination and transfer processes. For each new system of monomer, initiator and catalyst in ATRP kinetic studies have to be carried out to check the criteria described above. To verify the controlled nature of ATRP of 4-bromostyrene the first batch (**16a**) of polymerization reaction was performed and aliquots (**16a-1 – 16a-4**) were taken out from

---

<sup>103</sup> A. M. Kasko, A. M. Heintz, C. Pugh *Macromolecules* **1998**, 31, 256.

the reaction flask in definite time intervals. Via gas chromatography (GC) analysis the amount of unreacted monomer  $M_t$  contained in these samples was determined. Referring to the initial amount of monomer  $M_0$  at starting time  $t = 0$  the conversion was calculated using the following equation (Equation 8):

$$p = \frac{[M_0] - [M_t]}{[M_0]} \quad (\text{Equation 8})$$

$p$  = conversion

$[M_0]$  = initial monomer concentration at reaction time = 0

$[M_t]$  = monomer concentration at reaction time =  $t$

In Table 4-1 the conversions calculated from GC-data are outlined showing the increase of conversion with increasing reaction time.

**Table 4-1:** Conversion for definite reaction times determined via GC for aliquots **16a-1** – **16a-4** taken from ATRP of 4-bromostyrene with **3** as initiator and CuCl / PMDETA as catalytic system (molar ratio of reagents [monomer] : [initiator] : [CuCl] : [PMDETA] = 150 : 1 : 1 : 2).

polymer	time [min]	conversion
<b>16a-1</b>	60	0.156
<b>16a-2</b>	120	0.242
<b>16a-3</b>	180	0.279
<b>16a-4</b>	240	0.349

As there was no internal standard in this bulk polymerization a precise amount of anisole was added as external standard to an exactly determined sample weight. Before GC measurements the sample mixtures were diluted with THF.

In Figure 4-2  $\ln[M_0]/[M_t]$  also obtained from GC-measurements is plotted versus reaction time. The linear dependence of  $\ln[M_0]/[M_t]$  on time is suggesting that the rate of polymerization is much higher than the rate of termination reactions. Thus the controlled nature of ATRP of 4-bromostyrene in bulk at 60°C using **3** as initiator and CuCl / PMDETA as catalytic system was verified at least up to 40 % conversion, which was the range of interest for the preparation of low molecular weight polymers in this work.

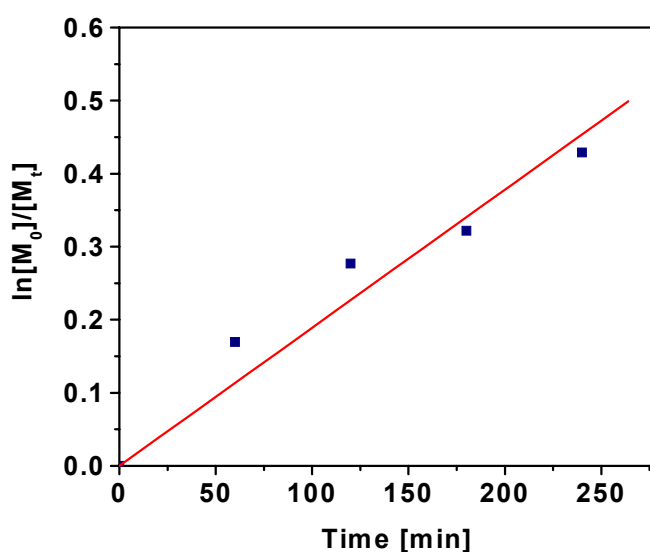


**Figure 4-2:** Dependence of  $\ln[M_0]/[M]$  on reaction time for aliquots **16a-1** to **16a-4**: ATRP of 4-bromostyrene in bulk at 60 °C ( $[M_0]$  = initial monomer concentration,  $[M_t]$  = monomer concentration after defined reaction time determined via GC analysis with anisole as external standard).

Shortly summarized it is obvious that the method described above offers an elegant way to produce “low molecular weight” polymers with defined chain lengths. By the use of the bipyridine initiator **3** for ATRP a bipyridine unit is incorporated in the polymer chain which can be metallated and the bromine substituents in the polymer chain can further be subjected to a polymeranalogous amination which will be discussed in the next sections.

The characterization of 4,4'-bis[poly(4-bromostyryl)methyl]-2,2'-bipyridines **16** was carried out using size exclusion chromatography as well as NMR spectroscopy. Especially SEC was important as long as this method could provide further data to verify the controlled nature of the polymerization reaction.

#### 4.1.2 Size exclusion chromatography (SEC)

To check the controlled nature of the polymerization, it was important to observe the time-dependence of the growth of molecular weight which was carried out via SEC. From the second reaction batch (**16b**) especially prepared for this purpose, aliquots were taken from the reaction flask at defined time intervals, the polymers were precipitated and analyzed via SEC. In Table 4-2 the SEC data of the polymer series **16b** are given. Figure 4-3 shows the monomodal elution curves of the polymers isolated from **16b-1** – **16b-5** and the graphical representation of the time dependence of molecular weight of the same polymers exhibiting linear behaviour.

**Table 4-2:** SEC data obtained at various time intervals for polymerization of 4-bromostyrene via ATRP in bulk at 60 °C using **3** as initiator and CuCl / PMDETA as catalytic system resulting in polymers **16b-1** – **16b-5**.

polymer	time [min]	M <sub>w</sub> [g/mol] <sup>a)</sup>	M <sub>n</sub> [g/mol] <sup>a)</sup>	PDI <sup>a)</sup>
<b>16b-1</b>	60	2240	1710	1.31
<b>16b-2</b>	120	3100	2340	1.33
<b>16b-3</b>	240	6290	4500	1.40
<b>16b-4</b>	300	8470	6070	1.40
<b>16b-5</b>	360	10810	7590	1.42

a) Determined via SEC with THF + 0.25 wt% TBAB as eluent, calibration versus polystyrene standards.

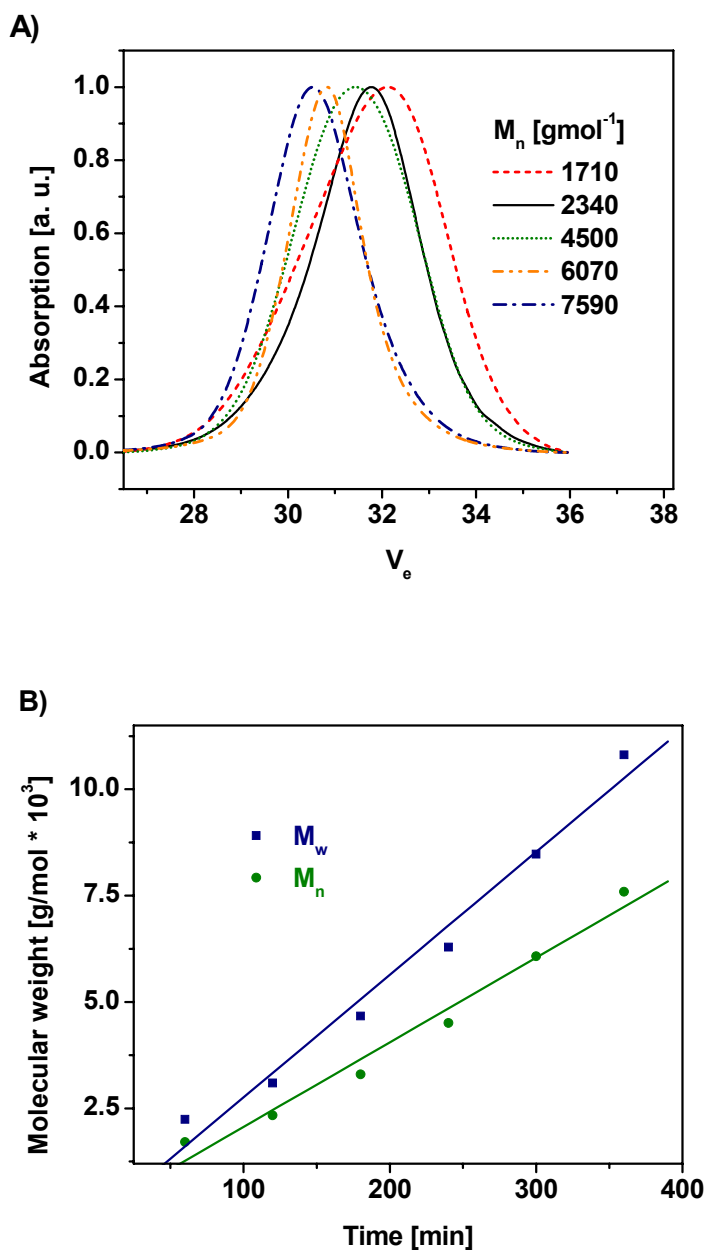


**Figure 4-3:** A) SEC elution curves for the series of polymers **16b-1** – **16b-5** with increasing molecular weights (THF + 0.25 wt% TBAB as eluent, calibration with polystyrene standards). B) Dependence of  $M_n$  and  $M_w$  on time for ATRP of 4-bromostyrene in bulk at 60 °C.

The eluograms as well as the data obtained for the **16b**-series show a constant increase in molecular weight with time. Both  $M_n$  and  $M_w$  exhibit a linear dependence on reaction time which is a measure of conversion. From these values the time to terminate the polymerization can be chosen to obtain a defined molecular weight of the desired polymer. Taking into account that the aim of this synthetic strategy is to prepare Ru(II) dyes carrying smaller chains of polymers in the end, the polymers with less repeating units are of more interest in this work. With less repeating units and less molecular weight the dye content will be higher in the end-product making the material more interesting for the application in dye-sensitized solar-cells.

It has to be noted that the polymers resulting from **16a** and **16b** were only prepared to obtain analytical data for the polymerization of 4-bromostyrene applying the system reported above. The 4,4'-bis[poly(4-bromostyryl)methyl]-2,2'-bipyridines **16c** – **16f** were used for further conversion to achieve Ru(II) centered hole transport polymers carrying TPA units and are listed in Table 4-3.

### 4.1.3 NMR-spectroscopy

4,4'-bis[poly(4-bromostyryl)methyl]-2,2'-bipyridines (**16a** – **f**) were characterized using  $^1\text{H}$ -NMR-spectroscopy. The spectra of all these polymers are very similar exhibiting the same characteristic signals. As an example the  $^1\text{H}$ -NMR spectrum of polymer **16f** ( $M_n = 26610 \text{ g mol}^{-1}$ ) will be discussed here (see Figure 4-4). For comparison, the spectrum of the monomer 4-bromostyrene is plotted in Figure 4-4 as well.

The proton NMR-spectra of **16f** was recorded in deuterated chloroform ( $\text{CDCl}_3$ ) and exhibits broad signals with low or even without resolution typical for polymers. Two doublets are present in the low field region at 6.29 ppm and 7.16 ppm respectively representing the 4 protons of the AA'XX' - spin system of the para-substituted aromatic ring of the 4-bromostyrene monomer unit. The polymer backbone is visible in a broad signal in the alkyl region from 1.25 ppm to 1.56 ppm showing an integral of 3 protons compared with the aryl resonance signals.

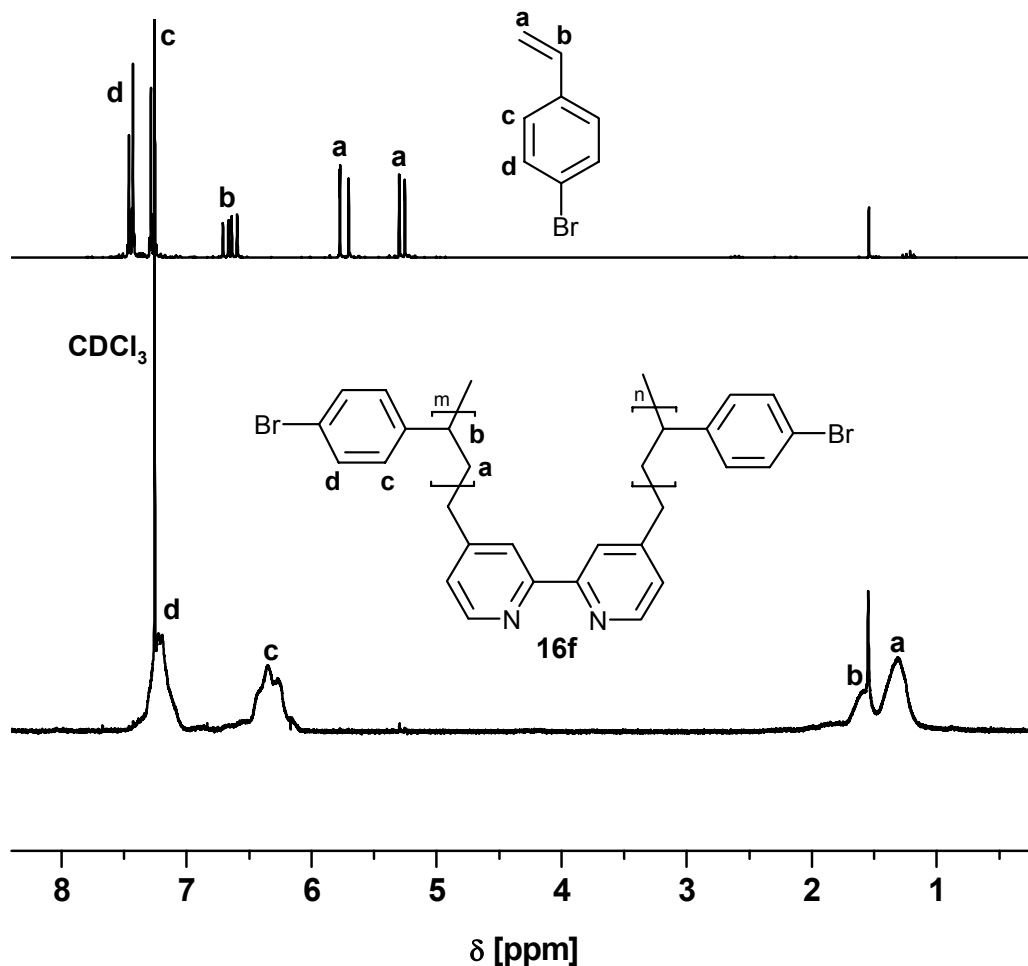


**Figure 4-4:**  $^1\text{H-NMR}$  spectra of polymer **16f** ( $M_n = 26610 \text{ g mol}^{-1}$ ; 144 repeating units) and 4-bromostyrene recorded in  $\text{CDCl}_3$  (250 MHz, 298 K).

The resonance signals of the bipyridine protons are hardly visible in the  $^1\text{H-NMR}$  spectrum of **16f** because the weight fraction of those within the polymer chain is insufficient for the detection. However, in polymer **16d** exhibiting lower molecular weight broad singlets at 8.03 ppm and 8.55 ppm could be detected which can be referred to protons of the bipyridine centre of the polymer chain.

## 4.1.4 Thermal properties: DSC and TGA

The thermal properties of the series **16 c – f** of 4,4'-bis[poly(4-bromostyryl)methyl]-2,2'-bipyridines have been characterized by Differential Scanning Calorimetry (DSC) and Thermo-Gravimetric Analysis (TGA). The data obtained by these measurements are summarized Table 4-3.

**Table 4-3:** Molecular weights and thermal properties of different 4,4'-bis[poly(4-bromostyryl)methyl]-2,2'-bipyridines (**16 c -f**) prepared via ATRP in bulk at 60 °C using **2** as initiator and CuCl / PMDETA as catalytic system.

polymer	$M_n$ [g/mol] <sup>a)</sup>	$M_w$ [g/mol] <sup>a)</sup>	PDI <sup>a)</sup>	$T_g$ [°C] <sup>b)</sup>	$T_{onset}$ [°C] <sup>c)</sup>
<b>16c</b>	2080	2890	1.39	104.7	230
<b>16d</b>	3107	4816	1.55	112.2	226
<b>16e</b>	10340	15322	1.48	126.8	236
<b>16f</b>	26610	31481	1.18	135.6	233

a) Determined with SEC with THF + 0.25 wt% TBAB as eluent, calibration versus polystyrene standards, UV-detection,  $PDI = M_w/M_n$ ; b) determined with DSC with heating / cooling rate of 10 Kmin<sup>-1</sup>; c) defined as temperature at which weight loss is starting; determined with TGA via heating from 30 to 650 °C with 10 Kmin<sup>-1</sup>.

The absence of any melting or recrystallization peaks in DSC points towards the amorphous nature of polymers **16 c – f**. In all cases, glass transitions were evident in the DSC-curves: The glass transition temperatures  $T_g$  of polymers **16 c – f** range between 104.7 °C for **16c** which exhibits the lowest molecular weight and 135.6 °C for **16f** which represents the polymer with the highest molecular weight in this series. A constant increase in  $T_g$  with molecular weight is recognizable in this series of 4,4'-bis[poly(4-bromostyryl)methyl]-2,2'-bipyridines.

All 4,4'-bis[poly(4-bromostyryl)methyl]-2,2'-bipyridines (**16c – f**) show appreciably good thermal stability having an onset of weight loss at temperatures around 230 °C.

## 4.2 Synthesis and characterization of 4,4'-bis[poly(4-vinyltriphenylamino) methyl]-2,2'-bipyridine (**17 c – f**)

In order to obtain a hole transport functionality the bromophenyl groups in polymers **16** were converted into triphenylamine moieties. For this purpose a method of Pd-catalyzed amination reaction with diphenylamine as coupling reagent was adopted. Similar reactions were reported to proceed smoothly and fast with a high degree of substitution using coupling reagents like carbazoles or phenazines<sup>104</sup>.

The general method of Pd-catalyzed amination reactions was intensively studied in the groups of Buchwald<sup>105</sup> and Hartwig<sup>106</sup> and it is known from literature that side reactions involving incorporation of phosphor and dehalogenation are possible if aryl halides containing electron-poor substituents are used. In order to avoid any undesired product and to obtain complete conversion in appreciably short periods, different combinations of Pd-catalysts and ligands were tested in model reactions of bromo benzenes with diphenylamine to find out the most efficient system. In this way it turned out that a combination of Pd(OAc)<sub>2</sub> and P(<sup>t</sup>Bu)<sub>3</sub> in the presence of NaO<sup>t</sup>Bu gave the best results with the reaction proceeding in extraordinarily short time of one to two hours. The Pd-catalyzed polymeranalogous amination reaction of the poly(4-bromostyrene) chains of macroligands **16 c – f** was carried out in a general procedure as shown in Scheme 4-2 and described in detail in the experimental part of this thesis. In this way poly(4-vinyltriphenylamine) carrying a bipyridine unit in the center could be obtained (**17 c – f**).

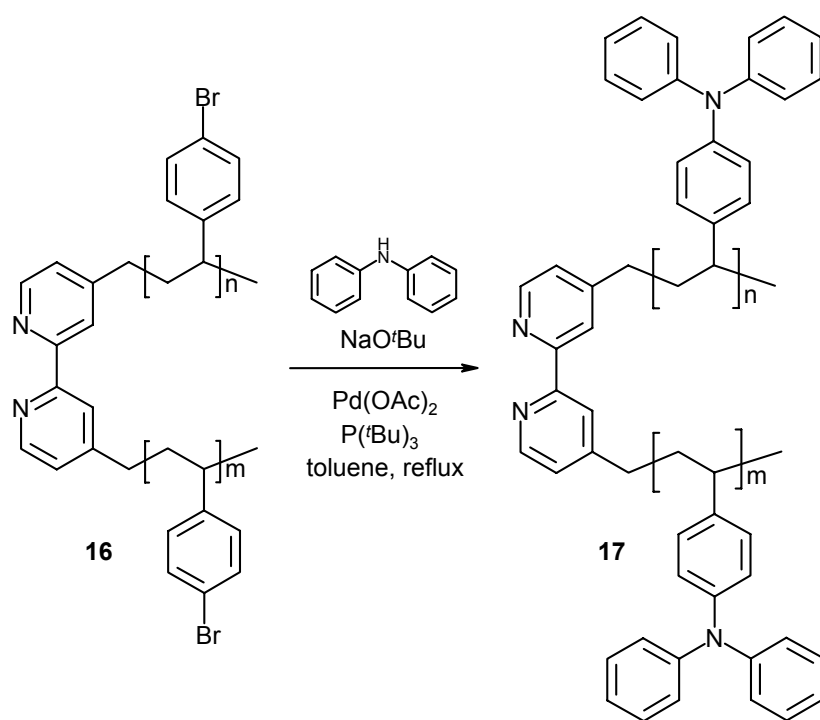
<sup>104</sup> T. Kanbara, Y. Yokokawa, K. Hasegawa *J. Polym. Sci.: Part A: Polymer Chemistry* **2000**, 38, 28.

<sup>105</sup> B. H. Yang, S. L. Buchwald *J. Organomet. Chem.* **1999**, 576, 125.

<sup>106</sup> F. E. Goodson, S. I. Hauck, J. F. Hartwig *J. Am. Chem. Soc.* **1999**, 121, 7527.

With the described catalytic system it was possible to achieve very high conversion of the aryl bromide to triphenylamine in less than two hours using the following procedure:

In a three-neck flask equipped with a condenser, an argon inlet and a septum the starting polymer and diphenylamine were dissolved in dry toluene. One after another the base NaO<sup>t</sup>Bu, the ligand P(<sup>t</sup>Bu)<sub>3</sub> and Pd(OAc)<sub>2</sub> were added. It must be noted that prior to use NaO<sup>t</sup>Bu has to be dried properly under vacuum at 110 °C. The ligand P(<sup>t</sup>Bu)<sub>3</sub> in toluene solution (1 g P(<sup>t</sup>Bu)<sub>3</sub> in 30 ml dry toluene) was stored under inert gas atmosphere and used as such making sure that water and oxygen is absolutely excluded. The reaction mixture was refluxed for 2 h before terminating the reaction. The working up procedure for further purification is also not very complicated.



**Scheme 4-2:** Schematic representation of the Pd-catalyzed polymeranalogous amination of 4,4'-bis[poly(4-bromostyryl)]-2,2'-bipyridine (**16**) with diphenylamine as coupling reagent and NaO<sup>t</sup>Bu, Pd(OAc)<sub>2</sub> and P(<sup>t</sup>Bu)<sub>3</sub> as catalytic system to yield 4,4'-bis[poly(4-vinyltriphenylamino)methyl]-2,2'-bipyridine **17**.

After cooling the reaction mixture to room temperature and filtration over alumina to remove the residual Pd, half of the solvent was evaporated and the poly(4-vinyltriphenylamine) (**17**) was precipitated in methanol.

Further reprecipitation from THF solution of the polymer into MeOH yielded about 90 % of the desired product. Thus **16 c – f** were converted into the corresponding 4,4'-bis[poly(4-vinyltriphenylamino)methyl]-2,2'-bipyridines **17 c – f** the characterization of which will be discussed here.

#### 4.2.1 NMR-spectroscopy

The polymeranalogous amination reaction was followed via NMR-spectroscopy and the spectra of 4,4'-bis[poly(4-bromostyryl)methyl]-2,2'-bipyridine **16f** and 4,4'-bis[poly(4-vinyltriphenylamino)methyl]-2,2'-bipyridine **17f** are both discussed here for comparison. The NMR-spectra of educt **16f** and product 4,4'-bis[poly(4-vinyltriphenylamino)methyl]-2,2'-bipyridine **17f** are given in Figure 4-5.

After about one hour of reaction, the signals of the aryl protons of polymer **16f** at 6.29 ppm and 7.17 ppm have completely disappeared. The new multiplets corresponding to triphenylamine protons appeared at about 6.5 – 7.0 ppm. As it is already described for polymers **16** the resonance signals of the bipyridyl protons are getting non-detectable with increasing molecular weight due to their low weight fraction within the polymer chain: For polymer **17d** broad singlets at 7.96 ppm and 8.29 ppm are indicating the bipyridine centre of the polymer chain whereas in **17f** the bipyridine protons could not be detected.

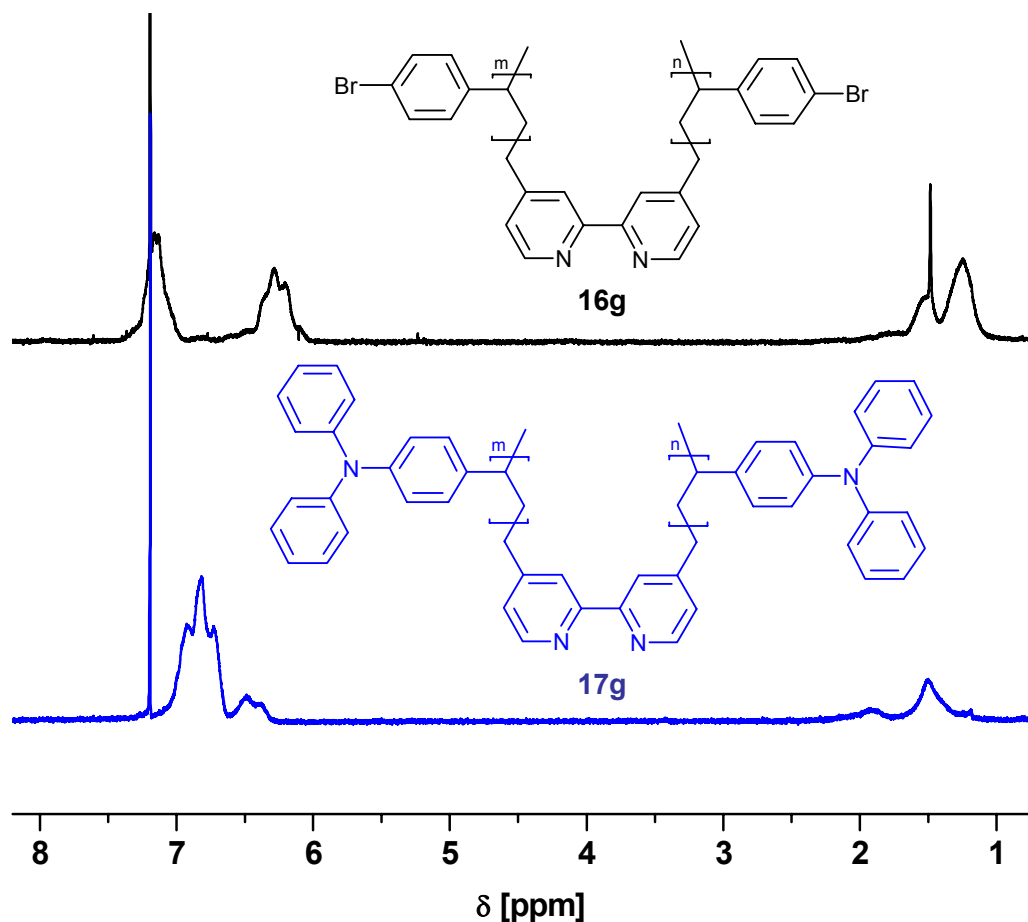


**Figure 4-5:** <sup>1</sup>H-NMR spectra of polymers **16f** and **17f** recorded in CDCl<sub>3</sub> (250 MHz, 298 K) showing the disappearance of the two broadened doublets from polymer **16f** (6.3 ppm, 7.2 ppm) and the appearance of the multiplets (6.5 – 7.0 ppm) corresponding to the aryl protons of polymer **17f** after about one hour of reaction.

Taking the results from the observation of the polymeranalogous reaction via NMR-spectroscopy into account it can be assumed that about 95 % of the amination reaction is complete after a reaction time of ca. one hour.

## 4.2.2 Elemental analysis

To compare the results obtained from NMR-spectroscopy about the conversion of **16** to **17**, an elemental analysis was carried out to determine the content of bromine in the resulting 4,4'-bis[poly(4-vinyltriphenylamino)methyl]-2,2'-bipyridine **17**. The conversion of polymer **16** to polymer **17** could be calculated from weight percentage of remaining bromine as determined by elemental analysis for a series of samples taken at different time intervals. An example how to calculate the conversion from elemental analysis results is given here: For polymer **16d** with a number average molecular weight  $M_n$  of 3107 g/mol, the number of repeating units was calculated as 16. This gives a theoretical weight of bromine as 41.2 wt%. The elemental analysis gave exactly the same value for bromine content and after 2 hours of polymer analogous reaction, the residual bromine content in the resulting 4,4'-bis[poly(4-vinyltriphenylamino)methyl]-2,2'-bipyridine **17d** was determined as 7.56 wt%, which corresponds to a conversion of 82 %. Thus the conversion for the polymeranalogous reaction for a polymer with higher molecular weight was monitored in the following. For this purpose a polymeranalogous reaction batch was prepared using **16f** with  $M_n = 26610$  g/mol as educt and samples were taken out at defined time intervals.

The 4,4'-bis[poly(4-vinyltriphenylamino)methyl]-2,2'-bipyridines isolated from these samples were investigated via elemental analysis to obtain the bromine content of each. For starting polymer **16f** with  $M_n = 22610$  g/mol (repeating units = 124, theoretical Br-content = 43.4 %) elemental analysis gave 43.9 % Br-content which is in close agreement with the theoretical value. The data of elemental analysis obtained for the described polymeranalogous amination reaction of polymer **16f** to **17f** are presented in Table 4-4. After a reaction time of 65 min the Br-content decreased to 7.20 wt% corresponding to a conversion of 84 % and after two hours of reaction, the residual bromine content was only 0.5 wt% which corresponds to 99 % conversion.

**Table 4-4:** Content of bromine determined via elemental analysis of samples taken out from a batch of polymeranalogous amination reaction at defined times using **16f** with  $M_n = 22610$  g/mol as starting polymer.

Time of conversion [min]	0	5	15	65	120
Br-content [wt. %]	43.9	30.0	21.3	7.2	0.5
conversion [%]	0	32	51	84	99

Figure 4-6 depicts the rest bromine content and the corresponding conversion in the samples taken out from the amination reaction (using **16f** as starting polymer) plotted against time of conversion resulting in an exponential behaviour as expected.

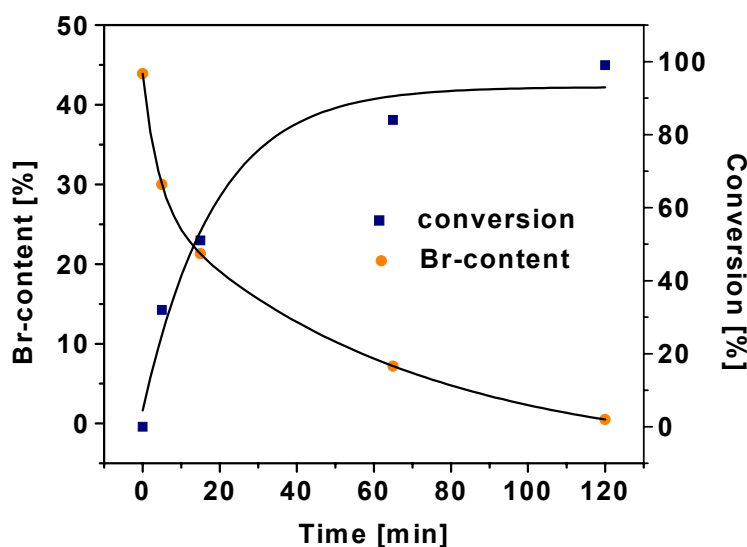


**Figure 4-6:** Plot of bromine content (weight percentage, ●) and corresponding conversion (■) determined from elemental analysis for polymer **17f** (starting from **16f**) at different time intervals of conversion. The solid lines represent the non-linear fits to the data points.

Considering the data from elemental analysis it is obvious that the polymer analogous reaction is completed within two hours yielding 4,4'-bis[poly(4-vinyltriphenylamino)methyl]-2,2'-bipyridine **17**.

#### 4.2.3 Molecular weight determination

The most common way of characterization of molecular weights via SEC turned out to be very difficult for 4,4'-bis[poly(4-vinyltriphenylamino)methyl]-2,2'-bipyridine (**17**). A comparison of the molecular weights of the new polymers **17** with **16** using a common SEC was not possible due to the difference in hydrodynamic volumes of these two classes of polymers and also due to lack of calibration standards for these new types of polymers. This results in low values of molecular weights for triphenylamine type polymers compared to precursor polymers **16** using the polystyrene calibration which does not reflect the reality. To overcome this problem, elution was also carried out in presence of added salts in THF or dimethylacetamide as solvent, but without any success. An alternative is to use MALDI-TOF MS analysis (see Figure 4-7).

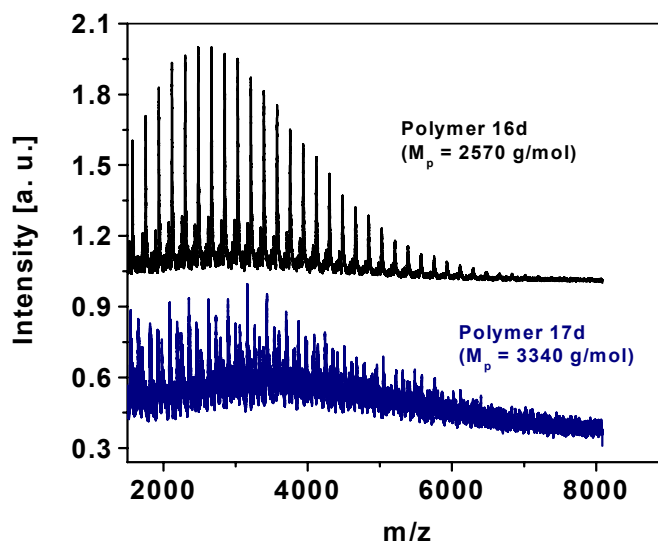


**Figure 4-7:** Comparison of MALDI-TOF mass spectra of polymers **16d** and **17d** (recorded with dithranol as matrix and Ag-triflate as additive).

As example MALDI-TOF MS was carried out for polymers **16d** and **17d** and the MALDI-TOF MS curves are given in Figure 4-7. The starting polymer **16d** has an  $M_n$ -value of 3107 g/mol as obtained from SEC. In MALDI-TOF MS measurement an  $M_n$  of 2720 g/mol was determined for polymer **16d** and  $M_n$  for polymer **17d** is 3350 g/mol. The peak molecular weights  $M_p$  for both polymers from MALDI-TOF MS are 2570 g/mol and 3340 g/mol. It can be seen obviously, that the two polymers **16d** and **17d** are monomodal and the difference in  $M_p$  between polymer **16d** and polymer **17d** corresponds to 92 % conversion for polymer amination reaction.

#### 4.2.4 Thermal analysis

4,4'-bis[poly(4-vinyltriphenylamino)methyl]-2,2'-bipyridines of the series **17c – f** having triphenylamine pendant groups exhibit thermal decay starting at about 225 °C and a glass transition temperature  $T_g$  at about 130°C - also for polymers with rather low molecular weight. A dependenc of  $T_g$  on molecular weight like it was recognized for polymers with structure **16** can not be ascertained for 4,4'-bis[poly(4-vinyltriphenylamino)methyl]-2,2'-bipyridines (**17**). No melting or recrystallization peaks were detected proving the amorphous structure of polymers **17**. The data obtained from thermal analysis via DSC and TGA are summarized in Table 4-5.

**Table 4-5:** Glass transition temperatures  $T_g$  and onset temperatures of thermal decay  $T_{onset}$  of polymers **17 c – f** determined via DSC and TGA.

polymer	<b>17c</b>	<b>17d</b>	<b>17e</b>	<b>17f</b>
$T_g$ [°C] <sup>a)</sup>	136.1	124.8	134.5	131.7
$T_{onset}$ [°C] <sup>b)</sup>	239	230	224	240

a) Heating / cooling rate = 10 Kmin<sup>-1</sup>; b) defined as temperature at which weight loss is starting; determined via heating from 30 to 650 °C with 10 Kmin<sup>-1</sup>.

#### 4.2.5 UV-Vis spectroscopy

The polymeranalogous reaction was also followed by UV-Vis spectroscopy exploiting the strong absorption maximum of triphenylamine derivatives at about  $\lambda_{\text{max}} = 305$  nm.

The absorption maxima of macroligand **16f** at 262, 270 and 278 nm have completely disappeared after about two hours of reaction time whereas the significant absorption maximum of 4,4'-bis[poly(4-vinyltriphenylamino)methyl]-2,2'-bipyridine **17f** appeared at  $\lambda_{\text{max}} = 305$  nm. The normalized absorption spectra of **16f** and **17f** are presented in Figure 4-8.

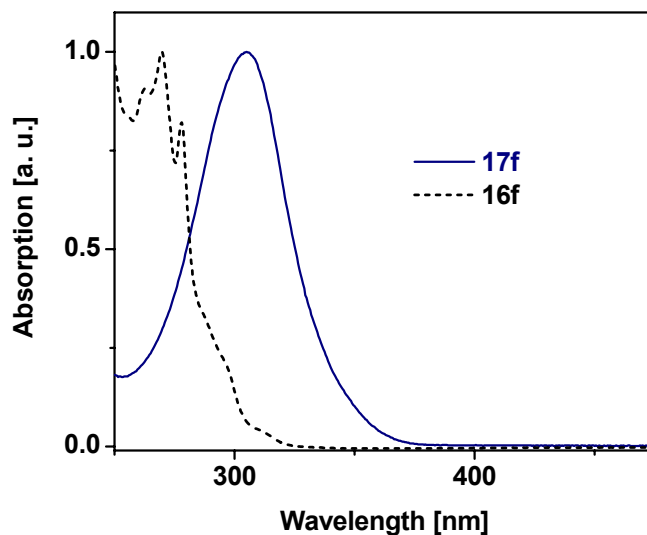


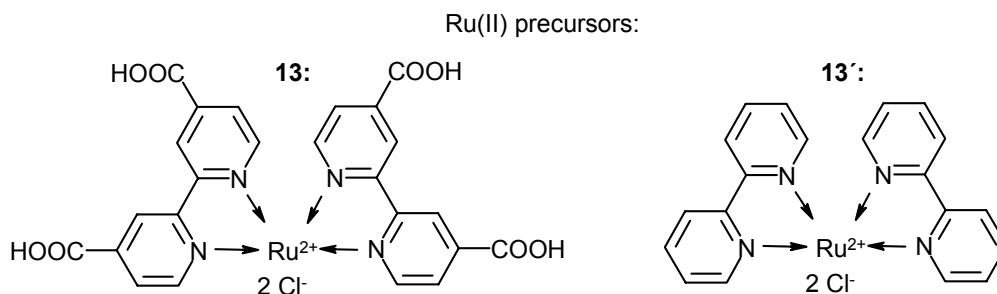
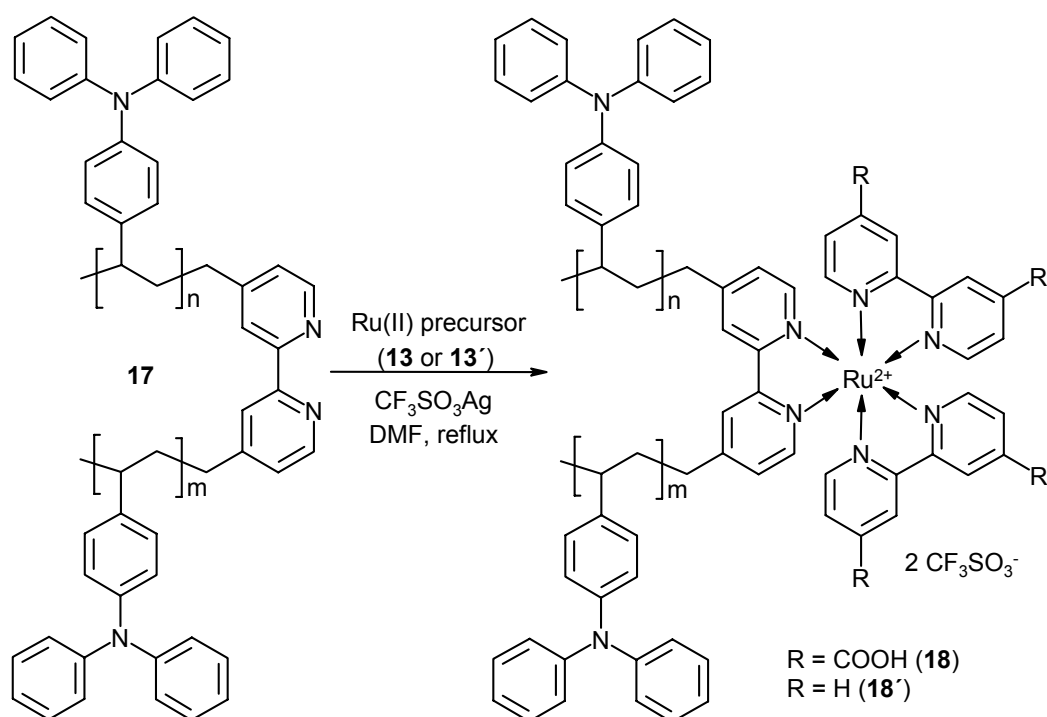
**Figure 4-8:** Normalized UV-Vis spectra of 4,4'-bis[poly(4-bromostyryl)]-2,2'-bipyridine (**16f**, dashed line) and the poly(4-vinyltriphenylamine) derivative **17f** (solid line).

### 4.3 Synthesis and characterization of bis[bipyridyl]-[4,4'-bis[poly(4-vinyltri-phenylamino)methyl]-2,2'-bipyridyl]-Ru(II) trifluoro-sulfonate (**18**)

The final step in the synthetic strategy was the metallation of polymer **17** with either Ru(II) precursor **13** (with COOH-anchor groups) or with the commercially available Ru(bpy)<sub>2</sub>Cl<sub>2</sub> · 2H<sub>2</sub>O **13'** (without anchor groups) carried out as shown in Scheme 4-3.

First the Ru(II) precursor **13** or **13'** was stirred with CF<sub>3</sub>SO<sub>3</sub>Ag in dry acetone to develop the complex Ru(bpy)<sub>2</sub>(CF<sub>3</sub>SO<sub>3</sub>)<sub>2</sub>(acetone)<sub>2</sub> which is much more active than the initial complex. The precipitate of AgCl was separated by filtration and acetone was removed in vacuum. In an argon flushed flask the residue was dissolved in dry DMF, polymer was added and the mixture was refluxed over night. After removal of half of the DMF the red-brown polymer complex was precipitated in methanol. By washing with methanol unreacted Ru(II) precursor or other low molecular weight Ru-complexes formed during the reaction were removed.

Polymers **17 c – f** were converted to the Ru(II) complexes via described metallation reaction resulting in products carrying COOH-anchor groups (**18e** and **18f**) and without anchor groups (**18c' - 18f'**).



**Scheme 4-3:** Complexation of the bipyridine unit in polymer **17** with  $\text{Ru}(\text{bpyCOOH})_2\text{Cl}_2 \cdot 2\text{H}_2\text{O}$  (**13**) or  $\text{Ru}(\text{bpy})_2\text{Cl}_2 \cdot 2\text{H}_2\text{O}$  (**13'**) using the activated silver salt method in DMF under reflux resulting in **18** or **18'** respectively.

#### 4.3.1 Thermal analysis of polymers **18**

The polymers bis[bipyridyl]-[4,4'-bis[poly(4-vinyltriphenylamino)methyl]-2,2'-bipyridyl]-Ru(II) bistrifluorosulfonate **18** resulting from the metallation of **17** are distinguished by their higher thermal stability.

This was ascertained by TGA measurements resulting in thermal decay starting above 265 °C as it is shown in Table 4-6. Also the glass transition temperatures  $T_g$  of the metal centered polymers are at least 10 - 20 °C higher in comparison with polymers **17** (except **18f** and **18f'**). The absence of melting or recrystallization peaks is pointing out to the amorphous nature of polymer structure **18**.

**Table 4-6:** Glass transition temperatures  $T_g$  and onset temperatures of thermal decay  $T_{onset}$  of polymers carrying COOH-anchor groups **18e** and **18f** and polymers **18c'** - **18f'** without COOH-anchor groups determined via DSC and TGA.

polymer	<b>18c'</b>	<b>18d'</b>	<b>18e</b>	<b>18e'</b>	<b>18f</b>	<b>18f'</b>
$T_g$ [°C] <sup>a)</sup>	143.3	148.4	152.7	153.4	131.7	131.7
$T_{onset}$ [°C] <sup>b)</sup>	286	287	279	266	278	278

a) Heating / cooling rate = 10 Kmin<sup>-1</sup>; b) defined as temperature at which weight loss is starting; determined via heating from 30 to 650 °C with 10 Kmin<sup>-1</sup>.

For better overview a comparison of second heating curves for a complete series of polymers **16c**, **17c** and **18c'** as obtained from DSC are shown in Figure 4-9.

In this graph the increase in glass transition temperature  $T_g$  first from bipyridine centered poly(4-bromostyrene) (**16c**,  $T_g = 104.7$  °C) followed by the poly(4-vinyltriphenylamine) derivative (**17c**,  $T_g = 136.1$  °C) and finally to the metal centered hole transport polymer (**18c'**,  $T_g = 143.3$  °C) is clearly visible.

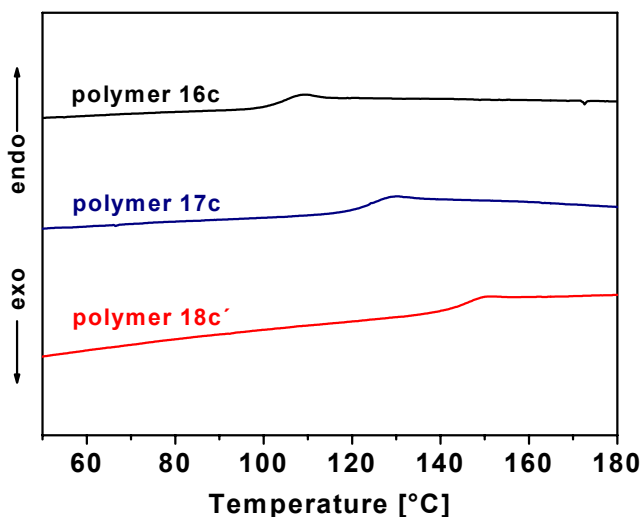


*Figure 4-9: Comparison of second heating curves for a series of polymers **16c**, **17c** and **18c'** obtained from DSC measurements (heating rate 10 Kmin<sup>-1</sup>).*

#### 4.3.2 Molecular weight determination

As already mentioned in section 4.2.3, the characterization and comparison of the molecular weights of the metal-free macroligands **16** and **17** with the polymer complex **18** using size exclusion chromatography (SEC) was not possible. As it also happened for polymers **17** SEC resulted in lower values of molecular weights for the polymer **18** compared to its precursors **16** and **17** (all measurements versus polystyrene standards). For this reason MALDI-TOF MS analysis was used to characterize at least the polymer complexes with low molecular weight **18c'** and **18d'**. For comparison and to get a better overview all three MALDI-TOF MS spectra and the resulting data of the series **16d**, **17d** and **18d'** are given in the next figure.

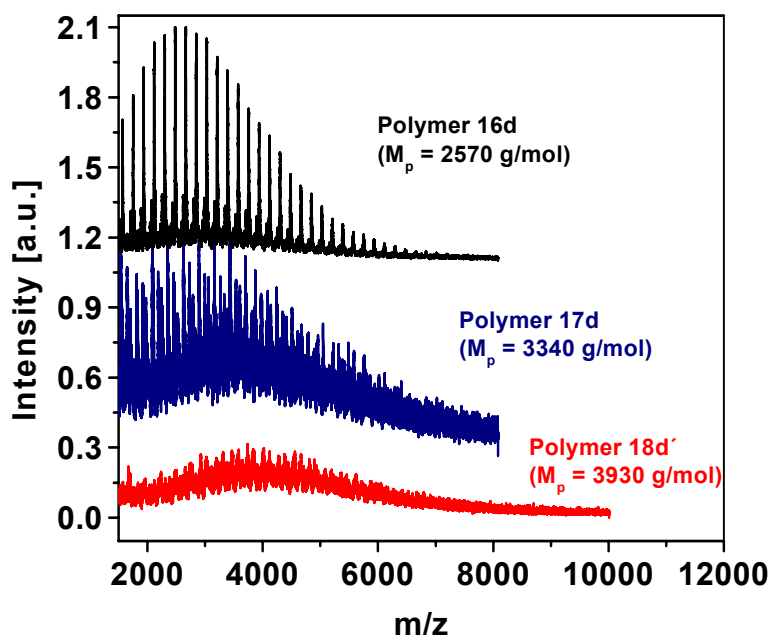


**Figure 4-10:** Comparison of MALDI-TOF mass spectra of polymers **16d**, **17d** and **18d'** (recorded with dithranol as matrix and Ag-triflate as additive).

In MALDI-TOF MS an  $M_n$ -value of 2720 g/mol was determined for **16d** and the  $M_n$ -values for polymer **17d** and polymer **18d'** are 3350 g/mol and 3940 g/mol, respectively. The peak molecular weights for all the three polymers from MALDI-TOF are 2570 g/mol, 3340 g/mol and 3930 g/mol, respectively. As presented in Figure 4-10 all the three polymers are monomodal and the weight difference between polymer **17d** and polymer **18d'** is 590 mass units indicating a successful metallation reaction with a conversion of 83 %. Using the method described here the weight fraction of Ruthenium-dye in final polymer can be varied over a wide range by varying the length of poly(4-bromostyrene) chains (from 5 wt% dye content for a molecular weight of 12300 g/mol up to 25 wt% dye content for a molecular weight of 2670 g/mol). The incorporation of COOH-anchor groups is also feasible for all of these polymers allowing an application of these materials in dye-sensitized TiO<sub>2</sub> solar cells.

### 4.3.3 UV-Vis spectroscopy

The progression of the metallation reaction was also followed via UV-Vis spectroscopy observing the characteristic absorption maximum of the Ru-complex. The MLCT-band representing the bis(bipyridine) Ru(II) precursor at 550 nm shifted to 456 nm, the characteristic MLCT-absorption wavelength of the tris(bipyridine) product. In Figure 4-11 the UV-Vis absorption spectra of polymers **17d** and **18d'** are given showing a clear absorption band at 456 nm for **18d'** and no absorption at 550 nm.

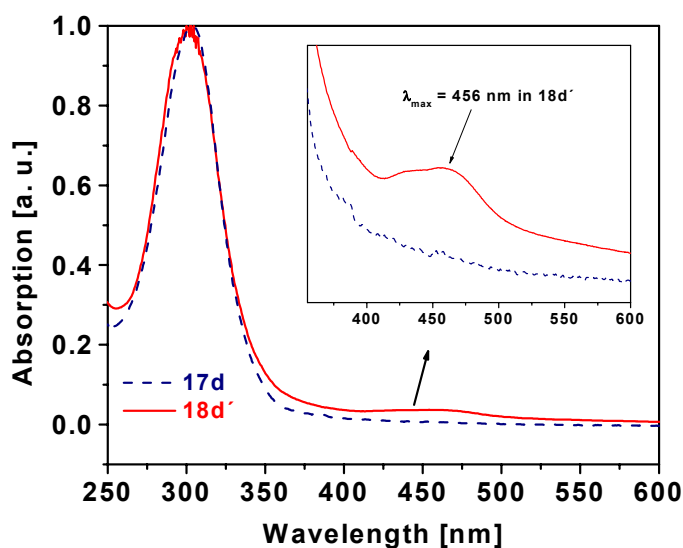


**Figure 4-11:** UV-Vis spectra of **17d** ( $M_n = 3350$  g/mol from MALDI-TOF, dashed line) and polymer **18d'** ( $M_n = 3940$  g/mol from MALDI-TOF, solid line) recorded in  $\text{CHCl}_3$ . The inset shows the magnified absorption maximum of the hexacoordinated Ru(II) core at 456 nm present only in polymer **18d'** and not in polymer **17d**.

The spectra were recorded using a polymer with rather low molecular weight to obtain definite information. With high-molecular weight polymers of structure **18** exhibiting  $M_n$  beyond 10000 g/mol the MLCT-band of the Ru(II) complex is superposed by the strong absorption of the triphenylamine monomer unit.

#### 4.3.4 Transient absorption spectroscopy of **18**

In order to study the potential of bis[bipyridyl]-[4,4'-bis[poly(4-vinyltriphenylamino) methyl]-2,2'-bipyridyl]-Ru(II) bistrifluorosulfonate (**18**) for interface modification in dye-sensitized TiO<sub>2</sub> solar cells transient absorption spectra of these were recorded by James Durrant and co-workers. The dynamics of the decay of the dye cation were investigated after coating the dyes onto a TiO<sub>2</sub> surface. In the next figure the transient absorption spectra of the low molecular weight model compounds **14** and **15** as well as that of polymer **18f** are given.

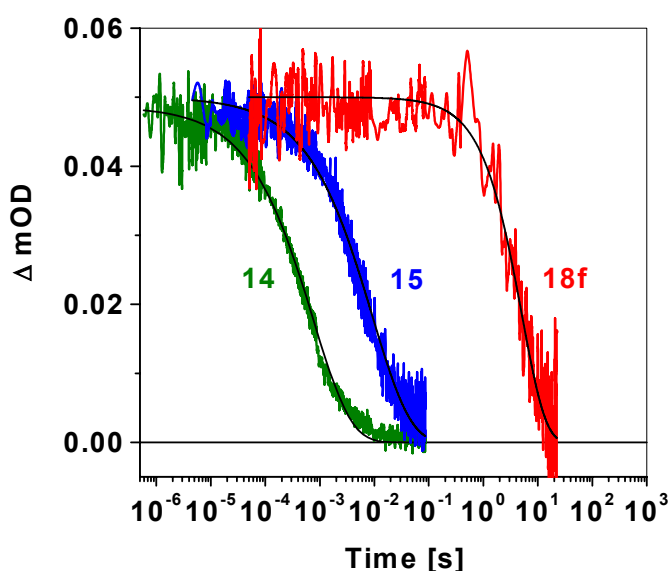


**Figure 4-12:** Decay of the dye cation of model compounds **14** and **15** in comparison with polymer **18f** monitored at 900 nm following pulsed laser excitation of dye sensitized TiO<sub>2</sub> films at 450 nm; experimental data (green, blue, red) and exponential fits (black solid lines).

It can be clearly seen in the graph that the decay of the dye cation of **18f** is extremely retarded in comparison to the model compounds. The decay half times  $t_{50\%}$  for **14** and **15** are 0.35 and 5 ms respectively, but for the polymeric structure **18f** the value of  $t_{50\%}$  is 4s which is three orders of magnitude higher than that of **15**.

Actually this is one of the highest values ever measured for a dye sensitized metal oxide film up to now. The remarkably slow charge recombination dynamics observed for the bifunctional polymer **18f** are suggested to be consistent with an increased physical separation of the HOMO orbitals of the dye from the TiO<sub>2</sub> surface. In order to prove this theory time dependent density functional theory (TD-DFT) ab-initio calculations were performed by Durrant and co-workers to determine the spatial distribution of the dye HOMO orbitals (see Figure 4-13).

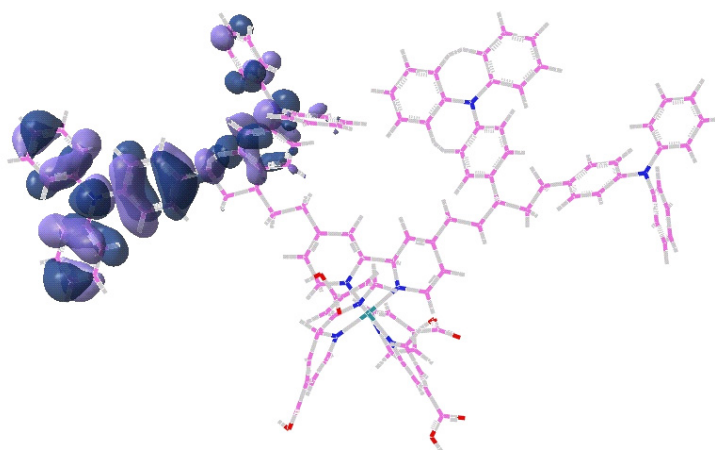


**Figure 4-13:** Graphical representation of the HOMO orbital of Ru-centred polymer **18f** as determined from the TD-DFT ab-initio calculations.

According to TD-DFT calculations the extreme retardation is attributed to an increased distance of the dye cation centre from the TiO<sub>2</sub> electrode surface due to localization of the cation somewhere on the TPA moieties in the polymer chain. The approximate distance of the excited state HOMO from the TiO<sub>2</sub> surface, as obtained from the TD-DFT ab-initio calculations, were found to be ~16.7 Å for the bifunctional polymer **18f** – a value, which is consistent with the observed retardation of the charge recombination dynamics. The recombination dynamics of **18f** exhibit an excellent fit to a mono-exponential decay which is indicative of the recombination dynamics being limited by interfacial electron dynamics which was the aim of the synthetic strategy.

In this chapter the synthesis of new polymers possessing hole transport functionality as well as light absorbing dye unit was reported. Via ATRP 4-bromostyrene was polymerized using 4,4'-bis(chloromethyl)-2,2'-bipyridine (**3**) as initiator resulting in 4,4'-bis[poly(4-bromostyryl)]-2,2'-bipyridines with defined molecular weights. These polymers with the structure **16** were subjected to a Pd-catalyzed polymeranalogous amination reaction incorporating the hole transport moiety yielding 4,4'-bis[poly(4-vinyltriphenylamino)methyl]-2,2'-bipyridines (**17**). In a metallation reaction the bipyridine center of these molecules could be converted with Ru(II) precursors to hexacoordinated Ru(II) complexes yielding bis[bipyridyl]-[4,4'-bis[poly(4-vinyltriphenylamino)methyl]-2,2'-bipyridyl]-Ru(II) trifluorosulfonate (**18**). By using 4,4'-bis[poly(4-vinyltriphenylamino)methyl]-2,2'-bipyridines with different molecular weights for metallation the Ru(II) weight fraction of the resulting complex could be varied over a broad range. The materials with the structure **18** exhibit excellent thermal stability as well as extraordinary slow recombination dynamics. By applying a polymeric hole transport ligand the decay half time of the Ru(II) cation was retarded by a factor of 1000 compared with the low molecular weight equivalents **14** and **15** which can be attributed to increased spatial separation of the dye cation centred from TiO<sub>2</sub>. This was confirmed by TD-DFT ab-initio calculations resulting in distances of the dye HOMO orbital from TiO<sub>2</sub> of ~10.8, ~15.6 and ~16.7 Å for the novel bifunctional dyes **14**, **15** and **18f** respectively.

## 5 Fully functionalized AB-diblock copolymers carrying hole transport and NLO-dye blocks

*In this chapter the synthesis of AB-diblock copolymers is reported which carry a hole transport block as well as a NLO-dye block unit. All polymers discussed here were prepared via ATRP starting from 4-bromostyrene. Poly(4-bromostyrene) was then used as macroinitiator to attach the second block for which silylated hydroxyethylmethacrylate (HEMA-TBDMS) was chosen as monomer. As the monomer units of both blocks exhibit functional groups it was possible to subject them to polymeranalogous reactions. The poly(4-bromostyrene) block was converted in a Pd-catalyzed amination reaction to yield poly(4-vinyltriphenylamine) which is a hole transport block and an NLO dye was attached to the HEMA-monomer units after removal of the protective group. The details of this multi-step synthesis yielding the desired bifunctional block copolymers carrying hole transport block and dye block will be discussed in the following section.*

Triphenylamine derivatives are of great interest as hole transport layers especially in light emitting devices and are extensively used in photocopying and laser printing industry<sup>107</sup>. Incorporating the triphenylamine functionality together with a dye into a block copolymer architecture could potentially lead to nanostructured optoelectronic devices in the future<sup>108</sup>. Especially for photorefractive applications this concept provides a great chance to enhance the to date materials which are mostly based on multi-component guest-host systems consisting of photoconducting polymers, low-molecular weight glasses and plasticizers together with non-linear optical (NLO) dyes. As long as plasticizers disturb the charge transport a lot of work has been done to get rid of this component<sup>109</sup> by going for block copolymer strategy.

In the present work the block copolymer concept should be realized with the aim to obtain bifunctional AB-diblock copolymers carrying poly(4-vinyltriphenylamine) as hole transport block as well as a second block functionalized with NLO (non linear optic)-dye units. For the preparation of block copolymers a method of controlled polymerization was needed which enables the sequential polymerization of different monomers. To realize this concept atom transfer radical polymerization (ATRP) will be tested which is known as easy to perform for a variety of monomers and has rather low sensitivity to the presence of water and oxygen compared with other controlled living polymerization techniques for example anionic polymerization<sup>110, 111</sup>. The homopolymers prepared via ATRP possess an halide as active chain-end as long as no termination reaction occurs.

---

<sup>107</sup> "Polymers for Light Wave and Integrated Optics" (Editor: L. A. Hornak), Marcel Dekker, New York, **1983**.

<sup>108</sup> G. N. Tew, M. U. Pralle, S. I. Stupp *Angew. Chem.* **2000**, 112, 3, 527.

<sup>109</sup> A. Leopold, U. Hofmann, M. Grasmuck, S. J. Zilker, D. Haarer, J. Ostrauskaite, J. V. Grazulevicius, M. Thelakkat, C. Hohle, P. Strohsriegl, H.-W. Schmidt, A. Bacher, D. D. C. Bradley, M. Redecker, M. Inbasekaran, W. W. Wu, E. P. Woo *Proceedings of SPIE* **2000**, Vol. 4104, 95.

<sup>110</sup> "Controlled / Living Radical Polymerization" (Editor: K. Matyjaszewski), ACS, Washington, DC, **2000**.

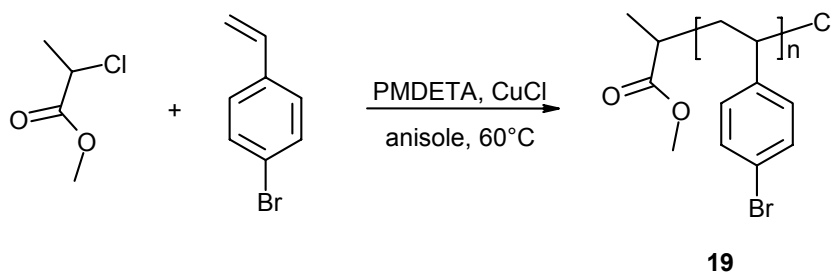
<sup>111</sup> J. Jagur-Grodzinski *Reactive & Functional Polymers* **2001**, 49, 1.

For this reason the homopolymers resulting from ATRP can function as macroinitiators and can initiate the polymerization of another monomer making the preparation of block copolymers feasible. During the proceeding of this PhD work the polymerization of 4-bromostyrene via ATRP as well as the Pd-catalyzed polymeranalogous amination of this monomer unit has been studied intensively as reported in previous chapters. Also here 4-bromostyrene was chosen as monomer for building the first block and the use of the resulting poly(4-bromostyrene) as macroinitiator for the polymerization of a second monomer to get AB-diblock copolymer structures was tested. The polymerization of 4-bromostyrene via ATRP not only yielded macroinitiators which should initiate the polymerization of a second block but also it gave the opportunity to incorporate hole transport functionalities via Pd-catalyzed polymeranalogous amination reaction with diphenylamine on the bromine substituent of the 4-bromostyrene monomer unit. For the preparation of the second block *t*-butyldimethylsiloxyethyl methacrylate (HEMA-TBDMS) was used as monomer and poly(4-bromostyrene) as macroinitiator. HEMA-TBDMS also provides the possibility of polymeranalogous reactions taking place on the hydroxy function of HEMA after removal of the protective silyl-group. Onto the hydroxy pendant group, carboxylic acid chloride derivative of an NLO azo-dye can be attached via polymeranalogous esterification reaction resulting in a second block carrying an NLO-dye. The synthetic strategy for the preparation of the fully functionalized AB-diblock copolymers as well as details of the multi-step synthesis will be reported in the following section.

## 5.1 Synthesis and characterization of poly(4-bromostyrene) macroinitiators (19)

The synthesis of poly(4-bromostyrene) macroinitiators was carried out via ATRP using  $\alpha$ -chloromethylpropionate (MCP), a standard initiator for ATRP, and PMDETA / CuCl as catalytic system in anisole as solvent at a temperature of 60 °C. 4-bromostyrene, solvent and catalytic system PMDETA / CuCl were stirred for about one hour to form the

Cu-ligand complex, then the initiator  $\alpha$ -chloromethylpropionate (MCP) was added and the mixture was degassed by the freeze-pump-thaw method already reported in previous sections. The mixture was immersed into an oilbath maintained at a temperature of 60 °C. After a definite time the reaction was quenched by cooling and exposing the reaction mixture to air. It is crucial to treat the macroinitiator very carefully due to the danger of losing the chlorine end-group under stringent conditions. In the next reaction step, this chlorine end-group is needed to initiate the polymerization of the second monomer HEMA-TBDMS. For this reason the poly(4-bromostyrene) macroinitiators were precipitated in dried n-hexane, isolated, dried in vacuum and stored under inert gas atmosphere to be promptly used in the next reaction step.



**Scheme 5-1:** Schematic representation of the synthesis of poly(4-bromostyrene) macroinitiator via ATRP using methylchloropropionate as initiator and PMDETA / CuCl as catalytic system. The reaction was carried out in anisole at 60 °C.

Further purification steps were not carried out and the product was directly used as obtained after precipitation to initiate the polymerization of HEMA-TBDMS for preparation of the desired AB-diblock copolymers. A series of poly(4-bromostyrene) macroinitiators (**19 a – e**) with different molecular weights have been prepared and the characterization of these will be given in the following sections. The control of the polymerization of 4-bromostyrene via ATRP using MCP as initiator and PMDETA and CuCl as catalytic system was tested via GC analysis.

### 5.1.1 GC analysis of ATRP of 4-bromostyrene with standard initiator MCP

In order to verify the controlled nature of the polymerization of 4-bromostyrene in anisole using  $\alpha$ -chloromethylpropionate (MCP) as initiator a batch of ATRP was prepared for the purpose of GC analysis as reported in section 4.1.1. Aliquots were taken out of the reaction flask in reasonable time intervals and were analyzed via gas chromatography (GC). The samples were diluted in chloroform before GC-measurement and anisole (used as solvent for the polymerization) was set as internal standard.

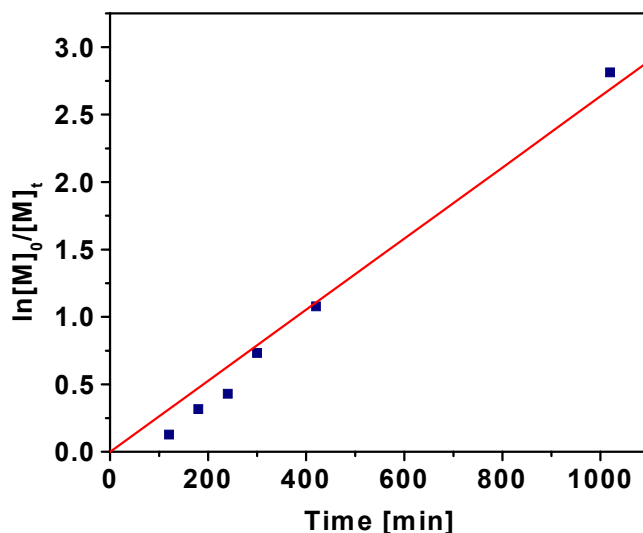


**Figure 5-1:** Dependence of  $\ln[M]_0/[M]_t$  on reaction time for ATRP of 4-bromostyrene in anisole at 60 °C ( $[M]_0$  = initial monomer concentration,  $[M]_t$  = monomer concentration after defined reaction time determined via GC analysis with anisole as internal standard). The ratio of the reactands is  $[M]_0 : [\text{Initiator}] : [\text{CuCl}] : \text{PMDETA} = 55 : 2 : 1 : 1$ .

The linear dependence of  $\ln[M]_0/[M]$  on time shown in the graph clearly ascertains the controlled nature of ATRP of monomer 4-bromostyrene up to long reaction times using

standard initiator MCP, PMDETA / CuCl as catalytic system and anisole as solvent. Thus the method adopted here seems to be suitable for the preparation of macroinitiators with a defined chain length which have the ability to initiate the polymerization of a second monomer in a controlled way.

### 5.1.2 Size exclusion chromatography (SEC)

To determine molecular weights and polydispersities the poly(4-bromostyrene) macroinitiators (**19**) were characterized via size exclusion chromatography (SEC) using THF + 0.25 wt% tetrabutylammoniumbromide as eluent. All polymers of the structure **19** exhibit monomodal elution curves and polydispersities appreciably low for ATRP. As an example the elution curve for **19c** is shown in Figure 5-2.

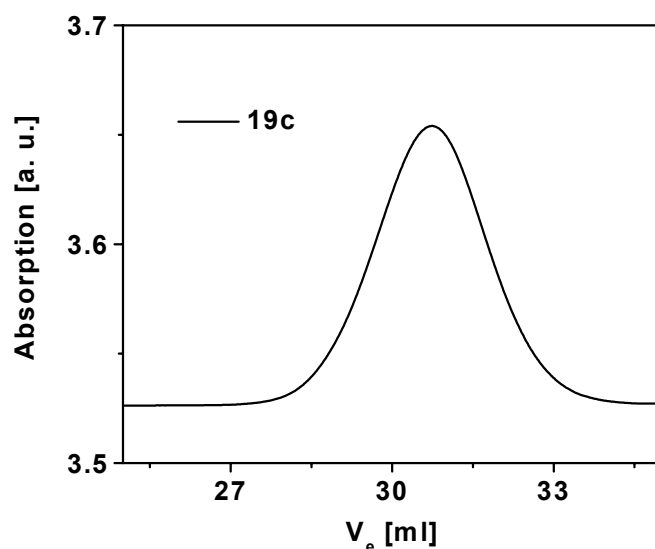


*Figure 5-2: SEC elution curve for polymer 19c (THF + 0.25 wt% TBAB as eluent, calibration with polystyrene standards).*

In the following table the number average molecular weights ( $M_n$ ), weight average molecular weights ( $M_w$ ) and polydispersities (PDI) of the series of polymers with structure **19** obtained from size exclusion chromatography (SEC) are listed.

**Table 5-1:**  $M_n$ ,  $M_w$  and PDI of a series poly(4-bromostyrene) macroinitiators (**19 a - e**) prepared via ATRP in anisole at 60 °C using MCP as initiator and CuCl / PMDETA as catalytic system.

polymer	$M_n$ [g/mol] <sup>a)</sup>	$M_w$ [g/mol] <sup>a)</sup>	PDI <sup>b)</sup>
<b>19a</b>	4714	6668	1.41
<b>19b</b>	6016	8221	1.37
<b>19c</b>	6534	8573	1.31
<b>19d</b>	13184	18163	1.38
<b>19e</b>	25042	28176	1.13

a) Determined via SEC with THF + 0.25 wt% TBAB as eluent, calibration versus polystyrene standards, UV-detection; b) PDI =  $M_w/M_n$ .

The series of polymers to be used as macroinitiators exhibit molecular weights in a range from 4714 g/mol to 25042 g/mol. By applying macroinitiators with different chain length a dependence of block copolymer formation on molecular weight was investigated and will be reported later.

### 5.1.3 Thermal analysis

The thermal properties of poly(4-bromostyrene) macroinitiators (**19 a – e**) have been determined by differential scanning calorimetry (DSC) and thermo gravimetric analysis (TGA). Glass transition temperatures and onset temperature of thermal decay obtained by this characterization methods are summarized in Table 5-2.

**Table 5-2:** Glass transition temperatures  $T_g$  and onset temperatures of thermal decay  $T_{onset}$  of polymers **19 a – e** determined via DSC and TGA.

polymer	<b>19a</b>	<b>19b</b>	<b>19c</b>	<b>19d</b>	<b>19e</b>
$T_g$ [°C] <sup>a)</sup>	94.4	118.8	117.3	119.3	125.1
$T_{onset}$ [°C] <sup>b)</sup>	240	227	247	245	245

a) Heating / cooling rate = 10 Kmin<sup>-1</sup>; b) defined as temperature at which weight loss is starting; determined via heating from 30 to 650 °C with 10 Kmin<sup>-1</sup>.

The glass transition temperatures are in an appreciable range for poly(4-bromostyrene) homopolymers and very similar to  $T_g$  of poly(styrene). None of the heating or cooling curves show any peak referring to melting processes or recrystallization giving hint to the amorphous nature of the macroinitiators **19**. All polymers with the structure **19** exhibit thermal stability up to at least 226 °C being in good agreement with the values reported for bipyridine centered poly(4-bromostyrenes) (**16**) discussed in a previous chapter of this thesis.

#### 5.1.4 NMR-spectroscopy

To verify the structure of poly(4-bromostyrene) macroinitiators <sup>1</sup>H-NMR spectroscopy was carried out. <sup>1</sup>H-NMR-spectra of all polymers **19** recorded in deuterated chloroform (CDCl<sub>3</sub>) exhibit very similar resonance signals, therefore the spectrum of **19c** will be discussed here as example: The polymer backbone is represented by a broad signal without resolution ranging from 1.25 to 1.56 ppm and the integral value of this signal was set to 3 protons. At 6.29 ppm and 7.16 ppm the signals for the AA'XX' -spin system of the para-substituted aromatic ring of the 4-bromostyrene monomer unit are visible representing an integral value of 4 protons.

Resonance signals corresponding to the initiator MCP could not be detected presumably due to its low weight fraction within the polymer chain.

## 5.2 Synthesis and characterization of poly(4-bromostyrene)-*block*-poly(HEMA-TBDMS) (**21**)

The synthesis of AB-diblock copolymers poly(4-bromostyrene)-*block*-poly(HEMA-TBDMS) was carried out via ATRP in solution using poly(4-bromostyrene) macroinitiators (**19**) and PMDETA /CuCl as catalytic system. The synthesis of monomer HEMA-TBDMS (**20**) as well as the details of the preparation of the block copolymers will be reported here.

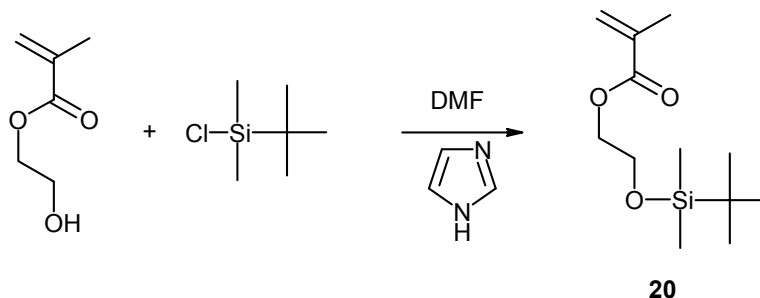
### 5.2.1 Synthesis and characterization of *t*-butyldimethylsiloxyethyl methacrylate (HEMA-TBDMS) (**20**)

Hydroxyethyl methacrylate (HEMA) was chosen as monomer for the second block in the desired AB-diblock copolymer structure. The hydroxy function of this molecule provides the opportunity to perform further polymeranalogous reactions after HEMA was incorporated into a block copolymer structure. As the AB-diblock copolymers had to withstand the polymeranalogous amination of the poly(4-bromostyrene) block, a protective group had to be attached to the hydroxy function. The *t*-butyldimethylsilyl (TBDMS) group was found to form silylethers with high stability against aqueous and alcoholic bases<sup>112</sup> and was therefore chosen as protective group for HEMA. The incorporation of the TBDMS protective group was carried out by a modification of a procedure reported in literature<sup>113</sup> and is presented in Scheme 5-2.

---

<sup>112</sup> E. J. Corey, A. Venkateswarlu *J. Am. Chem. Soc., Communication to the Editor* **1972**, 6190.

<sup>113</sup> H. Mori, O. Wakisaka, A. Hirao *Macromolecular Chemistry & Physics* **2003**, 195, 2313.



**Scheme 5-2:** Schematic representation of the synthesis of *t*-butyldimethylsilyloxyethyl methacrylate (HEMA-TBDMS, **20**).

Hydroxyethylmethacrylate and an excess of imidazole as base were dissolved in dry DMF, cooled to  $-20\text{ }^{\circ}\text{C}$  and a solution of *t*-butyldimethylsilylchloride in dry DMF was added dropwise. After the reaction mixture got turbid it was heated up to room temperature, stabilizer 2,6-di(*tert*.butyl)-4-methylphenol was added and it was stirred for three days under argon atmosphere. DMF was removed in high vacuum and the residue was extracted with  $\text{H}_2\text{O}$  until it was neutral. The aqueous fractions were extracted with diethylether and the combined organic fractions were dried over  $\text{Na}_2\text{SO}_4$ . Removal of the solvent yielded *t*-butyldimethyl-siloxyethylmethacrylate (HEMA-TBDMS, **20**) which had to be purified further by fractional distillation in high vacuum. It is essential that HEMA-TBDMS (**20**) is stored over  $\text{CaH}_2$  under inert gas atmosphere and distilled in high vacuum directly before use for polymerization.

The structure of HEMA-TBDMS was verified via NMR-spectroscopy clearly showing the resonance signals of the protective group, i. e. two singulets at 0.04 ppm and 0.86 ppm corresponding to the methyl substituents (integral value 6) and the *t*-butyl group (integral value 9) respectively. Shifted to lower field at 3.28 ppm and 4.20 ppm two triplets representing the ethylene unit are present exhibiting an overall integral of 4. The two protons of the vinyl group are represented by two singulets at 5.53 ppm and 6.09 ppm each having an integral value of 1.

### 5.2.2 Synthesis of poly(4-bromostyrene)-*block*-poly(HEMA-TBDMS) (**21**)

The synthesis of the AB-diblock copolymer, poly(4-bromostyrene)-*block*-poly(HEMA-TBDMS) (**21**) via ATRP seemed to be very challenging due to the difficulty to introduce the second block. The main problem was the difference in polarity and solubility between *t*-butyldimethylsiloxyethylmethacrylate (HEMA-TBDMS, **20**), macroinitiator **19** and the desired AB-diblock copolymer **21**. In literature AB-diblock copolymers are reported mostly consisting of blocks with very similar polarity for example poly(HEMA) and poly(ethylene glycol) polymerized via ATRP in ethylene glycol<sup>114</sup> or even aqueous media<sup>115</sup>. Thus a solvent combination had to be found in which HEMA-TBDMS (**20**), the poly(4-bromostyrene) macroinitiator (**19**) as well as poly(4-bromostyrene)-*block*-poly(HEMA-TBDMS) (**21**) are totally soluble. After screening a series of solvents and solvent combinations the mixture of ethylmethylketone / isopropanol (80 : 20 v/v)<sup>116</sup> turned out to be very promising for the realization of the synthetic strategy.

Further it was investigated if it was possible to use the isolated macroinitiator before block copolymerization or if the active chlorine group at the chain-end is abstracted by the procedure of precipitation during purification of the macroinitiator. Therefore in one reaction batch a macroinitiator was prepared. After a definite time, half of the reaction mixture was taken out and solvent and residual monomer were removed from this fraction by vacuum distillation resulting in a solid mixture consisting of catalyst and macroinitiator. The other half of the reaction batch was used to precipitate the macroinitiator into dry n-hexane followed by filtration and drying in vacuum. Both the isolated and the “non-purified” macroinitiators were used to initiate the polymerization of HEMA-TBDMS under standard conditions reported in the experimental part.

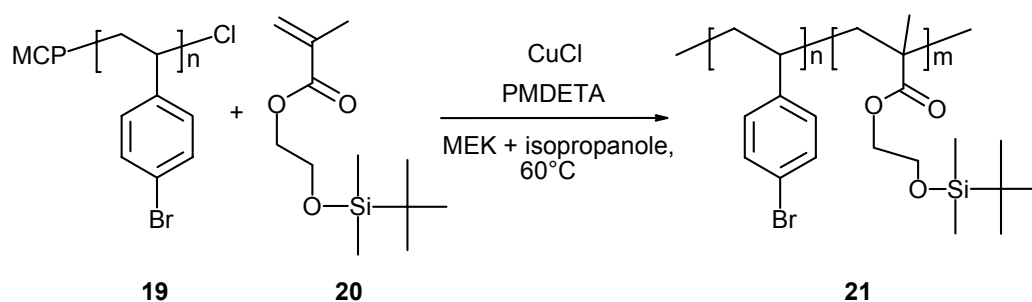
---

<sup>114</sup> B. Reinig, H. Keul, H. Hoecker, *Polymer* **2002**, 43, 3139.

<sup>115</sup> T. A. von Werne, D. S. Germack, E. C. Hagberg, V. V. Sheares, C. J. Hawker, K. R. Carter, *J. Am. Chem. Soc.* **2003**, 125, 3831.

<sup>116</sup> K. L. Beers, S. Boo, S. G. Gaynor, K. Matyjaszewski, *Macromolecules* **1999**, 32, 5772.

It was found that both macroinitiators were able to initiate the polymerization of the second block proving that the active chain-end is not abstracted by purification. Only slight differences in molecular weights of the resulting AB-diblock copolymer were observed. Due to reasons of purity, the block copolymerizations reported in this chapter were all prepared applying a macroinitiator which was isolated before further use.



**Scheme 5-3:** Schematic representation of the synthesis of poly(4-bromostyrene)-*b*-poly(HEMA-TBDMS) (**21**) via ATRP in MEK : isopropanol = 80 : 20 (v/v).

In a general procedure PMDETA and CuCl were added to a mixture of MEK / isopropanol (80 : 20 v/v) and stirred for one hour. Subsequently poly(4-bromostyrene) macroinitiator **19** was added and the reaction mixture was stirred until the macroinitiator was fully dissolved. Carefully excluding oxygen and water HEMA-TBDMS was filtrated in argon stream over a small column packed with alox N to remove stabilizer and was added to the reaction flask. After degassing using the freeze-pump-thaw method, the sealed flask was immersed to an oilbath maintained at 60 °C. The polymerization was quenched after 16.5 h by rapid cooling and exposing to air and the product was precipitated directly into MeOH. Further purification was carried out by reprecipitation from THF into MeOH.

The aim was to prepare a series of AB-diblock copolymers poly(4-bromostyrene)-*block*-poly(HEMA-TBDMS) starting from the macroinitiators **19 a – e** discussed in the section before. After several experiments it was found that it is not possible to initiate polymerization of the second monomer (HEMA-TBDMS, **20**) using macroinitiators with

molecular weights above ~7000 g/mol such as **19d** ( $M_n = 13184$  g/mol) and **19e** ( $M_n = 25042$  g/mol). One reason for this is the decreased solubility observed for high molecular weight macroinitiators in the chosen solvent combination (MEK : isopropanol = 80 : 20 v/v). Moreover, there may be kinetic and diffusion-limited reasons making it impossible for the HEMA-TBDMS monomer to reach the active chain end of the macroinitiator being hidden within the polymer coil structure.

The preparation of AB-diblock copolymers **21 a – 21 c** was successfully carried out using **19 a – 19 c** as macroinitiators. The molar ration of the reactands [macroinitiator **19**] : [HEMA-TBDMS] were 1:20, 1:25 and 1:28 for **21a**, **21b** and **21c**, respectively. These block copolymers were characterized via SEC and NMR-spectroscopy as reported in the following paragraph and also the thermal properties were determined.

### 5.2.3 Size exclusion chromatography (SEC)

To verify the AB-diblock copolymer structure **21 a – c** the polymers were characterized via size exclusion chromatography using THF + 0.25 wt% TBAB as eluent. All polymer-batches **21 a – c** clearly exhibit monomodal elution curves without any shoulder signals of residual macroinitiator or side-products proving the formation of an AB-diblock copolymer structure. For example the elution curves of macroinitiator **19c** and the corresponding AB-diblock copolymer **21c** are presented in Figure 5-3.

Comparing the molecular weights of polymers **19** and corresponding polymers **21** obtained from SEC the weight fraction of the poly(HEMA-TBDMS) block ( $\chi_1$ ) can be calculated by applying Equation 9.

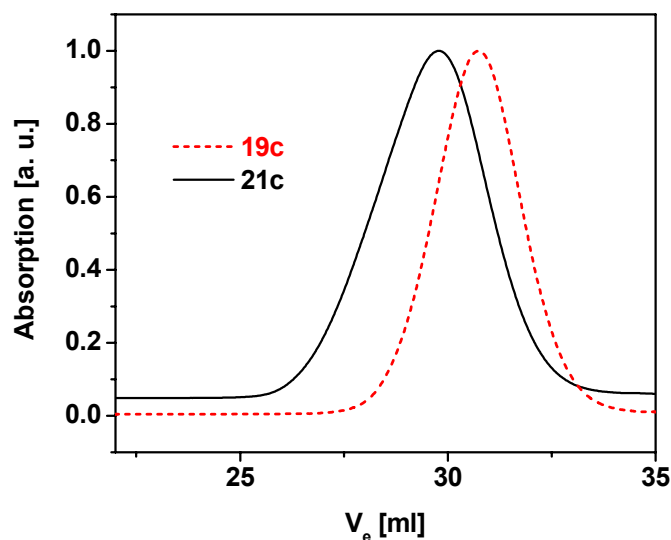


**Figure 5-3:** Elution curves for polymers **19c** (dashed) and **21c** (solid) recorded in THF + 0.25 wt% TBAB as eluent; calibration with polystyrene standards.

$$\chi_1 = \frac{M_n(\text{blockcopolymer21}) - M_n(\text{macroinitiator19})}{M_n(\text{blockcopolymer21})} \quad (\text{Equation 9})$$

The results as well as the molecular weights and polydispersities of all polymers **21 a – c** determined via SEC are summarized in Table 5-3. In comparison with the corresponding macroinitiators all AB-diblock copolymers show a considerable increase in molecular weight and polydispersities ranging from 1.44 to 1.57 which are appreciably low for AB-diblock copolymers prepared via ATRP.

**Table 5-3:** SEC-data of AB-diblock copolymers (**21 a – c**) prepared via ATRP in MEK / isopropanole at 60 °C using macroinitiators **19 a – c** and CuCl / PMDETA as catalytic system; weight fraction of poly(HEMA-TBDMS) block ( $\chi_1$ ) calculated from  $M_n$ .

polymer	$M_n$ [g/mol] <sup>a)</sup>	$M_w$ [g/mol] <sup>a)</sup>	PDI <sup>b)</sup>	$\chi_1$ (poly(HEMA-TBDMS)) [wt%]	$\chi_1$ (theory) [wt%]
<b>21a</b>	6034	9503	1.57	21.9	50
<b>21b</b>	8304	11943	1.44	27.6	50
<b>21c</b>	9620	14527	1.51	32.1	50

a) Determined via SEC with THF + 0.25 wt% TBAB as eluent, calibration versus polystyrene standards, UV-detection; b) PDI =  $M_w/M_n$ .

#### 5.2.4 NMR-spectroscopy

The AB-diblock copolymers **21** were characterized via <sup>1</sup>H-NMR spectroscopy and the spectra recorded in CDCl<sub>3</sub> exhibit a combination of broad resonance signals corresponding to the poly(4-bromostyrene) macroinitiator **19** and those representing poly(HEMA-TBDMS) (see Figure 5-4). As the spectra of the series **21** are very similar the spectrum of **21c** will be discussed here as an example. The singlets corresponding to the TBDMS-protective group are clearly present at 0.06 ppm and 0.89 ppm. The ethylene group of HEMA is present as two broad singlets at 3.76 ppm and 3.95 ppm whereas signals at 6.33 ppm and 7.22 ppm represent the para-substituted aromatic ring of the poly(4-bromostyrene) block.

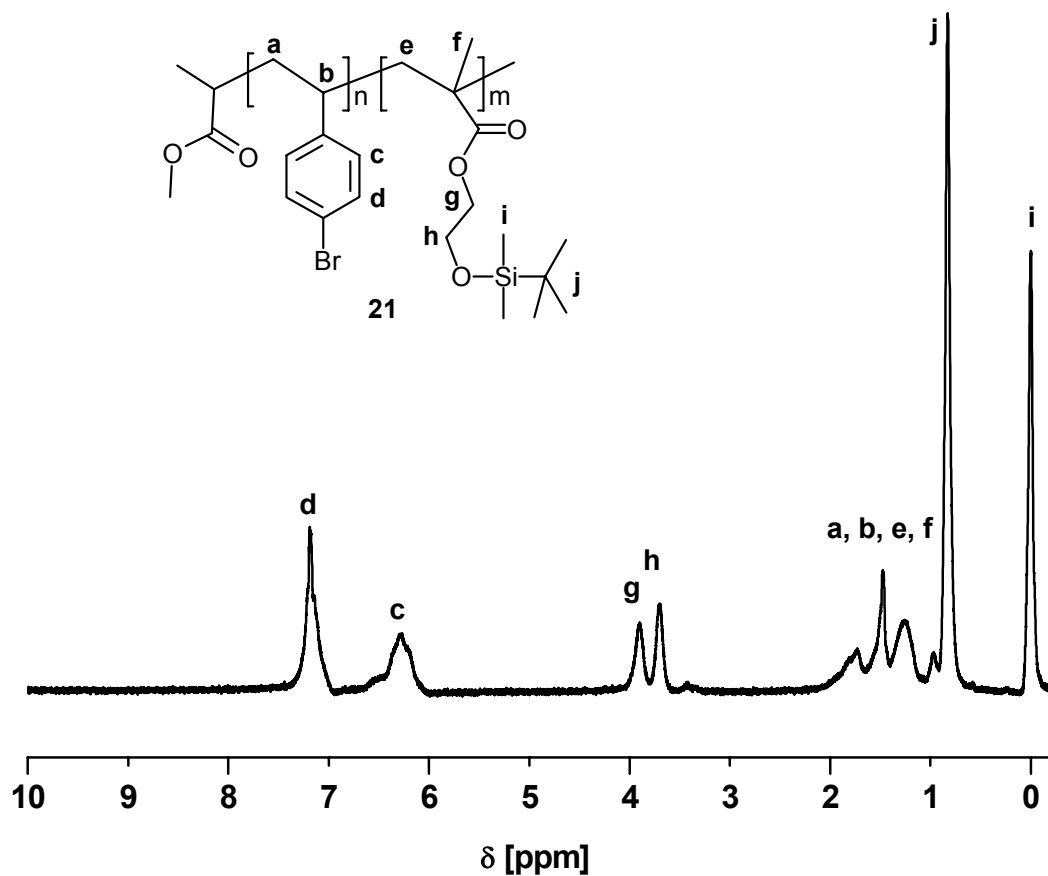


**Figure 5-4:**  $^1\text{H}$ -NMR spectrum of poly(4-bromostyrene)-block-poly(HEMA-TBDMS) (**21**) recorded in  $\text{CDCl}_3$  (250 MHz, 298 K).

### 5.2.5 Calculation of composition

Using characteristic signals of the different monomer units and their integrals from  $^1\text{H}$ -NMR spectra of the AB-diblock copolymer it is possible to calculate the composition of the polymers with the following equations.

$$\chi = \frac{\text{Integral}_1 \cdot \text{MW}_1}{\text{Integral}_2 \cdot \text{MW}_2} \quad (\text{Equation 10})$$

$$\chi_2 = \frac{1}{1 + \chi} \cdot 100 \quad (\text{Equation 11})$$

$\chi$  = weight ratio of the block 1 to block 2

$\text{Integral}_1$  = integral value of characteristic  $^1\text{H-NMR}$  signal of monomer unit 1

$\text{Integral}_2$  = integral value of characteristic  $^1\text{H-NMR}$  signal of monomer unit 2

$MW_1$  = molecular weight of monomer 1;  $MW(\text{HEMA-TBDMS}) = 244.4 \text{ g/mol}$

$MW_2$  = molecular weight of monomer 2;  $MW(4\text{-bromostyrene}) = 183.05 \text{ g/mol}$

$\chi_2$  = weight fraction of block 2 in wt%.

Using the data obtained in  $^1\text{H-NMR}$  for **21c** an example for the calculation will be given here: As characteristic signal for the poly(HEMA-TBDMS) block a broad singlet of one of the methylene group at 3.76 ppm was chosen and the integral value was set to two ( $\text{Integral}_1$ ). The signal chosen for the poly(4-bromostyrene) block is situated in the aromatic region and exhibits an corresponding integral of 3.68 protons ( $\text{Integral}_2$ ). Using equation 2 with the appropriate molecular weights given above followed by applying equation 3 the result is  $\chi_2 = 58 \text{ wt\%}$  for the poly(4-bromostyrene) block and thus 42 wt% for the poly(HEMA-TBDMS) block. In Table 5-4 the results of this calculations for polymers **21 a – c** are summarized.

**Table 5-4:** Weight fractions of poly(HEMA-TBDMS) and poly(4-bromostyrene) in AB-diblock copolymers **21** calculated from  $^1\text{H-NMR}$ .

polymer	$\chi_1$ (poly(HEMA-TBDMS))	$\chi_2$ (poly(4-bromostyrene))
	[wt%]	[wt%]
<b>21a</b>	35	65
<b>21b</b>	32	68
<b>21c</b>	42	58

It has to be noted that the weight fractions  $\chi_1$  and  $\chi_2$  of the two block segments in **21 a – c** calculated using NMR-data differ distinctly from those obtained from SEC in chapter 5.2.3. The values for poly(HEMA-TBDMS) block  $\chi_1$  determined from proton NMR are about 10 % higher than those taking into account the molecular weights from SEC. The reason for this deviation may be the fact that the method of SEC does not result in absolute values but uses calibration standards. Thus it is advisable to give preference to  $\chi_1$  and  $\chi_2$  calculated from integrals in  $^1\text{H-NMR}$  spectra.

### 5.2.6 Thermal analysis

The thermal properties of the AB-diblock copolymers were determined via differential scanning calorimetry (DSC) and thermo gravimetric analysis (TGA) and are summarized in Table 5-5.

**Table 5-5:** Glass transition temperatures  $T_g$  and onset temperatures of thermal decay  $T_{onset}$  of **21 a – c** determined via DSC and TGA.

Polymer	<b>21a</b>	<b>21b</b>	<b>21c</b>
$T_{g1}$ [ $^{\circ}\text{C}$ ] <sup>a)</sup>	20.9	-	29.6
$T_{g2}$ [ $^{\circ}\text{C}$ ] <sup>a)</sup>	107.2	133.5	119.0
$T_{onset}$ [ $^{\circ}\text{C}$ ] <sup>b)</sup>	205	240	223

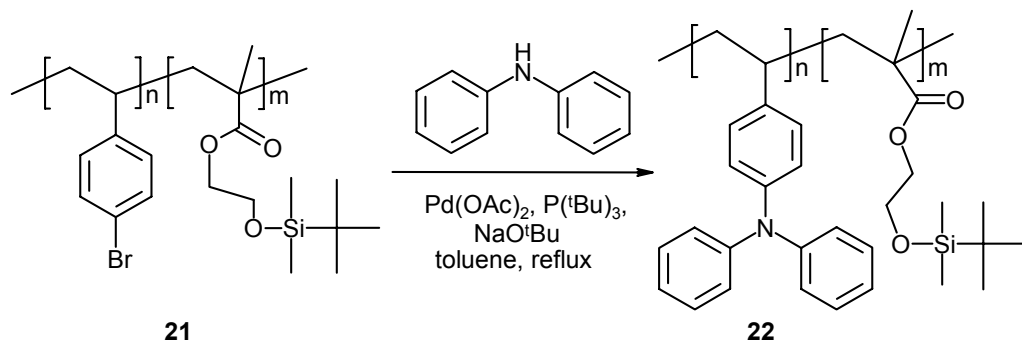
a) Heating / cooling rate = 10  $\text{Kmin}^{-1}$ ; b) defined as temperature at which weight loss is starting; determined via heating from 30 to 650  $^{\circ}\text{C}$  with 10  $\text{Kmin}^{-1}$ .

As expected for AB-diblock copolymers a second glass transition could be detected for polymers **21a** and **21c** caused by the poly(HEMA-TBDMS) block ( $T_{g1}$ ) beside the glass transition corresponding to poly(4-bromostyrene) ( $T_{g2}$ ). For **21b** the first glass transition could not be detected.

Compared with the glass transition temperature of poly(HEMA-TBDMS) homopolymer ( $T_g = 24.1$  °C) prepared as reference via living anionic polymerization a good agreement was observed. The absence of any melting or recrystallization peak indicates a totally amorphous structure of the novel polymers of the series **21 a – c**.

### 5.3 Synthesis and characterization of poly(4-vinyl-triphenylamine)-*block*-poly(HEMA-TBDMS) (**22b**, **22c**)

In the next reaction step the hole transport functionality has to be incorporated into poly(4-bromostyrene)-*block*-poly(HEMA-TBDMS) (**21**) applying a suitable procedure of a polymeranalogous reaction. The principle of Pd-catalyzed amination of poly(4-bromostyrene) has already been exploited for bipyridine centered poly(4-bromostyrene) homopolymers resulting in hole transport poly(4-vinyltriphenylamine) derivatives in extraordinarily short reaction times and good yields as reported in chapter 4. This optimized method using Pd(OAc)<sub>2</sub>, P(*t*Bu)<sub>3</sub> and NaO*t*Bu as catalytic system were adopted here also for the introduction of the hole transport block into poly(4-bromostyrene)-*block*-poly(HEMA-TBDMS) (**21**) as presented in Scheme 5-4. The conversion of **21** to poly(4-vinyltriphenylamine)-*block*-poly(HEMA-TBDMS) (**22**) was carried out in toluene with four-times molar excess of diphenylamine. Polymer **21** and diphenylamine were dissolved in toluene followed by the addition of the catalytic system (Pd(OAc)<sub>2</sub>, P(*t*Bu)<sub>3</sub> and NaO*t*Bu) as shown in Scheme 5-4. The reaction mixture was refluxed over night, then half of the toluene was distilled off the flask. The residue was diluted with THF and the solution was filtered over a small column packed with alox N to remove rest catalyst. After evaporating the solvent the desired product **22** was precipitated into methanol. Further purification was carried out by reprecipitation from THF into methanol yielding white powder. By this method **21b** and **21c** were converted to the corresponding AB-diblock copolymers **22b** and **22c** carrying triphenylamine units as hole transport functionality.



**Scheme 5-4:** Pd-catalyzed polymeranalogous amination of poly(4-bromostyrene)-block-poly(HEMA-TBDMS) **21** using  $\text{Pd(OAc)}_2$ ,  $\text{P(tBu)}_3$  and  $\text{NaOtBu}$  as catalytic system.

The resulting polymers were characterized via NMR-spectroscopy and the thermal properties were determined via DSC and TGA. Size exclusion chromatography was also carried out but did not deliver reasonable results.

### 5.3.1 Size exclusion chromatography (SEC)

SEC was carried out to determine the molecular weights of poly(4-vinyltriphenylamine)-block-poly(HEMA-TBDMS) **22b** and **22c**. As already reported SEC characterization of polymers carrying triphenylamine moieties turned out to be very difficult due to differences in intrinsic viscosities and hydrodynamic volumes of these polymers compared to the calibration standard. For this reason a comparison of molecular weights of poly(4-vinyltriphenylamine)-block-poly(HEMA-TBDMS) (**22**) with those of the precursor polymers **21** using standard SEC was not possible. The triphenylamine units presumably interact strongly with the stationary phase leading to delayed elution and tailing effect which results in lower molecular weights for polymers with the structure **22** compared to poly(4-bromostyrene)-block-poly(HEMA-TBDMS) (**21**) as shown in Table 3-1.

**Table 5-6:** Molecular weights and polydispersities of poly(4-vinyltriphenylamine)-block-poly(HEMA-TBDMS) **22b** and **22c** and corresponding polymers **21b** and **21c**.

polymer	$M_n$ [g/mol] <sup>a)</sup>	$M_w$ [g/mol] <sup>a)</sup>	PDI <sup>b)</sup>
<b>21b</b>	8304	11943	1.44
<b>21c</b>	9620	14527	1.51
<b>22b</b>	4322	5656	1.31
<b>22c</b>	5818	8407	1.45

a) Determined via SEC with THF + 0.25 wt% TBAB as eluent, calibration versus polystyrene standards, UV-detection; b) PDI =  $M_w/M_n$ .

Elution of the new materials **22** was also tested using dimethylacetamide in combination with LiCl as eluent at 70 °C which resulted in multiple signals suggesting decomposition of the samples. Also MALDI-TOF did not provide an alternative method of molecular weight determination also because of decomposition of the AB-diblock copolymers **22** during measurement.

### 5.3.2 NMR-spectroscopy

<sup>1</sup>H-NMR-spectroscopy was carried out to confirm the structure suggested for polymers **22b** and **22c**. The chemical shifts of **22c** will be given here as example:

The signals of the poly(4-bromostyrene) block of **21c** at 6.33 ppm and 7.22 ppm disappeared fully followed by the appearance of a characteristic multiplet at 6.43 – 7.11 ppm corresponding to the poly(4-vinyltriphenylamine) unit of the novel polymer **22c**. The resonance signals of the protective TBDMS-group are still present at 0.06 ppm and 0.89 ppm ascertaining no abstraction has taken place during the polymeranalogous amination reaction under the reported conditions.

A broad multiplet in the alkyl-region (1.03 ppm – 1.88 ppm) can be attributed to the polymer backbone and the ethylene moiety of HEMA-TBDMS monomer unit is represented by two broad singlets at 3.76 ppm and 3.96 ppm respectively supporting the structure suggested for the AB-diblock copolymer **22c**. According to the data obtained from  $^1\text{H-NMR}$  an almost full conversion of the poly(4-bromostyrene) block to poly(4-vinyltriphenylamine) within the limits of detection is assumed.

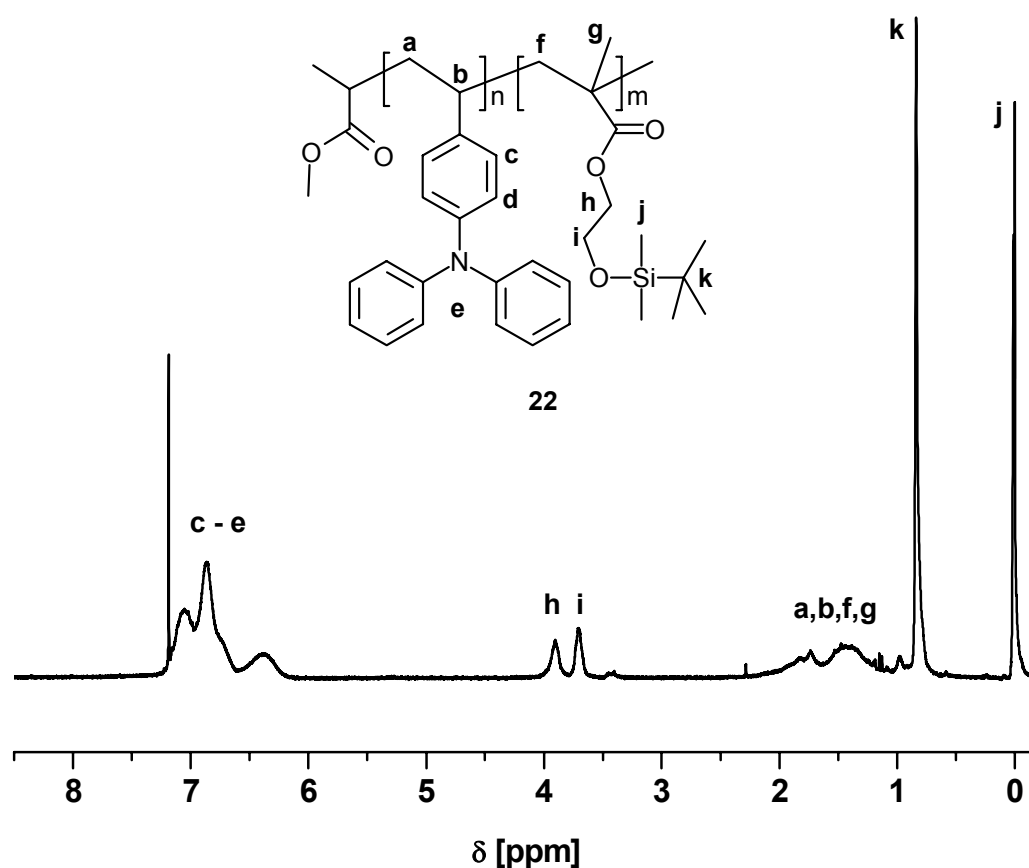


**Figure 5-5:**  $^1\text{H-NMR}$  spectrum of poly(4-vinyltriphenylamine)-block-poly(HEMA-TBDMS) (**22 c**) recorded in  $\text{CDCl}_3$  (250 MHz, 298 K).

### 5.3.3 Thermal analysis

The determination of the thermal properties of poly(4-vinyltriphenylamine)-b-poly(HEMA-TBDMS) **22b** and **22c** was performed via DSC and TGA. The glass transitions temperatures  $T_g$  as well as onset temperatures of thermal decay  $T_{onset}$  are given in Table 5-7.

**Table 5-7:** Glass transition temperatures ( $T_{g1}$  and  $T_{g2}$ ) and onset temperatures of thermal decay ( $T_{onset}$ ) of polymers **22b** and **22c**:

polymer	<b>22b</b>	<b>22c</b>
$T_{g1}$ [°C] <sup>a)</sup>	31.1	24.9
$T_{g2}$ [°C] <sup>a)</sup>	135.6	121.6
$T_{onset}$ [°C] <sup>b)</sup>	247	251

a) Heating / cooling rate = 10 Kmin<sup>-1</sup>; b) defined as temperature at which weight loss is starting; determined via heating from 30 to 650 °C with 10 Kmin<sup>-1</sup>.

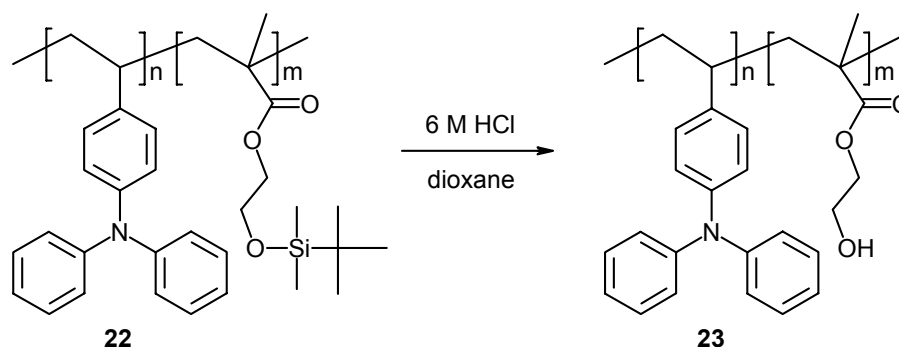
As expected for AB-diblock copolymers both **22b** and **22c** exhibit two glass transitions at temperatures  $T_{g1}$  and  $T_{g2}$ . The glass transitions detected at 24.9 °C and 31.1 °C ( $T_{g1}$ ) correspond to the poly(HEMA-TBDMS) block and is in good agreement to the DSC-data obtained for poly(HEMA-TBDMS) homopolymer which is  $T_g = 24.1$  °C. The glass transitions at higher temperatures (121.6 °C and 135.6 °C,  $T_{g2}$ ) can be attributed to the poly(4-vinyltriphenylamine) block resulting from the polymeranalogous amination reaction. According to TGA results the decomposition of polymers **22b** and **22c** starts at a temperature of about 250 °C pointing out to a good thermal stability of the block copolymers carrying hole transport functionality.

## 5.4 Synthesis and characterization of poly(4-vinyl-triphenylamine)-*block*-poly (HEMA-DNPP) (**28**)

In a last step of synthesis the NLO-dye functionality will be attached to the AB-diblock copolymers **22b** and **22c**. In order to enable photorefractive investigations of the target materials the NLO-dye 2,5-dimethyl-4-(4-nitrophenylazo) phenol (DNPP, **24**) was chosen as dye suitable for the present concept. In order to realize the plan of synthesis the *tert*.butyldimethylsilyl (TBDMS) protective group of (4-vinyltriphenylamine)-*block*-poly (HEMA-TBDMS) **22** has to be removed. Moreover, DNPP has to be synthesized and modified to its carboxylic acid chloride derivative to enable the attachment to the HEMA repeating units within the AB-diblock copolymer. This was performed in several reaction steps reported in the following sections.

### 5.4.1 Synthesis of poly(4-vinyltriphenylamine)-*block*-poly(HEMA) (**23**)

Poly(4-vinyltriphenylamine)-*block*-poly(HEMA) (**23**) was prepared by removing the *tert*.-butyldimethylsilyl (TBDMS) protective group from poly(4-vinyltriphenylamine)-*block*-poly (HEMA-TBDMS) (**22**) as presented in Scheme 5-5. As TBDMS groups exhibit sensitivity against acid media the abstraction was carried out in a mixture of dioxane and HCl. The polymer was dissolved in dioxane followed by the slow addition of 6 M HCl and stirring for 2h. The acid solution was poured into water and was extracted several times with chloroform. Concentration of the combined organic fractions was followed by precipitation of the target polymer **23** into methanol.



**Scheme 5-5:** Schematic representation of the synthesis of poly(4-vinyltriphenylamine)-block-poly(HEMA) **23** in dioxane and 6 M HCl.

#### 5.4.2 Size exclusion chromatography (SEC)

The molecular weights of polymers of the type poly(4-vinyltriphenylamine)-b-poly(HEMA) (**23**) was investigated by size exclusion chromatography (SEC). In order to facilitate the elution of the highly polar samples THF + 0.25 wt% TBAB was used as eluent. Nevertheless SEC resulted in multimodal elution curves which might be a sign for the formation of aggregates which are not cracked by the addition of salt (TBAB) to the eluent. For this reason it was not possible to obtain reasonable molecular weights from polymers **23b** and **23c** and the successful removal of the protective group was verified by NMR-sepectroscopy.

#### 5.4.3 NMR-spectroscopy

The most characteristic feature of the  $^1\text{H}$ -NMR-spectrum of polymers with the structure **23** in comparison to those still carrying the TBDMS-group (**22**) is the disappearance of the significant singlets of the TBDMS-protective group at 0.06 ppm and 0.89 ppm. The polymer backbone is still present in a bulk of resonance signals in the range of 0.95 ppm – 1.91 ppm.

The hydroxy function as well as the methylene units of the polyHEMA-block are detected in form of diffuse broad singulets at 3.47 ppm, 3.82 ppm and 4.08 ppm. The signals for the methylene units are shifted to lower field due to the direct neighbourhood to the polar hydroxy function after removal of the TBDMS-group. In the aromatic region of the spectrum, the protons of the poly(4-vinyltriphenylamine) block are present in a broad multiplet ranging from 6.41 ppm to 7.09 ppm.

#### 5.4.4 Thermal analysis

Thermal properties of the polymers poly(4-vinyltriphenylamine)-*block*-poly(HEMA) **23b** and **23c** were investigated. The glass transition temperatures  $T_g$  as well as onset temperatures of thermal decay  $T_{onset}$  are outlined in Table 5-8.

**Table 5-8:** Glass transition temperatures ( $T_g$ ) and onset temperatures of thermal decay ( $T_{onset}$ ) of polymers **23b** and **23c**:

polymer	<b>23b</b>	<b>23c</b>
$T_g$ [°C] <sup>a)</sup>	138.4	128.4
$T_{onset}$ [°C] <sup>b)</sup>	266	260

a) Heating / cooling rate = 10 Kmin<sup>-1</sup>; b) defined as temperature at which weight loss is starting; determined via heating from 30 to 650 °C with 10 Kmin<sup>-1</sup>.

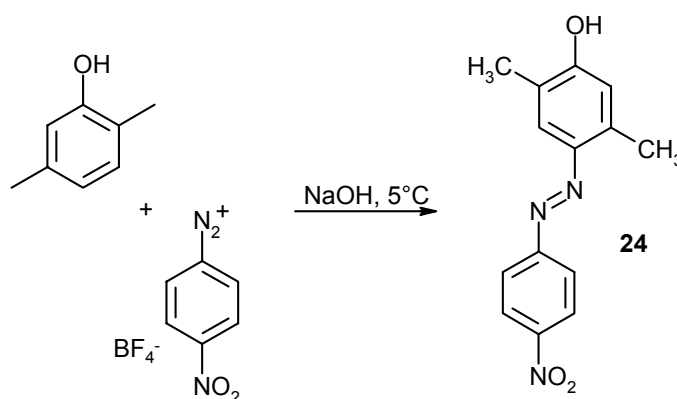
After removal of the TBDMS-protective groups both polymers with the structure **23** exhibit one glass transition at about 130 °C which can be assigned to the presence of the poly(4-vinyltriphenylamine) block. The glass transition corresponding to the poly(HEMA) could not be detected. With  $T_{onset}$  of about 260 °C, the block copolymers **23b** and **23c** show higher thermal stability than the polymers still carrying the protective group (**22b** and **22c**).

### 5.4.5 Synthesis and characterization of 1-[(2,5-dimethyl-4-(4-nitrophenylazo) phenoxy] butyric acid chloride (**27**)

The incorporation of the dye-unit was carried out via subjecting the poly(HEMA) block to polymeranalogous reaction with an appropriate derivative of the NLO-dye DNPP. Thus the acid chloride derivative of 2,5-dimethyl-4-(4-nitrophenylazo)-phenol (DNPP) **24** was prepared to enable a polymeranalogous esterification reaction with the hydroxy function of the HEMA monomer unit of the AB-diblock copolymers. 2,5-dimethyl-4-(4-nitrophenylazo) phenol (DNPP) **24** was prepared via azo coupling followed by a three-step conversion to the desired 1-[(2,5-dimethyl-4-(4-nitrophenylazo) phenoxy] butyric acid chloride (**27**).

#### *Synthesis and characterization of 2,5-dimethyl-4-(4-nitrophenylazo) phenol (DNPP) (24)*

The preparation of 2,5-dimethyl-4-(4-nitrophenylazo) phenol (DNPP) **24** was carried out in an azo coupling reaction with 2,5-dimethylphenol and the diazonium salt 4-nitrobenzenediazonium tetrafluoroborate as shown in Scheme 5-6.



**Scheme 5-6:** Schematic representation of the synthesis of 2,5-dimethyl-4-(4-nitrophenylazo)-phenol (DNPP) **24**.

To a solution of 2,5-dimethylphenol in aqueous NaOH, an equimolar amount of the diazonium salt dissolved in diluted acetic acid was added after cooling both solutions to

0°C. The pH value of the reaction mixture had to be above 7 during this procedure and was therefore adjusted by addition of aqueous NaOH when necessary. The alkaline solution was stirred at 5 °C for 1h followed by precipitation of the product by adding acetic acid and shifting pH below 7. The product was isolated by filtration and washed excessively with water to remove any traces of acid or salt.

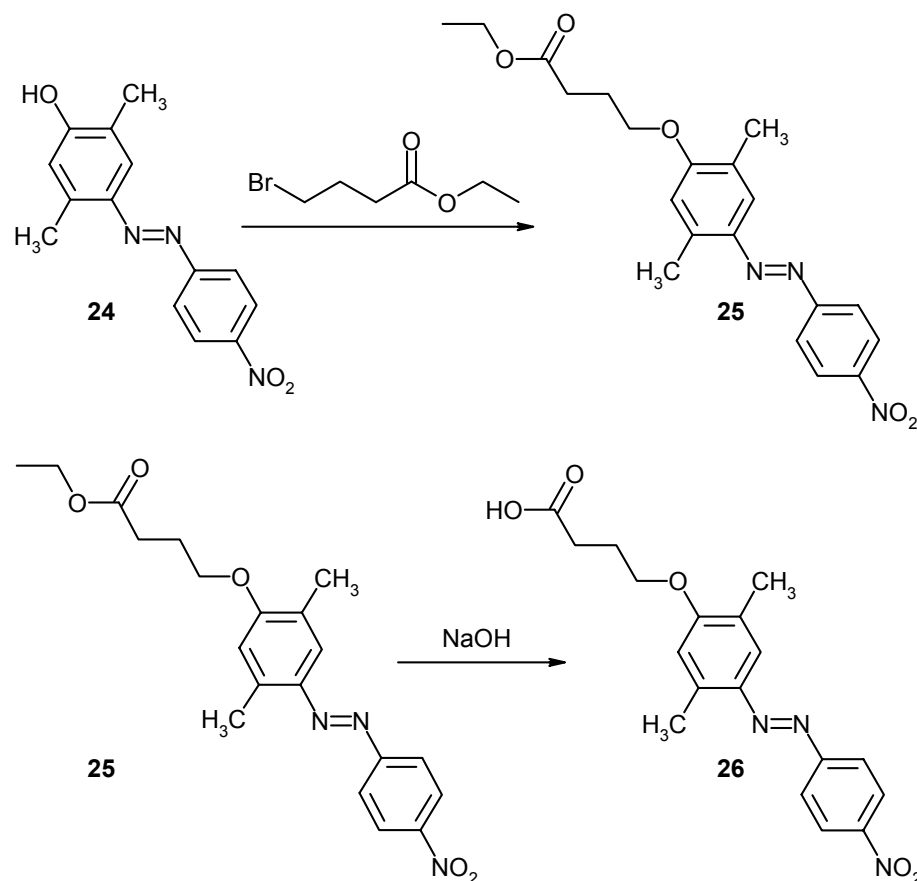
The structure of DNPP (**24**) was verified via NMR-spectroscopy resulting in resonance signals clearly representing the substitution pattern of the aromatic rings: Two singlets at 6.74 ppm and 7.61 ppm respectively correspond to two aromatic protons of the phenol ring; the methyl groups in 2,5-position are represented by two significant singlets at 2.26 ppm and 2.67 ppm and the hydroxy proton is visible in a broad singlet at 5.18 ppm. Two doublets shifted to lower field at 7.92 ppm and 8.32 ppm correspond to the AA'XX'-spin system of the nitro-substituted arom. The structure is supported by <sup>13</sup>C-NMR spectroscopy and mass-spectrometry as reported in the experimental part.

*Synthesis and characterization of 1-[2,5-dimethyl-4-(4-nitrophenylazo) phenoxy] butyric acid (26)*

1-[2,5-dimethyl-4-(4-nitrophenylazo) phenoxy] butyric acid (**26**) was prepared in two reaction steps starting with an etherification reaction of 2,5-dimethyl-4-(4-nitrophenylazo)-phenol with 1-bromoethylbutyrate with K<sub>2</sub>CO<sub>3</sub> and KI in acetone as shown in Scheme 5-7. The reaction mixture was refluxed for at least two days and quenched when the educt was fully consumed (TLC-control). The product 1-[2,5-dimethyl-4-(4-nitrophenylazo) phenoxy] ethylbutyrate **25** was isolated by evaporation of acetone and no further purification was carried out. In a second reaction step, the ethylbutyrate was converted to the carboxylic acid by saponification of the ethylester with NaOH in ethanol / water (1:1 v/v). After stirring for 1h the solution was acidified with HCl and the product was precipitated. Filtration and washing yielded pure 1-[2,5-dimethyl-4-(4-nitrophenylazo) phenoxy] butyric acid **26**.

The two DNPP-derivatives **25** and **26** were characterized via <sup>1</sup>H-NMR spectroscopy. The protons at 1.25 ppm and 4.13 ppm in the spectrum of **25** can be attributed to the ethyl ester group.

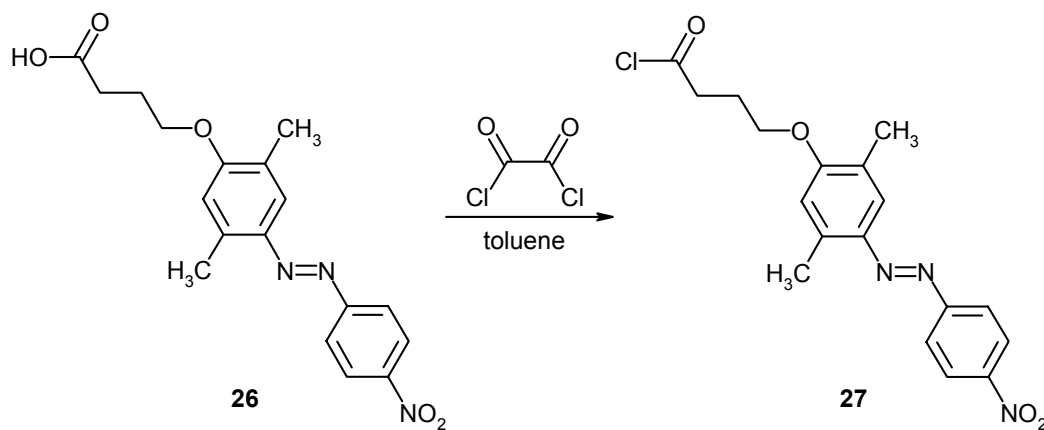
These signals disappeared in the  $^1\text{H-NMR}$  spectrum of **26** and the proton corresponding to the carboxylic acid group at 12.17 ppm was visible. The details of the spectroscopic characterization as well as  $^{13}\text{C-NMR}$  and mass spectrometry data supporting the structure of **25** and **26** are given in the experimental section.



**Scheme 5-7:** Schematic representation of the two-step synthesis of 1-[2,5-dimethyl-4-(4-nitrophenylazo) phenoxy] butyric acid (**26**).

In a subsequent reaction step presented in Scheme 5-8 1-[2,5-dimethyl-4-(4-nitrophenylazo) phenoxy] butyric acid **26** was converted to the corresponding acid chloride **27** via reaction with oxalyl chloride. The reaction was carried out in dried toluene with a 7 times excess of oxalyl chloride.

After refluxing the reaction mixture for 3 h most of the oxalyl chloride together with half of the toluene were removed from the flask via vacuum distillation. Dry toluene, n-hexane and a small amount of  $K_2CO_3$  were added and the deep red solution was refluxed for additional 2 h. After filtration of the hot reaction mixture it was cooled down to 4 °C until the product **27** appeared in form of red crystals out of the solution. Ensuring the exclusion of humidity 1-[2,5-dimethyl-4-(4-nitrophenylazo) phenoxy] butyric acid chloride **27** was isolated by filtrating the crystals from the mother liquor under argon stream.



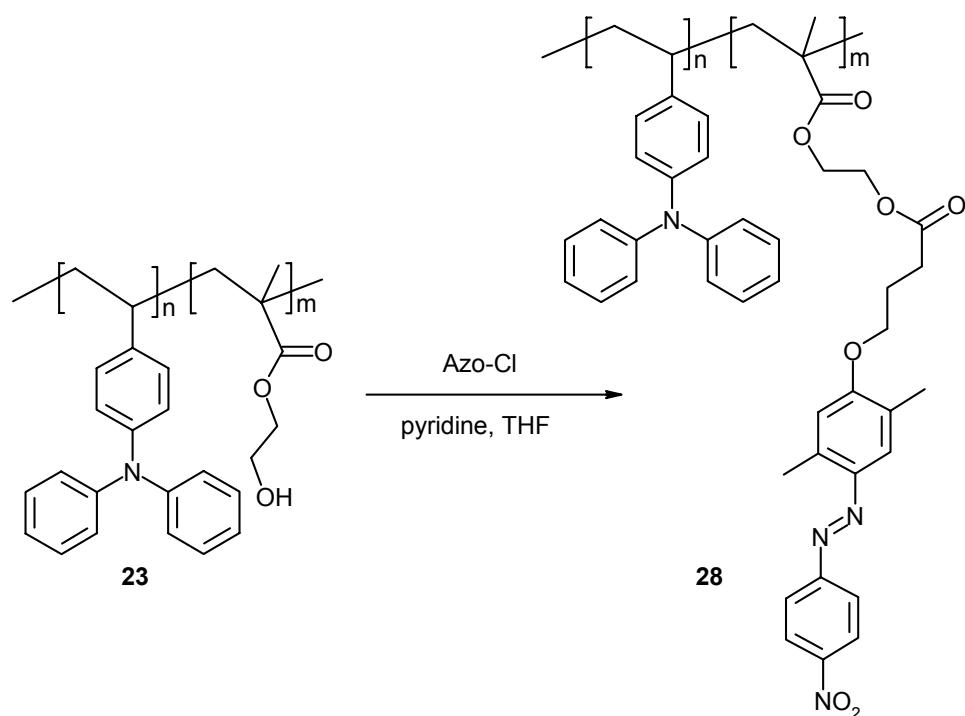
**Scheme 5-8:** Schematic representation of the synthesis of 1-[2,5-dimethyl-4-(4-nitrophenylazo) phenoxy] butyric acid chloride (**27**) using oxalyl chloride in dried toluene.

1-[2,5-dimethyl-4-(4-nitrophenylazo) phenoxy] butyric acid chloride was characterized using proton NMR-spectroscopy resulting in a very similar spectrum in comparison to the educt **26**. In the spectrum of **27** almost all signals are shifted to lower field. For example, for compound **27** the methylene group adjacent to the carbonyl carbon is situated at 3.16 ppm whereas it was present at 2.43 ppm in the spectrum of **26**. Moreover the proton of the carboxylic acid function has disappeared in the spectrum of **27** confirming a successful conversion to the acid chloride derivative.

#### 5.4.6 Synthesis and characterization of poly(4-vinyltriphenylamine)-*block*-poly(HEMA-DNPP)

In a last reaction step the dye functionality was incorporated into the polymer chain of poly(4-vinyltriphenylamine)-*b*-poly(HEMA) of polymers **23b** and **23c** via esterification reaction with 1-[2,5-dimethyl-4-(4-nitrophenylazo) phenoxy] butyric acid chloride (**27**) as presented in Scheme 5-9. The reaction was carried out in THF with pyridine as catalyst under water free conditions. The start of this reaction was indicated by the precipitation of pyridinium hydrochloride as white powder from the reaction solution. After a total reaction time of 24 h the product was precipitated directly from the reaction mixture into methanol yielding an orange coloured powder. <sup>1</sup>H-NMR spectrum of the raw product recorded in THF-d<sub>8</sub> revealed a huge amount of unreacted azo-dye presumably hydrolyzed to the carboxylic acid derivative **26** mixed with fully functionalized polymers **28**. To remove the residual azo dye, the polymer was soxhlet extracted with methanol but with unsatisfying results. The isolation of pure **28** was successfully carried out exploiting the different solubilities of polymer and low-molecular azo-dye in chloroform. After preparing a suspension of the raw product in chloroform the low-molecular weight dye **26** could be removed by filtration as it did not dissolve in chloroform yielding pure poly(4-vinyltriphenylamine)-*b*-poly (HEMA-DNPP) (**28**).

The characterization of the novel AB-diblock copolymers **28b** and **28c** carrying dye moiety as well as hole transport block was performed via NMR-spectroscopy. The molecular weight determination was carried out via SEC and static light scattering which will be discussed in the following sub-section.



**Scheme 5-9:** Schematic representation of the synthesis of poly(4-vinyltriphenylamine)-*b*-poly(HEMA-DNPP) (**28**).

#### 5.4.7 Size exclusion chromatography (SEC)

Size exclusion chromatography of polymers **28a** and **28b** carried out in THF + 0.25 wt% TBAB as eluent resulted in monomodal elution curves with very low polydispersities. As it is shown in Table 3-1 the molecular weights of the resulting fully functionalized AB-diblock copolymers are lower than those of the corresponding non-functionalized starting polymers **21b** and **21c**.

**Table 5-9:** Comparison of molecular weights and polydispersities of block copolymers **21c** and **21b** with those of bifunctional polymers **28b** and **28c**.

polymer	<b>21b</b>	<b>21c</b>	<b>28b</b>	<b>28c</b>
$M_n$ [g/mol] <sup>a)</sup>	8304	9620	4077	4448
$M_w$ [g/mol] <sup>a)</sup>	11943	14527	4826	5058
<b>PDI</b> <sup>b)</sup>	1.44	1.51	1.18	1.14

a) Determined via SEC with THF + 0.25 wt% TBAB as eluent, calibration versus polystyrene standards, UV-detection; b) PDI =  $M_w/M_n$ .

The reason for this are probably problems with the method of SEC which appears to be not suitable for the newly prepared materials **28b** and **28c**: As already reported in previous sections there might be enormous differences between hydrodynamic volume of the sample materials and the calibration standards which are polystyrenes.

#### 5.4.8 NMR-spectroscopy

The fully functionalized diblock copolymers **28** were characterized via  $^1\text{H}$ -NMR spectroscopy recorded in deuterated THF. It is remarkable that the resonance signals corresponding to the dye-functionlized HEMA-block are very diffuse which suggests agglomeration between the dye moieties. From earlier work in the group of MC I it is known that with lowering the dye content within the polymer chain the signal start to fade and finally disappear<sup>117</sup>. The chemical shifts and spectral features for polymer **28c** will be given as example in the following: As already reported the polymer backbone is present in a bulk of resonance signals in the range of 0.89 ppm – 1.29 ppm. At 2.46 ppm a singlet is visible which can be assigned to the methyl substituents of the phenyl group of the NLO-dye attached to poly(HEMA-block).

<sup>117</sup> A. Fuchs, *joint group discussion*.

The methylene units of HEMA-monomer unit is hardly visible in form of a very broad signal at 4.08 ppm. From 6.55 ppm to 7.09 ppm the aromatic protons of poly(4-vinyltriphenylamine) block are present. Three broad singulets at 7.58 ppm, 7.86 ppm and 8.26 ppm can be attributed to aromatic protons of the azo-dye supporting the suggested structure for poly(4-vinyltriphenylamine)-b-poly(HEMA-DNPP) **28c**.

#### 5.4.9 Thermal analysis

In Table 5-10 the thermal properties ( $T_g$  and  $T_{onset}$ ) of the newly synthesized poly(4-vinyltriphenylamine)-b-poly(HEMA-DNPP) **28b** and **28c** are summarized.

**Table 5-10:** Glass transition temperatures ( $T_g$ ) and onset temperatures of thermal decay ( $T_{onset}$ ) of polymers **28b** and **28c**.

polymer	<b>28b</b>	<b>28c</b>
$T_g$ [°C] <sup>a)</sup>	134.2	130.1
$T_{onset}$ [°C] <sup>b)</sup>	237	233

a) Heating / cooling rate = 10 Kmin<sup>-1</sup>; b) defined as temperature at which weight loss is starting; determined via heating from 30 to 650 °C with 10 Kmin<sup>-1</sup>.

With the introduction of the dye functionality via polymeranalogous esterification the thermal stability of the AB-diblock copolymers decreases distinctly. Whereas polymers **23** without azo-dye attached exhibit  $T_{onset}$  of about 260 °C the thermal decay of the novel materials with the structure **28** already starts little over 230°C with  $T_{onset}$  being 236.8 °C and 232.9 °C for **28b** and **28c** respectively. For the fully functionalized AB-diblock copolymers **28b** and **28c** only one glass transition above 130 °C was detected which corresponds to the poly(4-vinyltriphenylamine) block. The glass transition for the dye-functionalized block could not be observed.

### 5.4.10 UV-Vis Spectroscopy

The method of UV-Vis spectroscopy was used to determine the content of the NLO-dye within polymers **28b** and **28c**. First of all the extinction coefficient of the dye-unit was determined: An UV-Vis spectrum of 2,5-dimethyl-4-(4-nitro-phenylazo)-phenol (DNPP) **24** which is defined here as the basic dye unit was recorded and the extinction coefficient was calculated from optical density at maximum absorption wavelength (395 nm) and concentration using Equation 7. Applying this result in Equation 12 and Equation 13 reveals the weight percentage of dye of **28b** and **28c**:

$$c_{dye} = \frac{OD}{\varepsilon_{dye} \cdot l} \quad (\text{Equation 12})$$

$$\chi_{dye} = \frac{c_{dye} \cdot M_{dye}}{c_{polymer}} \cdot 100 \quad (\text{Equation 13})$$

$c_{dye}$  = molar dye concentration [mol/l]

$OD$  = optical density

$l$  = thickness of sample [cm]

$\varepsilon_{dye}$  = extinction coefficient of **24** [ $\text{lmol}^{-1}\text{cm}^{-1}$ ]

$\chi_{dye}$  = weight percentage of basic dye unit **24** [%]

$M_{dye}$  = molecular weight of **24** = 271.15 [g/mol]

$c_{polymer}$  = defined concentration of polymer **28** [g/l]

From the UV-Vis spectrum of a solution of polymer **28** in chloroform with the defined concentration  $c_{polymer}$  the molar dye concentration  $c_{dye}$  of dye units within this solution was calculated (Equation 12). With this information it is possible to calculate the ratio of dye concentration and polymer concentration (Equation 13). The factor of the molecular weight of the dye is needed to equal the units and via multiplication with the factor 100 the result can be obtained in weight percentage.

**Table 5-11:** Weight percentage of dye in polymers **28b** and **28c** calculated from UV-Vis spectra recorded in chloroform.

polymer	<b>28b</b>	<b>28c</b>
$\chi_{\text{dye}}$ [wt%]	9.6	41.2

The normalized UV-Vis spectra of both polymers **28b** and **28c** are plotted in the next figure to make the results more clear.

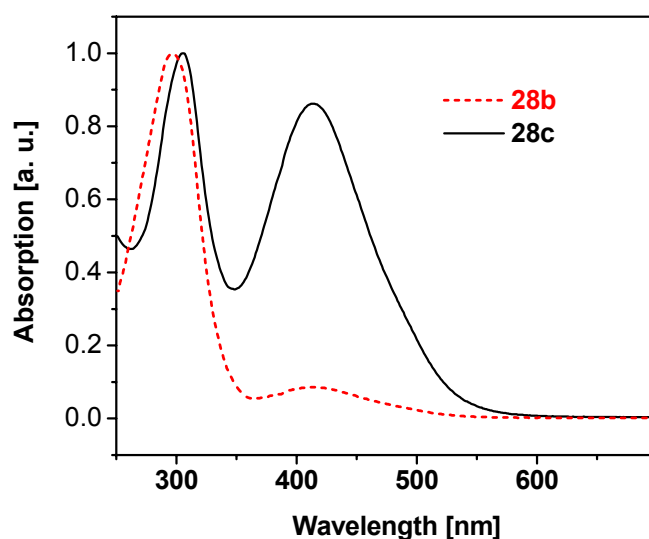


**Figure 5-6:** Normalized UV-Vis spectra of polymers **28b** (dashed line) and **28c** (solid line) recorded in  $\text{CHCl}_3$ .

The spectrum of **28b** exhibits a strong absorption band at 300 nm which represents the poly(4-vinyltriphenylamine) block whereas the absorption of the block functionalized with the NLO-dye at 410 nm is weak pointing out to the low dye content of 9.6 %. In contrast to that the absorption band of the dye moieties is very strong in the UV-Vis spectrum of polymer **28c** supporting the dye content in **28c** being high.

The goal of synthesis of fully functionalized AB-diblock copolymers of the structure poly(4-vinyltriphenylamine)-b-poly(HEMA-DNPP) was successfully attained using a multi-step synthetic strategy based on the method of ATRP. Poly(4-bromostyrene) macroinitiators (**19**) were prepared by carrying out ATRP of 4-bromostyrene using CuCl and PMDETA as catalytic system and anisole as solvent. It was possible to start the polymerization of HEMA-TBDMS (**20**) which was chosen as monomer unit for the second block using macroinitiators **19** resulting in block copolymers with the structure poly(4-bromostyrene)-b-poly(HEMA-TBDMS) (**21**). The poly(4-bromostyrene) block was converted to the hole transport triphenylamine functionality adopting a Pd-catalyzed amination reaction which has been investigated extensively in previous sections of this thesis. The incorporation of the dye unit was performed via esterification reaction of an acid chloride derivative of an NLO-dye (**27**). Using this synthetic strategy it was possible to obtain fully functionalized AB-diblock copolymers **28b** and **28c** with a dye content of 9.6 % and 41.2 % respectively.

Thus polymers **28b** and **28c** are fully functionalized AB-diblock copolymers carrying a hole transport block and an NLO-dye block. These polymers are of interest to study the photorefractive properties in block copolymers and may open the way to a new field of material science.

## 6 Summary

This thesis is dealing basically with synthesis of organic materials for electro-optical applications and interfacial modifications in such applications. It is structured into two major sections each of which presenting a new concept of bifunctional materials:

*I. Bifunctional Ru(II) dyes carrying hole transport units*

*II. Fully functionalized AB-diblock copolymers*

In the following paragraphs the different concepts and synthetic pathways are summarized and outstanding results will be presented in compact form.

*I. Bifunctional Ru(II) dyes carrying hole transport units for interface modification in solid-state dye-sensitized nc-TiO<sub>2</sub> solar cells*

The main concern in this part of this work was the improvement of the TiO<sub>2</sub> / dye / hole conductor interfaces in solid-state dye-sensitized TiO<sub>2</sub> solar cells. Therefore novel concepts of bifunctional materials carrying light absorbing Ru(II) dye centre as well as hole transport triphenylamine moieties were developed for the following reasons:

- Improvement of wetting between polar Ru(II) dye layer and the non-polar spiro-hole conductor.
- Spatial separation of excited dye cation centre (HOMO) away from the TiO<sub>2</sub> surface.
- Retardation of recombination of holes in the dye molecule with electrons in TiO<sub>2</sub>.

In order to reach these goals, novel bipyridine ligands carrying hole transport units (bpy-TPA **6** and bpy-TPD **11**) with bipyridine centre for coordination of a transition metal atom have been prepared (see Figure 6-1).

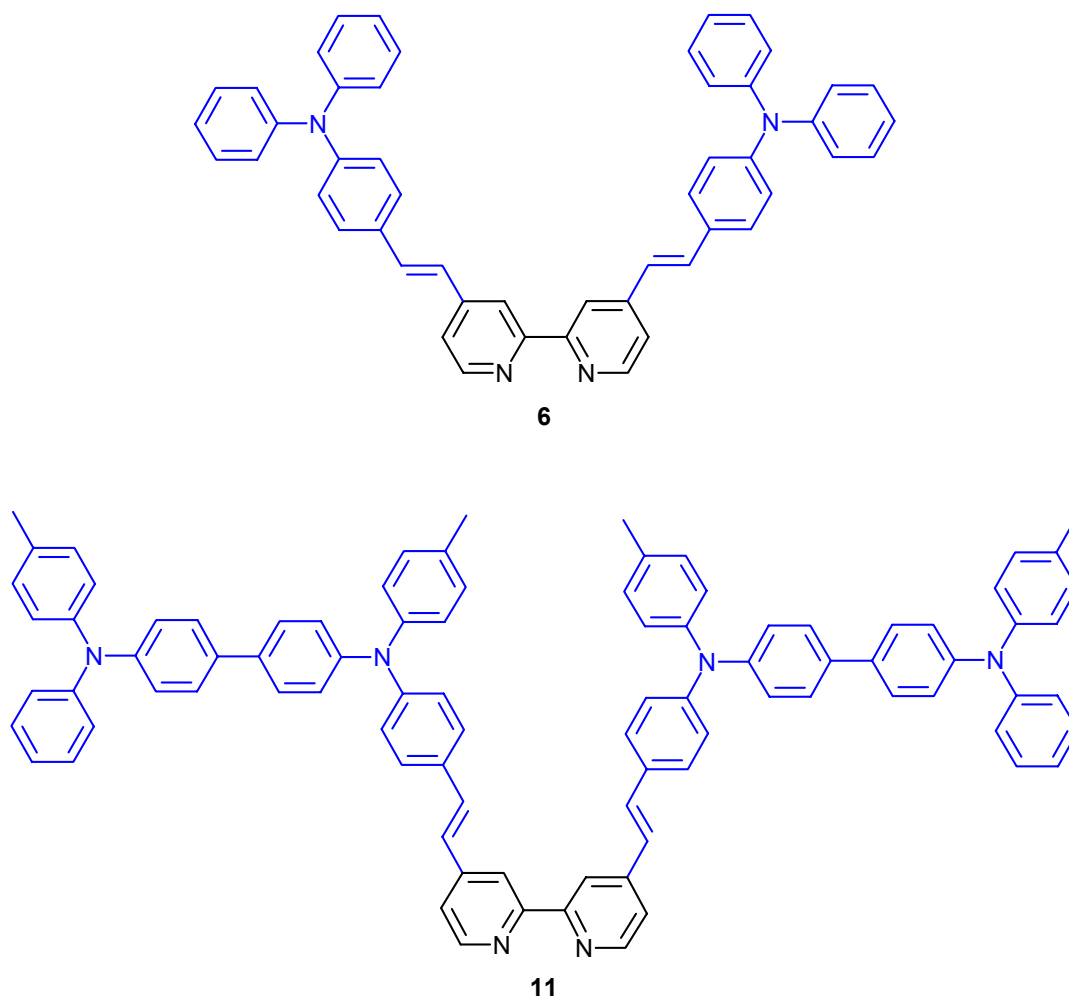


**Figure 6-1:** Chemical structures of novel bipyridine ligands *bpy-TPA* (**6**) and *bpy-TPD* (**11**) carrying hole transport units covalently attached to a bipyridine centre for coordination of a transition metal atom.

According to Figure 6-2 the new bifunctional Ru(II) dyes **14** and **15** have been prepared in a metallation reaction applying Ru(II) precursor and characterized. The structures of these bifunctional compounds are given in Figure 6-3. Both new dyes **14** and **15** exhibit a tremendous increase in the extinction coefficients  $\epsilon$  as determined via UV-Vis spectroscopy in comparison to standard dyes which do not carry these hole transport units.

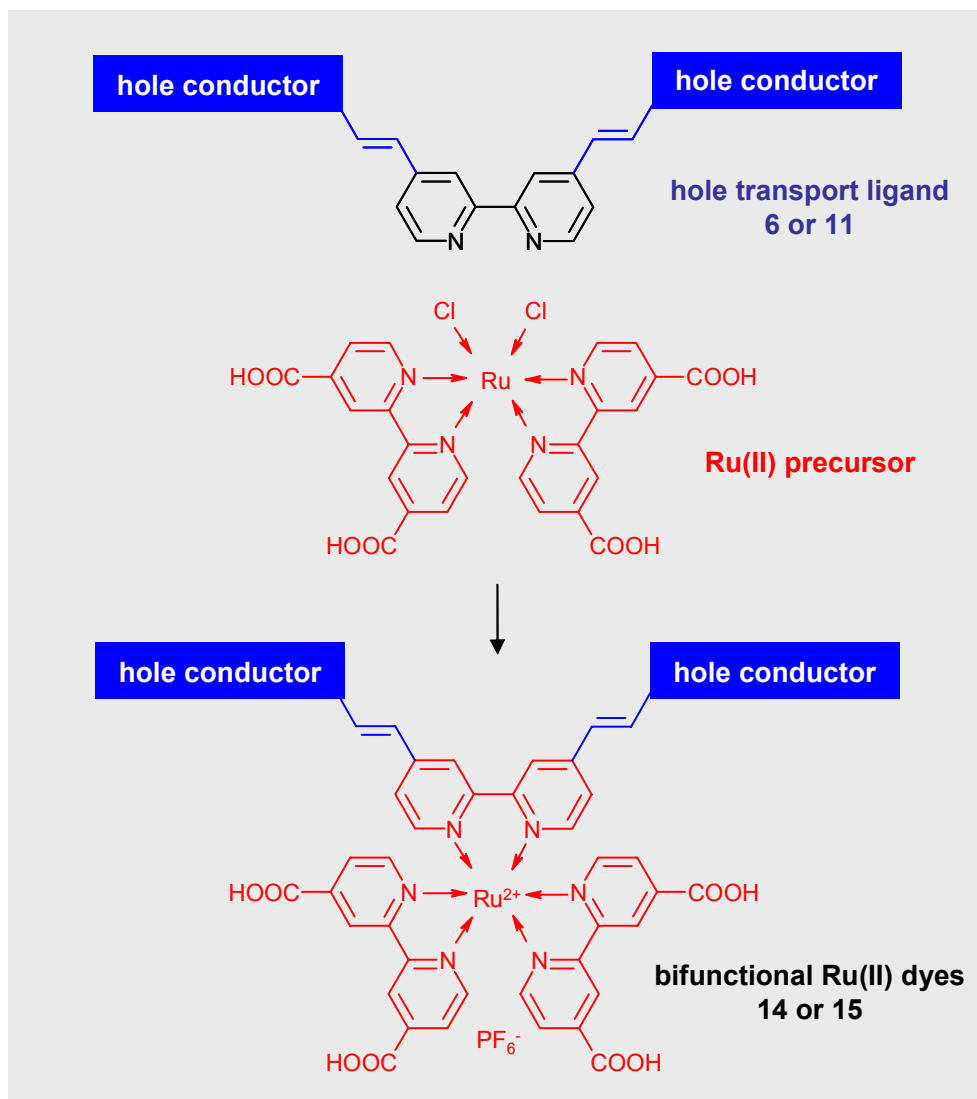


**Figure 6-2:** Schematic representation of the metallation of bipyridine ligands **6** and **11** applying a Ru(II) precursor resulting in novel bifunctional Ru(II) dyes **14** and **15**.

The new dye **14** exhibit  $\epsilon$  of  $51\,900\text{ lcm}^{-1}\text{mol}^{-1}$  at  $405\text{ nm}$  which is more than three times higher than that of conventional dyes at the appropriate wavelength. For bifunctional dye **15**  $\epsilon$  is  $64\,500\text{ lcm}^{-1}\text{mol}^{-1}$  at  $349\text{ nm}$ , also being more than three times higher than the value for conventional dyes.

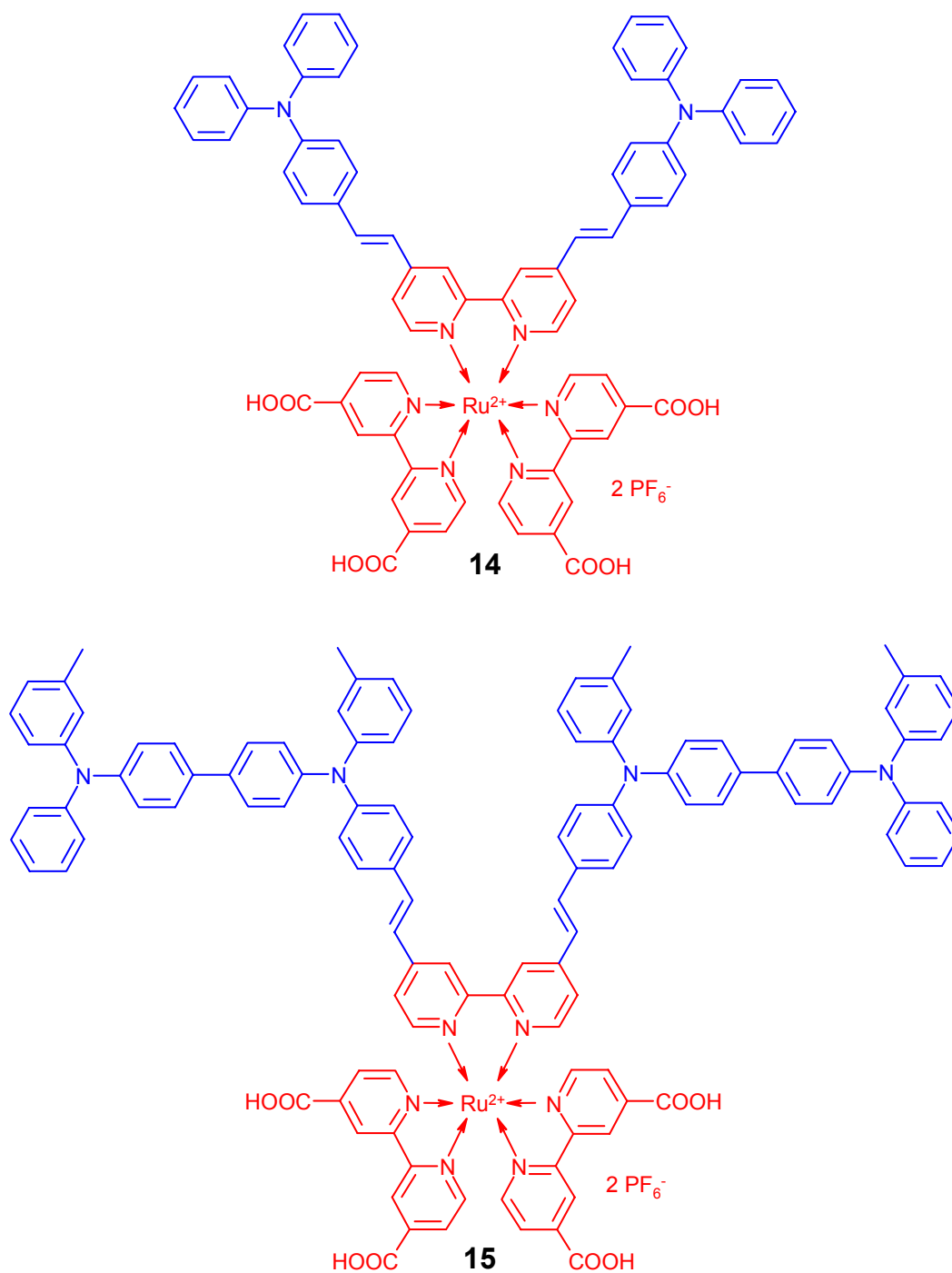


**Figure 6-3:** Chemical structures of new bifunctional materials **14** and **15** carrying triarylamine moieties for hole transport and Ru(II) dye centre as light absorbing unit.

This makes them very promising for the use in dye-sensitized TiO<sub>2</sub> solar cells. As an example compound **14** was tested as interface modification agent and dye in various compositions with standard dye N 719 in solid-state dye-sensitized TiO<sub>2</sub> solar cells.

The application of this material resulted in a considerable improvement of all photovoltaic parameters using a 1 : 1 mixture of dyes as shown in Table 6-1. Short circuit current I<sub>SC</sub> was improved up to 60 %, open circuit voltage U<sub>OC</sub> by 25 % and finally a power conversion efficiency was increased more than by a factor of two by using a 1 : 1 mixture of standard dye N 719 and **14** (see Table 6-1).

**Table 6-1:** Photovoltaic parameters of solar cells prepared using different dye compositions of N 719 and **14** (white light source, AM 1.5, 77 mWcm<sup>-2</sup>).

dye composition N 719 : 14	I <sub>SC</sub> [mA]	U <sub>OC</sub> [V]	FF [%]	η [%]
N 719	1.95	645	40	0.70
3 : 1	2.49	720	33	0.76
1 : 1	3.18	755	51	1.63
1 : 3	1.84	750	41	0.73
14	1.07	810	42	0.48

An important question was, if the spatial separation of the positive hole from the TiO<sub>2</sub> surface really could be increased by using bifunctional dyes carrying a hole transport unit. This was proved successfully by transient absorption spectroscopy performed by the group of Durrant at Imperial College, London, UK: The dye cations were generated by photo excitation of the dyes after chemisorption onto a TiO<sub>2</sub> surface. It could be shown that the decay half time (t<sub>50%</sub>) of the dye cation for bifunctional dyes **14** and **15** chemisorbed onto a TiO<sub>2</sub> surface was 0.35 ms and 5 ms respectively before the decay by recombination.

This means that by extending the conjugation of the bipyridine ligands bpy-TPA and bpy-TPD in **14** and **15** respectively,  $t_{50\%}$  could be increased by three orders of magnitude and recombination could be retarded tremendously. Furthermore, a spatial separation of the HOMO orbitals of the dyes away from TiO<sub>2</sub> surface was assumed. This was verified by time-dependent density functional theory (TD-DFT) ab-initio calculations which was also carried out in the group of Durrant to determine the spatial distribution of the HOMO orbitals of the dyes after excitation. It was calculated that the HOMO orbitals of dye **14** are delocalized over the bipyridine unit and the triphenylamine groups. In contrast to that, the HOMO orbitals of **15** are spread only over the TPD moieties resulting in increased spatial separation from the TiO<sub>2</sub> surface compared to **14** assuming the anchoring of the dye units onto TiO<sub>2</sub> via the carboxylic acid anchor groups present in these dyes.

The concept of bifunctional materials was further extended to polymers by the preparation of Ru(II) centred dyes carrying poly(4-vinyltriphenylamine) units as hole conductor chains. It was assumed that by further extension of the hole transport ligand the spatial separation of the dye cation from TiO<sub>2</sub> may become even larger and thus recombination even more retarded. Thus a strategy for the synthesis of the bifunctional polymers was developed which is shown in Figure 6-4.

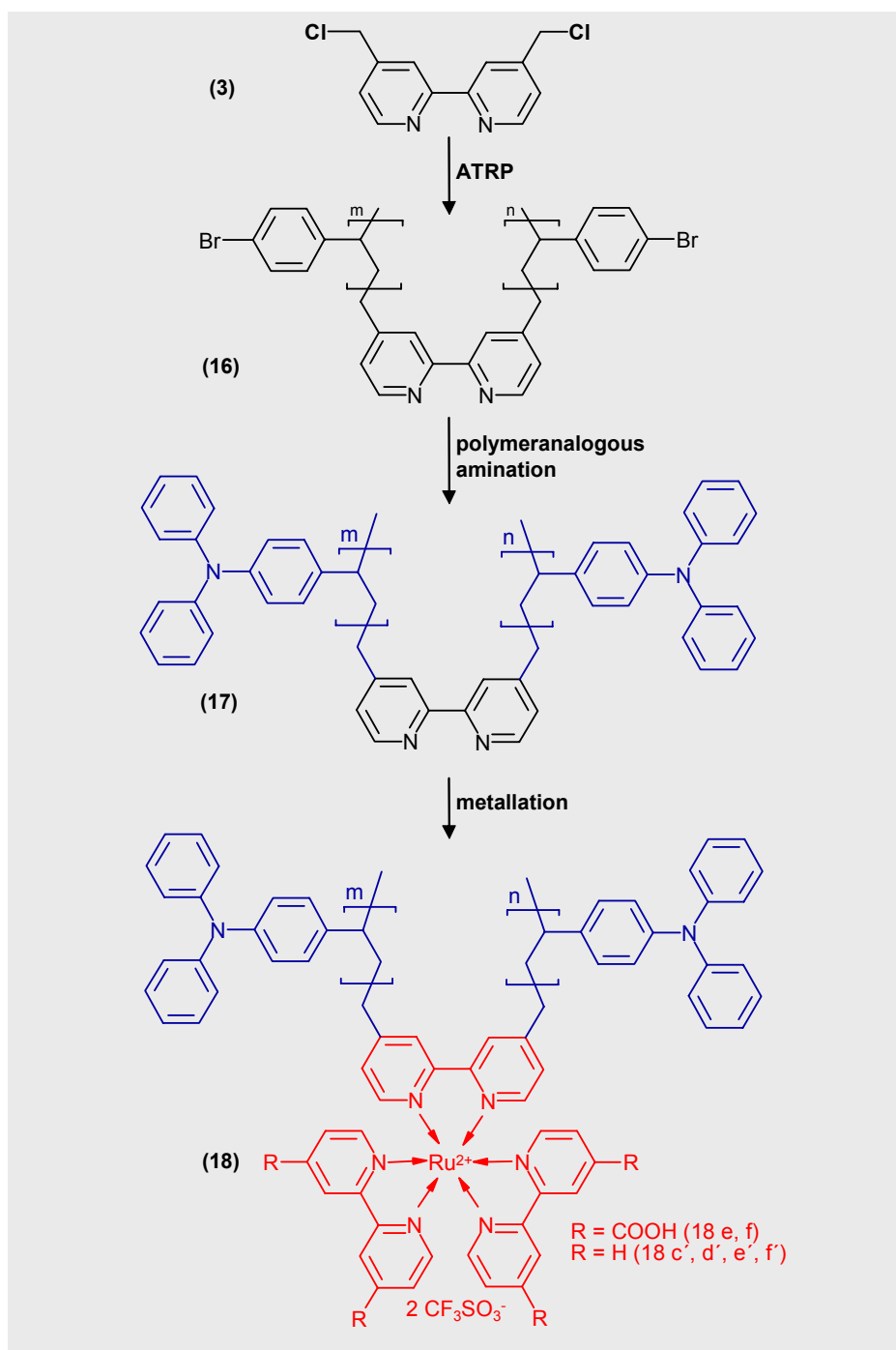


**Figure 6-4:** Schematic representation of the synthesis of bifunctional polymers (**18 e, f** and **18c' - f'**) via ATRP followed by polymeranalogous amination and metallation with Ru(II) precursors.

For the synthesis of the polymers the method of atom transfer radical polymerization (ATRP) was adopted starting with the polymerization of 4-bromostyrene using 4,4'-bis(chloromethyl)-2,2'-bipyridine (**3**) as initiator and CuCl / PMDETA as catalytic system. The polymerization conditions were optimized and thus it was possible to control the molecular weight of the polymers and to obtain appreciably low polydispersities. The resulting 4,4'-bis[poly(4-bromostyryl)methyl]-2,2'-bipyridines (**16**) were subjected to a Pd-catalyzed polymeranalogous amination reaction with diphenylamine yielding 4,4'-bis[poly(4-vinyl-triphenylamino)methyl]-2,2'-bipyridines (**17**) with high conversion in extraordinarily short reaction times. Metallation of polymers **17** with Ru(II) precursors with and without COOH-anchor groups resulted in the desired bifunctional polymeric Ru(II) dyes **18 e, f** and **18 c', d', e', f'** as shown in Figure 6-4. The synthetic procedure presented here is of a general nature and the dye content in such polymers could be tuned between 2 % and 20 % by controlling the length of the polymer chains. These complexes have been characterized and their thermal properties determined. Transient absorption studies of the bifunctional polymeric Ru(II) dyes **18 e, f** and **18 c' - f'** were of particular interest considering the extreme retardation of recombination observed for the low molecular weight bifunctional dye **15**. For polymer **18f** with anchor groups and ~ 144 repeating units of 4-vinyltriphenylamine in the polymer chain a decay half time  $t_{50\%}$  of the dye cation of 4 s was determined which is actually the highest value ever measured for Ru(II) dyes on metal-oxide films. A comparison of the decay studies of all new bifunctional materials **14**, **15** and **18f** is given in Figure 6-5 showing the relative decrease in optical density ( $\Delta mOD$ ) of the different radical cations as a function of time.

According to TD-DFT ab-initio calculations the dye HOMO orbitals are delocalized over the poly(4-vinyltriphenylamine) chain showing increased spatial separation away from the TiO<sub>2</sub> surface than observed for low molecular weight dyes **14** and **15**. All these facts point out that the new polymeric dyes exhibit considerably slower charge recombination rates than more simple molecular dyes which are nowadays used in dye-sensitized TiO<sub>2</sub> solar cells.

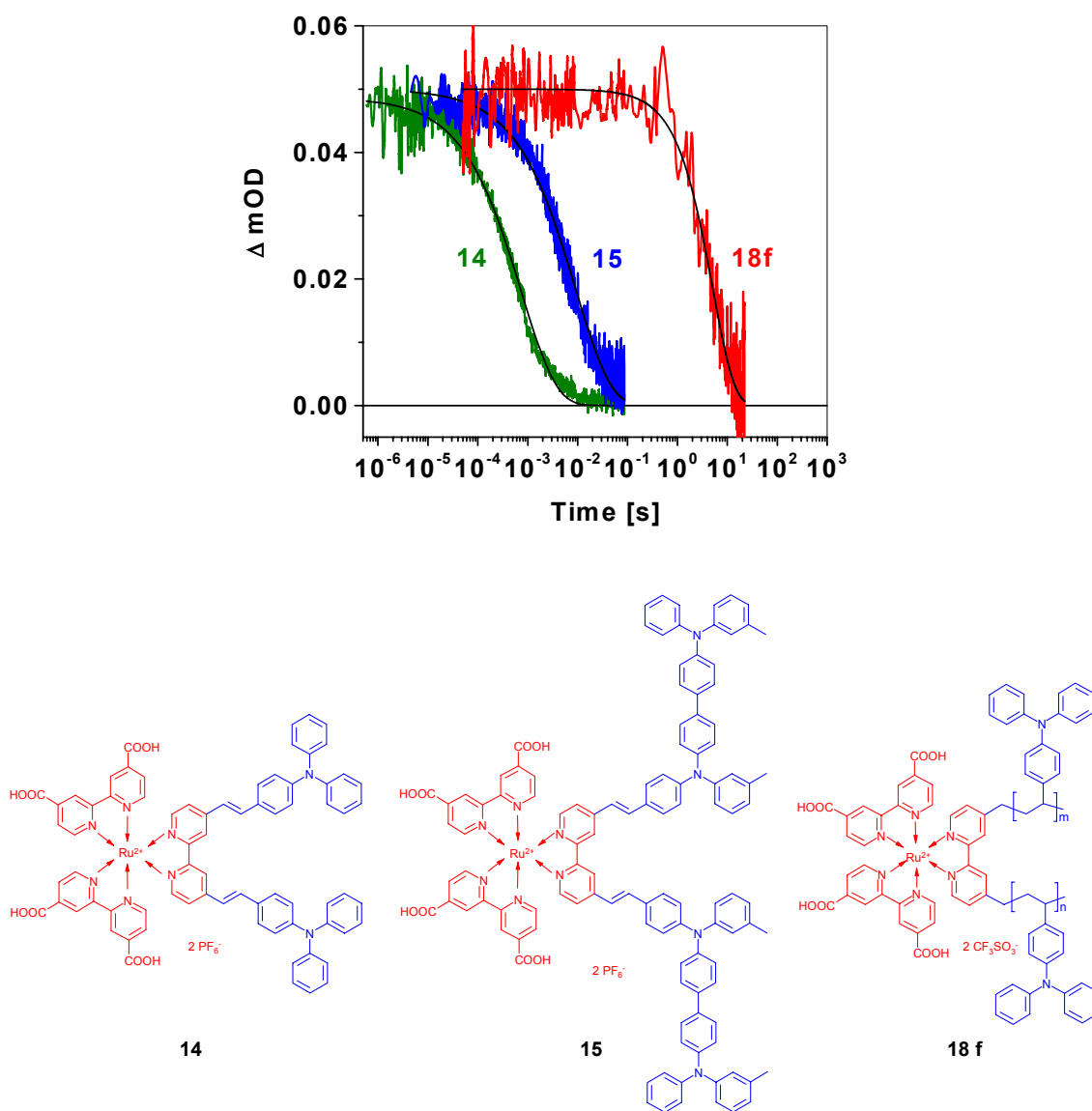


**Figure 6-5:** Decay of the dye radical cation of model compounds **14** and **15** in comparison with polymer **18f** (144 vTPA-repeating units) monitored at 900 nm following pulsed laser excitation of dye sensitized TiO<sub>2</sub> films at 450 nm; experimental data (green, blue, red) and exponential fits (black solid lines). The structures of **14**, **15** and **18f** are given below the graph.

Considering the results above, it is very clear that the new synthetic concept was realized successfully. Novel bifunctional materials with low molecular weight (**14** and **15**) as well as polymers (**18 e, f** and **18 c' - f'**) have been prepared which turned out to match all criteria for interface modification agents in dye-sensitized TiO<sub>2</sub> solar cells. This was also verified using compound **14**. Especially, the polymeric complexes exhibit extraordinarily long decay half times  $t_{50\%}$  in the range of seconds which is the longest-living radical cation ever measured on dye-sensitized TiO<sub>2</sub> films.

## *II. Fully functionalized AB-diblock copolymers carrying hole transport and NLO-dye blocks*

Another synthetic approach of this thesis was to explore the suitability of the polymerization technique ATRP for the synthesis of fully functionalized AB-diblock copolymers for photorefractive applications. For this purpose, 4-bromostyrene was polymerized via ATRP using  $\alpha$ -chloromethylpropionate as initiator and CuCl / PMDETA as catalytic system yielding poly(4-bromostyrene) macroinitiators (**19 a – e**). The control of this polymerization reaction was verified by GC analysis before the macroinitiators had been used to initiate the polymerization of HEMA-TBDMS which was applied as monomer for the second block. By this method, AB-diblock copolymers have been prepared consisting of a poly(4-bromostyrene) block and a poly(HEMA-TBDMS) block (**21**). The total scheme of synthesis of poly(4-bromostyrene)-*block*-poly(HEMA-TBDMS) (**21**) is shown in Figure 6-6.

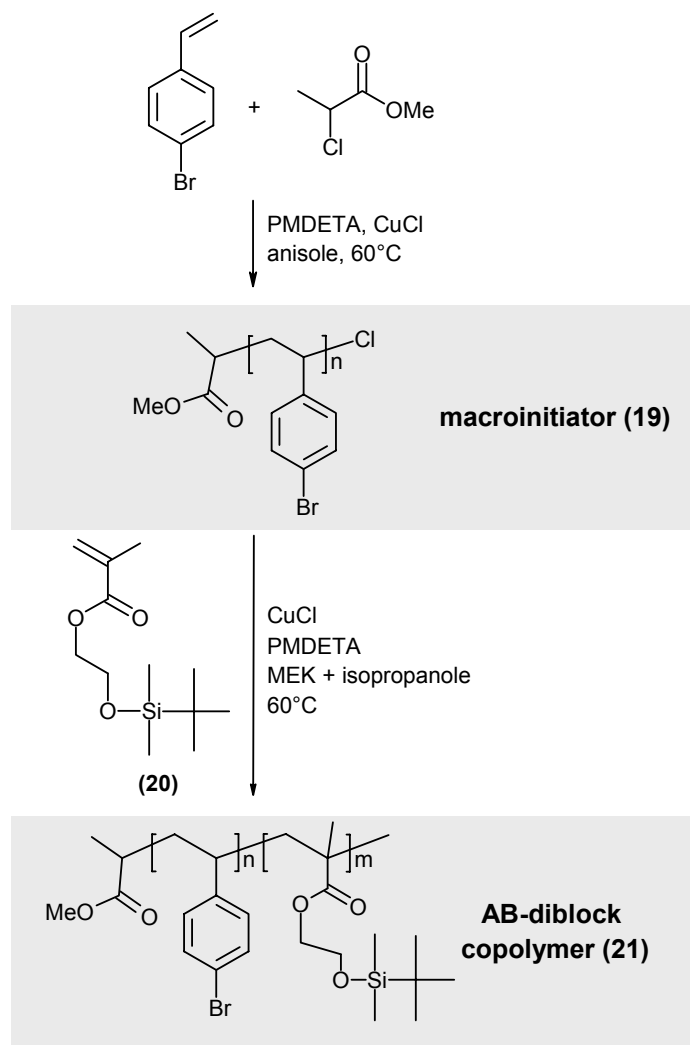
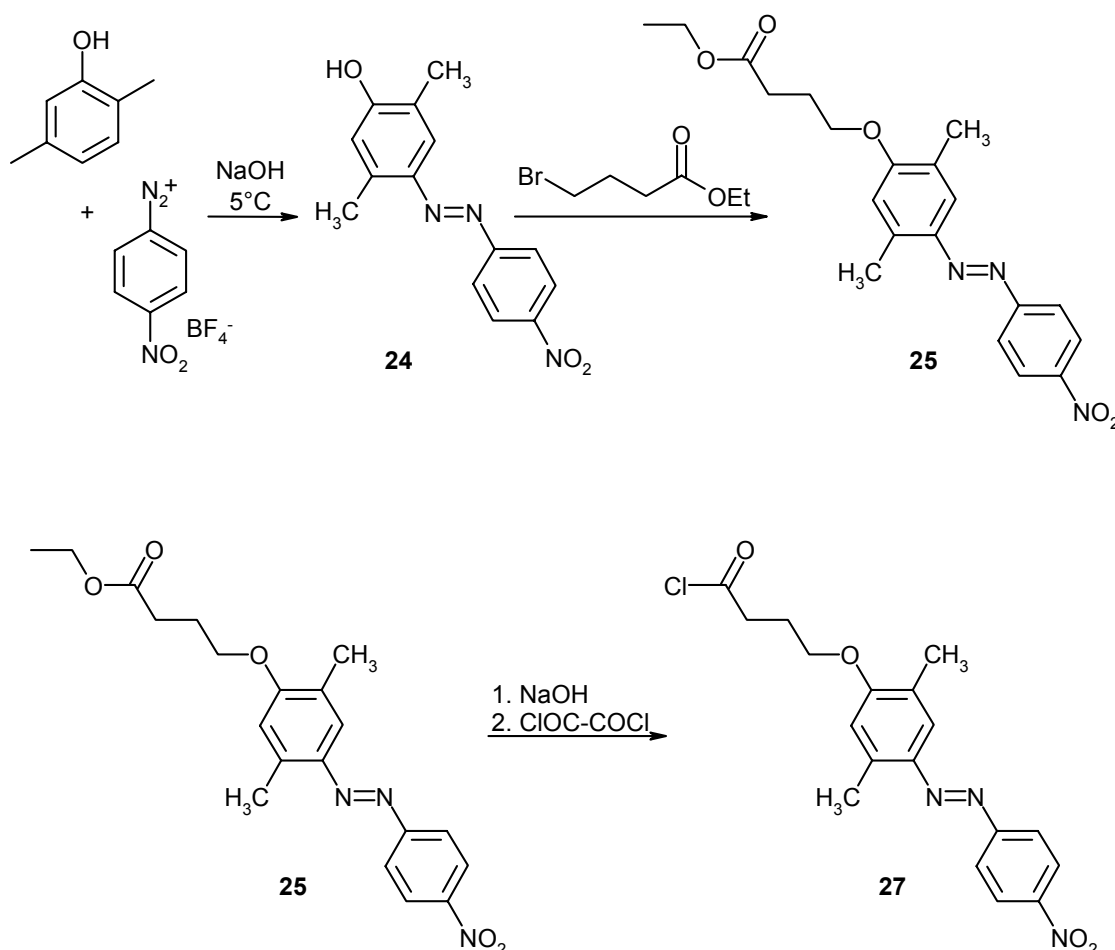


**Figure 6-6:** Schematic representation of the synthesis of AB-diblock copolymers poly(4-bromostyrene)-block-poly(HEMA-TBDMS) (21).

In a Pd-catalyzed polymeranalogous amination reaction with diphenylamine the poly(4-bromostyrene) block was converted into a poly(4-vinyltriphenylamine) hole transport moiety which represents the photoconductor functionality in these macromolecules. The NLO-dye functionality was introduced in an esterification reaction on the hydroxy function of the HEMA monomer units after removal of the TBDMS protective groups.

For this purpose, the acid chloride derivative of a dye with non-linear optical properties (DNPP) was synthesized in a multi-step reaction resulting in 1-[2,5-dimethyl-4-(4-nitrophenylazo) phenoxy] butyric acid chloride (**27**) (see Scheme 6-1).



**Scheme 6-1:** Schematic representation of the synthesis of 1-[2,5-dimethyl-4-(4-nitrophenylazo) phenoxy] butyric acid chloride (**27**).

The fully functionalized AB-diblock copolymers exhibit a poly(4-vinyltriphenylamine) hole transport functionality as well as different weight fractions of a non-linear optical dye moiety (see Figure 6-7).

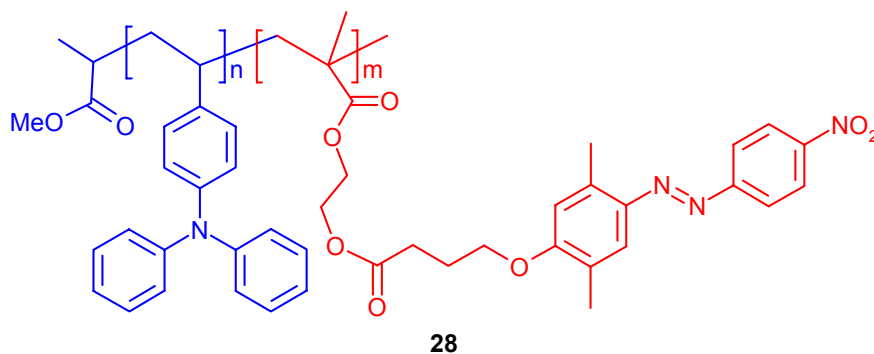


**Figure 6-7:** Chemical structure of fully functionalized AB-diblock copolymer poly(4-vinyltriphenylamine)-block-poly(HEMA-DNPP) (**28**).

In summary, the synthesis of fully functionalized AB-diblock copolymers had been carried out with success using the method of ATRP for polymerization and various polymeranalogous reactions for introduction of the different functionalities. The synthetic concept developed in this work opens the field to a great variety of materials as different hole transport or dye units may be attached to the polymer chains by the polymeranalogous reactions applied here. The novel fully functionalized AB-diblock copolymers bring a new class of photorefractive materials. The future plan regarding this field is to study the potential of nanoscale phase separation of these new bifunctional AB-diblock copolymers (**28**). Since film preparation, generation of nanoscale phase separation and related characterization techniques exceeded the dimensions of this thesis there is the perspective to explore this topic with the new materials in the future.

## 7 Zusammenfassung

Diese Arbeit beschäftigt sich mit organischen Materialien für elektro-optische Anwendungen und der Modifikation der ihrer Grenzflächen. Sie ist in zwei Hauptabschnitte gegliedert in denen jeweils ein neues Konzept bifunktionaler Materialien vorgestellt wird:

- I. Bifunktionelle Ru(II)-Farbstoffe mit Lochtransport-Einheiten*
- II. Vollfunktionalisierte AB-Diblock-Copolymere*

In den folgenden Abschnitten sind alle neuen Konzepte und Synthese-Strategien zusammengefasst. Besondere, herausragende Ergebnisse werden in zusammengefasster Form präsentiert.

### *I. Bifunktionelle Ru(II)-Farbstoffe mit Lochtransporteinheiten zur Grenzflächenmodifikation in farbstoffsensibilisierten TiO<sub>2</sub>-Feststoff-Solarzellen*

Das Hauptanliegen dieser Teilarbeit war die Verbesserung der TiO<sub>2</sub> / Farbstoff / Lochleiter-Grenzfläche in farbstoffsensibilisierten TiO<sub>2</sub>-Feststoff-Solarzellen. Es wurden dazu neuartige Konzepte bifunktionaler Materialien entwickelt, die sowohl ein lichtabsorbierendes Ru(II)-Farbstoff-Zentrum als auch lochtransportierende Triphenylamin-Einheiten tragen. Die Lösung folgender Problemstellungen wurde angestrebt:

- Verbesserung der Benetzung der polaren Ru(II) Farbstoff-Schicht mit unpolarem Spiro-Lochleiter.
- Räumliche Trennung des Farbstoff-Radikalkations (HOMO) von der TiO<sub>2</sub>-Oberfläche.
- Verzögerung der Rekombination von Löchern in den Farbstoff-Molekülen mit Elektronen im TiO<sub>2</sub>.

Um die angestrebten Ziele zu erreichen, wurden neuartige Bipyridin-Liganden mit Lochtransporteinheiten (bpy-TPA **6** und bpy-TPD **11**) und Bipyridin-Zentren für die Koordination von Übergangsmetallatomen hergestellt (vgl. Abb. 7-1).

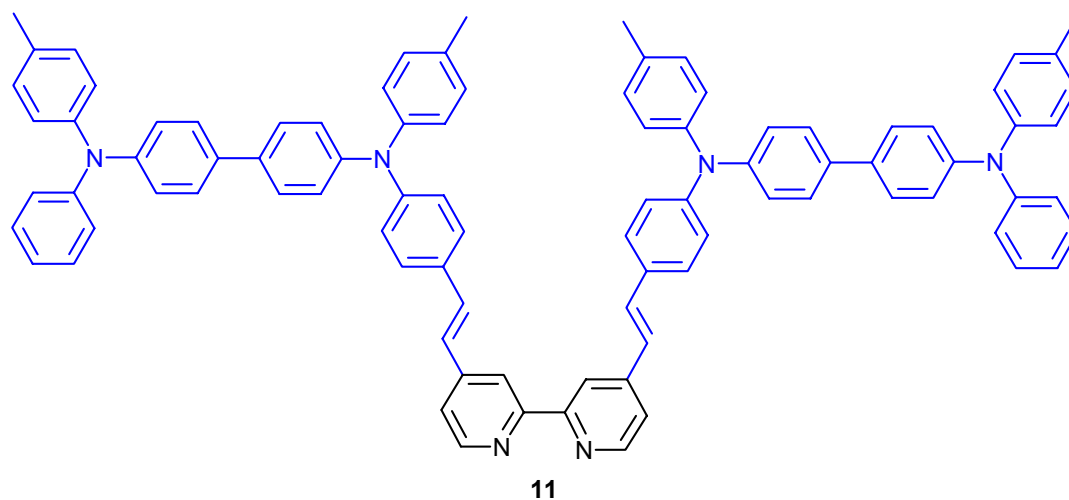
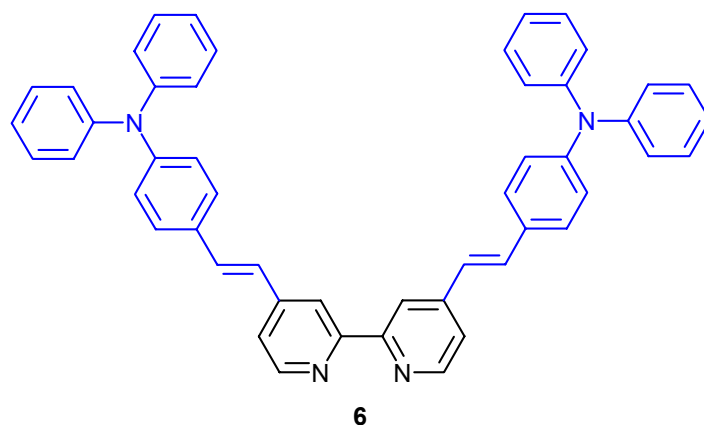


**Abb. 7-1:** Strukturformeln der neuartigen Bipyridin-Liganden bpy-TPA (**6**) und bpy-TPD (**11**) mit Lochtransporteinheiten, die kovalent an ein Bipyridin-Zentrum gebunden sind, welches für die Koordination von Übergangsmetall-atomen dient.

Aus den Liganden wurden die bifunktionellen Ru(II)-Farbstoffe **14** und **15** wie in Abb. 7-2 dargestellt in einer Metallierungs-Reaktion mit Ru(II)-Precursorkomplexen hergestellt; die Strukturen der neuen bifunktionellen Ru(II)-Komplexe **14** und **15** sind in Abb. 7-3 zu sehen.

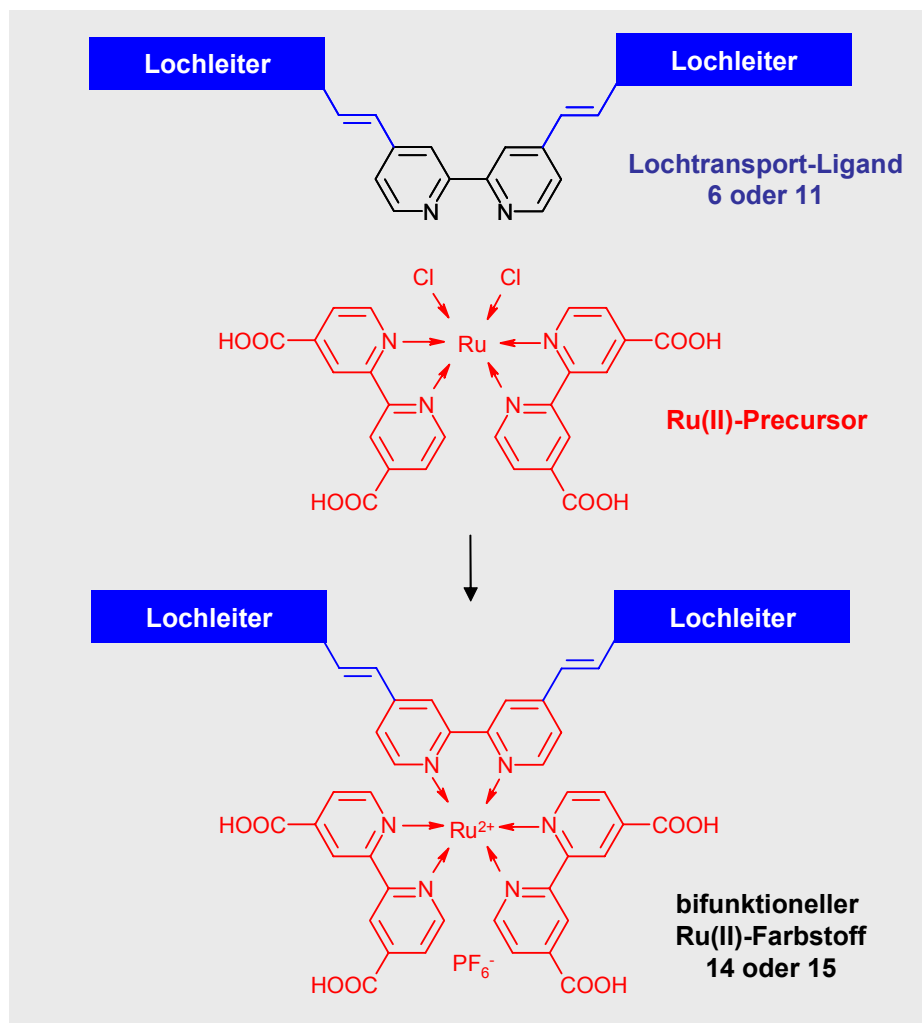


**Abb. 7-2:** Schematische Darstellung der Metallierung der Bipyridin-Liganden **6** und **11** unter Anwendung von Ru(II)-Ausgangskomplexen mit den bifunktionellen Ru(II)-Farbstoffen **14** und **15** als Endprodukte.

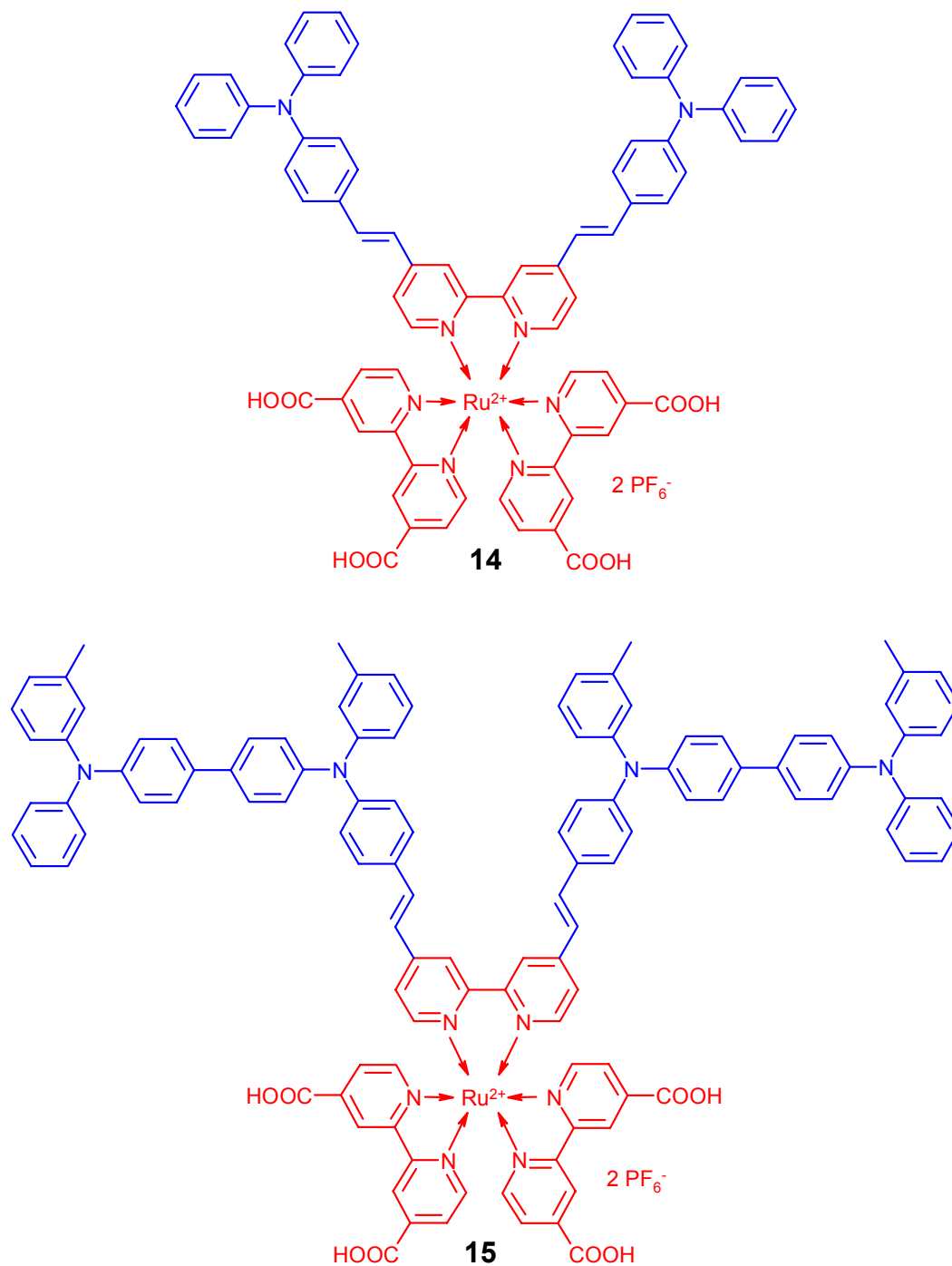


**Abb. 7-3:** Strukturformeln der neuen bifunktionellen Materialien **14** und **15** mit Triphenylamin-Substituenten für den Lochtransport und Ru(II)-Farbstoff-Zentren als lichtabsorbierende Einheiten.

Beide neu-synthetisierten Ru(II)-Farbstoffe **14** und **15** zeigen im Vergleich zu Standard-Farbstoffen, die keine zusätzlichen Lochtransporteinheiten tragen, einen enorm hohen Extinktionskoeffizienten  $\epsilon$ . Die  $\epsilon$ -Werte wurden aus den Ergebnissen der UV-Vis-Spektroskopie-Messungen berechnet. Ru(II)-Farbstoff **14** besitzt einen Extinktionskoeffizienten  $\epsilon$  von  $51\,900\text{ lcm}^{-1}\text{mol}^{-1}$  bei 408 nm, also mehr als dreimal so hoch wie  $\epsilon$  von konventionellen Farbstoffen bei der entsprechenden Wellenlänge. Für den bifunktionellen Farbstoff **15** beträgt der Wert für  $\epsilon$   $64\,500\text{ lcm}^{-1}\text{mol}^{-1}$  bei 349 nm, was im Vergleich zu Standard-Farbstoffen eine Verbesserung um mehr als einen Faktor drei bedeutet. Durch diese Ergebnisse erweisen sich die neuen Materialien **14** und **15** als sehr vielversprechend für die Anwendung in farbstoff-sensibilisierten TiO<sub>2</sub>-Solarzellen. Als Beispiel wurde Verbindung **14** für die Modifikation von Grenzflächen und als Farbstoff in verschiedenen Mischungen mit Standard-Farbstoff N 719 in *nc*-TiO<sub>2</sub> Solarzellen getestet. Die Anwendung von **14** in einer 1:1-Mischung mit N 719 führte zu einer beträchtlichen Verbesserung aller photovoltaischen Parameter (vgl. Tabelle 7-1).

***Tabelle 7-1:** Photovoltaische Parameter von Solarzellen, die mit verschiedenen Farbstoff-Kompositionen aus **14** und N 719 hergestellt wurden (weiße Lichtquelle, AM 1.5, 77 mWcm<sup>-2</sup>).*

Farbstoff-Komposition	I <sub>sc</sub> [mA]	U <sub>oc</sub> [V]	FF [%]	$\eta$ [%]
N 719 : 14				
N 719	1.95	645	40	0.70
3 : 1	2.49	720	33	0.76
1 : 1	3.18	755	51	1.63
1 : 3	1.84	750	41	0.73
14	1.07	810	42	0.48

Unter Verwendung einer 1:1-Mischung aus Standard-Farbstoff N 719 und **14**, konnte der Kurzschluss-Strom  $I_{SC}$  um bis zu 60 % verbessert werden, Leerlauf-Spannung  $U_{OC}$  wurde um 25 % erhöht und der Gesamtwirkungsgrad  $\eta$  mehr als verdoppelt (vgl. Tabelle 7-1).

Die wichtige Frage stellte sich, ob die räumliche Trennung der positiven Löcher zur  $TiO_2$ -Oberfläche vergrößert werden könnte, indem man bifunktionelle Farbstoffe mit kovalent angebondenen Lochtransporteinheiten verwendete. Dies konnte erfolgreich durch transiente Absorptions-Spektroskopie nachgewiesen werden, die in der Gruppe von Durrant am Imperial College in London (UK) durchgeführt wurde: Die Farbstoff-Radikalkationen wurden durch Laseranregung generiert, nachdem die Farbstoffe auf eine  $TiO_2$ -Oberfläche chemisorbiert wurden. Es wurde festgestellt, daß die Rekombinationshalbwertszeiten  $t_{50\%}$  der Radikalkationen für die auf  $TiO_2$  chemisorbierenden bifunktionellen Farbstoffe **14** und **15** 0.35 ms beziehungsweise 5 ms betragen. Das bedeutet, daß man durch Erweiterung der Konjugation der Bipyridin-Liganden bpy-TPA und bpy-TPD in **14** bzw. **15** die Halbwertszeiten um drei Größenordnungen erhöhen und damit die Rekombination von Elektronen und Löchern in einem enormen Ausmaß verzögern kann. Es wurde daher eine räumliche Trennung der HOMO-Orbitale der Farbstoffe zur  $TiO_2$ -Oberfläche angenommen.

Diese Annahme konnte durch TD-DFT (time-dependent density functional theory) ab-initio Berechnungen, mit denen man die räumliche Verteilung der HOMO-Orbitale der Farbstoffe nach ihrer Anregung bestimmen kann, bestätigt werden. Diese Berechnungen wurden ebenfalls in der Gruppe von Durrant durchgeführt. Es wurde berechnet, daß die HOMO-Orbitale von **14** über den Bipyridin-Einheiten und dem Triphenylamin-Substituenten verteilt sind. Im Gegensatz dazu konnte eine Delokalisierung der HOMO-Orbitale des Farbstoffs **15** über den TPD-Einheiten festgestellt werden, was im Vergleich zu **14** zu einer Erhöhung des räumlichen Abstands von der  $TiO_2$ -Oberfläche führte. Man geht dabei von einer Anhaftung durch die Carboxylsäure-Ankergruppen der Farbstoffmoleküle auf der  $TiO_2$ -Oberfläche. Aufgrund dieser Ergebnisse wurde prognostiziert, daß durch weitere Ausdehnung des Lochtransport-Liganden die räumliche Trennung weiter vergrößert und dadurch Rekombinationsprozesse noch mehr verzögert

werden könnten. Daher wurde eine Synthese-Strategie für Polymere entwickelt, die in Abb. 7-4 aufgezeigt wird.

Für die Synthese der Polymere wurde Atom Transfer Radikalische Polymerisation (ATRP) als Methode ausgeschöpft:

Zunächst wurde 4-Bromstyrol polymerisiert mit 4,4'-Bis(chloromethyl)-2,2'-bipyridin (**3**) als Initiator und CuCl / PMDETA als katalytischem System. Die Bedingungen für diese Polymerisationsreaktion wurden optimiert, man erzielte gute Kontrolle des Molekulargewichts und erhielt geringe Polydispersitäten.

Die 4,4'-Bis[poly(4-bromstyryl)methyl]-2,2'-bipyridine (**16**) wurden einer Pd-katalysierten polymeranalogen Aminierung mit Diphenylamin unterworfen, bei der man nach Optimierung in außergewöhnlich kurzen Reaktionszeiten sehr hohe Umsätze mit 4,4'-Bis[poly(4-vinyltriphenylamino)methyl]-2,2'-bipyridin als Produkt (**17**) erzielen konnte.

Die Metallierung der Polymere **17** mit Ru(II)-Precursorkomplexen sowohl mit als auch ohne COOH-Ankergruppen lieferte die angestrebten bifunktionellen, polymeren Ru(II)-Farbstoffe **18 e, f** und **18c' - f'** als Endprodukte (vgl. Abb. 7-4). Durch den Syntheseweg, der hier vorgestellt wurde, kann man den Farbstoffgehalt der Endpolymere zwischen 2 % und 20 % durch Veränderung der Länge der Polymerketten variieren. Die polymeren Komplexe **18 e, f** und **18c' - f'** wurden charakterisiert und ihre thermischen Eigenschaften bestimmt.

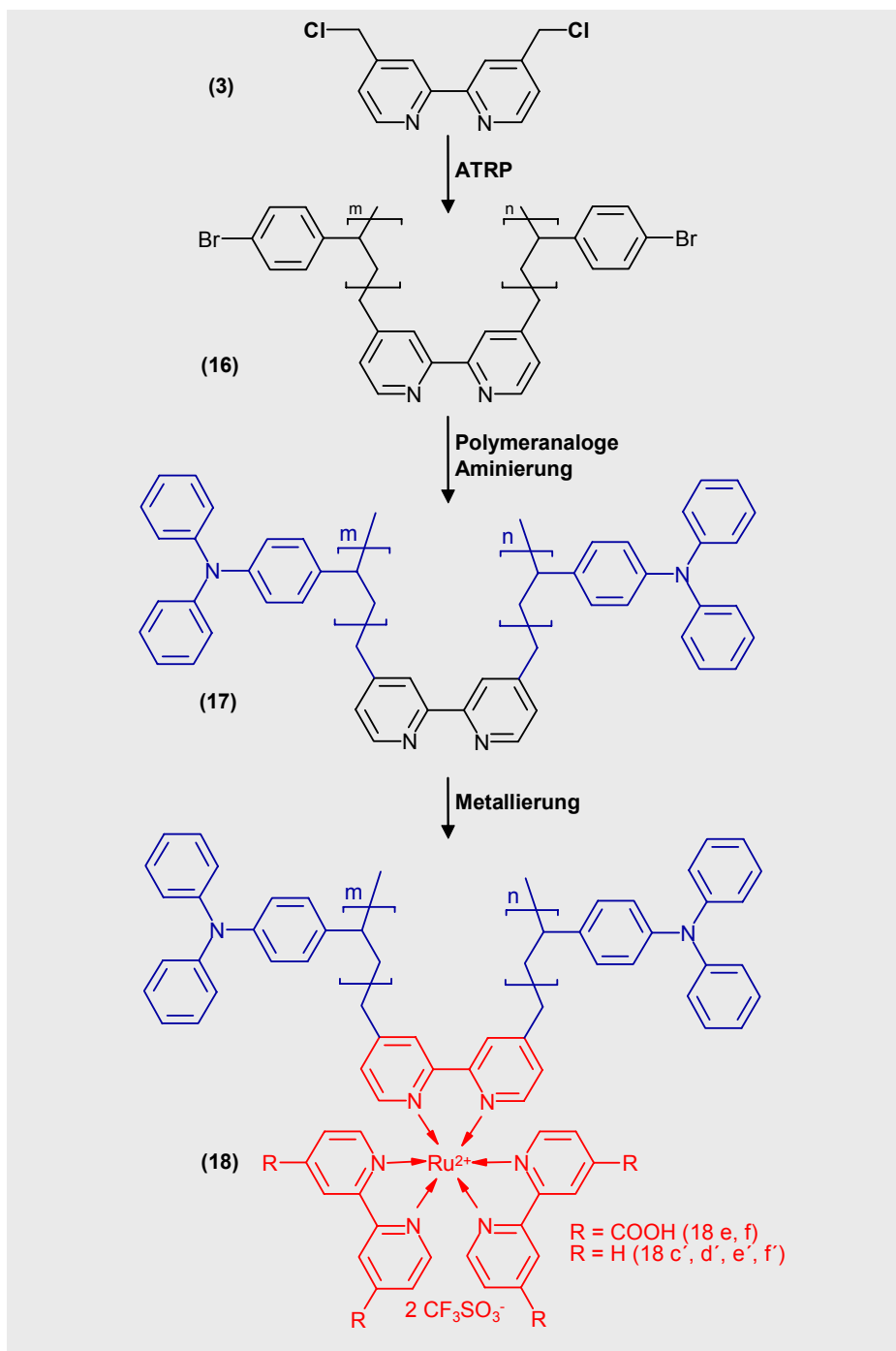


**Abb. 7-4:** Schematische Darstellung der Synthese von bifunktionellen Polymeren (**18 e, f** und **18 c'-f'**) durch ATRP gefolgt von einer polymeranalogen Aminierung und Metallierung mit Ru(II)-Precursoren.

Transiente Absorptionsspektroskopie dieser Verbindungen war von besonderem Interesse, da bereits für den niedermolekularen Farbstoff **15** eine extreme Verzögerung der Rekombination festgestellt wurde. Die entsprechenden Studien von Polymer **18f** (mit COOH-Ankergruppen und ~ 144 Wiederholungseinheiten von 4-Vinyltriphenylamin in den Polymerketten) ergaben dabei eine Rekombinationshalbwertszeit  $t_{50\%}$  der Farbstoff-Radikalkationen von 4 s. Es handelt sich dabei um den höchsten Wert, der bislang für einen Ru(II)-Farbstoff gemessen wurde, der auf einen Metalloxid-Film chemisorbiert wurde. Ein Vergleich der Zerfallsstudien aller neuen bifunktionellen Materialien **14**, **15** und **18f** ist in Abb. 7-5 zu sehen. Dazu wurde die relative Veränderung der optischen Dichte ( $\Delta mOD$ ) der verschiedenen Radikalkationen als Funktion der Zeit aufgetragen.

Laut TD-DFT ab-initio Berechnungen sind die HOMO-Orbitale der Radikalkationen im Fall **18f** über den Poly(4-vinyltriphenylamin)-Ketten delokalisiert. Das resultiert in einer drastischen Erhöhung der räumlichen Trennung der HOMOs von der TiO<sub>2</sub>-Oberfläche im Vergleich zu den niedermolekularen Farbstoffen **14** und **15**. Die Resultate zeigen deutlich, daß die neuen polymeren Farbstoffe im Vergleich zu einfacheren Farbstoffstrukturen, die heutzutage in Solarzellen eingesetzt werden, zu einer beträchtlichen Verzögerung der Rekombination von Elektronen und Löchern führt.

Aus den Endergebnissen geht eindeutig hervor, daß das neue Synthesekonzept erfolgreich realisiert wurde. Neuartige bifunktionelle, niedermolekulare Materialien (**14** und **15**) und Polymere (**18 e, f** und **18c' - f'**) wurden hergestellt, die alle Kriterien zur Grenzflächenmodifikation in farbstoffsensibilisierten TiO<sub>2</sub>-Solarzellen erfüllen. Außergewöhnlich lange Halbwertszeiten der Radikalkationen im Bereich von Sekunden konnten für die polymeren Ru(II)-Farbstoffe festgestellt werden. Es wird nochmals betont, daß es sich dabei um die langlebigsten Radikalkationen handelt, die bislang nach Farbstoff-Chemisorbtion auf einem TiO<sub>2</sub>-Film untersucht wurden.

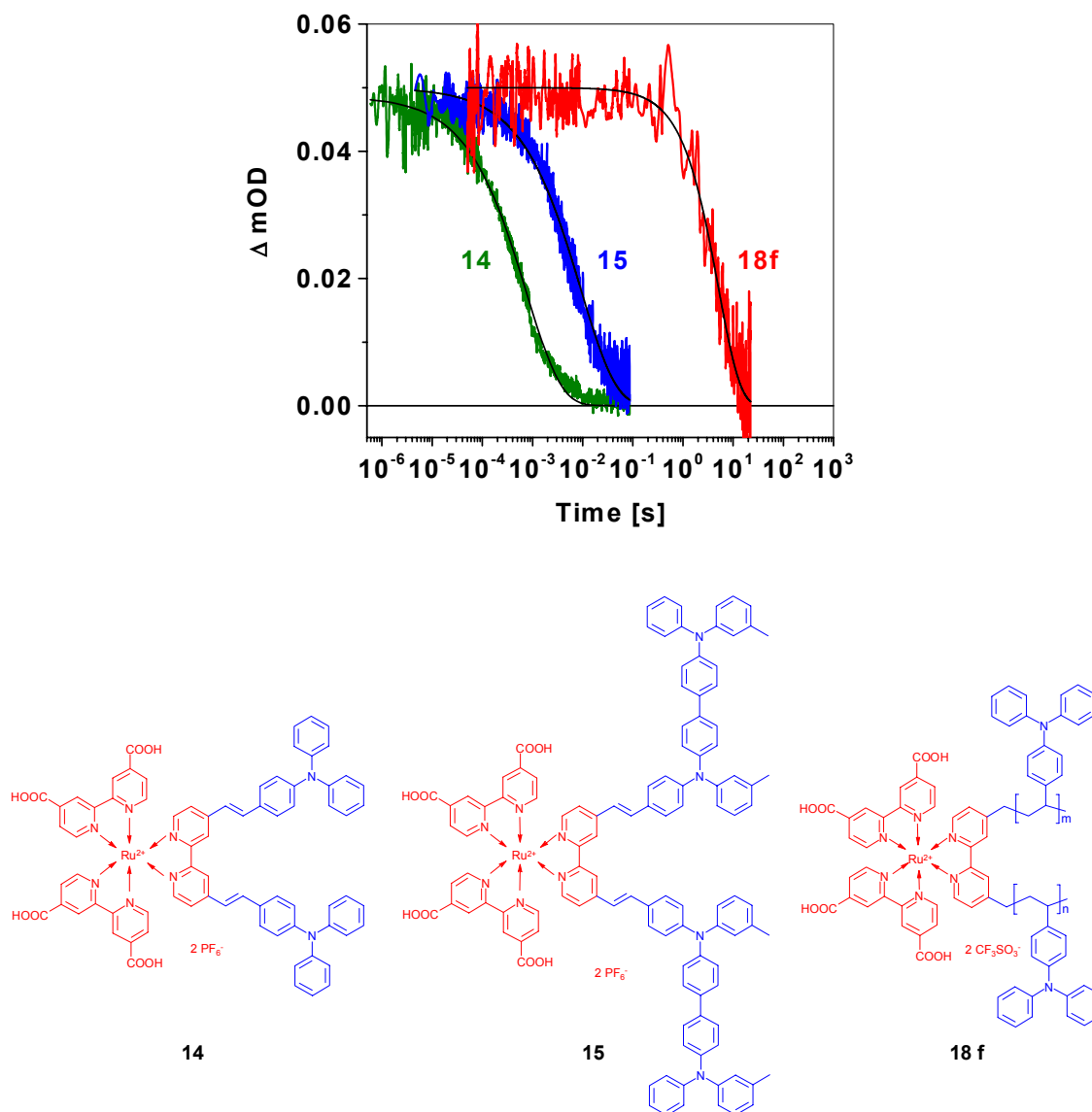


**Abb. 7-5:** Zerfallskurven der Modellverbindungen **14** und **15** im Vergleich zu Polymer **18f** (144 vTPA-Wiederholungseinheiten), aufgezeichnet nach Laseranregung (450 nm) von farbstoffsensibilisierten  $TiO_2$ -Filmen bei einer Detektionswellenlänge von 900 nm; experimentelle Daten (grün, blau, rot) und exponentielle Anpassungen der Messkurven (schwarze Linien). Unterhalb des Graphen sind die Strukturen der Verbindungen **14**, **15** und **18f** angegeben.

## *II. Vollfunktionalisierte AB-Diblock-Copolymere mit Lochtransport-Block und NLO-Farbstoff-Block*

Ein anderer synthetischer Ansatz dieser Arbeit bestand in der Untersuchung der Tauglichkeit der Polymerisations-Technik ATRP für die Herstellung von vollfunktionalisierten AB-Diblock-Copolymeren für photorefraktive Anwendungen. Dazu wurde 4-Bromstyrol durch ATRP unter Anwendung von  $\alpha$ -Chlormethylpropionat als Initiator und CuCl / PMDETA als katalytischem System polymerisiert. Man erhielt die Makroinitiatoren **19 a – e**. Die Kontrolle dieser Polymerisation wurde durch Gaschromatographie (GC) nachgewiesen, bevor die Makroinitiatoren zur Initiierung der Polymerisation der zweiten Monomers eingesetzt wurden. HEMA-TBDMS wurde dabei als Monomer für den zweiten Block ausgewählt. Durch diese Methode wurden AB-Diblock-Copolymere synthetisiert, die aus einem Poly(4-bromstyrol)-Block und einem poly(HEMA-TBDMS)-Block bestehen (**21**). Eine Gesamtübersicht der Synthese von Poly(4-bromstyrol)-*block*-poly(HEMA-TBDMS) (**21**) ist in Abb. 7-6 dargestellt.

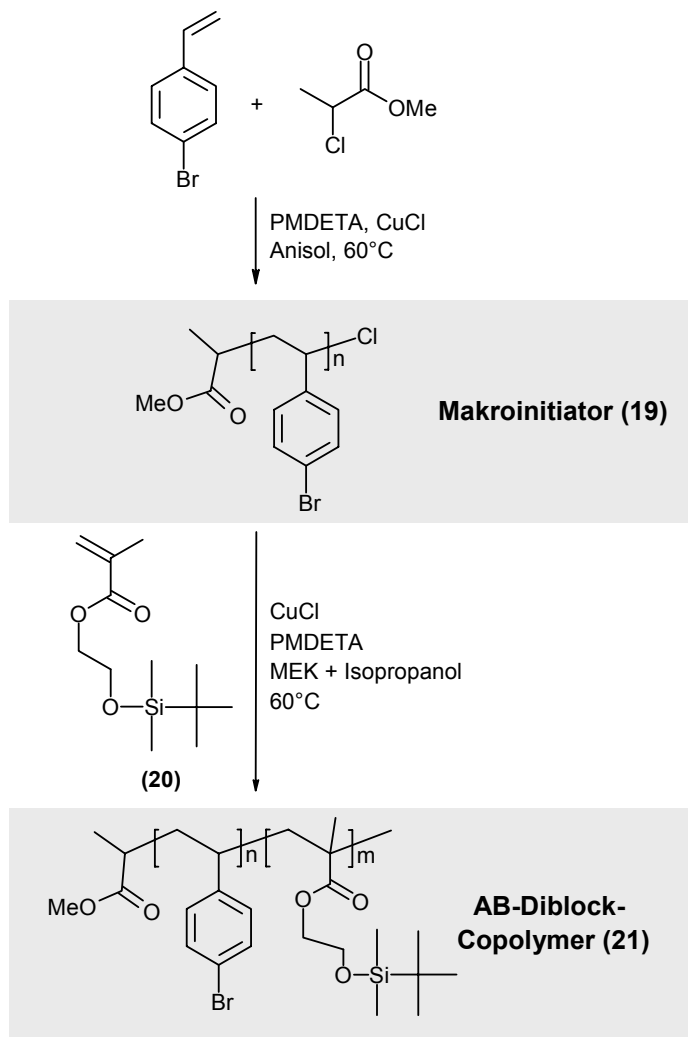
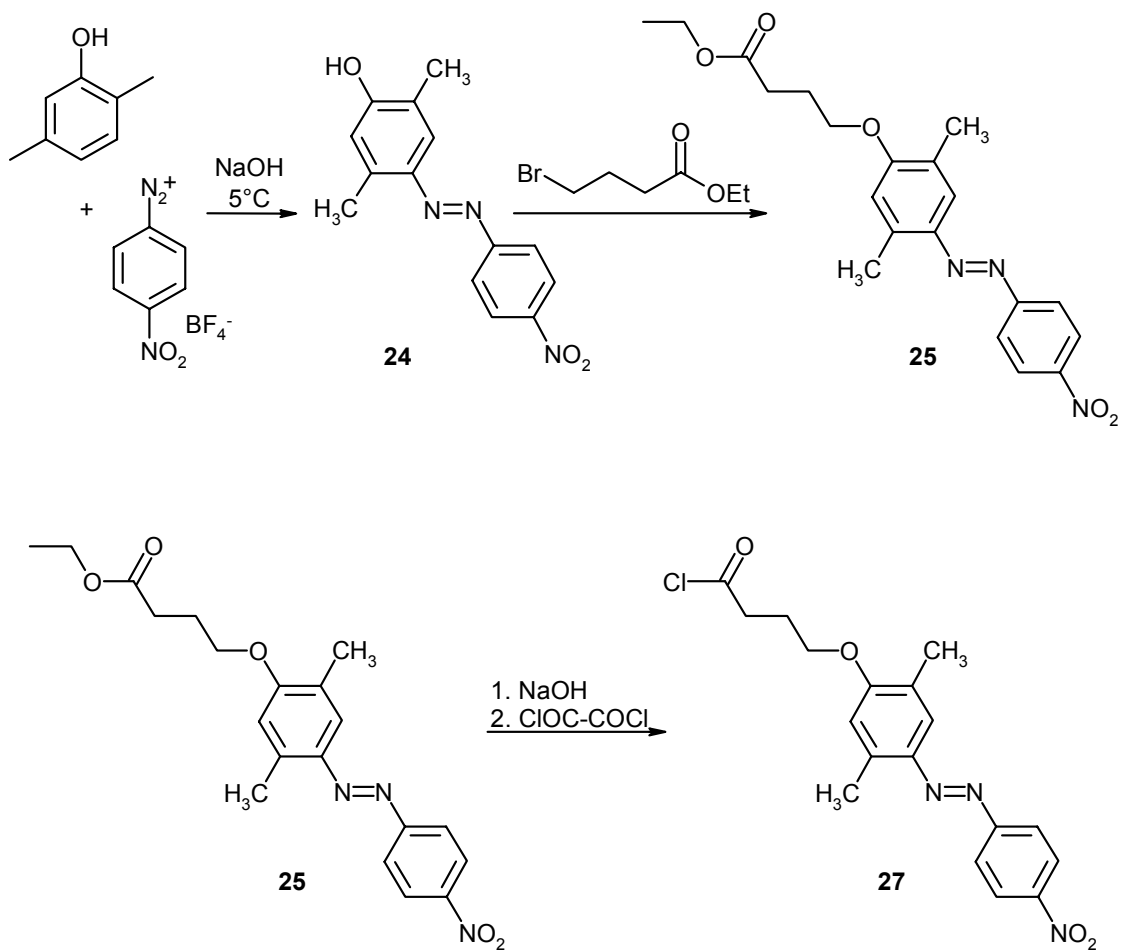


**Abb. 7-6:** Schematische Darstellung der Synthese der AB-Diblock-Copolymere Poly(4-bromostyrol)-block-poly(HEMA-TBDMS) (21).

In einer Pd-katalysierten polymeranalogen Aminierungsreaktion mit Diphenylamin wurde der Poly(4-bromostyrol)-Block zu einer Poly(4-vinyltriphenylamin)-Lochtransporteinheit umgewandelt, welche den Photoleiter in diesen Makromolekülen darstellt. Die NLO-Funktionalität wurde durch Veresterung der Hydroxy-Funktionen der entschützten HEMA-TBDMS Monomer-Einheiten eingeführt. Dazu synthetisierte man das Säurechlorid-Derivat eines nicht-linear-optischen Farbstoffes (DNPP): 1-[2,5-Dimethyl-4-(4-nitrophenylazo)phenoxy]buttersäurechlorid (27) (vgl. Schema 7-1).



**Schema 7-1:** Reaktionsschema der mehrstufigen Synthese von 1-[2,5-Dimethyl-4-(4-nitrophenylazo)phenoxy]buttersäurechlorid (27).

Die angestrebten AB-Diblock-Copolymere besitzen schließlich sowohl einen Poly(4-vinyltriphenylamin)-Block als Lochtransporteinheit als auch eine nicht-linear-optische Farbstoffeinheit in verschiedenen Gewichtsanteilen. Die Struktur der vollfunktionalisierten Endprodukte ist in Abb. 7-7 dargestellt.

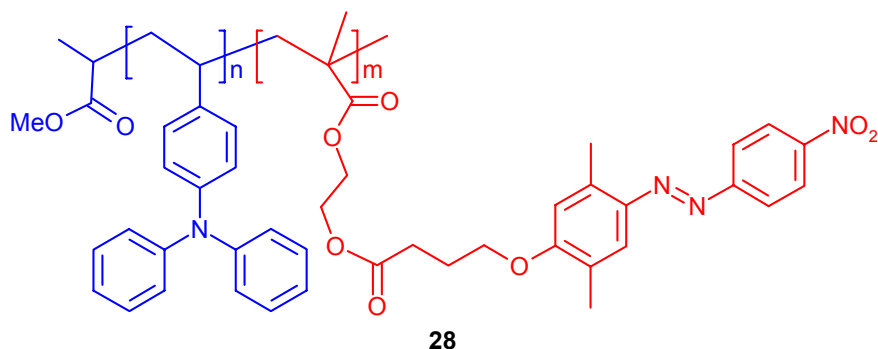


**Abb. 7-7:** Chemische Struktur eines vollfunktionalisierten AB-Diblock-Copolymers Poly(4-vinyltriphenylamin)-block-poly(HEMA-DNPP) (**28**).

Zusammenfassend ist festzustellen, daß die Synthese von vollfunktionalisierten AB-Diblock-Copolymeren (**28**) unter Anwendung von ATRP als Polymerisations-Methode gefolgt von einer Reihe polymeranaloger Umsetzungen zur Einführung der Funktionalitäten mit Erfolg durchgeführt wurde. Das neue Synthesekonzept, das während dieser Arbeit entwickelt wurde, öffnet den Zugang zu einer enormen Vielfalt an Materialien. Durch die optimierten polymeranalogen Umsetzungen, bietet sich nämlich die Möglichkeit, verschiedene Lochtransport- oder Farbstoff-Funktionalitäten an die Polymerketten anzubinden. Insbesondere stellen die vollfunktionalisierten Blockcopolymeren **28**, die hier beschrieben wurden, eine neue Klasse an photorefraktiven Materialien dar. Die Perspektiven, die aus dieser Arbeit resultieren, beinhalten daher eine Untersuchung des Potentials der neuen Polymere, Filme mit Phasenseparation im Nanometerbereich zu bilden und zu charakterisieren. Sowohl Filmpräparation als auch die verschiedenen Methoden zur Filmcharakterisierung überschreiten jedoch das Ausmaß dieser Arbeit, so daß diese Thematik als Ausblick für die Zukunft festgehalten wird.

## 8 Experimental

*In this chapter methods and devices for characterization are described and briefly discussed. For the investigation of the photovoltaic properties of solar cells built with the new materials a special set up was used which is given in this section. The solvents and reagents which were used for synthesis are introduced and the purification methods applied for them are given. Moreover the synthetic procedures to obtain the materials reported in this work are presented and the data of characterization are specified in details.*

## 8.1 Methods and devices for characterization

### 8.1.1 Differential scanning calorimetry (DSC)

Differential scanning calorimetry was carried out with a PERKIN-ELMER Diamond DSC with heating / cooling rates of 10 or 20 Kmin<sup>-1</sup>. Samples were prepared in 40 µl pans using 7 – 15 mg of substance.

### 8.1.2 Elemental analysis

For elemental analysis samples were sent to Mikroanalytisches Labor Pascher (An der Pulvermühle 1, 53424 Remagen, Germany). This laboratory provides the possibility of exact detection especially of small amounts of halides (Br) and metals (Cu) in solid-state materials.

### 8.1.3 Fluorescence spectroscopy

Fluorescence spectroscopy was carried out using a Shimadzu RF-5301 PC spectral fluorometer. All samples were measured in solution with concentrations of about 10<sup>-6</sup> mol l<sup>-1</sup>. The excitation wavelength was determined via UV-VIS spectroscopy (maximum absorption wavelength) before.

### 8.1.4 Fourier transformed infrared spectroscopy (FT-IR)

Fourier transformed infrared spectroscopy was performed with a BIO-RAD Digilab FTS-40. All measurements were carried out by embedding the substance into a KBr pellet using 32 scans and a resolution of 4 cm<sup>-1</sup> (transmission mode).

### 8.1.5 MALDI-TOF spectrometry

MALDI-ToF spectra were recorded using a Reflex 3 from BRUKER equipped with a Nitrogen laser with a wavelength of 342 nm.

### 8.1.6 Mass spectrometry

Mass spectrometry was carried out on a Finnigan MAT 8500 and Varian MAT 112 spectrometer using a ionization energy of 70 eV (electron impact). The  $m/z$  – values are given.

### 8.1.7 Nuclear magnetic resonance spectroscopy (NMR)

$^1\text{H}$ -NMR spectra were recorded using an AVANCE AC 250 spectrometer (250 MHz) from BRUKER. For sample preparation about 10 mg of substance was dissolved in deuterated solvents like  $\text{CDCl}_3$ ,  $\text{DMSO-d}_6$ ,  $\text{THF-d}_8$  etc. and filled into high precision NMR-tubes. All measurements were carried out at 298 K using a minimum of 16 scans. For signal characterization the following abbreviations were used: s (singlet), d (doublet), t (triplet), q (quadruplet), m (multiplet, signal without resolution).  $^{13}\text{C}$ -NMR spectra were recorded on the same spectrometer (62.5 MHz). For  $^{13}\text{C}$ -NMR 30-40 mg of substance have to be used with a minimum of 1024 scans.

### 8.1.8 Size exclusion chromatography (SEC)

#### *Electrolyte-SEC:*

Electrolyte size exclusion chromatography was carried out using a polymer-SEC setup equipped with an UV-Detector (Waters 486, 254 nm) and an RI-Detector (Waters 410). As eluent a solution of 0.25 wt% tetrabutylammoniumbromide (TBAB) in THF was used. Calibration was carried out using polystyrene standards (PSS).

The device was equipped with SDV-Columns (300 x 8 mm; 5  $\mu\text{m}$  particle size) with pore sizes of  $10^2$  -  $10^5$   $\text{\AA}$  and an SDV-guard-column (50 x 8 mm; 5  $\mu\text{m}$  particle size) with a pore size of 100  $\text{\AA}$  (PSS). The eluent was pumped with constant flow of  $0.5 \text{ mlmin}^{-1}$  using a P100 from Spectra Physics. All measurements were carried out at room temperature using o-dichlorobenzene as internal standard.

### *High-temperature SEC:*

High-temperature SEC was performed with a Waters 150CV setup equipped with an RI-detector. As eluent a solution of 0.05 mol % LiCl in DMAc was used. Calibration was carried out with polystyrene standards (PSS). The device features PSS Gram-columns (300 x 8 mm; 5  $\mu\text{m}$  particle size) with pore sizes of  $10^2$  and  $10^3$   $\text{\AA}$  and an SDV-guard-column (50 x 8 mm; 5  $\mu\text{m}$  particle size) with a pore size of 100  $\text{\AA}$ . All measurements were carried out at 70  $^\circ\text{C}$  using o-dichlorobenzene as internal standard.

### 8.1.9 Thermo gravimetric analysis (TGA)

Thermo gravimetric analysis was carried out using a METTLER TOLEDO TGA / SDTA 851 $^\circ$ . Samples were prepared by filling 6- 12 mg of substance into alox crucibles. All measurement were performed under nitrogen flow ( $75 \text{ cm}^3\text{min}^{-1}$ ) in a temperature range from 30 to 650  $^\circ\text{C}$  at a heating rate of  $10 \text{ Kmin}^{-1}$ .

### 8.1.10 Thin layer chromatography (TLC)

Thin layer chromatography was performed on POLYGRAM SIL G/UV254 and POLYGRAM ALOX N/UV cards purchased from Roth GmbH. Substances in solution were applied via capillary glass tubes ( $\text{\O} 0.6 \text{ mm}$ , Marienfeld GmbH, Germany) and separation of the substances was carried out using appropriate solvent combinations.

### 8.1.11 UV-Vis spectroscopy

UV-Vis spectra were recorded on a HITACHI U-3000 spectro photometer. The measurements were carried out in solution ( $\text{CHCl}_3$ , MeOH etc.) using quartz glass cuvettes with 1 cm thickness and concentrations of about  $10^{-5} \text{ mol l}^{-1}$ .

### 8.1.12 Preparation and characterization of solar cells

#### *Materials for solar cell preparation*

Glass substrates (Type TEC8, 3 mm thick) covered with a layer of fluorine-doped tin oxide (FTO) having a sheet resistance of 8 ohms per square, were purchased from Hartfordglass (Indiana, USA). Titanium(IV) bis(acetylacetonato) diisopropoxide (TAA) and N-lithiobis(trifluoromethanesulfonimide) ( $\text{CF}_3\text{SO}_2$ )<sub>2</sub>NLi (Li-salt) were purchased from Aldrich. TAA was used as received and Li-salt was dried in vacuum before use. Nanocrystalline titanium dioxide (*nc*-TiO<sub>2</sub>) precursor paste (Ti-oxide TSP) and ruthenium-dye (Ru-535 bisTBA or N 719) were bought from Solaronix (Aubonne, Switzerland). The N 719 dye, *cis*-bis(isothiocyanato)-bis-(2,2'-bipyridyl-4,4'-dicarboxylato)-ruthenium(II)-bis(tetrabutylammonium) has a shortened formula of  $\text{RuL}_2(\text{NCS})_2(\text{TBA})_2$ , where L = 2,2'-bipyridyl-4,4'-dicarboxylic acid and TBA = tetrabutylammonium. 2,2',7,7'-Tetrakis(N,N-di-4-methoxyphenyl amino)-9,9'-*spiro*-bifluorene (*spiro*-OMeTAD) was obtained from Covion Semiconductors, Frankfurt. The *spiro*-OMeTAD radical cation salt (abbreviated as *ox. spiro*) was obtained by single electron transfer oxidation of *Spiro*-OMeTAD with excess of  $\text{AgSbF}_6$  in toluene. Other solvents and common chemicals were purchased from Aldrich or Fluka and used as received without further purification.

#### *Instrumentation for solar cell preparation and characterization*

The spray pyrolysis deposition (SPD) and screen-printing (see Figure 8-1) were carried out using home-made instruments. The thicknesses of the blocking layers have been measured by field-emission scanning electron microscopy (FE-SEM LEO 1530).

The photovoltaic current-voltage measurements have been carried out by a Keithley 6517 Source-Measure unit under AM 1.5 solar spectral conditions (Xenon arc lamp, Air Mass Filters from Oriel).

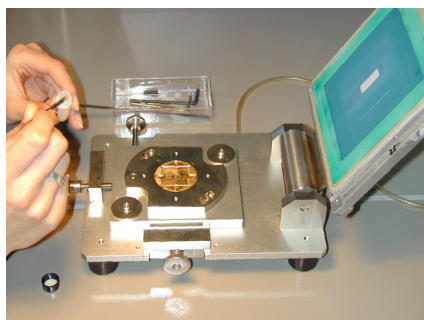


*Figure 8-1: Experimental setup for screen-printing of the nanoporous TiO<sub>2</sub>-layer.*



*Figure 8-2: Experimental setup for current-voltage characterization of solar cells (light sources: Xe-lamp, solar light simulator).*

The intensity of light was calibrated with a standard Si-reference cell from the Fraunhofer Institut (ISE), Freiburg as 77 mW/cm<sup>2</sup>. Au was deposited by electron beam deposition in a vacuum chamber of BA 510 type from Unaxis.

## 8.2 Solvents, chemicals and inert gas

### *Solvents:*

acetone	was stirred over CaSO <sub>4</sub> , distilled and stored under Argon atmosphere
anisole	was refluxed over sodium, distilled and stored under Argon atmosphere
chloroform	was distilled with glass packed column
cyclohexane	was distilled with glass packed column
dichloromethane	was distilled with glass packed column
diethylether	was refluxed over sodium, distilled and stored under Argon atmosphere
dimethylformamide (DMF)	was stirred over CaH <sub>2</sub> , distilled under reduced pressure and stored under Argon atmosphere
1,4-dioxane	was refluxed over sodium, distilled and stored under Argon atmosphere
ethanol	was purchased from MERCK in p. a. quality
ethylacetate	was distilled with glass packed column
o-dichlorobenzene	was stirred over CaH <sub>2</sub> , distilled under reduced pressure and stored under Argon atmosphere
tetrahydrofuran (THF)	was refluxed over potassium, distilled and stored under Argon atmosphere

Deuterated solvents (CDCl<sub>3</sub>, DMSO-d<sub>6</sub>, THF-d<sub>8</sub>, d<sub>3</sub>-MeOD, CF<sub>3</sub>COOD) for NMR-spectroscopy were purchased from Deutero GmbH (Am Ring 29, 56288 Kastellaun, Germany) and used as received.

### Chemicals:

4,4'-dimethyl-2,2'-bipyridine	was purchased from Aldrich
4-bromostyrene	was purchased from ACROS, stirred over CaH <sub>2</sub> , distilled in vacuum and stored under Argon atmosphere at -10 °C
4-diphenylamino benzaldehyde	was purchased from FLUKA
Bis(2,2'-bipyridine)dichloro-Ruthenium(II)monohydrate	was purchased from Aldrich and STREM
caesium fluoride (CsF)	was purchased from Aldrich, dried in vacuum and stored under Argon atmosphere
18-crown-6	was purchased from Aldrich
CuCl, CuBr	was purchased from MERCK, purified with glacial acetic acid as reported by Keller et al. <sup>118</sup> and stored under Argon atmosphere
4,4'-dijodobiphenyl	was purchased from Fluka and sublimed before use
diisopropylamine	was distilled before use
diphenylamine	was purchased from ACROS
ethylbromoisobutyrate (EBiB)	was purchased from Aldrich, distilled and stored under Argon atmosphere
hexachloroethane	was purchased from Aldrich
hydroxyethylmethacrylate	was purchased from Aldrich, stirred over CaH <sub>2</sub> and distilled in vacuum
imidazole	was purchased from Aldrich

---

<sup>118</sup> R. N. Keller, H. D. Wycoff *Inorg. Synth.* **1946**, 2, 1.

---

methylchloropropionate (MCP)	was purchased from Aldrich , distilled and stored under Argon atmosphere
3-methyldiphenylamine	was purchased from Aldrich
n-butyllithium (n-BuLi)	was purchased from ACROS (1.6 M in n-hexane) packed in septum bottles
palladium acetate (Pd(OAc) <sub>2</sub> )	was purchased from Aldrich
phosphorylchloride	was purchased from MERCK and freshly distilled for prompt use
potassium carbonate (K <sub>2</sub> CO <sub>3</sub> )	was purchased from FLUKA and dried at 110 °C
pyridine	purchased from Aldrich in Sure/Seal™ bottle
Ruthenium trichloride	was purchased from Lancaster
sodium-tert.butoxide	was purchased from Aldrich, dried and stored at 110 °C in the oven for prompt use
tert.butyldimethylsilylchloride	was purchased from Aldrich
trimethylsilylchloride	was purchased from Aldrich packed in Sure/Seal™ bottle under Nitrogen
triphenylphosphine	was purchased from FLUKA
tri-tert.butylphosphine	was purchased from Aldrich and ACROS and used as toluene solution (1g in 30 ml toluene) under Argon atmosphere

*Inert gases:*

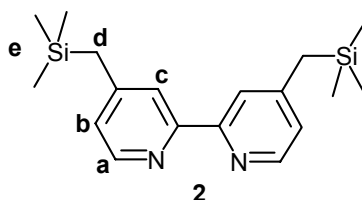
**Argon** and **Nitrogen** were used as inert gases for air and water sensitive reactions. Also for storage of water-free and air sensitive solvents and chemicals an inert gas atmosphere was required. **Argon** and **Nitrogen** were dried by passing through potassium powder adsorbed on alumina N and molecular sieve.

## 8.3 Synthesis and characterization

### 8.3.1 4,4'-bis(trimethylsilylmethyl)-2,2'-bipyridine (**2**)

A mixture of 80 ml dried THF and 8.75 ml diisopropylamine (62.5 mmol) was cooled to -78 °C, 34.4 ml n-BuLi (1.6 M in n-hexane) was added via dropping funnel and the solution was stirred for 20 min at -78 °C. A solution of 4.61 g (25 mmol) 4,4'-dimethyl-2,2'-bipyridine in 60 ml dried THF was added dropwise. After stirring for additional 25 min at -78°C the solution was heated up to -50 °C and stirred for 20 min. After cooling to -78 °C 7.06 g (65 mmol) trimethylsilylchloride were added and the reaction was quenched after stirring for not more than 2 min by adding 15 ml of ethanol. The solution was heated to room temperature and poured into a separation funnel with 100 ml of aqueous NaHCO<sub>3</sub>. The mixture was extracted with ethylacetate (3 x 150 ml) and washed with brine. After drying the combined organic fractions over Na<sub>2</sub>SO<sub>4</sub> the solvent was evaporated resulting in a yellow powder of **2**. After filtration of a solution of **2** in diethylether over Alox N and cooling 5.99 g of white crystals were obtained (73 %).

*Characterization:*



<sup>1</sup>H-NMR (CDCl<sub>3</sub>, 250 MHz):      δ (ppm): 0.03 (s, 18 H, **e**), 2.18 (s, 4 H, **d**), 6.89 (d, 2 H, **a**), 8.02 (s, 2H, **c**), 8.43 (d, 2 H, **b**).

<sup>13</sup>C-NMR (CDCl<sub>3</sub>, 62.5 MHz):      δ (ppm): 27.4, 30.6, 120.5, 123.2, 150.9, 153.9, 155.7.

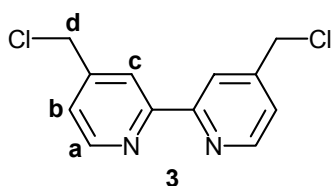
IR (KBr):      ν (cm<sup>-1</sup>): 3049, 2953, 2896, 1587, 1459, 1376, 1248, 1160, 1038, 859.

Mass spectrometry:      m/z = 328 (M<sup>+</sup>)

### 8.3.2 4,4'-bis(chloromethyl)-2,2'-bipyridine (**3**)

To a solution of 4,4'-bis(trimethylsilylmethyl)-2,2'-bipyridine (**2**) (43 mmol, 14.13 g) and  $\text{Cl}_3\text{CCl}_3$  (86 mmol, 20.26 g) in 150 ml dry DMF under inert gas atmosphere anhydrous CsF (86 mmol, 13.06 g) was added. The reaction mixture was stirred at room temperature until the starting TMS compound was fully consumed (TLC control). The reaction mixture was poured into a mixture of EtOAc and  $\text{H}_2\text{O}$  (200 ml each), the organic layer was separated and the aqueous layer was extracted three times with 100 ml EtOAc each. The combined organic fractions were dried over  $\text{Na}_2\text{SO}_4$ . Filtration and evaporation of the solvent gave yellowish product which was purified by washing with cold toluene to yield a white solid: 5.00 g (46 %).

*Characterization:*

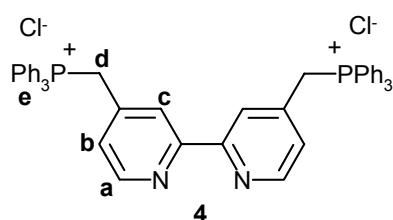


$^1\text{H-NMR}$ ( $\text{CDCl}_3$ , 250 MHz):	$\delta$ (ppm): 4.58 (s, 4 H, <b>d</b> ), 7.35 (d, 2 H, <b>a</b> ), 8.39 (s, 2 H, <b>c</b> ), 8.66 (d, 2H, <b>b</b> ).
$^{13}\text{C-NMR}$ ( $\text{CDCl}_3$ , 62.5 MHz):	$\delta$ (ppm): 44.2, 120.4, 132.1, 147.0, 149.6, 156.1.
IR (KBr):	$\nu$ ( $\text{cm}^{-1}$ ): 3001, 1594, 1558, 1457, 1376, 1279, 1216, 855.
Mass spectrometry:	$m/z = 252$ ( $\text{M}^+$ )

### 8.3.3 4,4'-bis(triphenylphosphonium-methyl)-2,2'-bipyridyl chloride (**4**)

In a 500 ml three-neck flask equipped with an thermometer, argon inlet and condenser 3.60 g (14.22 mmol) 4,4'-bis(chloromethyl)-2,2'-bipyridine (**3**) and 7.46 g (28.44 mmol)  $\text{P}(\text{Ph})_3$  were dissolved in 200 ml dry DMF and stirred at 120 °C for 48 h. After cooling to room temperature 300 ml of dry diethylether were added and the precipitate was isolated by filtration. Impurities were removed by excessively washing the product with diethylether, yielding 8.82 g (80 %) of almost white powder.

*Characterization:*



$^1\text{H-NMR}$ ( $\text{CDCl}_3$ , 250 MHz):	$\delta$ (ppm): 4.84 (d, 2 H, <b>d</b> ), 7.05 (m, 1 H, <b>a</b> ), 7.70-8.00 (m, 17 H, <b>c, e</b> ), 8.38 (m, 1H, <b>b</b> )
IR (KBr):	$\nu$ ( $\text{cm}^{-1}$ ): 3051, 3010, 2987, 2849, 2764, 1664, 1588, 1553, 1482, 1437, 1383, 1320, 1254, 1111, 994, 920, 852, 757, 720, 690.
Mass spectrometry:	$m/z$ = 444, 262, 183, 108, 36.

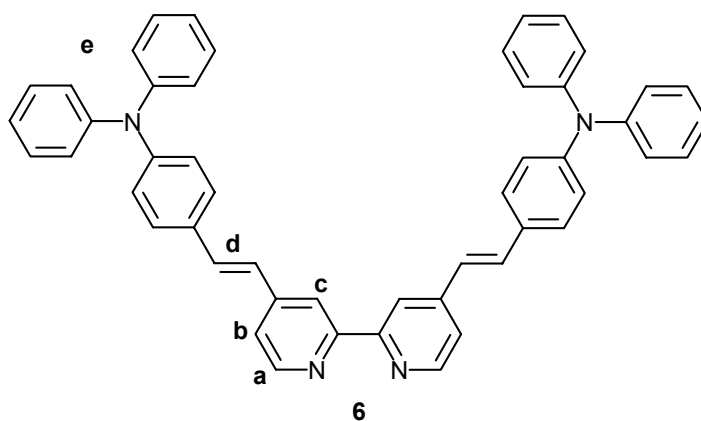
### 8.3.4 4,4'-bis[4-(diphenylamino)styryl]-2,2'-bipyridine (**6**)

Under argon atmosphere 4.5 g (5.8 mmol) of compound **4** and 3.17 g (11.6 mmol) 4-diphenylaminobenzaldehyde (**5**) were dissolved in 50 ml dried THF and heated up to 50

°C. A suspension of 2.23 g (23.2 mmol) NaOtBu in THF was slowly added to the reaction mixture via dropping funnel followed by stirring at 50 °C for 4 h.

After cooling to room temperature the reaction mixture was neutralized with acetic acid (10 %) and extracted with CH<sub>2</sub>Cl<sub>2</sub>. The combined organic fractions were washed with H<sub>2</sub>O (2 x) and with an aqueous solution of NaOAc (1 x). After drying over Na<sub>2</sub>SO<sub>4</sub> and evaporation of the solvent, the residue was purified via column chromatography (cyclohexane : EtOAc = 5 : 1) yielding a yellow powder: 2 g (50 %).

*Characterization:*



<sup>1</sup>H-NMR (CDCl<sub>3</sub>, 250 MHz): δ (ppm): 6.95 – 7.44 (m, 17 H, **a**, **d**, **e**), 8.49 (s, 1 H, **c**), 8.62 (d, 1H, **b**).

IR (KBr): ν (cm<sup>-1</sup>): 3027, 1631, 1583, 1492, 1376, 1330, 1282, 1176, 968, 835, 753, 685.

UV-VIS (CHCl<sub>3</sub>): λ<sub>max1</sub> = 298 nm, λ<sub>max2</sub> = 398 nm.

Mass spectrometry: m/z = 694 (M<sup>+</sup>)

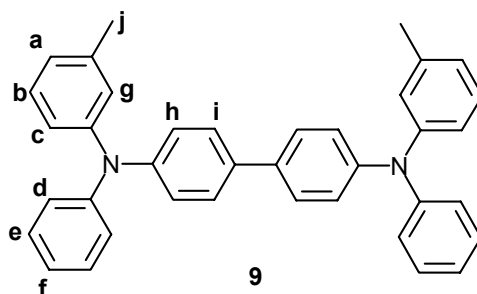
### 8.3.5 Synthesis of 4,4'-bis[N-(phenyl)-N'-(styryl)-N,N'-bis(3-methylphenyl)-1,1'-biphenyl-4,4'-diamino]-2,2'-bipyridine (**11**)

#### Step I:

#### *N,N'*-diphenyl-*N,N'*-bis(3-methylphenyl)-1,1'-biphenyl-4,4'-diamine (**9**)

In an argon flushed flask 6.9 g (17 mmol) 4,4'-dijodobiphenyl (**8**), 28.8 g (204 mmol)  $K_2CO_3$ , 6.48 g (102 mmol) Cu-powder, 1.32 g (5 mmol) 18-crown-6 and 9.35 g (51 mmol) 3-methyldiphenylamine (**7**) were dissolved in 50 ml dry o-dichlorobenzene and stirred for 1 h at 120 °C. After that, the reaction mixture was refluxed for 24 h, then cooled to room temperature and diluted with 50 ml THF. The solution was filtrated to remove catalyst, then the solvent was removed via distillation. After dissolving the residue in THF the product was precipitated into methanol. Filtration and washing three times with 250 ml methanol yielded 5.3 g of yellowish-white powder (yield: 60 %).

#### Characterization:



$^1H$ -NMR ( $CDCl_3$ , 250 MHz):  $\delta$  (ppm): 2.24 (s, 6 H, **j**), 6.82 – 7.49 (m, 26 H, **a - i**).

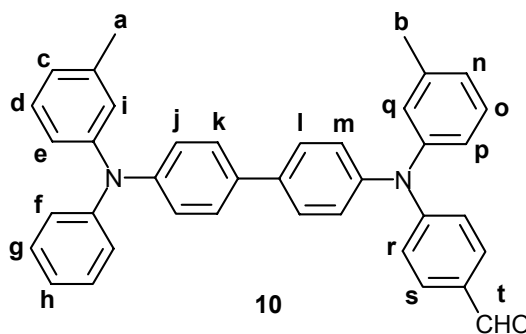
IR (KBr):  $\nu$  ( $cm^{-1}$ ): 3030, 2918, 1935, 1592, 1488, 1315, 1274, 1213, 1176, 1153, 1028, 830, 807, 744, 695, 678.

UV-VIS ( $CHCl_3$ ):  $\lambda_{max1} = 323$  nm,  $\lambda_{max2} = 353$  nm.

Mass spectrometry:  $m/z = 516$  ( $M^+$ )

*Step II:*

*N*-phenyl-*N'*-(*p*-formylphenyl)-*N,N'*-bis(3-methylphenyl)-1,1'-biphenyl-4,4'-diamine (**10**)  
 15 ml dry DMF were cooled to 0 °C, 0.53 g (3.48 mmol) POCl<sub>3</sub> were added and the mixture was stirred for 1 h letting it warm up to room temperature. After cooling again to 0 °C a solution of 1.5 g (2.9 mmol) of the diamine (**9**) synthesized in Step I dissolved in dry DMF was added dropwise. The solution was first stirred at room temperature for 1 h, then heated up to 60 °C and stirred until the diamine is totally consumed (TLC control). After cooling again to room temperature the mixture was poured into ice-water and neutralized with sodium acetate. The precipitate was isolated via filtration, washed with water and dried. After dissolving the raw product in 50 ml CH<sub>2</sub>Cl<sub>2</sub> the organic fraction was washed three times with H<sub>2</sub>O (50 ml each). The organic fraction was dried with Na<sub>2</sub>SO<sub>4</sub> and the solvent evaporated. Reprecipitation from THF into methanol yielded a yellow powder which was purified by column chromatography to separate residual educt and disubstituted bi-product yielding 13 % of the desired aldehyde.

*Characterization:*

<sup>1</sup>H-NMR (CDCl<sub>3</sub>, 250 MHz):      δ (ppm): 2.26 (s, 3 H, **a**), 2.52 (s, 3 H, **b**), 6.79 – 7.65 (m, 32 H, **c - s**), 10.04 (1 H, **t**).

IR (KBr):                              ν (cm<sup>-1</sup>): 3030, 2922, 2848, 1935, 1685, 1590, 1490, 1318, 1274, 1213, 1164, 1121, 1028, 1003, 824, 755, 696, 678, 625.

UV-VIS (CHCl<sub>3</sub>):  $\lambda_{\max 1} = 348 \text{ nm}$ ,  $\lambda_{\max 2} = 371 \text{ nm}$ .

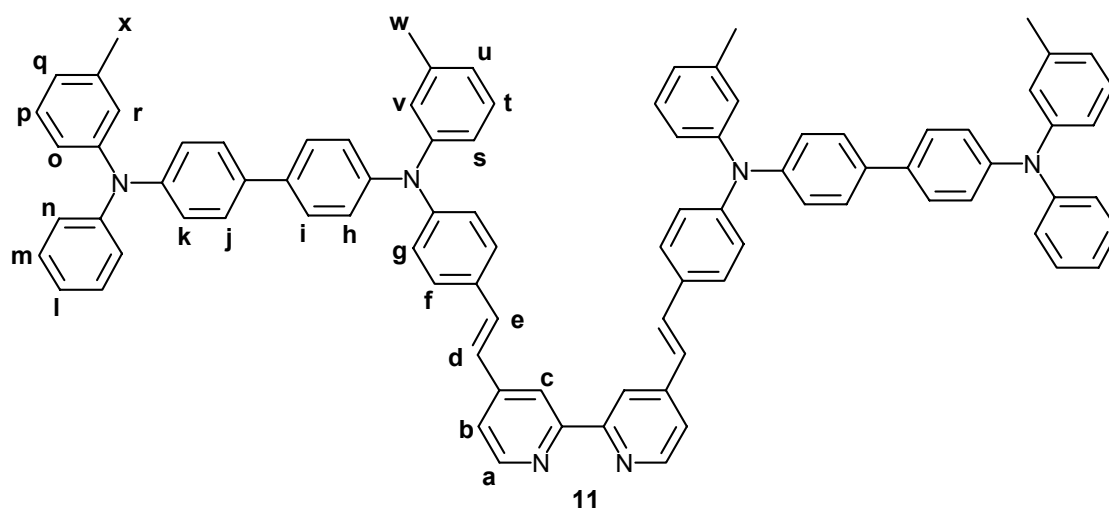
Mass spectrometry:  $m/z = 544 (M^+)$

*Step III:*

*4,4'-bis[N-(phenyl)-N'-(styryl)-N,N'-bis(3-methyl phenyl)-1,1'-biphenyl-4,4'-diamino]-2,2'-bipyridine (bpy-TPD ligand, 11)*

The TPD-ligand **11** was synthesized by coupling the aldehyde (**10**, from Step II) with the phosphonium salt **4**: Under argon atmosphere 0.544 g (1 mmol) of (**10**) and 0.302 g (0.5 mmol) **4** were dissolved in 25 ml dry THF. After heating to 50 °C a suspension of 0.192 g (2 mmol) NaOt-Bu in 25 ml dry THF was added dropwise and the mixture was stirred until the aldehyde **6** is fully consumed (TLC-control). The solution was cooled to room temperature and neutralized with acetic acid (10 % v/v). Extraction with CH<sub>2</sub>Cl<sub>2</sub> (three times, 50 ml each), drying of the combined organic fractions over Na<sub>2</sub>SO<sub>4</sub> and evaporation of the solvent resulted in a gold-coloured raw-product. This was reprecipitated from CH<sub>2</sub>Cl<sub>2</sub> into petrolether (40 – 60 °C) yielding 0.35 g of yellow powder: 57 %.

*Characterization:*

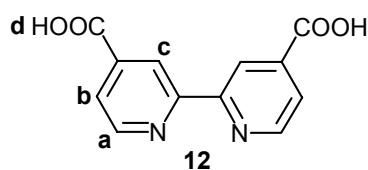


$^1\text{H-NMR}$ ( $\text{CDCl}_3$ , 250 MHz):	$\delta$ (ppm): 2.25 (s, 5 H, <b>w, x</b> ), 6.83 – 7.65 (m, 30 H, <b>a, d – v</b> ), 8.48 (s, 1 H, <b>c</b> ), 8.63 (d, 1 H, <b>b</b> )
IR (KBr):	$\nu$ ( $\text{cm}^{-1}$ ): 3030, 2952, 2920, 2860, 1585, 1492, 1375, 1317, 1273, 1178, 961, 744, 695.
UV-VIS ( $\text{CHCl}_3$ ):	$\lambda_{\text{max}1} = 309$ nm, $\lambda_{\text{max}2} = 352$ nm, $\lambda_{\text{max}3} = 403$ nm.
Mass spectrometry:	$m/z = 1236$ ( $\text{M}^+$ )

### 8.3.6 4,4'-dicarboxy-2,2'-bipyridine (**12**)

In 115 ml concentrated  $\text{H}_2\text{SO}_4$  5 g (27.14 mmol) 4,4'-dimethyl-2,2'-bipyridine was dissolved, 32.3 g (108.5 mmol) of  $\text{Na}_2\text{Cr}_2\text{O}_7 \cdot \text{H}_2\text{O}$  was added slowly and the solution was stirred at 75 °C over night. After cooling to room temperature the mixture was poured carefully to ice water and diluted with water. The precipitate was separated by filtration, dissolved in 6 M NaOH and the solution was filtrated again. After adding HCl (conc.) until pH 1 the product precipitated and could be isolated by filtration. Washing successively with  $\text{H}_2\text{O}$  to remove residual acid, then MeOH and diethylether and drying in vacuum gave 4.4 g of light grey powder (66 %).

*Characterization:*



$^1\text{H-NMR}$ ( $\text{DMSO-d}_6$ , 250 MHz):	$\delta$ (ppm): 7.90 (d, 2 H, <b>a</b> ), 8.84 (s, 2 H, <b>c</b> ), 8.90 (d, 2 H, <b>b</b> ), 13.81 (s, 2 H, <b>d</b> ).
$^{13}\text{C-NMR}$ ( $\text{CF}_3\text{COOD}$ , 62.5 MHz):	$\delta$ (ppm): 123.55, 127.79, 143.78, 147.21, 147.78, 167.15.

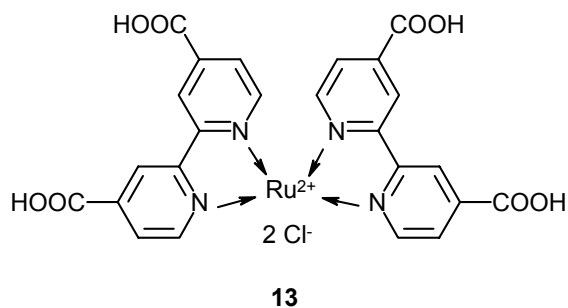
IR (KBr):  $\nu$  (cm<sup>-1</sup>): 3447, 3113, 2449, 1717, 1366, 1288, 1269, 1243, 766, 682.

Mass spectrometry:  $m/z = 244$  (M<sup>+</sup>)

### 8.3.7 Bis(4,4'-dicarboxy-2,2'-bipyridyl) Ru(II)dichloride (**13**)

In a three neck flask flushed with argon 360 mg (1.37 mmol) RuCl<sub>3</sub> · 3 H<sub>2</sub>O was dissolved in 100 ml dry DMF. A suspension of 678 mg (2.77 mmol) 4,4'-dicarboxy-2,2'-bipyridine (**12**) in 50 ml DMF was added very slowly and the reaction mixture was refluxed for 14 h. After cooling to room temperature the dark solution was poured over a glass filter and DMF was removed from the filtrate. The residue was recrystallized from acetone, isolated and dried in vacuum to yield 0.9 g of almost black powder (99 %).

*Characterization:*



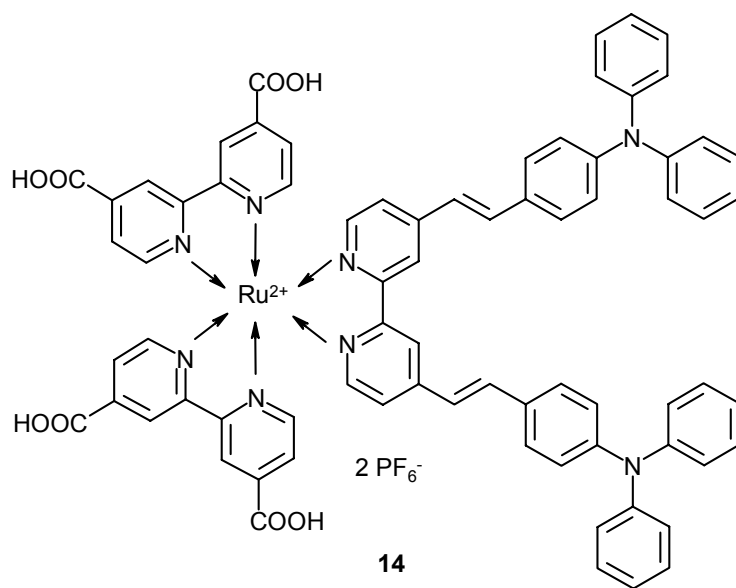
IR (KBr):  $\nu$  (cm<sup>-1</sup>): 3443, 2981, 2780, 2070, 1978, 1718, 1653, 1559, 1472, 1405, 1230, 1018, 771, 668.

UV-VIS (CHCl<sub>3</sub>):  $\lambda_{\max 1} = 310$  nm,  $\lambda_{\max 2} = 391$  nm,  $\lambda_{\max 3} = 536$  nm.

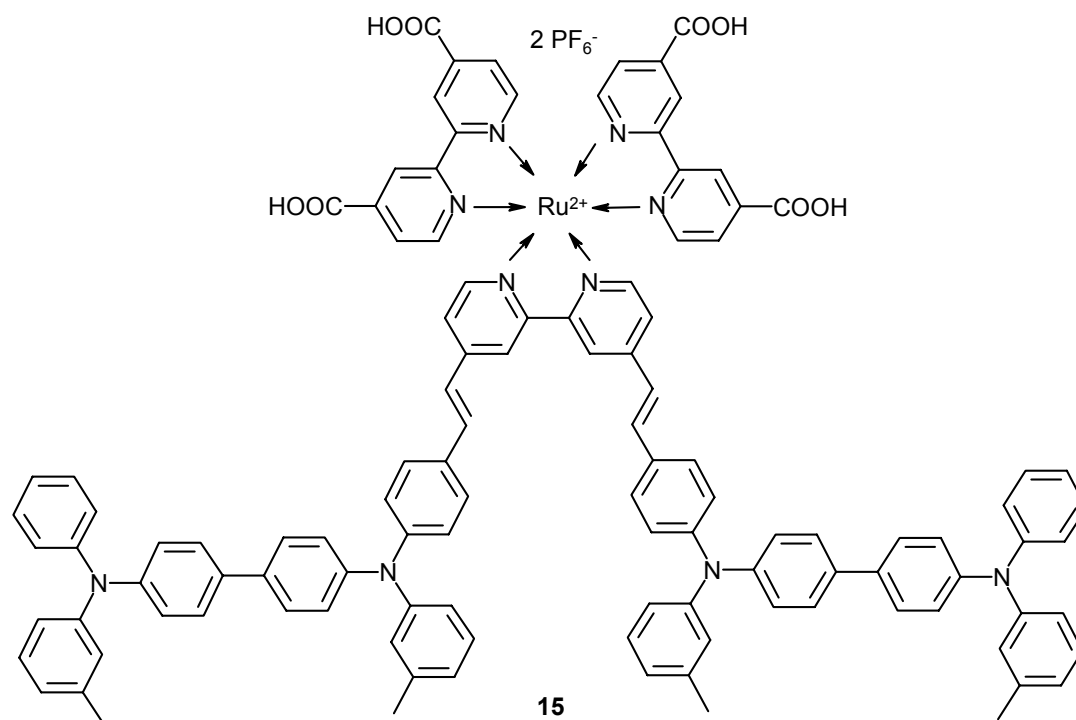
### 8.3.8 Synthesis of bifunctional dyes **14** and **15**

Equimolar amounts of the ligand (**6** or **11**) and Ru(II) precursor **13** were added to 20 ml dry DMF. After stirring for 1 h  $\text{CF}_3\text{SO}_3\text{Ag}$  was added in equimolar amounts and the reaction mixture was refluxed under argon atmosphere until the ligand was fully consumed (TLC control). The mixture was filtrated hot and then cooled to room temperature. A saturated aqueous solution of  $\text{KPF}_6$  was added and the mixture was refrigerated until the product precipitated. Reprecipitation from THF into petrol ether (40 – 60 °C) followed by filtration and drying yielded the Ru(II) complex (**14** or **15**) as red powder.

*Characterization of 14:*



Yield:	83 %
$^1\text{H-NMR}$ ( $\text{CDCl}_3$ , 250 MHz):	$\delta$ (ppm): 6.97 – 7.08 (m), 7.21 – 7.38 (m), 8.44 (s)
IR (KBr):	$\nu$ ( $\text{cm}^{-1}$ ): 3002, 2913, 1980, 1584, 1508, 1492, 1329, 1282, 1176, 968, 840.
UV-VIS ( $\text{CHCl}_3$ ):	$\lambda_{\text{max}1} = 301 \text{ nm}$ , $\lambda_{\text{max}2} = 405 \text{ nm}$

Characterization of **15**:

Yield: 51 %

$^1\text{H-NMR}$  (DMSO- $d_6$ , 250 MHz): 2.23 (s, 6 H), 6.87 – 7.55 (m, 36 H)

IR (KBr):  $\nu$  ( $\text{cm}^{-1}$ ): 3449, 3033, 2923, 1980, 1595, 1491, 1378, 1318, 1273, 832, 697.

UV-VIS ( $\text{CHCl}_3$ ):  $\lambda_{\text{max}1} = 304 \text{ nm}$ ,  $\lambda_{\text{max}2} = 413 \text{ nm}$

### 8.3.9 4,4'-bis[poly(4-bromostyryl)methyl]-2,2'-bipyridine (**16**)

*General procedure I:*

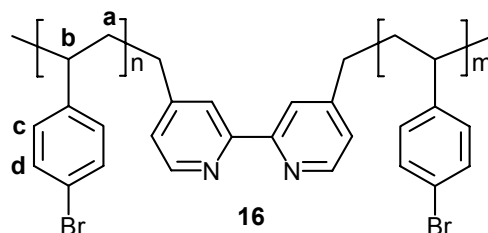
The monomer 4-bromostyrene and CuCl were placed in an argon flushed three-neck flask followed by the addition of PMDETA. The mixture turns brownish green when the ligand PMDETA was added. After stirring for 1 h 4,4'-bis(chloromethyl)-2,2'-bipyridine was added and the mixture was degassed in three cycles by the freeze-pump-thaw method. Equipped with a septum and a condenser, the flask was immersed in an oil bath maintained at 60°C and the initial time was recorded. After a certain reaction time the reaction was quenched by rapid cooling and exposing to air. After precipitation in n-hexane the slightly bluish polymers were filtrated, dried and washed first with methanol, then with an aqueous solution of NH<sub>4</sub>Cl to remove the residual copper catalyst. The polymers were reprecipitated from THF into methanol to give white solids.

To determine reaction kinetics, samples (2ml) were taken out of the reaction mixture at certain time intervals through the septum with an argon flushed syringe. They were cooled and exposed to air to terminate the polymerization and were used for GC analysis after dilution with THF.

Ratio of reactands = [4-bromostyrene] : [CuCl] : [PMDETA] : [**2**] = 150 : 1 : 2 : 1

*Example: Synthesis of 16f:*

28 g (153 mmol)	4-bromostyrene
101.0 mg (1.02 mmol)	CuCl
353.5 mg (2.04 mmol)	PMDETA
258.2 mg (1.02 mmol)	4,4'-bis(chloromethyl)-2,2'-bipyridine

*Characterization:*

$^1\text{H-NMR}$  ( $\text{CDCl}_3$ , 250 MHz):  $\delta$  (ppm): 1.25 (m, 2 H, **a**), 1.56 (m, 1 H, **b**), 6.29 (d, 2 H, **c**), 7.16 (d, 2 H, **d**).

IR (KBr):  $\nu$  ( $\text{cm}^{-1}$ ): 2924, 1592, 1486, 1407, 1073, 1009, 822.

UV-VIS ( $\text{CHCl}_3$ ):  $\lambda_{\text{max}} = 276 \text{ nm}$ .

SEC (THF + 0.25 % wt. TBAB):  $M_n = 26610 \text{ g/mol}$   
PDI = 1.18

DSC ( $10 \text{ Kmin}^{-1}$ ):  $T_g = 135.5 \text{ }^\circ\text{C}$

TGA:  $T_{\text{onset}} = 233 \text{ }^\circ\text{C}$

### 8.3.10 4,4'-bis[poly(4-vinyltriphenylamino)methyl]-2,2'-bipyridine (17)

*General procedure II:*

Polymer **16** and three times excess (referring to the monomer unit) of diphenylamine were dissolved in dry toluene.  $\text{NaO}^t\text{Bu}$ ,  $\text{Pd}(\text{OAc})_2$  and  $\text{P}^t\text{Bu}_3$  were added to the solution at room temperature. The dark brown reaction mixture was stirred at  $110^\circ\text{C}$  for 2h under an argon atmosphere. The reaction was quenched by cooling and flushing with air. After the removal of half of the toluene in vacuum the reaction mixture was diluted with THF and filtered over a small amount of Alox N.

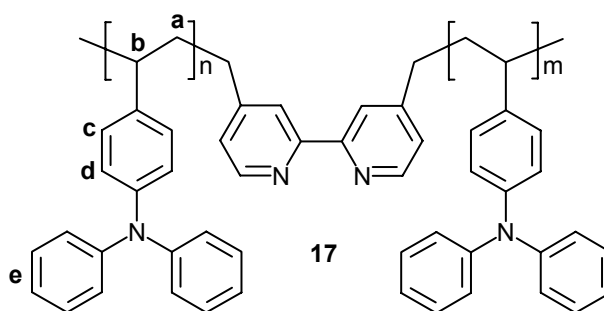
After evaporation of half of the THF, the bipyridine centred poly(4-vinyltriphenylamine) (**17**) was precipitated in methanol, filtrated and dried. For further purification the product was reprecipitated from THF into methanol to yield a light brown solid. It is possible to follow the progression of the reaction via analyzing samples taken from the reaction mixture with NMR or UV-VIS spectroscopy.

Ratio of reactands = [polymer **16**] : [diphenylamine] : [NaO<sup>t</sup>Bu] : [Pd(OAc)<sub>2</sub>] : [P(<sup>t</sup>Bu)<sub>3</sub>]  
= 1 : 3 : 1.5 : 0.025 : 1.5

*Example: Synthesis of 17f:*

1g (5.46 mmol of monomer unit)	<b>16f</b>
2.77 g (16.38 mmol)	diphenylamine
0.79 g (8.19 mmol)	NaO <sup>t</sup> Bu
30.60 mg (0.14 mmol)	Pd(OAc) <sub>2</sub>
165 mg (8.19 mmol)	P( <sup>t</sup> Bu) <sub>3</sub>
30 ml	toluene

*Characterization:*



Yield:	1.34 g
<sup>1</sup> H-NMR (CDCl <sub>3</sub> , 250 MHz):	δ (ppm): 1.57 (m, 4 H, <b>a</b> ), 1.97 (m, 2 H, <b>b</b> ), 6.48 – 6.99 (m, 14 H, <b>c</b> , <b>d</b> , <b>e</b> ).

IR (KBr):	$\nu$ (cm <sup>-1</sup> ): 3058, 3024, 2920, 2850, 1588, 1492, 1312, 1275, 826, 751, 694.
UV-VIS (CHCl <sub>3</sub> ):	$\lambda_{\text{max}}$ = 303 nm.
SEC (THF + 0.25 % wt. TBAB):	$M_n$ = 15140 g/mol PDI = 1.36
DSC (10 Kmin <sup>-1</sup> )	$T_g$ = 131.7 °C
TGA:	$T_{\text{onset}}$ = 240 °C

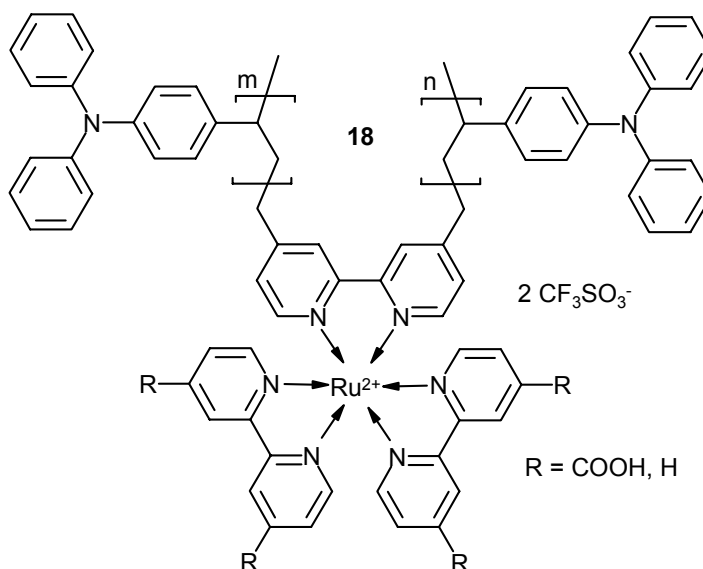
### 8.3.11 Bis[bipyridyl]-[4,4'-bis[poly(4-vinyltriphenylamino)methyl]-2,2'-bipyridyl]-Ru(II) trifluorosulfonate (**18**)

#### *General procedure III:*

CF<sub>3</sub>SO<sub>3</sub>Ag (2eq.) and Ru(bpy)<sub>2</sub>Cl<sub>2</sub>·2H<sub>2</sub>O or **13** (1eq.) were dissolved in 30 ml dry acetone and stirred under argon for 3 h. After filtration of AgCl over a filter paper, acetone was removed under reduced pressure at room temperature. The dark red residue was dissolved in 30 ml dry DMF and polymer **17** was added. The reaction mixture was refluxed for 24 h. At the end of reaction about 75% of the DMF was removed and the rest was dissolved in a small amount of CHCl<sub>3</sub>. The product (**18**) was precipitated by dropping the CHCl<sub>3</sub> solution into MeOH, filtered and washed repeatedly with MeOH until the washings were colourless. After drying in vacuum an orange powder was obtained in approximately 80 % yield.

#### *Example: Synthesis of 18d:*

96.3 mg (0.375 mmol)	CF <sub>3</sub> SO <sub>3</sub> Ag
97.5 mg (0.187 mmol)	Ru(bpy) <sub>2</sub> Cl <sub>2</sub> · 2H <sub>2</sub> O
0.7 g (2.6 mmol of monomer unit)	<b>17d</b>

*Characterization:*

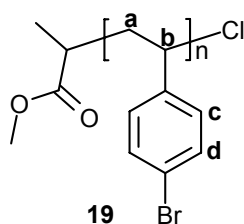
Yield:	0.54 g
$^1\text{H-NMR}$ ( $\text{CDCl}_3$ , 250 MHz):	$\delta$ (ppm): 1.57 (m, 2 H), 2.00 (m, 1 H), 6.59 - 6.89 (m, 9 H), 7.41 (m, 0.06 H), 7.54 (m, 0.06 H), 7.74 (m, 0.08 H), 7.91 (m, 0.12 H), 8.33 (m, 0.08 H).
IR (KBr):	$\nu$ ( $\text{cm}^{-1}$ ): 2940, 2899, 1567, 1492, 1437, 1318, 1235, 1063, 801.
UV-VIS ( $\text{CHCl}_3$ ):	$\lambda_{\text{max}} = 456 \text{ nm}$ .
MALDI-TOF MS	$M_n = 3940 \text{ g/mol}$
DSC ( $10 \text{ Kmin}^{-1}$ )	$T_g = 148.4 \text{ }^\circ\text{C}$
TGA:	$T_{\text{onset}} = 287 \text{ }^\circ\text{C}$

8.3.12 Synthesis of poly(4-bromostyrene) macroinitiator (**19**)*General procedure IV:*

In a three neck flask, 4-bromostyrene, CuCl and PMDETA were diluted with very few dried anisole. After stirring for 1h the initiator  $\alpha$ -chloromethylpropionate was added and the mixture was degassed three times via freeze-pump-thaw-method as it is reported before. The flask was immersed into an oil bath maintained at 60 °C. After 17 h the reaction was quenched by rapid cooling and exposing to air. The polymer was precipitated in dried n-hexane, isolated by filtration and dried in vacuum. Further purification steps were set aside due to the danger of losing the reactive end group. The product was stored under argon atmosphere and used up fast for the next reaction step.

*Example: Synthesis of 19c:*

10 g (54.6 mmol)	4-bromostyrene
98.99 mg (1 mmol)	CuCl
173.3 mg (1 mmol)	PMDETA
245.1 mg (2 mmol)	$\alpha$ -chloromethylpropionate
1 ml	anisole

*Characterization:*

Yield:	79 %
$^1\text{H-NMR}$ ( $\text{CDCl}_3$ , 250 MHz):	$\delta$ (ppm): 1.25 - 1.56 (m, 3 H, <b>a</b> , <b>b</b> ), 6.29 (m, 2 H, <b>c</b> ), 7.16 (m, 2 H, <b>d</b> ).

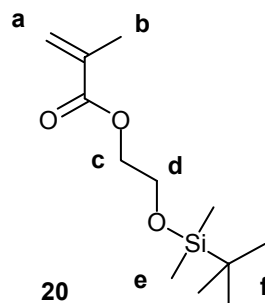
IR (KBr):	$\nu$ (cm <sup>-1</sup> ): 2924, 1592, 1486, 1407, 1073, 1009, 822.
SEC (THF + 0.25 % wt. TBAB):	$M_n = 6534$ g/mol PDI = 1.31
DSC (10 Kmin <sup>-1</sup> )	$T_g = 117.3$ °C
TGA:	$T_{\text{onset}} = 247$ °C

### 8.3.13 *Tert.*-butyldimethylsiloxyethylmethacrylate (**20**)

45.55 g (0.35 mol) hydroxyethylmethacrylate (HEMA) and 59.57 g (0.875 mol) imidazole were dissolved in 100 ml dry DMF and cooled to -20°C. In another flask 58.03 g (0.385 mol) *tert.*-butyldimethylsilylchloride was dissolved in 120 ml DMF with gentle heating and added to the DMF solution within 2h via dropping funnel. After the reaction mixture got clear and then again turbid, it was heated up to room temperature and stirred under argon for 3 days. Stabilizer was added before removing DMF in vacuum. The residue was extracted with water until pH = 7 and the water fraction was extracted with diethylether (4 x 100 ml). The combined organic fractions were dried over Na<sub>2</sub>SO<sub>4</sub>, filtrated and the solvent evaporated in vacuum.

The product HEMA-TBDMS was further purified via vacuum distillation ( $5 \cdot 10^{-2}$  mbar) under gentle heating (not over 60 °C) and stored over CaH<sub>2</sub> under inert gas atmosphere: 61 g (71 %).

*Characterization:*



$^1\text{H-NMR}$  ( $\text{CDCl}_3$ , 250 MHz):  $\delta$  (ppm): 0.04 (s, 6 H, **e**), 0.86 (s, 9 H, **f**), 1.92 (s, 3 H, **b**), 3.82 (t, 2 H, **d**), 4.19 (t, 2 H, **c**), 5.54 (s, 1 H, **a**), 6.09 (s, 1 H, **a**).

$^{13}\text{C-NMR}$  ( $\text{CDCl}_3$ , 62.5 MHz):  $\delta$  (ppm): 18.6, 18.7, 26.2, 61.6, 66.3, 125.8, 136.7, 167.7.

### 8.3.14 Poly(4-bromostyrene)-b-poly(HEMA-TBDMS) (**21**)

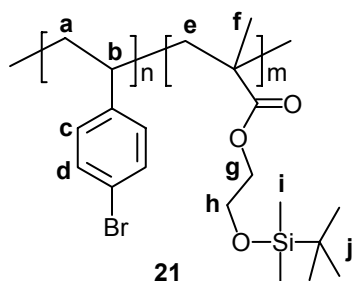
#### *General procedure V:*

A mixture of ethylmethylketone and isopropanol was prepared resulting in an initiator concentration of  $0.02 \text{ mol l}^{-1}$ . The macroinitiator **19** (5 g, 0.765 mmol of monomer unit), CuCl (75.7 mg, 0.765 mmol) and PMDETA (0.265 mg, 1.53 mmol) were added to the mixture of solvents in an argon-flushed schlenk-flask and stirred for 1 h. The macroinitiator definitely has to be dissolved completely. A small column ( $\text{Ø}$  2 cm) was packed with alumina N (2 cm height) which was stored in the oven at  $110 \text{ }^\circ\text{C}$  for several days before use. Monomer **20** was filtrated fast over alox N column and immediately added to the reaction mixture.

After degassing by freeze-pump-thaw method like reported before the flask was immersed into an oil bath maintained at  $60 \text{ }^\circ\text{C}$ . The reaction was quenched after 16.5 h via rapid cooling and exposing to air. The product was precipitated into methanol, filtrated, washed and dried. For further purification polymer **21** was reprecipitated from THF into methanol.

*Example: Synthesis of 21c:*

5 g (0.765 mmol of monomer unit)	macroinitiator <b>19c</b>
75.7 mg (0.765 mmol)	CuCl
0.265 mg (1.53 mmol)	PMDETA
5.24 g (21.42 mmol)	HEMA-TBDMS ( <b>20</b> )
30.6 ml	MEK
7.65 ml	isopropanol

*Characterization:*

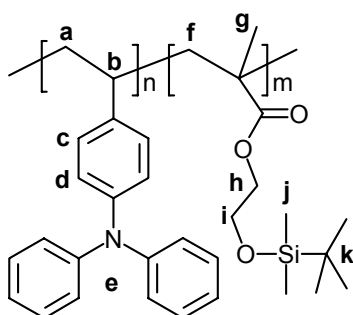
Yield:	7.4 g (72 %)
$^1\text{H-NMR}$ ( $\text{CDCl}_3$ , 250 MHz):	$\delta$ (ppm): 0.06 (s, 6 H, <b>i</b> ), 0.89 (s, 10.8 H, <b>j</b> ), 1.03 – 1.87 (m, 3.6 H, <b>a, b, e</b> ), 3.76 (s, 1.9 H, <b>h</b> ), 3.95 (s, 1.8 H, <b>g</b> ), 6.33 (m, 3.6 H, <b>c</b> ), 7.22 (m, 3.7 H, <b>d</b> ).
IR (KBr):	$\nu$ ( $\text{cm}^{-1}$ ): 2930, 2857, 1731, 1486, 1407, 1256, 1106, 1009, 834, 778.
SEC (THF + 0.25 % wt. TBAB):	$M_n = 9620$ g/mol PDI = 1.51
DSC (10 $\text{Kmin}^{-1}$ ):	$T_{g1} = 29.6$ °C $T_{g2} = 119.0$ °C
TGA:	$T_{\text{onset}} = 223$ °C

8.3.15 Poly(4-vinyltriphenylamine)-b-polyHEMA-TBDMS (**22**)*General procedure VI:*

The block copolymer **21** and four times excess of diphenylamine were dissolved in dry toluene. Na-*tert*.butoxide, Pd(OAc)<sub>2</sub> and P(*tert*.Bu)<sub>3</sub> were added. The reaction mixture was refluxed over night, cooled and most of the toluene was evaporated resulting in a very concentrated suspension. After adding THF the mixture was filtrated over Alox N to remove the catalyst. Then the solution was concentrated and the polymer was precipitated in methanol. For purification the product could be reprecipitated from THF in methanol, yielding a white powder after isolating and drying in vacuum.

*Example: Synthesis of 22c:*

2.5 g (7.92 mmol of 4-bromostyrene units)	polymer <b>21c</b>
5.36 g (31.68 mmol)	diphenylamine
1.14 g (11.88 mmol)	Na- <i>tert</i> .butoxide
44.4 mg (0.198 mmol)	Pd(OAc) <sub>2</sub>
0.320 g (1.584 mmol)	P( <i>tert</i> .Bu) <sub>3</sub>
100 ml	toluene
100 ml	THF

*Characterization:***22**

$^1\text{H-NMR}$ ( $\text{CDCl}_3$ , 250 MHz):	$\delta$ (ppm): 0.06 (s, 6 H, <b>j</b> ), 0.89 (s, 9 H, <b>k</b> ), 1.03 – 1.88 (m, 10.4 H, <b>a</b> , <b>b</b> , <b>f</b> , <b>g</b> ), 3.76 (s, 2 H, <b>i</b> ), 3.96 (s, 2 H, <b>h</b> ), 6.43 – 7.11 (m, 23.5 H, <b>c</b> – <b>e</b> ).
IR (KBr):	$\nu$ ( $\text{cm}^{-1}$ ): 2930, 2857, 1731, 1486, 1407, 1256, 1106, 1009, 834, 778.
SEC (THF + 0.25 % wt. TBAB):	$M_n = 5818$ g/mol PDI = 1.45
DSC ( $10 \text{ Kmin}^{-1}$ ):	$T_{g1} = 24.9$ °C $T_{g2} = 121.6$ °C
TGA:	$T_{\text{onset}} = 251$ °C

### 8.3.16 Poly(4-vinyltriphenylamine)-b-polyHEMA (**23**)

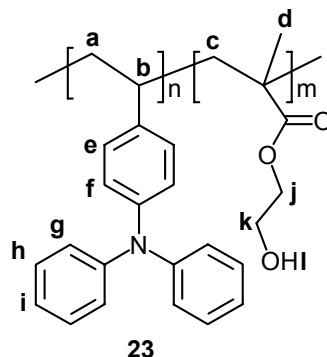
#### *General procedure VII:*

The removal of the protection group was carried out applying a modification of the procedure reported by C. Frenz<sup>119</sup>. Polymer **22** was dissolved in dioxane and 6 M HCl was added carefully. After stirring for 2 h  $\text{CHCl}_3$  was added and the solution was poured into a separation funnel filled with water. The aqueous phase was extracted three times with  $\text{CHCl}_3$  and the organic fractions were combined. Concentrating of the organic solution followed by precipitation into MeOH, filtrating and drying yielded a white powder.

#### *Example: Synthesis of 23c:*

1 g	polymer <b>22</b>
3 ml	HCl (6 M)
100 ml	1,4-dioxane

<sup>119</sup> C. Frenz, *Dissertation*, Bayreuth **2003**.

*Characterization:*

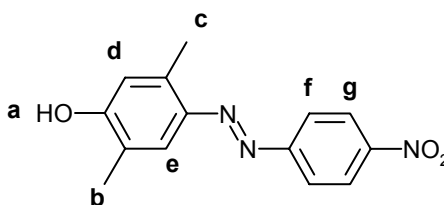
Yield:	0.840 g
$^1\text{H-NMR}$ ( $\text{CDCl}_3$ , 250 MHz):	$\delta$ (ppm): 0.95 – 1.91 (m, 44 H, <b>a – d</b> ), 3.47 (s, 1 H, <b>l</b> ), 3.82 (s, 2 H, <b>k</b> ), 4.08 (s, 2 H, <b>j</b> ), 6.41 – 7.09 (m, 90 H, <b>e – i</b> ).
SEC (THF + 0.25 % wt. TBAB):	$M_n = 5355$ g/mol PDI = 1.47
DSC ( $10 \text{ Kmin}^{-1}$ ):	$T_g = 128.4$ °C
TGA:	$T_{\text{onset}} = 260$ °C

8.3.17 2,5-dimethyl-4-(4-nitrophenylazo)phenol (**24**)

To a solution of 3 g (75 mmol) NaOH in 25 ml  $\text{H}_2\text{O}$ , 3.05 g (25 mmol) 2,5-dimethylphenol was added. Parallel to that, a solution of 5.92 (25 mmol) 4-nitrobenzene-diazonium tetrafluoroborate in 30 ml acetic acid and 30 ml  $\text{H}_2\text{O}$  was also prepared. After cooling both solutions to 0 °C, HCl was added dropwise to the alkaline reaction mixture. It is important to keep the reaction mixture alkaline if necessary via additional NaOH. The reaction mixture was stirred for 1 h at 5 °C and acidified with acetic acid to

precipitate the product. Filtration, washing with water and drying in vacuum yields 6.4 g of orange colored powder (94 %).

*Characterization:*



**24**

$^1\text{H-NMR}$  ( $\text{CDCl}_3$ , 250 MHz):  $\delta$  (ppm): 2.26 (s, 3 H, **b**), 2.67 (s, 3 H, **c**), 5.18 (s, 1 H, **a**), 6.74 (s, 1 H, **d**), 7.61 (s, 1 H, **e**), 7.92 (d, 2 H, **g**), 8.32 (d, 2 H, **f**).

$^{13}\text{C-NMR}$  ( $\text{CDCl}_3$ , 62.5 MHz):  $\delta$  (ppm): 15.6, 16.8, 116.3, 117.6, 122.9, 124.9, 140.3, 143.1, 147.4, 156.0, 160.8

IR (KBr):  $\nu$  ( $\text{cm}^{-1}$ ): 3422, 3204, 3068, 1631, 1613, 1591, 1558, 1507, 1471, 1448, 1381, 1327, 1285, 1265, 1253, 1182, 1168, 1107, 1087, 1012, 891, 852.

Mass spectrometry:  $m/z = 271$  ( $\text{M}^+$ )

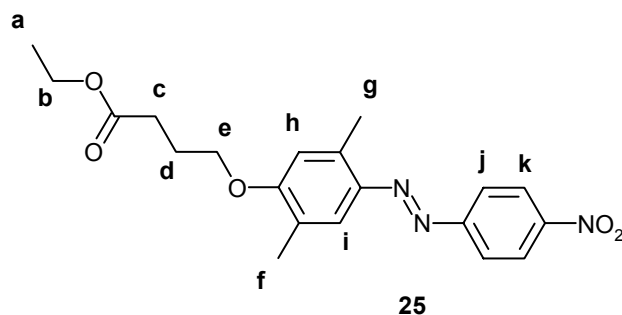
UV-VIS ( $\text{CHCl}_3$ ):  $\lambda_{\text{max}} = 395$  nm

### 8.3.18 1-[(2,5-dimethyl-4-(4-nitrophenylazo) phenoxy] ethylbutyrate (**25**)

2 g (7.4 mmol) of 2,5-dimethyl-4-(4-nitrophenylazo)phenol (**24**), 2.17 g (11.1 mmol) 1-bromoethylbutyrate 1.53 g (11.1 mmol)  $\text{K}_2\text{CO}_3$  and 0.153 g (0.925 mmol) KI were dissolved in 50 ml dry acetone and heated to reflux for at least 2 d.

After consumption of the azo educt (TLC control) the hot reaction mixture was filtrated and the residue was extracted with hot acetone (3 x 20 ml). From the combined acetone fractions the solvent was evaporated and the product dried in vacuum: 2.3 g (80 %).

*Characterization:*



$^1\text{H-NMR}$  ( $\text{CDCl}_3$ , 250 MHz):  $\delta$  (ppm): 1.25 (t, 3 H, **a**), 2.20 (m, 5 H, **f**, **d**), 2.54 (t, 2 H, **c**), 2.71 (s, 3 H, **g**), 4.10 (t, 2 H, **e**), 4.13 (t, 2 H, **b**), 6.73 (s, 1 H, **h**), 7.62 (s, 1 H, **i**), 7.95 (d, 2 H, **k**), 8.31 (d, 2 H, **j**).

$^{13}\text{C-NMR}$  ( $\text{CDCl}_3$ , 62.5 MHz):  $\delta$  (ppm): 15.6, 17.3, 18.9, 25.9, 32.1, 62.5, 68.5, 113.8, 119.1, 124.4, 126.1, 127.0, 142.0, 145.8, 149.6, 157.9, 162.4, 174.5

IR (KBr):  $\nu$  ( $\text{cm}^{-1}$ ): 3078, 3005, 2933, 1731, 1607, 1579, 1515, 1442, 1340, 1250, 1182, 1093, 1027, 858.

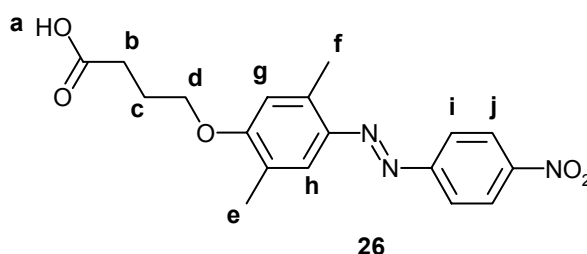
Mass spectrometry:  $m/z = 385$  ( $\text{M}^+$ )

UV-VIS ( $\text{CHCl}_3$ ):  $\lambda_{\text{max}} = 396$  nm

### 8.3.19 1-[(2,5-dimethyl-4-(4-nitrophenylazo) phenoxy]butyric acid (**26**)

In a mixture of H<sub>2</sub>O and Ethanol (1:1) 2.2 g (5.71 mmol) of the butyrate (**25**) and 0.343 g (8.57 mmol) NaOH were refluxed for 1.5 h. With 6 N HCl, pH of the solution is adjusted to 1 and the precipitate was filtrated after 20 min of stirring. Washing with water and drying in vacuum gave 1.90 g orange powder (93 %).

*Characterization:*



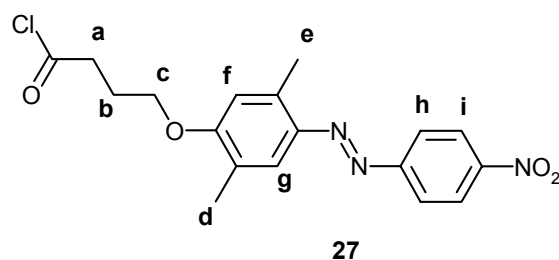
<sup>1</sup> H-NMR (DMSO, 250 MHz):	δ (ppm): 2.01 (q, 2 H, <b>c</b> ), 2.15 (s, 3 H, <b>e</b> ), 2.43 (t, 2 H, <b>b</b> ), 2.68 (s, 3 H, <b>f</b> ), 4.11 (t, 2 H, <b>d</b> ), 6.99 (s, 1 H, <b>g</b> ), 7.55 (s, 1 H, <b>h</b> ), 7.99 (d, 2 H, <b>j</b> ), 8.35 (d, 2 H, <b>i</b> ), 12.17 (s, 1 H, <b>a</b> )
<sup>13</sup> C-NMR (DMSO, 62.5 MHz):	δ (ppm): 15.6, 17.1, 24.2, 30.2, 67.2, 113.0, 117.1, 123.0, 124.8, 125.0, 140.5, 143.6, 147.6, 155.8, 160.8, 174.0
IR (KBr):	ν (cm <sup>-1</sup> ): 3004, 2995, 2709, 2384, 1775, 1642, 1585, 1509, 1447, 1362, 1266, 1123, 972, 848.
Mass spectrometry:	m/z = 357 (M <sup>+</sup> )
UV-VIS (CHCl <sub>3</sub> ):	λ <sub>max</sub> = 401 nm

## 8.3.20 1-[(2,5-dimethyl-4-(4-nitrophenylazo) phenoxy]

butyric acid chloride (**27**)

The carboxylic acid derivative (**26**) and 7 times excess of oxalyl chloride were added to 30 ml toluene and the suspension was stirred at room temperature for 45 min. After refluxing for 3 h half of the toluene was distilled from the deep red solution. After adding toluene and n-hexane (50 ml; 1:6) and a spatula of  $K_2CO_3$  the mixture was heated to reflux for 2 h and then hot filtered under an argon atmosphere. The solution is stored in the refrigerator under inert gas atmosphere until red crystals developed. Filtration in argon stream yielded the desired product.

*Characterization:*



$^1H$ -NMR ( $CDCl_3$ , 250 MHz):  $\delta$  (ppm): 2.21 – 2.26 (m, 5 H, **b**, **d**), 2.71 (s, 3 H, **e**), 3.16 (t, 2 H, **a**), 4.11 (t, 2 H, **c**), 6.71 (s, 1 H, **f**), 7.62 (s, 1 H, **g**), 7.93 (d, 2 H, **i**), 8.32 (d, 2 H, **h**).

UV-VIS ( $CHCl_3$ ):  $\lambda_{max} = 391$  nm

8.3.21 Poly(4-vinyltriphenylamine)-b-poly-(HEMA-DNPP) (**28**)

*General procedure VIII:*

In a three neck flask equipped with a condenser, inert gas inlet and a septum polymer **23** was dissolved in dry THF. Dry pyridin was added dropwise. In a second flask a THF

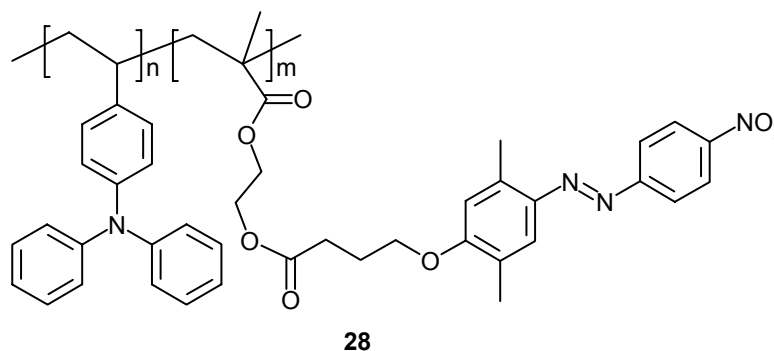
solution of the acid chloride derivative **27** was prepared and added to the reaction flask via syringe. After some minutes, the solution became turbid, then a white precipitate of pyridinium hydrochlorid developed. The reaction mixture was stirred at room temperature for 20 h, then 4 h more at a temperature of 50 °C. From this suspension the product was directly precipitated into methanol yielding an orange powder consisting of desired product **28** and unreacted low-molecular weight azo-dye which had to be removed. By preparing a chloroform suspension of the product mixture followed by filtration over low pore-size paper filter it was possible to isolate pure **28**. After concentrating the CHCl<sub>3</sub> filtrate the polymer could be precipitated in methanol. Filtrating and drying yielded the target molecule (**28**).

Ratio of reactands = [HEMA monomer units of polymer **23**] : [**27**] : [pyridine] = 1 : 4 : 12

*Example: Synthesis of 28c:*

140 mg (0.197 mmol of HEMA monomer units)	polymer <b>23c</b>
296 mg (0.788 mmol)	<b>27</b>
187 mg (2.364 mmol)	pyridine
10 ml	THF

*Characterization:*



## 8 Experimental

---

$^1\text{H-NMR}$ (THF- $d_8$ , 250 MHz):	$\delta$ (ppm): 0.89 – 1.29 (m, 3 H), 2.14 (m, 4 H), 2.46 (s, 3 H), 2.67 (m, 1 H), 4.08 (s, 1 H), 6.55 – 7.09 (m, 15 H), 7.58 (s, 1 H), 7.86 (s, 1 H), 8.26 (s, 1 H).
IR (KBr):	$\nu$ ( $\text{cm}^{-1}$ ): 3034, 2923, 1735, 1606, 1589, 1463, 1336, 1247, 1170, 1091, 855, 753, 695.
SEC (THF + 0.25 % wt. TBAB):	$M_n = 4448$ g/mol PDI = 1.14
DSC (20 $\text{Kmin}^{-1}$ ):	$T_g = 130.1$ °C
TGA:	$T_{\text{onset}} = 233$ °C
UV-VIS ( $\text{CHCl}_3$ ):	$\lambda_{\text{max}1} = 304$ nm, $\lambda_{\text{max}2} = 413$ nm





## Erklärung

Hiermit erkläre ich, daß ich die vorliegende Arbeit selbständig verfasst und keine anderen als die von mir angegebenen Quellen und Hilfsmittel benutzt habe.

Ferner erkläre ich, daß ich weder anderweitig mit oder ohne Erfolg versucht habe, diese Dissertation einzureichen, noch eine gleichartige Doktorprüfung an einer anderen Hochschule endgültig nicht bestanden habe.

.....

*Ort, Datum*

.....

*Katja Peter*